UNIVERSITÉ DE STRASBOURG

THÈSE

présentée pour obtenir le grade de

DOCTEUR de l'UNIVERSITÉ DE STRASBOURG

Par

Guangyan Du

Micrometric Contraction and Extension of Telescopic Supramolecular Polymers.

Soutenue publiquement le 28 septembre 2012 devant le jury composé de:

Professeur Gwénaël Rapenne (CEMES - CNRS, Université Paul Sabatier, Toulouse) - Rapporteur

Professeur Patrice Woisel (UMR 8207, CNRS - Université de Lille 1, Lille) - Rapporteur

Professeur Valérie Heitz (LSAMM, Université de Strasbourg, Strasbourg) - Examinateur

Professeur Eric Buhler (Laboratoire MSC, Université Paris Diderot) – Membre invité

Professeur Nicolas Giuseppone (ICS, Université de Strasbourg, Strasbourg) - Directeur de thèse

TABLE OF CONTENTS

ABSTRACT ***7***

ACKNOWLEDGMENTS ***11***

ABBREVIATIONS AND SYMBOLS ***13***

GENERAL INTRODUCTION ***15***

THEORETICAL PART ***19***

Chapter 1 : Bibliography **21**

1/ Supramolecular Chemistry 21

2/ Mechanically Interlocked Molecules (MIMs) 23

a) Definition and concept 23

b) Catenanes 24

c) Rotaxanes 26

d) Synthetic routes to rotaxanes 26

e) Polyrotaxanes 28

3/ Molecular Machines and Shuttles (or Switches) 30

a) Definitions and concepts 30

b) Rotaxanes as molecular shuttles 31

i. pH-controlled Shuttles 33

ii. Light-driven isomerisation shuttles 36

iii. Electrochemically-driven shuttles 37

iv. Metalation and demetalation-driven shuttles 39

c) Molecular muscles 41

i. Polymer-based artificial muscles 42

ii. Bistable rotaxane molecular muscles at the molecular level 44

iii. Attempts to extend bistable rotaxane molecular muscles at the macroscopic level 47

4/ Supramolecular Polymers 51

a) Definitions and classifications 51

b) Hydrogen-bonding supramolecular polymers 51

c) Metallo-supramolecular polymers 54

d) Self-healing 55

Chapter 2 : Synthesis and Characterization of Covalently Polymerized Rotaxanes **57**

1/ Retrosynthetic Approach 57

2/ Synthesis and characterization of pseudo-rotaxanes 59

a) Crown-ether aldehyde 5 59

b) Primary amine linker 9 60

c) Synthesis and characterization of pseudo-rotaxanes 61

d) Pseudo-rotaxanes stereoisomers 61

e) Acid-base titration for the switching process 63

3/ Synthesis and characterization of symmetric dumbbell 23 (n=1) 64

4/ Polymerization and characterization of the symmetric dumbbell with pseudo-rotaxane by click chemistry 68
5/ Synthesis of donor-acceptor amphiphilic rotaxane systems (J. J. Cid, A. Wolf, F. Niess) 70
6/ Conclusion on Covalently Polymerized Rotaxanes 71

Chapter 3 : Synthesis and Characterization of Metallo-Supramolecular Polymers 73
1/ Retrosynthetic Approach 74
2/ Synthesis of the unsymmetric dumbbell 45 (n = 1) 74
3/ Synthesis and characterization of model rotaxane (n=0) 81
4/ Characterization of the metallo-supramolecular polymers 84
a) ^{1}H NMR experiments 85
b) UV-Vis experiments 85
c) Light and neutron scattering experiments 86
d) Conclusions 92
5/ Self-healing behavior of the metallo-supramolecular polymers connected by tristerpyridine 93
6/ Oligophenylacetylene dumbbell functionalied triarylamine-fullerene dyads 96
7/ Conclusions 96

Chapter 4 : Synthesis and Characterization of Hydrogen-Bonding Supramolecular Polymers 99
1/ Synthesis of a model hydrogen-bonding rotaxane (DAD type) 99
a) Synthesis of the rotaxanes 2^{ext} and 2^{cont} 99
b) Synthesis of the complementary hydrogen-bonding dumbbell 26 104
2/ Characterization of the model hydrogen-bonding polymeric rotaxanes 105
a) ^{1}H NMR experiments 106
b) Light and neutron scattering experiments 107
c) TEM microscopy 109
3/ Synthesis of a model hydrogen-bonding rotaxane (ADA type) 109
4/ Conclusions 112

Conclusion and Perspectives 115

EXPERIMENTAL PART 117

Synthesis and characterization of organic compounds 119
1/ General Procedures 119
a) Solvent and chemical reagents 119
b) Chromatographic methods 119
c) Analytical methods and instruments 119
2/Synthesis of compounds 127
Compound 3 129
Compound 4 129
Compound 5 130
Compound 6 130
Compound 7 127
Compound 8 127
Compound 9 128

Compound 10 131
Compound 11 132
Compound 12 137
Compound 13 147
Compound 14 148
Compound 15 154
Compound 16 154
Compound 17 156
Compound 18 156
Compound 21 156
Compound 22 156
Compound 23 156
Compound 24 154
Compound 25 154
Compound 26 156
Compound 27 156
Compound 28 156
Compound 16 156
Compound 29 156
Compound 30 167
Compound 31 169
Compound 33 170
Compound 34 132
Compound 38 135
Compound 39 136
Compound 40 137
Compound 41 138
Compound 42 139
Compound 44 141
Compound 45 142
Compound 48 144
Compound 49 144
Compound 50 145
Compound 1^{ext} 157
Compound 1^{cont} 158
Procedures for polymerization of terpyridine rotaxanes 158
Procedures for acidic-basic titrations of monomers 1^{ext} and 1^{cont} 159
Compound 51 159
Compound 58 160
Compound 59 161
Compound 60 162
Compound 2^{ext} 162
Compound 2^{cont} 163
Compound 61 159
Compound 62 160
Compound 64 161
Procedures for acidic-basic titrations of monomer 2^{cont} 165
Procedures for polymerization of Hydrogen-bonding rotaxanes 165

Compound 65..... 151
Compound 67..... 152
Compound 68..... 153
Compound 69..... 171
Compound 70..... 147
Compound 71..... 147
Compound 72..... 172
Compound 73..... 172

Annex 1 –Superimposed ^{1}H NMR Spectra of compounds 10, 23 and 24 175

Annex 2 –^{1}H NMR Spectrum of compound 45.....176

Annex 3 – Superimposed ^{1}H NMR Spectra of compounds 64, 2^{ext}, 2^{cont} and polymers $[64 \bullet 2]^{cont}$ and $[64 \bullet 2]^{ext}$ 177

ABSTRACT

One of the targeted challenges in nanotechnologies consists in coupling together defined individual molecular motions for the production of macroscopic response. This objective requires first to control the precise motional features of discrete molecular switches or motors and second, to coordinate them in space and time in order to amplify the nanomechanical output by several orders of magnitude.

The main objective of my PhD work was to develop an acid-base-controllable supramolecular polymer based on bistable [2] rotaxane monomers which can contract and extend upon pH modulation. For that, we designed a double-threaded molecular shuttle in which two rings switch between two different recognition sites on a dumbbell component, allowing two stable states of the molecular shuttle in either contracted or expanded configurations (Figure A). The ends of each dumbbell were attached to a functional recognition unit, e.g., which can complex to metal ions , or form hydrogen-bonding recognition motifs, and these monomers were subsequently engaged in a supramolecular polymerization with the aim of collectively synchronizing and amplifying the individual monomer motions.

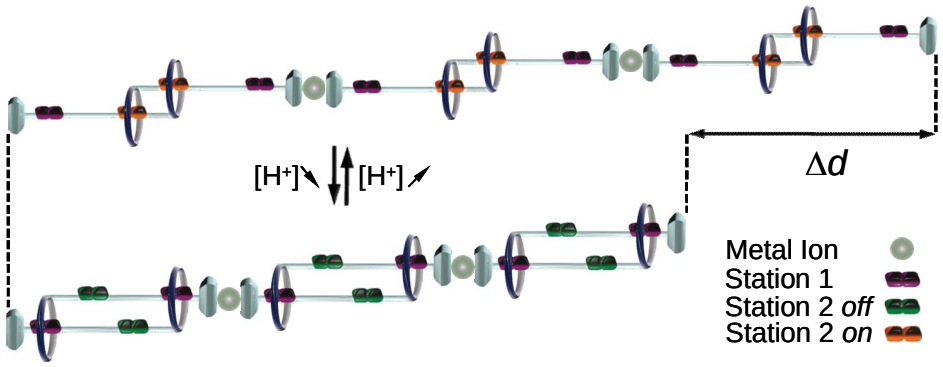

Figure A | General representation of the extension and the contraction of a telescopic supramolecular polyrotaxane upon pH modulation.

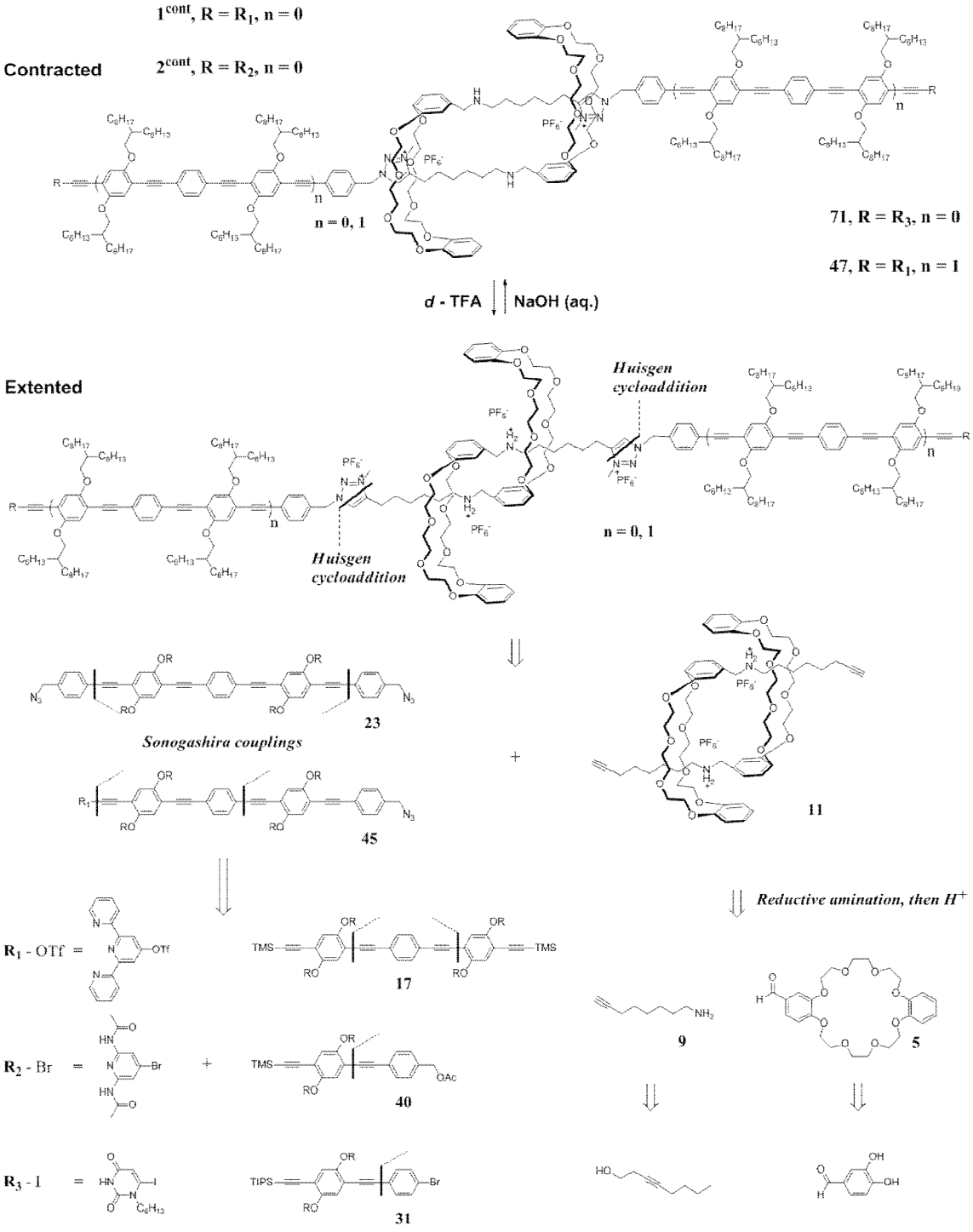

Scheme A | Target daisy chain bistable rotaxanes **1**^{cont}, **2**^{cont}, **47**, **71** and associated retrosynthetic strategy

From a molecular point of view, monomers (**1**^{cont}, **2**^{cont}, **47**, **71**) consist in two functional oligophenylacetylene dumbbells (**23**, **45**) and a bistable rotaxane (**11**, Scheme A). One of the recognition sites is a secondary dialkylammonium ($R_2NH_2^+$) center and the other site is a

triazolium unit. The macrocyclic $DB_{24}C_8$ part is known to have a better affinity for the N-benzylammonium template than for the triazolium one, and no affinity at all for the N-benzylamine moiety, thus allowing the two states of the molecular shuttle (contraction and expansion) depending on the protonation state. The syntheses of dumbbells (**23**, **45**) were envisioned through two unsymmetrical intermediates TMS-benzyl acetate **40** (8 steps) and TIPS-acetylene bromo aryl **31** (7 steps) which were obtained by iterative Sonogashira couplings and silyl groups deprotections. The hetero-coupling of **31** with **40** afforded the TIPS-benzyl acetate compound which was subsequently attached to a terpyridine unit. Finally, the terpyridine-benzyl-azide **45** was obtained with good yields. In the meantime, the symmetrical bis-benzyl-azide **23** (11 steps) was synthesized from bis-TMS protected oligophenylacetylene **17** to prepare covalent polymers obtained by click chemitry for comparison with the supramolecular ones.

Having our key building blocks in hands, we polymerized the bistable rotaxanes and analyzed their supramolecular structures by various techniques. For instance, metallosupramolecular polymers having two terpyridine ends (and with n=0) were polymerized in the presence of Zn(II) or Fe(II) ions. Characterization by a combination of static light scattering (SLS), dynamic light scattering (DLS) and small angle neutron scattering (SANS) revealed the formation of high molecular weight single chain polymers (up to 8×10^6 g.mol^{-1}) (see Fig. B).

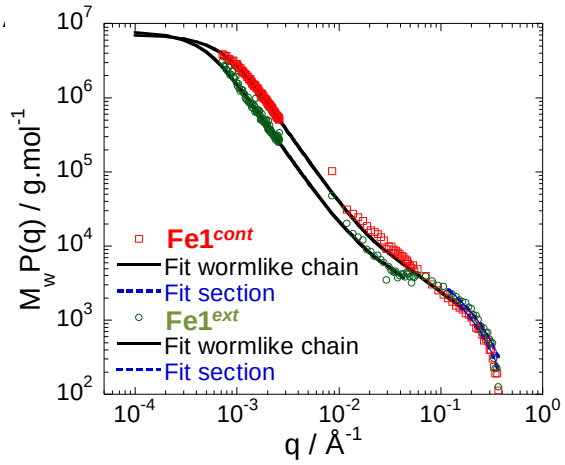

	Extended	Contracted
DP	2937	2937
L_c (Å)	**158614**	**93980**
M_L (g/mol/Å)	49.8	74.8

ΔL_P = 6.4µm ± 0.7

Figure B | SANS and SLS studies showing the micrometric contraction and extension of Fe (II) telescopic supramolecular polyrotaxanes and their characteristic values

Both samples exhibit a perfect wormlike-chain behavior, which represents a very interesting result regarding the high functionality of the polymer. In addition, the pH-triggered

contraction/extension process was clearly demonstrated by these datas as for the extended polymer sample (**1**^{ext} **Fe**) we observe *(i)* an increase of the contour length (L_c) of the whole supramolecular polymer chain by several micrometers in length, which was consistent with the theoretical calculation (the degree of polymerisation (DP) being similar to that of contracted polymer (**1**^{cont} **Fe**)), and *(ii)* a reduction of the linear mass density (M_L) upon extension which is also in agreement with the amplified motion.

In another example, consisting in a rotaxane monomer (**2**^{cont}, n=0) ended by pyridine bis-imide units which can form donor-acceptor-donor type hydrogen-bonding with an appropriate connector, we were able to combine several level of hierarchical organization (Fig. C). The acid / base titration process of the rotaxane and the corresponding polymer with the connector was studied by ^{1}H NMR and neutron scattering. TEM studies showed the formation of bundles of fibers, a promissing structuring to cross the scales up to macroscopic motions in films or gels.

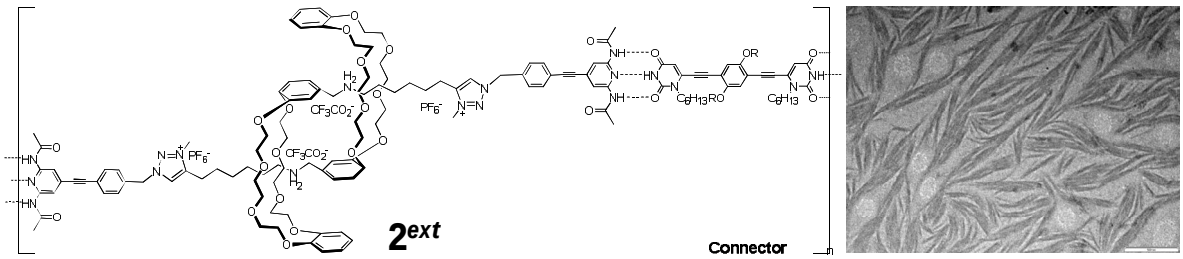

Figure C | TEM of Extended H-bonding Polyrotaxane (**2**^{ext})

In this PhD work, we have described the synthesis and characterization of a series of bistable single chain polyrotaxanes and their related higher aggregation state in fibers. Their molecular motions have been successfully translated from the nanometer to the tens of the micrometers. This represents the first example in the literature showing this synchronization of thousands of molecular machines to cross several length scales and as such, it is considered as a major step in supramolecular chemistry at its interface with nanotechnologies.

ACKNOWLEDGMENTS

First I would like to thank my PhD advisor Nicolas Giuseppone, Professor at the University of Strasbourg and director of the SAMS research group, where I was accepted to work. I have been grateful to work on the ambitious project he proposed to me and I enjoyed the time we spent working, investigating, and thinking together. I thank him for the trust he gave to me, for his patience, his knowledge, for the scientific formation and the advices I could benefit from his side, and for the multiple opportunities I was offered to improve and demonstrate my skills.

I greatly appreciated Dr. Emilie Moulin, permanent researcher of the SAMS team for her help, her advices, and the scientific and technical management she gave to me.

I want to thank Dr. Polavarapu Prasad, for his personal friendshiop, and the scientific collaboration in this project.

I appreciated the technical support of Celine Devignes and I thank her for the daily work and maintaining of the SAMS laboratories.

I thank Pr. Jean-François Legrand, Director of Institute Charles Sadron, for his trust in the project and for greeting me inside the institute where I could benefit efficient facilities for my work.

I am grateful to Oberlé Virginie, and Lea Koch for the administrative support during my PhD period in the Institute Charles Sadron.

I appreciated the collaboration of Pr. Eric Buhler and Dr. Nicolas Jouault from the university of Paris-Diderot 7 in Light and neutron scattering experiments. Their scientific contribution allowed great advancements in the project.

I thank Dr. Niess Frédéric and Schwartz Pierre-Olivier for their precious help in the part of this project.

I also thank Dr. Busseron Eric and Dr. Juan Cid-Martin for their collaboration. Their work permits us to explore new aspects of the project.

During my PhD work I was provided with various analysis equipments in ICS and I want to thank all the people in charged with these equipments: Yves Guilbert (NMR), and Dr. Fuks Gad (Microscopy).

I fully appreciated the good atmosphere in the SAMS team and thank all the people who had scientific or general discussion with me: Dr. Cormos Gabriela, Dr. Neviani Paolo, Dr. Weiss Jan, Zanirati Stefano (PhD student), Wolf Adrian (PhD student), Xiang Yunjie (PhD student), Dr. El Badri Faris.

I also want to thank all the people from ICS for the advices and scientific discussions, and good moments we spared in the Institute: Dr. Loic Jierry, Patricia Tirado, Dr. Johana Davida, Dr. Lara Tauk and other researchers and students who worked in ICS.

I would greatly thank my parents, my brother, my sister and all the people in my family who encouraged me in my will to make this PhD.

I also thank my friends (Mengchao Cui, Chencong Shi, Dr. Ting Wang, Dr. Xiaomin, Wei, Dr. Ying Zhang, Dr. Zhan Shi, Dr. Xiang Li et al.) for their help and all the good moments we spared in Strasbourg.

I want to thank the University of Strasbourg where I performed my PhD, and the China Scholarship Council (CSC) for funding my works for four years.

Finally, I thank Pr. Gwénaël Rapenne, Pr. Patrice Woisel, Pr. Valérie Heitz, and Pr. Eric Buhler for examinating my work and I am honoured by their attention.

ABBREVIATIONS AND SYMBOLS

Ac	Acetyl
Å	Angström
aq	aqueous
Bn	Benzyl
°C	Celsius Degree
DABCO	1,4-diazabicyclo[2.2.2]octane
DB24C8	Dibenzo-24-crown-8
DCM	Dichloromethane
DMF	Dimethylformamide
DMSO	Dimethylsulfoxide
DLS	Dynamic Light Scattering
EA	Elementary Analysis
eq., equiv.	Equivalent
ESI-MS	Mass Spectrometry with ElectroSpray Ionisation
EtOAc	Ethyle ccetate
h.	hour
HPLC	High Performance Liquid Chromatography
HRMS	High Resolution Mass Spectrometry
J	Coupling Constant
K	Kelvin
Kd	Dissociation Constant
L_c	Contour Length
LC/MS	Liquid Chromatography coupled to Mass Spectrometry
λ_{max}	Maximum of emission/absorption wavelength
MALDI-TOF	Matrix-assisted laser desorption/ionization –Time of Flight
MIMs	Mechanically Interlocked Molecules
µL	microliter
µm	micrometer
mL	Milliliter
M_L	Linear Mass Density
MS	Mass Spectrometry
nm	nanometer
NMR	Nuclear Magnetic Resonance
ppm	Parts per million
R_f	Retardation factor
R_g	Radius of gyration
RT	Room Temperature
SANS	Small Angle Neutron Scattering

SEM	Scanning Electron Microscopy
SLS	Static Light Scattering
T	Temperature
TEM	Transmission Electronic Microscopy
THF	Tetrahydrofuran
TLC	Thin Layer Chromatography
TMSA	Trimetylsilylacetylene
Ts	Tosyl (p-$CH_3C_6H_4SO_2$)
TfO	Triflate
UPLC	Ultra Performance Liquid Chromatography
UV	Ultra-violet
CuAAC	Copper-catalysed 1,3-dipolar azide-alkyne cycloaddition

GENERAL INTRODUCTION

Mechanically interlocked molecules (MIMs) are true molecular entities as a result of their interlocked components being intrinsically linked to one another and which prevent their dissociation unless one or more covalent bonds are cleaved. Within MIMs, the dynamic nature of mechanical bonds allows for the components to undergo relative internal movements, i.e. translation and circumrotation. Artificial molecular actuators, which can convert chemical, electrochemical, or photochemical energy into mechanical motion, have the potential for spawning nanomechanical systems. Current investigations have focused on the development of a "bottom-up" approach, which is centered on the design and manipulation of macromolecules and molecular assemblies, either biological or artificial, with the aim of transferring molecular phenomena towards motions at larger scales.

In particular, functional interlocked molecules constitute an active focus of interest in molecular electronics and nanotechnology as they can be a source of components for molecular-based devices. Although many examples of nanomachines / nanoswitches operating at the molecular level have been developed, such as catenanes and rotaxanes, the control of their collective behavior to produce macroscopic motions has not been achieved yet.

With these ideas in mind, the objective of this PhD work was to develop a new kind of responsive material which can contract upon pH modulation. We decided to investigate how well-designed rotaxane-based supramolecular polymers (Fig. 1) could lead to these structures by programmed self-assemblies and how a nanoscopic molecular motion could be translated to microscopic length scales and above.

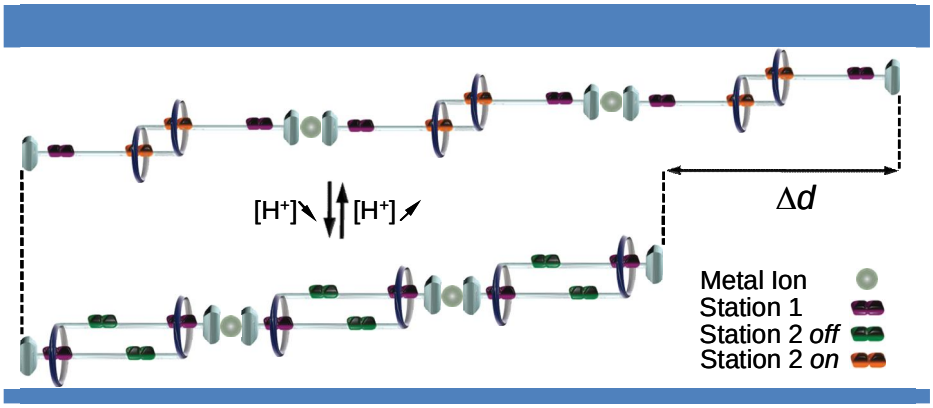

Figure 1 | General representation of the extension and contraction of a telescopic supramolecular polyrotaxane upon pH modulation.

In particular, this thesis focuses on the synthesis and characterization of a series of acid–base-controllable bistable single chain polyrotaxanes and of their related higher aggregation state in single-chain polymers bundled fibers (Fig. 1). Two examples of rotaxane monomer were envisioned, e.g., one able to complex to metal ions, or another able to form hydrogen-bonding. These monomers were expected to yield supramolecular polymerization with the hope to synchronize and amplify the monomer motions.

The rotaxane monomer was envisioned as a bistable rotaxane: one of the recognition sites (station) being a secondary dialkylammonium ($R_2NH_2^+$) center and the other site being a triazolium unit (Scheme 1). The macrocyclic DB24C8 part is known to have a better affinity for the N-benzylammonium template than for the triazolium one, and no affinity at all for the N-benzylamine moiety, thus allowing the two states of the molecular shuttle (contraction and extension) depending on the protonation. Then the monomers were expected to polymerize by metal-coordination or H-bonding interactions.

We have also decided to explore the syntheses of two functional oligophenylacetylene dumbbells to introduce them in covalent polyrotaxanes (see Scheme 1). The syntheses of dumbbells (**23, 45**) were envisioned through two unsymmetrical intermediates TMS-benzyl acetate **40** (8 steps) and TIPS-acetylene bromo aryl **31** (7 steps) which were planned by iterative Sonogashira couplings and silyl groups deprotections. The hetero-coupling of **31**with **40** should afford the TIPS-benzyl acetate compound which can be subsequently attached to a terpyridine unit. In the meantime, the symmetrical bis-benzyl-N_3 **45** was envisaged from the bis-TMS protected oligophenylacetylene **17** to prepare the covalent polymers for comparison with the supramolecular ones.

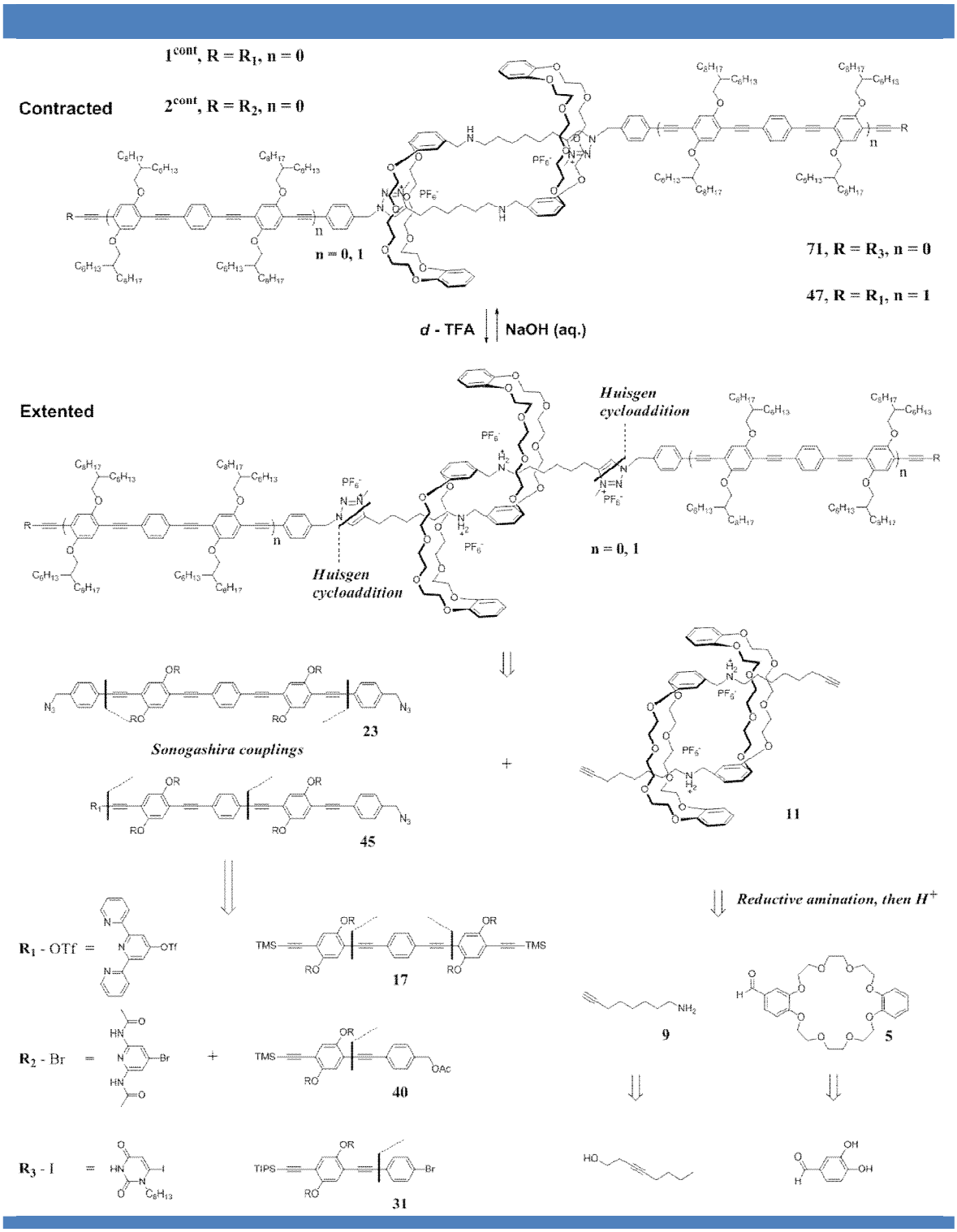

Scheme 1 | Target daisy chain bistable rotaxanes **1**^{cont}, **2**^{cont}, **47**, **71** and associated retrosynthetic strategy.

A combination of ^{1}H NMR, static light scattering, dynamic light scattering and small angle neutron scattering techniques was planned to characterize these polymers, e.g., molecular

weight, liner density, hydrodynamic radius, pH-triggered contraction/extension process. We also envisioned TEM and SEM imaging to characterize the related higher aggregation states.

My manuscript is composed of 4 chapters. The first part gives a bibliographic overview of the concepts and scientific achievements related to the project, and which are: rotaxane and mechanically interlocked molecules (MIMs), as well as supramolecular polymers.

The second chapter concerns the synthesis of the covalent polyrotaxanes, and the characterization of the molecules needed to the achievement of the project. An efficient and general scheme was developed to obtain each molecule in a large-scale synthesis.

The third chapter describes the synthesis of metallo-supramolecular polymer rotaxanes. Two metal ions were studied and perfect wormlike chain supramolecular polymers were obtained. Dynamic light scattering, static light scattering and small angle neutrons scattering techniques are discussed for the analysis of the micrometric contraction and extension of the polymers.

The fourth chapter deals with the synthesis of hydrogen-bonding polymer with appropriate connectors. The acid / base titration process of the rotaxane and of the corresponding polymer was studied by ^{1}H NMR, neutron scattering, and TEM imaging, revealing the formation of bundled fibers.

THEORETICAL PART

Chapter 1 : Bibliography

1/ Supramolecular Chemistry

Supramolecular chemistry, which has been defined as the "chemistry beyond the molecule" by Jean-Marie Lehn in 1978, is a field of research which has grown exponentially over the last few decades. [1] "Supermolecules" are composed of two or more molecules (or ions) held together and organized in space by non-covalent interactions such as hydrogen bonding, metal coordination, ion-ion, ion-dipole, dipole-dipole, van der Waals, π-π stacking interactions and hydrophobic or solvophobic effects. [2]

Supramolecular chemistry encompasses two broad categories: host-guest chemistry and self-assembly processes. For instance, crown ethers, cyclodextrins, calixarenes, cucurbiturils, and cyclophanes are typical host molecules [3] which have produced a blueprint for the subsequent growth of supramolecular chemistry.

Self-assembly is the process by which several molecules combine to produce more complex structures without guidance or management from an outside source.[4] This process is usually spontaneous and is also influenced by solvation or template effects *etc*. The understanding of these principles has led to an increasing insight into many biological processes, such as catalysis, transport, and replication. Concomitantly, chemists began to recognize and study synthetic structures based on non-covalent interactions, such as micelles and microemulsions. Variety of shapes and sizes of nanostructures were obtained using molecular self-assembly by non-covalent interactions [5] in the range of 1 to 100 nm. [6] This so-called "bottom up" approach which was inspired primarily by nature to construct

[1] (a) Lehn, J.-M. *Supramolecular Chemistry: Concepts and Perspectives* (VCH, Weinheim, 1995)； (b) Lehn, J.-M. Supramolecular Chemistry - Scope and Perspectives. Molecules, Supermolecules, and Molecular Devices (Nobel Lecture), *Angew. Chem. Int. Ed. Engl.* **27**, 89–112 (1988); (c) Desiraju, G. R. Chemistry beyond the molecule**.** *Nature* **412**, 397–400 (2001).
[2] Schneider, H.-J. Binding Mechanisms in Supramolecular Complexes. Angew. Chem. Int. Ed. 48, 3924–3977 (2009).
[3] (a) Pedersen, C. J. Cyclic polyethers and their complexes with metal salts. *J. Am. Chem. Soc.* **89**, 7017 (1967); (b) Szejtli J. *Cyclodextrin Technology*; Springer, New York, 1988; (c) David, G. C. *Calixarenes.* Cambridge: Royal Society of Chemistry, 1989; (d) Freeman, W. A.; Mock, W. L.; Shih, N. Y. Cucurbituril. *J. Am. Chem. Soc.* **103**, 7367 (1981); (e) Gabard, J.; Collet, A. Synthesis of a (D3)-bis(cyclotriveratrylenyl) macrocage by stereospecific replication of a (C3)-subunit. *Journal of the Chemical Society - Chemical Communications*, **21**, 1137–1139 (1981).
[4] Williams, D. H.; Westwell, M. S. Aspects of weak interactions. *Chem. Soc. Rev*., **27**, 57 (1998).
[5] Katsuhiko, A.; Hill, J. P; Lee, M. V.; Vinu, A.; Charvet, R.; Acharya, S. Challenges and breakthroughs in recent research on self-assembly. *Sci. Technol. Adv. Mater*. **9**, 014109 (2008).
[6] (a) Rebek, J. Jr. Molecular Recognition with Model Systems. *Angew. Chem. Int. Ed. Engl.* **29**, 245-255 (1990); (b) Vögtle, F. *Supramolecular Chemistry*; John Wiley & Sons: New York, 1991; (c) Amabilino, D. B.; Stoddart, J. F. Interlocked and Intertwined Structures and Superstructures. *Chem. Rev*. **95**, 2725-2828 (1995); (d) Fyfe, M. C. T.; Stoddart, J. F. Synthetic Supramolecular Chemistry. *Acc. Chem. Res*. **30**, 393-401 (1997); (d) Harada, A.; Li, K.; Kamachi, M. Double-stranded inclusion complexes of cyclodextrin threaded on poly(ethylene glycol). *Nature* **370**, 126-128 (1994).

nanostructures and devices has appeared advantageous over the "top down" approach because of the physical intrinsic limits below 30nm. [7]

Supramolecular chemistry has also had a huge impact on assistance to molecular synthesis, [8] also referred to as self-assembly followed by covalent modification (Figure 2). [9]

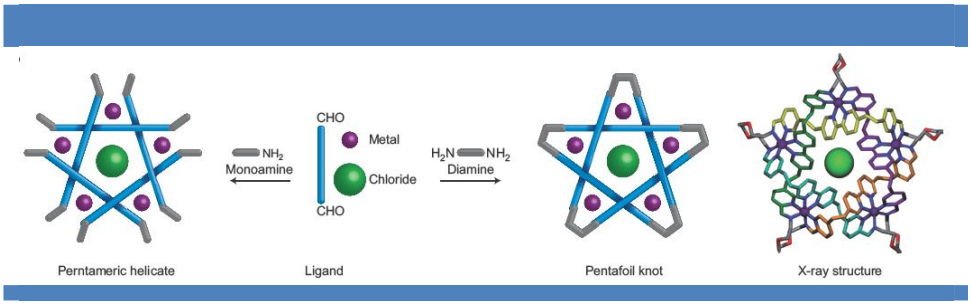

Figure 2 | One-pot synthesis of pentameric helicates (left) and a pentatoil knot (right) including X-ray crystallographic analysis that confirms the knotted topology.[9]

Supramolecular assistance to covalent synthesis has been exploited in the construction of more complex systems, such as molecular knots and interlocked molecular compounds (for example, catenanes and rotaxanes) as well as container molecules (molecular capsules). [10] Finally, if noncovalent synthesis has given access to finite supermolecules and infinite supramolecular arrays, the appealing prospect of synthesizing these types of compounds with complex molecular architectures using reversible covalent bond has also led to the development of dynamic covalent chemistry.

Overall, chemists are now able to synthetically program the formation of many supramolecular architectures, [11] and in particular with the aim of finely modulating their properties (magnetic, optoelectronic, rheological, *etc.*). [12] In the past years, chemists have developed more and more materials and devices and we will discuss further only one particular category defined as mechanically interlocked molecules.

[7] (a) Steed,J. W. ; Atwood, J. L. *Supramolecular Chemistry*, 2nd Edition. (VCH, Weinheim, 2009); (b) Kelly, M. J. Intrinsic top-down unmanufacturability. *Nanothechnology*, **22**, 245303 (2011).
[8] Anderson, S.; Anderson, H. L.; Sanders, J. K. M. Expanding roles for templates in synthesis. *Acc. Chem. Res*. **26**, 469-475 (1993).
[9] Ayme, J. F. ; Beves, J. E. ; Leigh, D. A. ; McBurney, R. T. ; Rissanen, K. ; Schultz, D. A Synthetic Molecular Pentafoil Knot. *Nature Chem*, **4**, 15-20 (2012).
[10] (a) Moulin, E.; Cormos, G.; Giuseppone, N. Dynamic combinatorial chemistry as a tool for the design of functional materials and devices. *Chem. Soc. Rev*. **41**, 1031-1049 (2012). (b) Lehn, J.-M. Dynamic combinatorial chemistry and virtual combinatorial libraries, *Chem. Eur. J*. **5**, 2455 (1999). (c) Maeda, T.; Otsuka, H.; Takahara, A. Dynamic covalent polymers: Reorganizable polymers with dynamic covalent bonds. *Progress in Polymer Science*, **34**, 581 (2009). (d) Gasparini, G.; Molin, M. D.; Lovato, A.; Prins, L. J. Gasparini, G., Dal Molin, M., Lovato, A.; Prins, L. J. Dynamic Covalent Chemistry. *Supramolecular Chemistry: From Molecules to Nanomaterials. Supramolecular Chemistry: From Molecules to Nanomaterials*, (VCH, Weinheim, 2012); (e) Rowan, S. J.; Cantrill, S. J.; Cousins, G. R. L.; Sanders, J. K. M.; Stoddart, J. F. Dynamic covalent chemistry, *Angew. Chem. Int. Ed*. **41**, 898-952 (2002).
[11] Lehn, J. M. in Supramolecular Science: *Where It Is and Where It Is Going*, Ungaro, R.; Dalcanale, E. Eds. 287-304, (Kluwer, Dordrecht, Netherlands, 1999).
[12] Lehn, J. M. Toward Self-Organization and Complex Matter. *Science* **295**, 2400-2403 (2002).

2/ Mechanically Interlocked Molecules (MIMs)

a) Definition and concept

Supramolecular complexes are mainly based on host-guest interactions with variable stabilities. In the 1990s, supramolecular chemistry became more sophisticated, with researchers such as J. P. Sauvage and J. F. Stoddart developing molecular machinery and highly complex self-assembled structures such as mechanically interlocked molecules (Figure 3). [13]

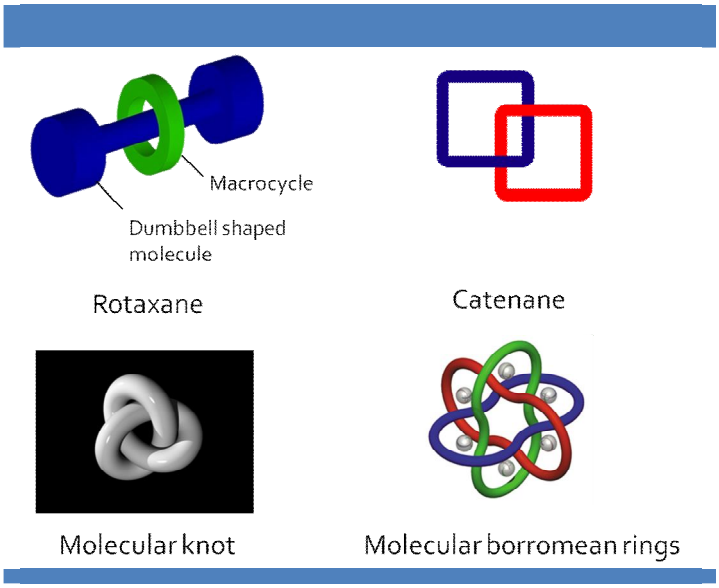

Figure 3| Examples of mechanically interlocked molecular architectures.[13]

Mechanically interlocked molecules are composed of two or more species threaded through (or around) one another thus forming a single entity. [14] Some noncovalent interactions may exist between the different interlocked components (often those that were used for the construction of the system), but covalent bonds do not.

Rotaxanes, catenanes, molecular knots, and molecular borromean rings are four typical examples of MIMs. Due to the great deal of interest in developing artificial molecular machines, [15] many efforts have been pursued by manipulating the relative position of the components, especially for the catenanes and rotaxanes.

[13] Amabilino, D. B.; Stoddart, J. F. Interlocked and Intertwined Structures and Superstructures. *Chem. Rev.* **95**, 2715-2828 (1995).
[14] Bruns, C. J., Stoddart, J. F. The Mechanical Bond: A Work of Art. *Top Curr. Chem.* **323**, 19-72 (2011).
[15] (a) Balzani, V.; Credi, A.; Raymo, F. M.; Stoddart, J . F. Artificial molecular mashines, *Angew. Chem. Int. Ed.* **39**, 3349 – 3391 (2000); (b) Kay, E. R.; Leigh, D. A. ; Zerbetto, F. Synthetic Molecular Motors and Mechanical Machines. *Angew. Chem. Int. Ed.* **46**, 72 – 191 (2007).

b) Catenanes

A catenane is a mechanically-interlocked molecular architecture consisting of two or more interlined macrocycles. The different rings cannot be separated without breaking the covalent bonds of the macrocycles. The construction of such a structure has been for a long time considered as a challenge for chemists since strategies for their synthesis relied initially on statistical approaches or on the use of covalent templates. [16] These protocols suffer from yields of less than 1%, or require many synthetic steps. Sauvage and co-workers opened up the field in 1983 when they introduced metal coordination template as an efficient route to the formation of catenanes (Figure 4). [17]

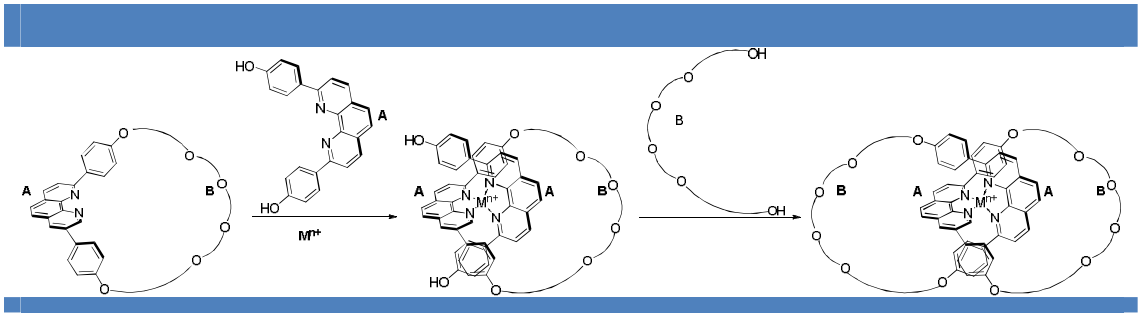

Figure 4 | Sauvage's metal templation of a catenane.[17]

This particular example involves a phenanthroline derivative A having two functional groups (for example OH) that may react with complementary functional units contained in a B unit. A and B generate the corresponding macrocycle AB. One equivalent of a macrocycle AB forms, with one equivalent of A and one equivalent of an appropriate metal ion M (like Cu(I)), the complex MA(AB). This complex further reacts with one equivalent of B to give the catenate $M(AB)_2$.

After this major breakthrough in the beginning era of MIMs, more complex systems were developed. One main achievement was reported by Leigh's group with the synthesis of a mechanically interlocked molecular rotor that presents a net unidirectional circumrotation. [18]

[16] Schill, G. *Catenanes, Rotaxanes and Knots*, Academic Press, New York, 1971.
[17] Dietrich-Buchecker C. O.; Sauvage, J. P. Une nouvelle famille de molecules : les metallo-catenanes. *Tet. Lett.* **24,** 5095-5098 (1983).

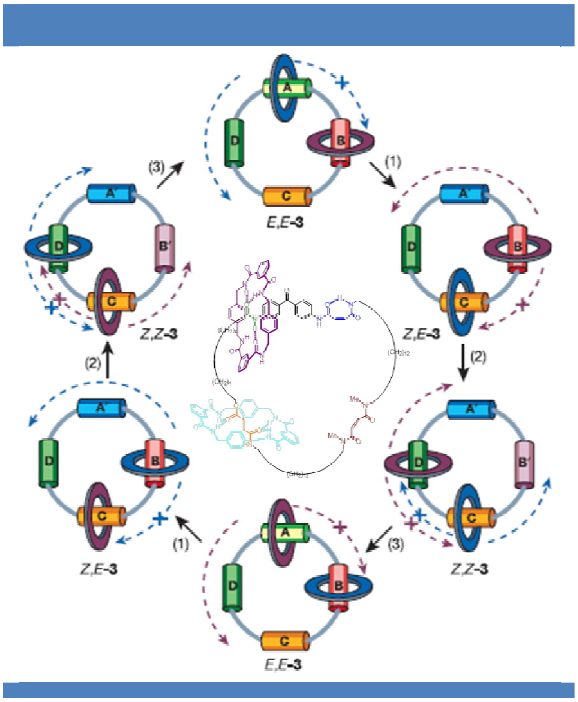

Figure 5 | Stimuli-induced net unidirectional circumrotation in a four-station [3]catenane.[18]

The [3]catenane system (Figure 5) consists of a larger macrocycle which contains four stations with different binding affinities for the macrocycle. Initially the blue and purple small rings are bound to stations A and B, respectively. With long wavelength UV light irradiation (process 1) A is converted into A' with lower binding affinity for the small blue ring, which becomes free to move. The purple ring stays at the B station blocking any clockwise movement of the blue ring, which has to move counterclockwise to arrive at station C, which now has the highest binding affinity. Irradiation with short wavelength UV light (process 2) transforms B into B' breaking the hydrogen bonds that hold the purple ring. The purple ring moves counterclockwise to station D, where it is bound again. The clockwise direction is blocked by the blue ring. White light irradiation (process 3) then resets the system by switching A' back to A and B' back to B, which makes the blue ring moving to B and the purple ring moving to A in a unidirectional manner. The blue and the purple ring have exchanged places by following each halfway around the large macrocycle. To complete a full rotation steps 1 to 3 have to be repeated. Each ring has then performed one clockwise and three counterclockwise movements, which amounts to a net relative unidirectional motion.

[18] Leigh, D. A.; Wong, J. K. Y.; Dehez, F.; Zerbetto, F. Unidirectional Rotation in a Mechanically Interlocked Molecular Rotor. *Nature*, **424**, 174 – 179 (2004).

c) Rotaxanes

Rotaxanes consist of macrocyclic rings trapped onto a linear dumbbell unit (the 'thread') by two bulky substituents (the 'stoppers'). The two components are kinetically trapped since the 'stoppers' can prevent the dissociation of the macrocycle sliding off the dumbbell without cleavage of one or more covalent bonds (Figure 6). [19]

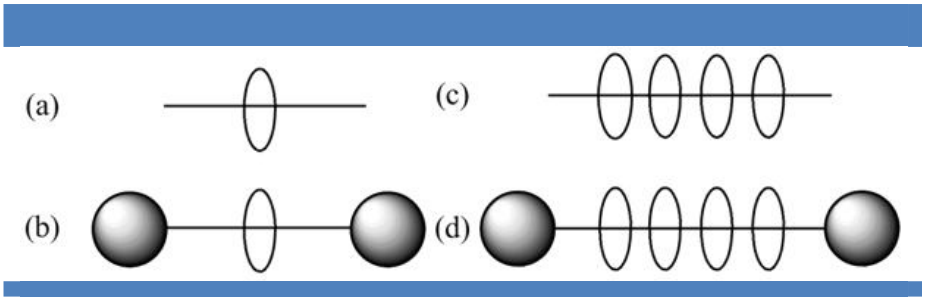

Figure 6 | A schematic representation of (a) a pseudorotaxane, (b) a [2] rotaxane, (c) a pseudopolyrotaxane, (d) a polyrotaxane.[19]

Without the locking end groups, the supramolecule can be called pseudorotaxane (a). When multiple ring-like molecules are threaded on one linear molecule, the prefix "poly" is added to the terms above (c, d).

d) Synthetic routes to rotaxanes

Since the earliest rotaxane had been reported in 1967, [20] much of the research concerning rotaxanes and other mechanically-interlocked molecular architectures has been focused on their efficient synthesis. Thus, the synthesis of rotaxanes has advanced significantly and efficient yields can be obtained by preorganizing the components utilizing hydrogen bonding, metal coordination, hydrophobic forces, covalent bonds, or coulombic interactions. [21] Supramolecular chemistry and template-directed synthesis in particular, are keys for the efficient access to these particular compounds. In general, the three main methods for preparing rotaxanes are the so-called 'capping', 'clipping', and 'slipping' procedures (Figure 7). [22]

[19] Collin, J. P.; Durot, S.; Sauvage, J. P.; Trolez, Y. Synthesis of [2]-, [3]-, and [4]rotaxanes whose axis contains two bidentate and two tridentate chelates. *New J. Chem.*, **35**, 2009-2012 (2011).
[20] Harrison, I. T.; Harrison, S. Synthesis of a stable complex of a macrocycle and a threaded chain. *J. Am. Chem. Soc.* **89**. 5723–5724 (1967).
[21] (a) Bravo, J. A.; Raymo, F. M.; Stoddart, J. F.; White, A. J. P.; Williams, D. J. High Yielding Template-Directed Syntheses of [2]Rotaxanes. *Eur. J. Org. Chem.* **11**, 2565–2571 (1998); (b) Gatti, F. G.; León, S.; Wong, J. K. Y.; Bottari, G.; Altieri, A.; Morales, A. M. F.; Teat, S. J.; Frochot, C.; Leigh, D. A.; Brouwer, A. M.; Zerbetto, F. Photoisomerization of a Rotaxane Hydrogen Bonding Template: Light-induced Acceleration of a Large Amplitude Rotational Motion, *Proc. Natl. Acad. Sci. USA*, **100**, 10-14 (2003).

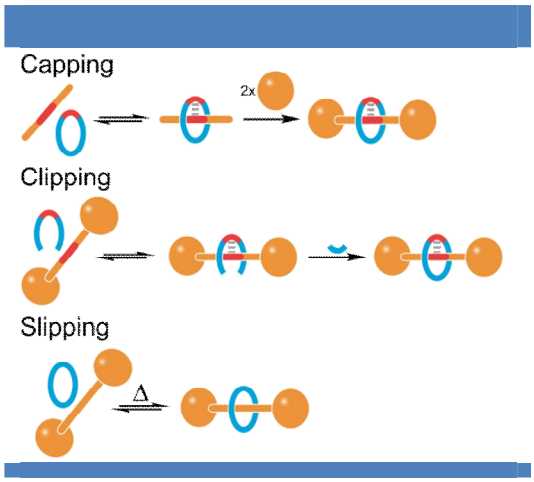

Figure 7 | Types of rotaxane syntheses by template mechanisms.[22]

The ‘capping’ method relies strongly upon a thermodynamically driven template effect. The ‘thread’ is held within the "macrocycle" by non-covalent interactions. This dynamic complex (or ‘pseudorotaxane’) is then converted to the rotaxane by reacting the ends of the threaded guest with large groups (‘stoppers’), preventing dissociation. The ‘clipping’ method is similar to the capping reaction except that in this case the dumbbell shaped molecule is complete and is bound to a partial macrocyle. The partial macrocycle then undergoes a ring closing reaction around the dumbbell-shaped molecule, forming the rotaxane. In the ‘slipping’ method, the preformed ring is forced over one of the blocking groups and onto a thermodynamically stable area on the axle.

One particular strategy, so called active template synthesis, was developed by D. A. Leigh to overcome the limitations associated with passive metal template routes. [23] The catalytic properties of metal ions are used to enhance covalent bond formation, as well as their ability to direct the bond formation; in this way, the metal ion is active as it plays a dual functionality. This synthesis relies on a macrocycle that is able to bind a metal ion in its cavity, promoting the formation of a covalent bond between two half-threaded units to form a rotaxane. As the metal ion is locked into position, the mechanical bond is selectively formed through the macrocycle (Figure 8).

[22] Aricó, F.; Badjic, J. D.; Cantrill, S. J.; Flood, A. H.; Leung, K. C.-F.; Liu, Y.; Stoddart, J. F. Templated Synthesis of Interlocked Molecules. *Top Curr. Chem.* **249**, 203–259 (2005).
[23] (a)Aucagne, V.; Berná, J.; Crowley, J. D.; Goldup, S. M., Hänni, K. D.; Leigh, D. A.; Lusby, P. J.; Ronaldson, V. E.; Slawin, A. M. Z.; Viterisi, A.; Walker, D. B. Catalytic “Active-Metal” Template Synthesis of [2]Rotaxanes, [3]Rotaxanes, and Molecular Shuttles, and Some Observations on the Mechanism of the Cu(I)-Catalyzed Azide−Alkyne 1,3-Cycloaddition *J. Am. Chem. Soc.* **129**, 11950 (2007). (b) Crowley, J. D.; Goldup, S. M.; Lee, A. L.; Leigh, D. A.; McBurney, R. T. Active metal template synthesis of rotaxanes, catenanes and molecular shuttles. *Chem. Soc. Rev.*, **38**, 1530–1541 (2009).

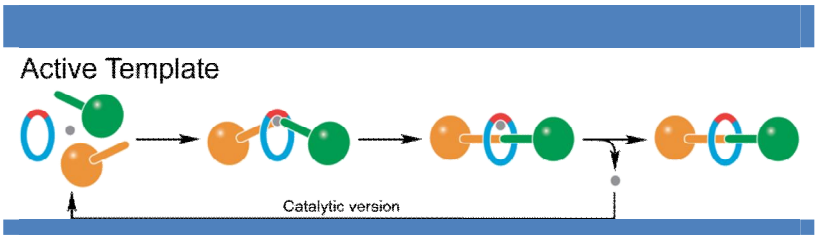

Figure 8 | Catalytic active metal template synthesis of a rotaxane.[23]

e) Polyrotaxanes

The chemistry of rotaxanes has well progressed in accordance with the interest in their unique structures and the expectation to develop molecular machines or molecular devices. In particular, polymers comprising several of these structures as key repeating units, i.e. interlocked polymers or polyrotaxanes, have been developped to combine individual units. [24]

The first polyrotaxane was synthesized by Harada *et al* in 1992, [25] and consists of α-cyclodextrins (α-CD) and polyethylene glycol chains (PEG). It represents a typical example of topological supramolecular architecture, which consists of multiple cyclic molecules threaded onto a linear polymer chain capped with bulky end-groups. By capping the polymer ends, dethreading of cyclic molecules is effectively prevented. The most distinctive property of polyrotaxane is that cyclic molecules can slide along and rotate around the main chain retaining the spatial constraints on a polymer backbone.

To date, various polyrotaxanes have been investigated as new building blocks to construct nanostructures as well as to achieve novel functions (Figure 9).[26] They can be mainly categorized into two types: main chain polyrotaxanes and side chain polyrotaxanes, but other interesting topologies have been produced. Especially, the linear daisy-chain polyrotaxane will be discussed in the following chapter.

[24] Harada, A. ; Hashidzume, A.; Yamaguchi, H.; Takashima, Y. Polymeric Rotaxanes. *Chem. Rev.* **109**, 5974–6023 (2009).
[25] Harada, A. ; Li, J.; Kamachi M. The molecular necklace-a rotaxane containing many threaded α-cyclodextrins. *Nature*, **356**, 325–327 (1992).

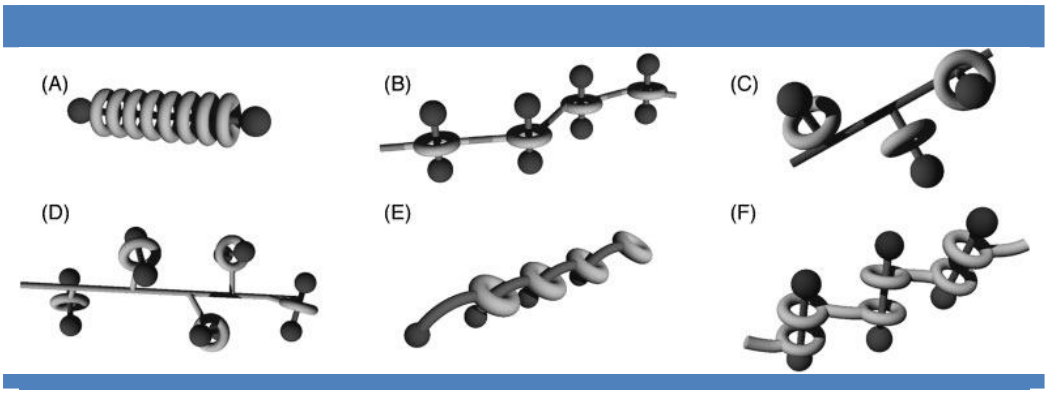

Figure 9| Typical structures of polyrotaxanes.(A), (B) main chain-types, (C), (D) side chain-types, (E) daisy-chain type, and (F) poly[3]rotaxane.[26]

The main difference between polyrotaxanes compared to classical polymers should reside in their physical or mechanical properties. Such characteristics enable for instance the application of polyrotaxane to stimuli-responsive smart materials and to various nanoscale molecular devices such as molecular tubes, insulated molecular wires, molecular shuttles, drug delivery systems, and multivalent ligand systems. [27] Especially, main-chain polyrotaxanes (Figure **9A**) are one of the most extensively studied categories of mechanically bonded macromolecules and have been well investigated as insulated molecular wires. [28] Many examples of main-chain oligo- and polyrotaxanes, relying on the threading of cyclodextrins, [29] macrocyclic oligoethers, [30] and cucurbiturils, [31] have also been reported in the literature.

In recent years, a new series of main-chain [*n*]polyrotaxanes have been developed by the ‘‘clipping’’ approach, using π-donor–acceptor rotaxanes (Figure 10). [32] Such [*n*]rotaxanes are composed of a linear polymeric dumbbell-shaped component, containing 2*n* dioxynaphthalene (DNP) units as the π-electron donors, and *n* cyclobisparaquat(*p*-phenylene) ($CBPQT^{4+}$) cyclophanes as the π-electron acceptors.

[26] (a) Kohsaka, Y.; Konishi, G.; Takata, T. Synthesis of A Main Chain-Type Polyrotaxane Consisting of Poly(crown ether) and *sec*-Ammonium Salt Axle and Its Application to Polyrotaxane Network. *Polymer Journal*, **39**, 861–873 (2007). (b) Fang, L.; Olson, M. A.; Beni´tez, D.; Tkatchouk, E.; Goddard, W. A.; Stoddart, J. F. Mechanically bonded macromolecules. *Chem. Soc. Rev.*, **39**, 17–29 (2010).
[27] (a) Ichi, T.; Watanabe, J.; Ooya, T.; Yui, N. Controllable Erosion Time and Profile in Poly(ethylene glycol) Hydrogels by Supramolecular Structure of Hydrolyzable Polyrotaxane. *Biomacromolecules*, **2**, 204-210 (2001); (b) Fujimoto, M.; Isobe, M.; Yamaguchi, S.; Amagasa, T.; Watanabe, A.; Ooya, T.; Yui, N. Poly(ethylene glycol) hydrogels cross-linked by hydrolyzable polyrotaxane containing hydroxyapatite particles as scaffolds for bone regeneration. *J Biomat Sci - Polym E*, **16**, 1611-1621 (2005).
[28] Frampton , M. J.; Anderson, H. L.; Insulated Molecular Wires. *Angew. Chem., Int. Ed.*, **46**, 1028–1064 (2007).
[29] (a) Harada, A.; Li, J.; Nakamitsu, T.; Kamachi, M. Preparation and Characterization of Polyrotaxanes Containing Many Threaded α-Cyclodextrins. *J. Org. Chem.*, **58**, 7524-7528 (1993). (b) Cacialli, F.; Wilson, J. S.; Michels, J. J.; Daniel, C.; Silva, C.; Friend, R. H.; Severin, N.; Samori, P.; Rabe, J. P.; O’Connell, M. J.; Taylor, P. N.; Anderson, H. L. Cyclodextrin-threaded conjugated polyrotaxanes as insulated molecular wires with reduced interstrand interactions. *Nat. Mater.*, **1**, 160–164 (2002).
[30] Gong, C. G.; Gibson, H. W.; Synthesis and Characterization of a Polyester/Crown Ether Rotaxane Derived from a Difunctional Blocking Group. *Macromolecules*, **29**,7029–7033 (1996).
[31] Whang, D.; Jeon, Y. M.; Heo, J.; Kim, K.; Self-Assembly of a Polyrotaxane Containing a Cyclic “Bead” in Every Structural Unit in the Solid State: Cucurbituril Molecules Threaded on a One-Dimensional Coordination Polymer. *J. Am. Chem. Soc.*, 1996, **118**, 11333–11334.

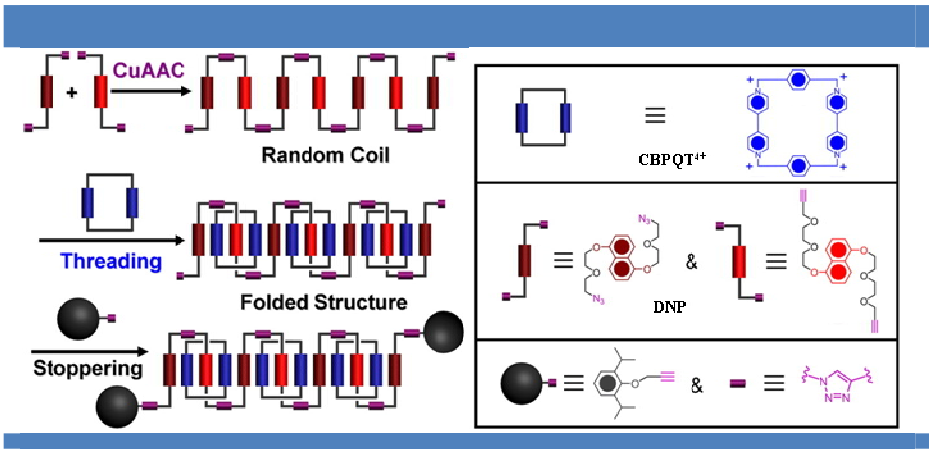

Figure 10| Schematic representation of the formation of polymer thread and corresponding polyrotaxane from two DNP-containing monomers by the ‘‘threading-followed-by-stoppering’’ approach.[32]

The prediction of the secondary structure of higher order donor–acceptor [*n*]rotaxanes (n > 10) was also explored by ^{1}H NMR spectroscopy, quantum mechanical calculations, molecular dynamics, molecular mechanics minimisations, X-ray structure diffractions. This analogue was predicted to adopt a random coil conformation, indicating that the instalment of the polyether macrocycles on the dumbbell molecules exerts significant effect on the secondary structure in such [π…π] stacking-based systems, compared to the hydrogen-bond based structure.

3/ Molecular Machines and Shuttles (or Switches)

a) Definitions and concepts

The term "molecular machine" first entered the vocabulary of science in the late 1980's. [33] According to the definition, a molecular machine is: "A mechanical device that performs a useful function using components of nanometer scale and defined structure, includes both artificial nanomachines and naturally occurring devices found in biological systems, which leaves open the possibility that man-made machines could function in the same way". [34]

A wide variety of rather simple molecular machines have been synthesized by chemists.

[32] (a) Wu, J.; Leung, K. C.-F.; Stoddart, J. F.; Efficient production of [*n*]rotaxanes using template-directed clipping reactions. *Proc. Natl. Acad. Sci. USA*, **104**, 17266-17271 (2007). (b) Zhang, W.; Dichtel, W. R.; Steig, A. Z.; Benitez, D.; Gimzewski, J. K.; Heath, J. R.; Stoddart, J. F. Proc. Folding of a donor-acceptor polyrotaxane using secondary noncovalent bonding interactions, *Natl. Acad. Sci. USA*, **105**, 6514-6519 (2008).
[33] (a) Alberts, B. M. The DNA enzymology of protein machines. *Cold Spring Harb. Symp. Quant. Biol.* **XLIV**, 1-12 (1984). (b) Schneider, T. D. Theory of molecular machines. I. Channel capacity of molecular machines. *J. Theor. Biol.* **148**, 83-123 (1991).
[34] Ballardini, R.; Balzani, V.; Credi, A.; Gandolfi, M. T.; Venturi, M. Artificial Molecular-Level Machines: Which Energy To Make Them Work? *Acc. Chem. Res.*, **34**, 445–455 (2001).

From a synthetic perspective, there are two important types of molecular machines: molecular shuttles (or switches) and molecular motors. They can consist of a single molecule; however, they are often constructed from mechanically-interlocked molecular architectures, such as rotaxanes and catenanes. [35]

b) Rotaxanes as molecular shuttles

It is known that there are naturally occurring rotaxanes that act as processive catalysts, promoting chemical changes while moving along a linear species. [36] Rotaxane threads can be designed in such a manner that they contain two different binding sites for the macrocycle. The preference for the macrocycle to bind to one site or the other can then be influenced by external factors, either chemically, electrochemically or photochemically. [37] The ring can therefore be moved back-and-forth along the axle and such functional assemblies are known as molecular shuttles (Figure 11).

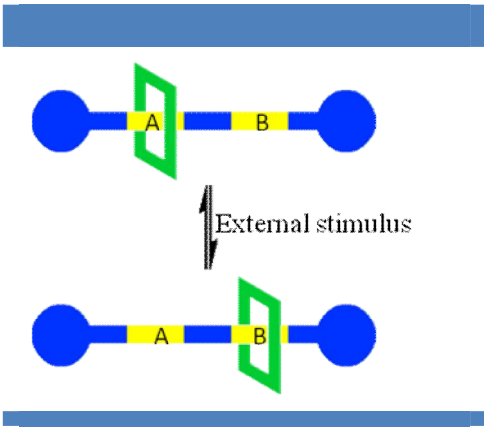

Figure 11│ A molecular shuttle, based on a rotaxane with two potential binding sites (A) and (B). A change in affinities by an external stimulus leads the macrocycle to be shifted to the alternate site.[37]

The first rotaxane-based molecular shuttle was reported by J. F. Stoddart [38] on which a molecular bead (tetracationic cyclophane based on two bipyridine groups and two *para*-phenylene groups) was able to shuttle between two docking stations (two arene groups) localed on a molecular thread (ethyleneglycol chain). The stoppers (bulky triisopropylsilyl groups) prevent the bead from slipping from the thread. (Figure 12). [39]

[35] Amabilino, D. B.; Perez-Garcıa, L. Topology in molecules inspired, seen and represented. *Chem. Soc. Rev.*, **38**, 1562–1571 (2009).
[36] Kinbara, K.; Aida, T. Toward Intelligent Molecular Machines: Directed Motions of Biological and Artificial Molecules and Assemblies. *Chem. Rev.*, **105**, 1377-1400 (2005).
[37] Credi, A.; Venturi, M. Molecular machines operated by light. *Cent. Eur. J. Chem.* **6**, 325–339 (2008).
[38] Anelli, P. L.; Spencer, N.; Stoddart, J. F. A molecular shuttle. *J. Am. Chem. Soc.*, **113**, 5131-5133 (1991).

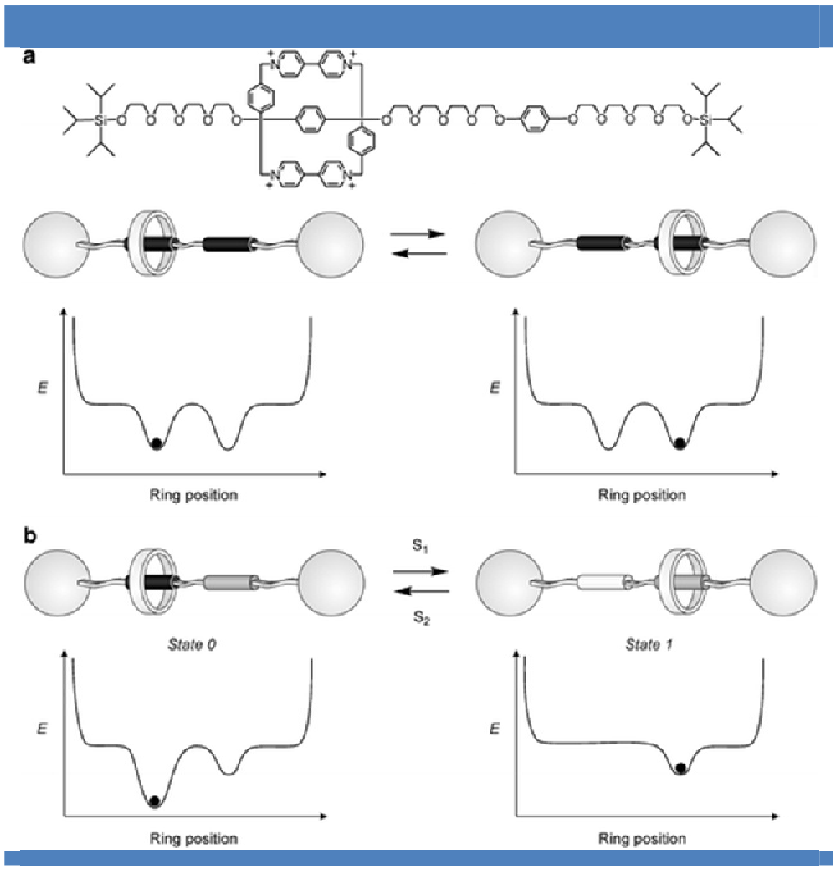

Figure 12 | (**a**) Structure of the first rotaxane-based molecular shuttle. (**b**) The two co-conformation associated with [2] rotaxane incoporationg two different recognition sites with dumbbell-shaped component can be interchanged by external stimuli S_1 and S_2.[39]

The bead is locked on one of the stations by π-π interactions but since the activation energy for migrating from one station to the other is only 13 kcal/mol (54 kJ/mol) the bead shuttles between them. Several structural, kinetic, and theoretical studies have been devoted to understand the deslipping process. [40] When the recognition sites (stations) of the dumbbell are chemically different, a rotaxane can exist as two different equilibrating conformations (Figure **12b**). The populations of each one reflect their relative free energies as determined primarily by the strengths of the two different sets of noncovalent bonding interactions. In the schematic representation shown in Figure **12b**, it has been assumed that the molecular shuttle resides preferentially in 'State 0' until a stimulus is applied that switches off the stronger of the two recognition sites, thus inducing the macrocycle to move to the second weaker

[39] (a) Balzani, V.; Credi, A.; Venturi, M.; *Molecular Devices and Machines—Concepts and Perspectives for the Nanoworld*. Weinheim, Germany: Wiley-VCH, 2008. (b) Stoddart, J. F.; Colquhoun, H. M.; Big and little Meccano. *Tetrahedron*. **64**, 8231-8263 (2008).

[40] (a) Affeld, A.; Hübner, G. M.; Seel, C.; Schalley, C. A. Rotaxane or pseudorotaxane? Effects of small structural variations on the deslipping kinetics of rotaxanes with stopper groups of intermediate size. *Eur. J. Org. Chem.***15**, 2877–2890 (2001). (b) Hübner, G. M.; Natchsheim, G.; Qian, Y. L.; Seel, C.; Vögtle, F. The spatial demand of dendrimers: deslipping of rotaxanes. *Angew. Chem. Int. Ed.* **39**, 1269–1272 (2000). (c) Leigh, D. A.; Troisi, A.; Zerbetto, F. Reducing molecular shuttling to a single dimension. *Angew. Chem. Int. Ed.* **39**, 350–353, (2000). (d) Schalley, C. A.; Beizai, K.; Vögtle, F. On the way to rotaxane-based molecular motors: studies in molecular mobility and topological chirality. *Acc. Chem. Res.* **34**, 465–476 (2001).

recognition site, 'State 1'. In appropriately designed rotaxanes, this nondegenerated process can be controlled reversibly by using chemical, electrochemical, or photochemical stimuli.

In the following discussion, we will illustrate some selected examples of rotaxanes in which the ring shuttling is induced by protonation–deprotonation, light-driven isomerisation, and other reversible processes which can be exploited to alter reversibly the stereo-electronic properties of one of the two recognition sites, thus affecting their relative capacities to sustain noncovalent bonds.

i. pH-controlled Shuttles

Many exanples of pH-controlled molecular shuttles have been reported by Stoddart, Leigh and others. [41] In an example from the group of Stoddart, the oxidation or protonation of the benzidine unit results in a loss of its affinity towards the $CBPQT^{4+}$ ring due to coulombic repulsion, and so the ring component migrates onto the biphenol station (Figure 13). [42]

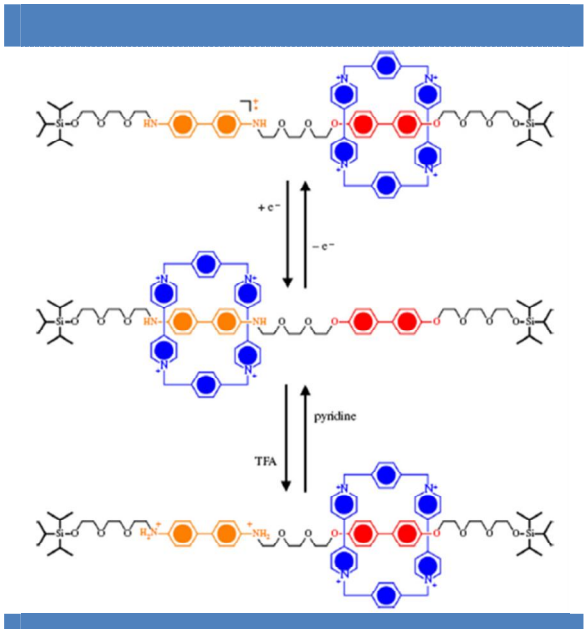

Figure 13 | A switchable donor–acceptor molecular shuttle. The $CBPQT^{4+}$ ring prefers to be located on the benzidine (orange) station until its oxidation or protonation moves the ring to the biphenol (red) station. Deprotonation or reduction results in the return of the ring to the benzidine station. [42]

[41] (a) Sindelar, V.; Silvi, S.; Kaifer, A. E. Switching a molecular shuttle on and off: simple, pH-controlled pseudorotaxanes based on cucurbit[7]uril. *Chem. Commun.*, 2185-2187 (2006) ; (b) Jiang, Q.; Zhang, H.; Han, M.; Ding, Z.; Liu, Y. pH-Controlled Intramolecular Charge-Transfer Behavior in Bistable [3]Rotaxane. *Org. Lett.*, **12**, 1728-1731 (2010); (c) Blanco, V.; Carlone, A.; Hänni, K. D.; Leigh, D. A.; Lewandowski, B. A Rotaxane-Based Switchable Organocatalyst, *Angew. Chem. Int. Ed.*, **51**, 5166-5169 (2012).

[42] Bissell, R. A.; Córdova, E.; Kaifer, A. E.; Stoddart, J. F. A chemically and electrochemically switchable molecular shuttle. *Nature* **369**, 133–137 (1994).

The process can be reversed upon reduction or deprotonation, resulting in the recovery of the initial state.

Another example of a pH-controllable rotaxane is built on a crown ether containing two electron-donor 1,2-dioxybenzene (DOB) moieties and a dumbbell-shaped component that comprises in its rod section a secondary ammonium ion and the already seen electron-acceptor bipyridinium unit (Figure 14). The crown ether macrocycle can establish hydrogen bonding interactions with the ammonium ion and charge transfer (CT) interactions with the bipyridinium unit. For the employed macrocycle, the hydrogen bonding interactions are much stronger than the CT ones, and therefore the stable structure of the rotaxane is the one in which the macrocycle surrounds the ammonium station. Such a structure can be, however, destabilized upon addition of a suitable base that, by deprotonating the ammonium ion, causes the complete displacement of the ring to the bipyridinium station. [43]

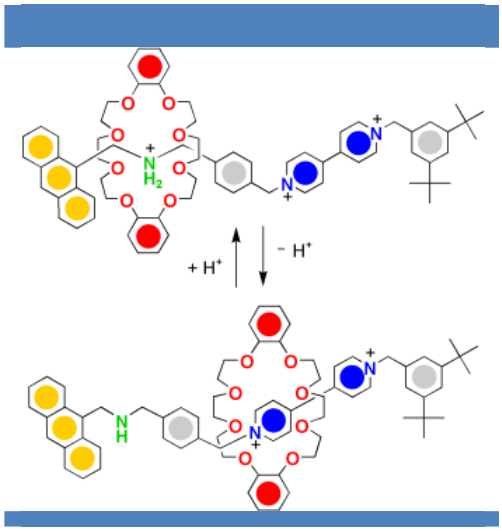

Figure 14 | Structure of the pH-controllable molecular shuttle.[43]

The first pH-switchable shuttle to exploit hydrogen bonding interactions with anions was reported by Leigh. [44] A succinamide station serves as the non-reactive station; as a second station, the thread includes a cinnamate derivative. In the neutral form, the phenolic cinnamate is a relatively poor hydrogen-bond acceptor, so the macrocycle resides on the succinamide station more than 95 % of the time (as evidenced by ^{1}H NMR), as it can form four strong hydrogen bonds with the amide carbonyls. Upon deprotonation of the phenol with

[43] (a) Ashton, P.R.; Ballardini, R.; Balzani, V.; Baxter, I.; Credi, A.; Fyfe, M. C.T.; Gandolfi, M. T.; Gómez-López, M.; Martínez-Díaz, M. V.; Piersanti, A.; Spencer, N.; Stoddart, J. F.; Venturi, M.; White, A. J. P.; Williams, D. J. Acid-base controllable molecular shuttles. *J. Am. Chem. Soc.* **120**, 11932–11942 (1998). (b) Garaudée, S.; Silvi, S.; Venturi, M.; Credi, A.; Flood, A. H.; Stoddart, J. F. Shuttling dynamics in an acid-base-switchable [2]rotaxane. *Chem. Phys. Chem.* **6**, 2145–2152 (2005).
[44] Keaveney, C. M.; Leigh, D. A. Shuttling through Anion Recognition. *Angew. Chem. Int. Ed.*, **43**, 1222-1224 (2004).

various bases (LiOH, NaOH, KOH, CsOH, Bu_4NOH, t-BuOK, DBU, and Schwesinger's phosphazine P_1 base), the macrocycle prefers binding the phenolate anion over the succinamide station in d_7-DMF. However, the shuttling was found to be extremely solvent-dependent (Figure 15).

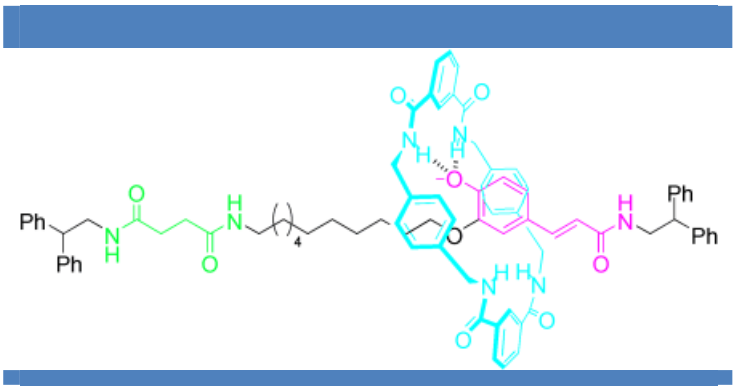

Figure 15 | Shuttling through anion recognition in a hydrogen-bonded bistable rotaxane.[44]

The construction and switching properties of a novel class of molecular shuttles based on imine-bonding stations were first reported by Kawai, H. (Figure 16). [45]

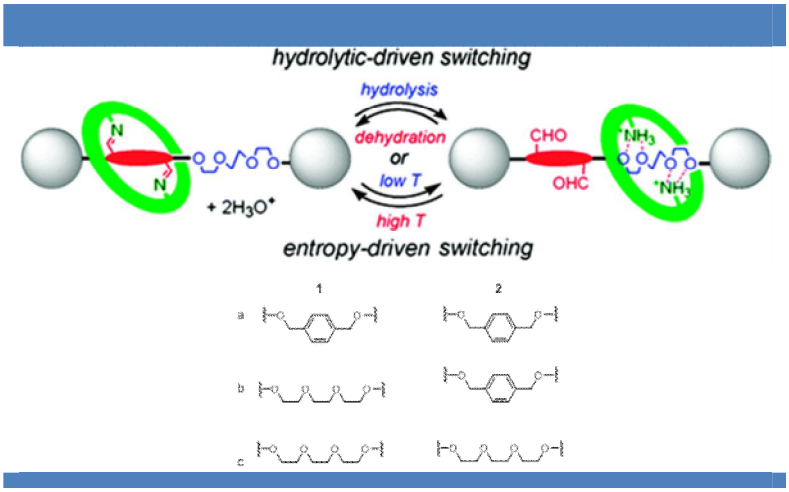

Figure 16| Hydrolytic control of positional switching of macrocycle in rotaxane-based molecular shuttles with/without hydrogen-bonding stations.[45]

Studies on dithioacetalized [2]rotaxane with two hydrogen-bonding stations and a masked imine-bonding station showed that protonation of a macrocycle increases the shuttling barrier due to hydrogen-bond formation between NH_3^+ groups and TEG (triethylene glycol)-stations. Hydrolysis of the imine bonds on the imine-bridged molecular shuttles **1**b,c with TEG-

[45] Umehara, T. ; Kawai, H. ; Fujiwara, K. ; Suzuki, T. Entropy- and Hydrolytic-Driven Positional Switching of Macrocycle between Imine- and Hydrogen-Bonding Stations in Rotaxane-Based Molecular Shuttles. *J. Am. Chem. Soc.* **130**, 13981–13988 (2008).

stations could exclusively give the [2]rotaxane **2**b,c $\cdot 2H^{2+}$, with the macrocycle hydrogen-bonded to the TEG-station. In contrast, **1**a, which does not contain TEG-stations, gave an equilibrated mixture of **1**a, monoimine, and **2**a $\cdot 2H^{2+}$ under similar acidic hydrolytic conditions. The equilibrium between **1**b,c and **2**b,c$\cdot 2H^{2+}$ to control the position of the macrocycle could be successfully switched to either side by applying acidic hydrolytic or dehydrating conditions. Furthermore, the equilibrium was largely biased to [2]rotaxane **2**b,c $\cdot 2H^{2+}$ under acidic hydrolytic conditions and could be reversed in favor of bis-imine **1**b,c just by heating. This is a successful example of a molecular shuttle exhibiting entropy-driven translational isomerism with remarkable positional discrimination. Examination of the thermodynamic parameters showed that imine-bond hydrolyses and hydrogen-bonds formation between the macrocycle and the station are thermodynamically matched processes, because both processes are enthalpically favored and accompanied by a loss of entropy. The combination of imine-bonding and hydrogen-bonding station in a rotaxane system seems to be the key for achieving a clear entropy-driven positional switching of the macrocycle.

This interplay could provide an important role in the design of entropy-driven molecular machines that exhibits a sharp transition in response to small temperature changes.

ii. Light-driven isomerisation shuttles

Although many examples of molecular switches based on MIMs have been reported, [46] constructing molecular devices from these switches has not been an easy task. Extracting useful work or energy from molecular switches has not yet truly been achieved either on the nano- or macroscale, although there are few examples in which the outcome of switching a MIM results in measurable work. Leigh demonstrated that the millimeter-scale directional transport of a liquid droplet can be achieved by using the biased Brownian motion of a molecular shuttle which results in a change of surface tension (Figure 17). [47]

[46] (a) Balzani, V.; Credi, A.; Venturi, M. *Molecular devices and machines*. Weinheim, Germany:Wiley VCH. 2008. (b) Avellini, T.; Li, H.; Coskun, A.; Barin, G.; Trabolsi, A.; Basuray, A. N.; Dey, S. K.; Credi, A.; Silvi, S.; Stoddart, J. F.; Venturi, M. Photoinduced Memory Effect in a Redox Controllable Bistable Mechanical Molecular Switch. *Angew. Chem. Int. Ed.* **51**, 1611-1615 (2012).

[47] Berná, J.; Leigh, D. A.; Lubomska, M.; Mendoza, S. M.; Perez, E. M.; Rudolf, P.; Teobaldi, G.; Zerbetto, F. Macroscopic transport by synthetic molecular machines. *Nat. Mater.* **4**, 704–710 (2005).

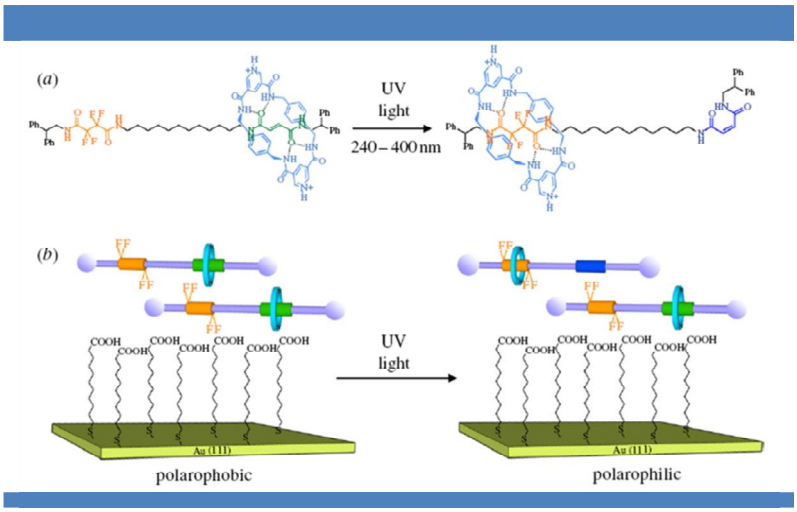

Figure 17 | A photoswitchable [2] rotaxane that changes its physical properties upon swithching from fluorophilic to polarophilic.[47]

The ring component resides initially on the fumaramide (green) station in the bistable [2]rotaxane. (*E*) - (*Z*) photoisomerization of the fumaramide to the maleimide (blue) results in the disruption of hydrogen-bonding interactions and the ring component shuttles onto the tetrafluorosuccinamide (orange) station. The concealment of the short fluoroalkane segment by the ring changes the surface properties such that it becomes polarophilic. This fact results in the directional transport of a diiodomethane droplet upon illumination which UV light focused on one side of the droplet. Photoisomerization-induced shuttling motion of the [2]rotaxane molecule can even move the droplet several millimetres up a 12° incline successfully.

iii. Electrochemically-driven shuttles

Sauvage and Balzani developped electrochemically driven shuttles stabilized by very different interactions than those used in the previously described systems. One of the studied rotaxane contains both a phenanthroline and a terpyridine unit in its dumbbell-shaped component (Figure 18), and a phenanthroline ligand on the threaded macrocycle. [48] Initially Cu (I) prefers to coordinate with the bidentate phenanthroline station in the axle but when Cu (I) gets oxidized to Cu (II) it would prefer to be in a five coordinate state and therefore the macrocycle glides along the axle to coordinate with the terdentate phenanthroline station.

[48] Armaroli, N.; Balzani, V.; Collin, J. P.; Gaviña, P.; Sauvage, J. P.; Ventura, B. Rotaxanes incorporating two different coordinating units in their thread: Synthesis and electrochemically and photochemically induced molecular motions. *J Am Chem Soc*.**121**, 4397–4408 (1999).

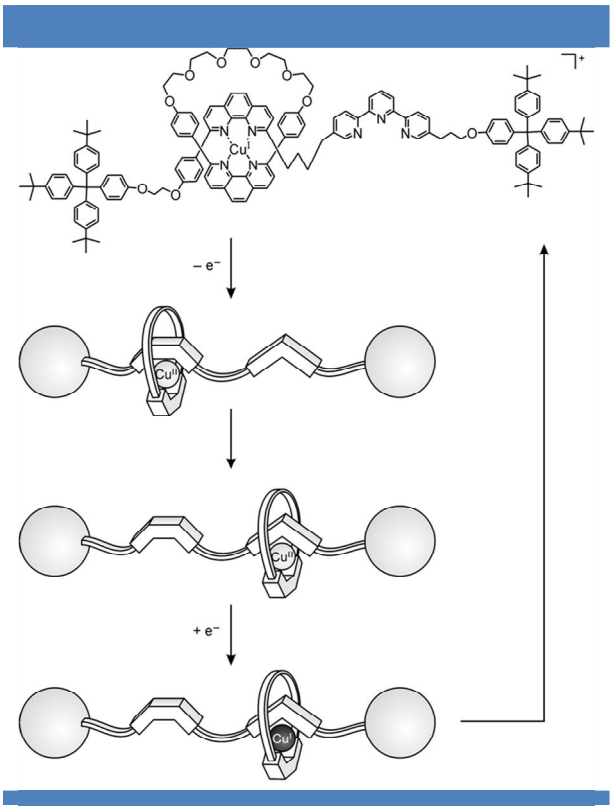

Figure 18 | Shuttling of a macrocyclic component electrochemically controlled by oxidation-reduction of the metal center.[48]

Very recently, this system has been improved by replacing the highly shielding and hindering phenanthroline moiety contained in the ring with a non-hindering biisoquinoline unit. [49] In this new rotaxane, the electrochemically driven shuttling of the ring is, indeed, at least four orders of magnitude faster than in the previous phenanthroline-based system. Many electrochemically driven shuttles had also been studied by Stoddart and co-workers, for instance, in a liquid-crystalline state, [50] or on the surface of silica nanoparticles (SNPs), [51] showing possible biomedical applications. [52]

One promising candidate is the ordered mesoporous silica material, which has shown interesting features such as high stability, important drug capacities and good biocompatibility. In a motif resembling the mechanized silica nanoparticles (MSNPs) which use enzymatic activation to release cargo, an integrated snap-top system was created that

[49] Durola, F.; Sauvage, J. P.; Fast electrochemically induced translation of the ring in a copper-complexed [2]rotaxane: the biisoquinoline effect. *Angew. Chem. Int. Ed.* **46**, 3537–3540 (2007).
[50] Yasuda, T.; Tanabe, K.; Tsuji, T.; Coti, K. K.; Aprahamian, I.; Stoddart, J. F.; Kato, T. A redox-switchable [2]rotaxane in a liquid-crystalline state. *Chem. Commun*. **46**, 1224-1226 (2010).
[51] Coskun, A.; Wesson, P. J.; Klajn, R.; Trabolsi, A.; Fang, L.; Olson, M. A.; Dey, S. K.; Grzybowski, B. A.; Stoddart, J. F. Molecular-Mechanical Switching at the Nanoparticle−Solvent Interface: Practice and Theory. *J. Am. Chem. Soc*., **132**, 4310–4320 (2010).
[52] Li, Z.; Barnes, J. C.; Bosoy, A.; Stoddart, J. F.; Zink, J. Z. Mesoporous Silica Nanoparticles in Biomedical Applications. *Chem. Soc. Rev.* **41**, 2590—2605 (2012).

utilizes mesoporous SNPs, functionalized with disulfide-containing [2]rotaxanes, to release their cargos selectively upon exposure to chemical reductants. [53] The snap-top system relies on the reductive cleavage of disulfide bonds in the stalks, which are encircled by either cucurbit[6]uril (CB[6]) or α-CD rings. When the reduction is performed in aqueous solution by adding dithiothreitol or 2-mercaptoethanol, the snapping of the stalks leads to the cargo (Rhodamine B) being released from the interiors of the SNPs.

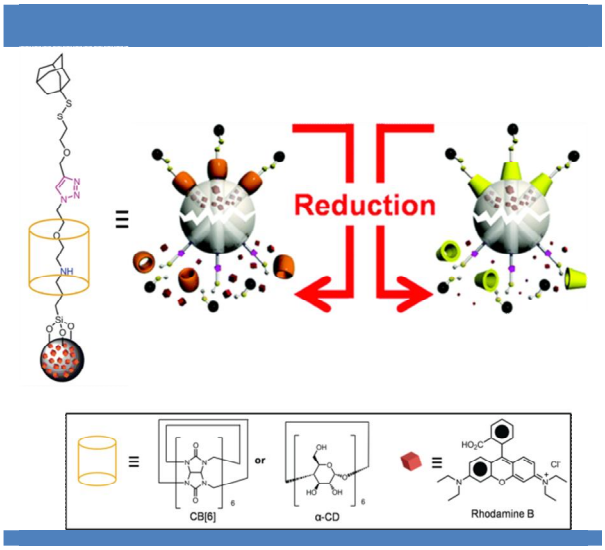

Figure 19 | Schematic representation of cargo being released from the nanopores of an MSNPs using rotaxanes as the external machinery.[53]

This particular integrated system is unique since it employs a highly modular approach to the piecing together of the individual building blocks that extend outward from the surfaces of the SNPs and hence is amenable rather easily to customization. It differs from previous redox-activated MSNPs systems in that it relies on an internal biological trigger, for example, glutathione inside of cells, to carry out the redox chemistry autonomously and does not require the use of an external chemical reductant to operate.

iv. Metalation and demetalation-driven shuttles

The group of Sauvage has played a major role in the development of this kind of shuttles in the last few years. For example, a cyclic [4]rotaxane, containing two roughly face-to-face porphyrinic plates whose mutual arrangement can be controlled by complexation of the four peripheral coordination sites of the rotaxane, has been synthesized using a quadruple

[53] Ambrogio, M. W.; Pecorelli, T. A.; Patel, K.; Khashab, N. M.; Trabolsi,A.; Khatib, H. A.; Botros, Y. Y.; Zink, J. I.; Stoddart, J. F. Snap-Top Nanocarriers. *Org. Lett.*, **12**, 3304-3307 (2010).

threading and stoppering reaction (Figure 20). [54]

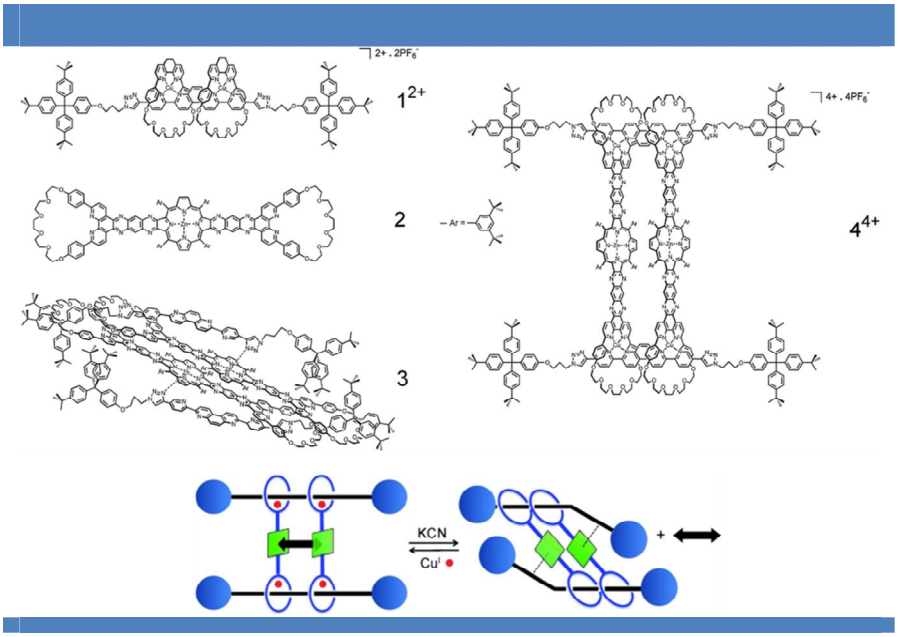

Figure 20 | A recognition process that is switched on and off by metalation or demetalation in a cyclic [4]rotaxane.[54]

The copper(I)-complexed form of the molecule $\mathbf{4}^{4+}$ acts as a specific receptor for rod-shaped substrates of various lengths (1,4-diazabicyclo[2.2.2]octane and 1,4-diaminobutane), with a certain length-selectivity. In contrast, the demetalated form of the [4]rotaxane **3**, has a totally different shape with a collapsed structure and it does not display any complexing ability anymore. In this respect, the receptor behaves as a switchable host, with an active form ($\mathbf{4}^{4+}$, the copper-complexed species) and a totally inactive form (**3**, the metal free state of the compound), both forms being quantitatively interconverted by coordination or decomplexation of the four copper(I) centres.

Another Cu-complexed [3]rotaxane consisting of two coordinating rings threaded by a two-binding-site axis has been prepared in good yield by the same group (Figure 21). [55] The geometry of the coordinating atoms belonging to the axis is such that the triazole groups can be either i) part of the coordinating fragments when the metal center is 5-coordinate, or ii) not at all involved in coordination to the metal when the latter is 4-coordinate.

[54] (a) Collin, J. P.; Durola, F.;Frey, J.; Heitz, V.; Reviriego, F.; Sauvage, J. P.; Trolez, Y.; Rissanen, K. Templated Synthesis of Cyclic [4]Rotaxanes Consisting of Two Stiff Rods Threaded through Two Bis-macrocycles with a Large and Rigid Central Plate as Spacer. *J. Am. Chem. Soc.*, **132**, 6840–6850 (2010). (b) Collin, J. P.; Durola, F.; Heitz, V.; Reviriego, F.; Sauvage, J. P.; Trolez, Y. A Cyclic [4]rotaxane that Behaves as a Switchable Molecular Receptor: Formation of a Rigid Scaffold from a Collapsed Structure by Complexation with Copper(I) Ions. *Angew. Chem. Int. Ed.* **49**, 10172–10175 (2010).

[55] Joosten, A.;Trolez, Y.; Collin,J. P.; Heitz, V.; Sauvage, J. P.; Copper(I)-Assembled [3]Rotaxane Whose Two Rings Act as Flapping Wings. *J. Am. Chem.Soc.* **134**, 1802−1809 (2012).

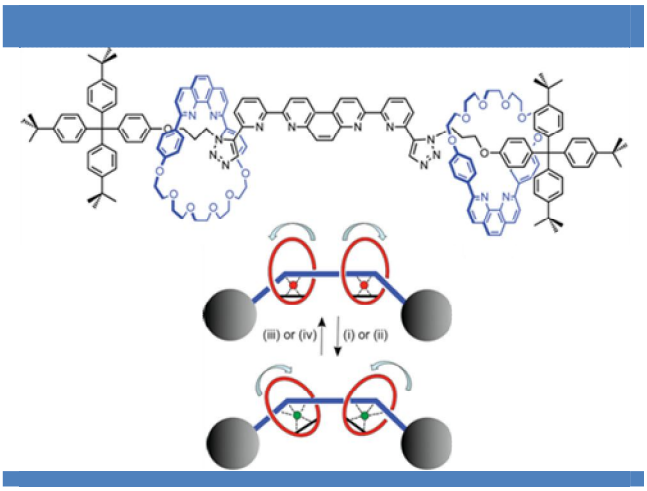

Figure 21 | (Cartoon representing the motions of the two binding macrocycles on a [3]rotaxane: (i) oxidation of Cu(I) to Cu(II), (ii) exchange of Cu(I) for Zn^{2+}, (iii) reduction of Cu(II) to Cu(I), (iv) exchange of Zn^{2+} for Cu(I).[55]

When the two complexed metal centers are monovalent Cu(I) centers, the triazoles are not included in the metal coordination sphere, whereas when the metal centers are Cu(II) or Zn(II), the triazole groups are bound to the metals, because Cu(I) is preferably 4-coordinate and Cu(II) and Zn(II) are 5-coordinate. The interconversion between both situations (4- or 5-coordinate) can be quantitatively induced by metal exchange (Cu(I)/Zn(II)) or by a redox process (Cu(II)/Cu(I)). It leads to important geometrical changes and in particular to a strong modification of the angle between the two rings. As a consequence, the two threaded rings undergo a motion which is reminiscent of a wing-flapping movement similar to that of birds. This flapping motion is fast and quantitative. Such a mechanical behavior may lead to new functional molecular machines in the future.

c) Molecular muscles

Muscles in the human body are responsible for movement by a complex process initiated by a potential travelling down a motor neuron and transmitted to a gliding filament of myosin and actine. Mimiking biological actuation devices is of particular interest in nanoscience. [56]

[56] (a) Mirfakhraia, T.; Maddena, J. D.W.; Baughmanb, R. H. Polymerartificialmuscles. *Materials today*. **10**, 30-38 (2007); (b) Bleger, D.; Yu, Z.; Hecht, S. Toward optomechanics: Maximizing the photodeformation of individual molecules. *Chem. Commun*., **47**, 12260-12266 (2011); (c) Spinks, G. M. Deforming Materials With Light: Photoresponsive Materials Muscle In On the Action. *Angew. Chem. Int. Ed.* **51**, 2285-2287 (2012); (d) Stuart, M. A. C.;Huck, W. T. S.; Genzer, J.; Müller, M.; Ober, C.; Stamm, M.; Sukhorukov, G. B.; Szleifer, I.; Tsukruk, V. V.; Urban, M.; Winnik, F.; Zauscher, S.;Luzinov, I.; Minko, S. emerging applications of stimuli-responsive polymer materials. *Nat. Mater*. **9**, 101–113 (2010). (e) Rogez, Z.; Martinoty, P. Mechanical properties of monodomain nematic side-chain liquid-crystalline elastomers with homeotropic and in-plane orientation of the director. *Eur. Phys. J. E.* **34**, 69 (2011); (f) Rogez, D.; Brommel, F.; Finkelmann, H.; Martinoty, P. Influence of Swelling on the Shear Mechanical Properties of Monodomain Side-Chain Liquid-Crystal Elastomers: Gaussian Versus Non-Gaussian Elasticity. *Macromol. Chem. Phys.* **212**, 2667-2673 (2011).

i. Polymer-based artificial muscles

Although very different from our approach based on MIMs, a first class of artificial candidates to produce contractions and extensions is based on electroactive polymers (EAPs). [57] The first group is known as ionic EAPs and includes ionic polymers, gels, ionomeric polymers, conductive polymers. [58] All these polymers work based on the movement of free ions which causes the material to bend. The disadvantage of these polymers is their need to stay wet. They are also usually encased between two flexible coatings which require a continuous supply of electricity. So, if the voltage is too high, there is a danger of permanently damaging the material. The second class of EAPs are electronic EAPs, which include ferroelectric polymers, dielectric elastomers and electroactive graft elastomers. [59] These polymers are stimulated by an electric field, and one of the particular advantage is that they can sustain high voltage and rapid movement. A typical characteristic property of an EAPs is that they can undergo a large amount of deformation (size or shape) while sustaining large forces. The usefulness of polymers containing ions originates from the strong intermolecular coulombic interactions between the ions.

There are many examples of ionic polymers, of which ionic polymer-metal composite (IPMC) devices are particularly interesting (Figure 22). [60]

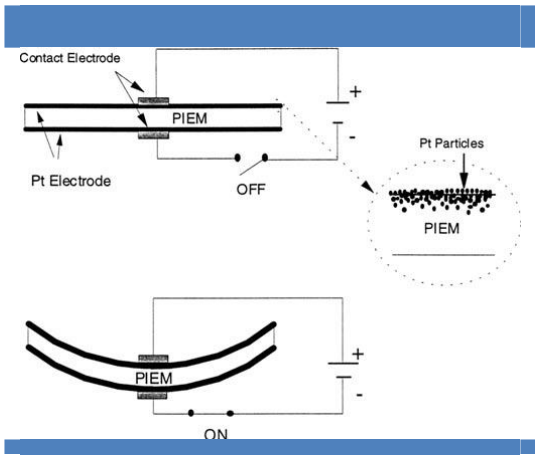

Figure 22 | An IPMC polymer molecular muscle sandwiched between porous Pt electrodes.[60]

[57] Bar-Cohen, Y. ELECTROACTIVE POLYMERS AS ARTIFICIAL MUSCLES-CAPABILITIES, POTENTIALS AND CHALLENGES. HANDBOOK ON BIOMIMETICS, Yoshihito Osada (Chief Ed.), Section 11, in Chapter 8, "Motion" paper **134**, publisher: NTS Inc., Aug. 2000.

[58] (a) Shahinpoor, M.; Bar-Cohen, Y.; Xue, T.; Simpson, J. O.; Smith, J. Ionic Polymer-Metal Composites (IPMC) as Biomimetic Sensors and Actuators, *Proceedings of SPIE's 5th Annual International Symposium on Smart Structures and Materials*, 1–5 March, 1998, San Diego, California. 3324-3327; (b) Fukushima, T.; Asaka, K.; Kosaka, A.; Aida, T. Fully Plastic Actuator through Layer-by-Layer Casting with Ionic-Liquid-Based Bucky Gel. *Angew. Chem. Int. Ed.* **44**, 2410-2413 (2005);

[59] (a) Pelrine, R.; Kornbluh, R.; Pei, Q.; Joseph, J. High-Speed Electrically Actuated Elastomers with Strain Greater Than 100%. *Science* **287**, 836–839 (2000) ; (b) Lovinger, A. J. Ferroelectric polymers. *Science* **220**, 1115–1121 (1983); (c) Wang, y.; Sun, C.; Zhou, E.; Su, J. Deformation Mechanisms of Electrostrictive Graft Elastomers. *Smart Mater. Struct.* , 13, 1407–1413 (2004).

[60] (a) Shahinpoor, M.; Kimm, K. J. The effect of surface-electrode resistance on the performance of ionic polymer–metal composite (IPMC) artificial muscles. *Smart Mater. Struct.* **9**. 543–551(2000); (b) Shahinpoor, M.; Bar-Cohen, Y.; Simpson, J. O.; Smith, J. Ionic polymer-metal composites (IPMCs) as biomimetic sensors, actuators and artificial muscles-a review. *Smart Mater. Struct.* **7**. R15 (1998).

Indeed, a strip of cationic IPMC can bend toward the anode if an electical potential is applied (and to the cathode with anionic IPMC). On the application of an electrical current, the material bends and when the current is switched off, the material contracts back to its original shape. Therefore, by alternating the current, the strip oscillates showing an analogy with muscles.

A second class of contracting/extending polymers is based on the binding of appropriate metal ions to linear ligand strands. For instance, hydrazone polycondensations generates channel-like complexes by reversible coiling of the ligand ***c.1***, thus allowing the generation of ion-induced, acid–base neutralisation fuelled, molecular nanomechanical contraction/extension motions of large amplitude (Figure 23). [61]

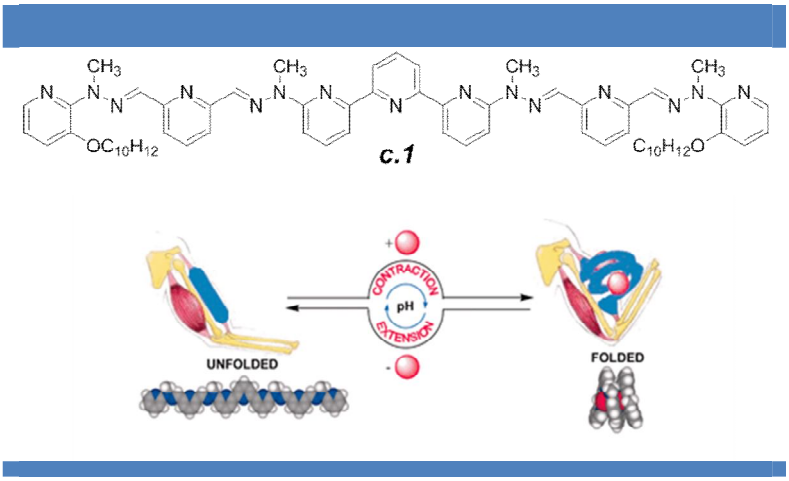

Figure 23 | A prototype pH-triggered molecular muscle based on coiling of a polyligand by Pb^{2+}.[61]

In the free state, the ligand ***c.1*** adopts an extended conformation (4 nm long). Upon binding Pb^{2+} ions, a Pb:ligand/2 :1 complex with a coiled structure of 0.71 nm long is formed. The complex is an example of thermodynamic self-assembly, which the complexation is reversible and the Pb^{2+} ions can be removed by addition of tris(2-aminoethy)amine (tren), regenerating the extended free ligand. Coiling and uncoiling can be made to cycle reversibly as a function of pH. Thus, addition of triflic acid to uncoiled ***c.1***/ Pb^{2+}/tren induces protonation of tren, thereby freeing Pb^{2+} to bind with ***c.1***, hence resulting in coiling. Alternatively, raising the pH by adding a base, such as triethylamine, deprotonates the tren, which then sequesters the Pb^{2+} ions and results in uncoiling.

[61] Stadler, A. M. ; Kyritsakas, N. ; Lehn, J. M. Reversible folding/unfolding of linear molecular strands into helical channel-like complexes upon proton-modulated binding and release of metal ions. *Chem. Commun.*, 2024-2025 (2004).

ii. Bistable rotaxane molecular muscles at the molecular level

Recently, examples of molecular mimics of muscle fibres have been described in the literature. Methods for synthesising them are centered on the formation of [2]-rotaxanes, which are well-suited for the construction of molecular machines as the relative motions of their mechanically interlocked components can be controlled. Pioneering work in the development of linear molecular muscles has been published by Sauvage, based on compounds prepared using transition metal-based templates for the formation of two-component interlocked molecules in which the design is bioinspired to display contraction and extension movements (Figure 24). [62]

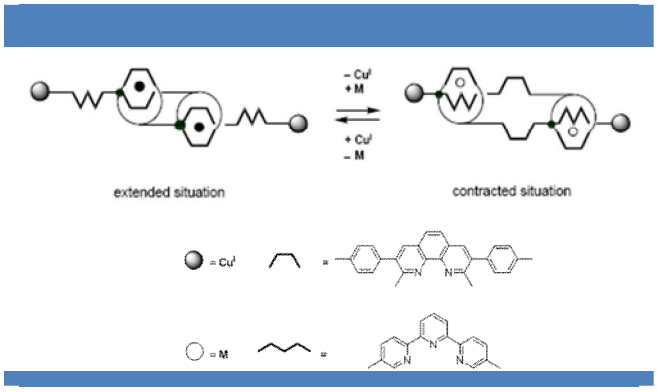

Figure 24 | Functioning principle of the unimolecular synthetic "muscle" published by Sauvage *et al.* [62]

As shown in Figure 24, the double-threaded compound can bind simultaneously two metal centers, either in a four-coordinate or a five-coordinate geometry. The four-coordinate situation results from the coordination of a copper(I) ion with two phenanthroline units and corresponds to an extended geometry (left part of Figure 24), whereas the five-coordinate situation results from the coordination of a divalent ion M (such as Zn(II)) with one phenanthroline and one terpyridine and leads to a contracted geometry (right part of Figure 24).

Easton *et al.* have developed a light-driven molecular muscle based on stilbene and α-cyclodextrin. [63] It rests on rotaxane 'daisy chain' dimers, in which a stilbene bonded to α-cyclodextrin molecule is threaded through another α-cyclodextrin bonded to a stilbene, with the stilbenes being capped with bulky alkyl groups to prevent unthreading of the components. Initially, both the stilbenes are in the *trans* conformation, and can therefore act as guests

[62] Jimenez, M. C. ; Buchecher, C. D. ; Sauvage, J. P. Towards Synthetic Molecular Muscles : Contraction and Stretching of a Linear Rotaxane Dimer. *Angew. Chem. Int. Ed.*, **39**, 3284-3287 (2000).
[63] Dawson, R. E. ; Lincoln, S. F. ; Easton, C. J. The foundation of a light driven molecular muscle based on stilbene and a-cyclodextrin. *Chem. Commun.*, 3980-3982(2008).

within the α-cyclodextrin. Upon irradiation with 350nm light, one or both of the stilbenes may isomerise, causing their release from the α-cyclodextrin and resulting in the extension of the rotaxane. This may be reversed by irradiation with 254nm light, causing the 'muscle' to contract or expand with light irradiation (Figure 25).

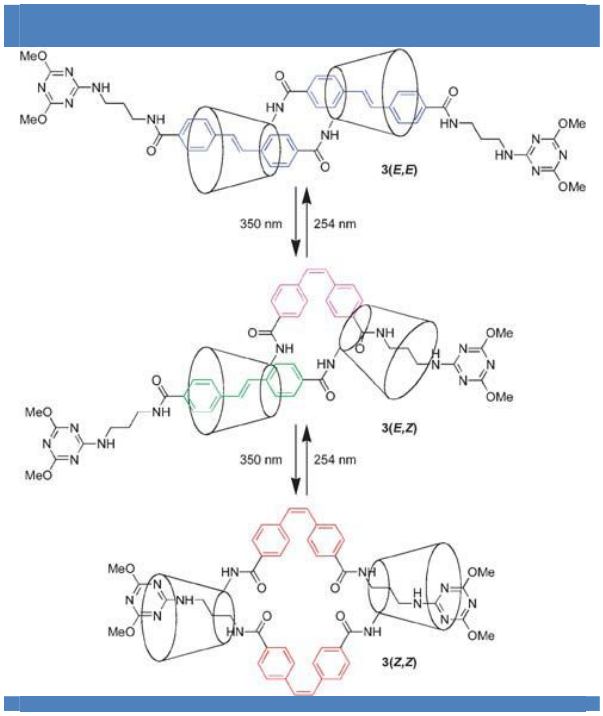

Figure 25 | Light triggered molecular muscle based on stilbene and α-cyclodextrin.[63]

The present system, based on photonic inputs, expands the field in a very significant fashion, by using light as physical trigger.

In another work, a pH-switchable glycol [c2]daisy chain molecular shuttle muscle was prepared by the group of Coutrot based on the idea of a pH-controllable molecular shuttle (Figure 26). [64] The target monomer molecular muscle includes a side arm which contains two different recognition sites (i.e. benzylammonium and triazolium units). Because of the better affinity of the DB24C8 for the benzylammonium compared to the triazolium, and because of the lack of affinity for the benzylamine unit (deprotonated benzylammonium unit), the interwoven dimer could contract or stretch by changing the pH of the solution, thus exhibiting a muscle-like behavior at the molecular level.

[64] (a) Coutrot, F.; Romuald, C.; Busseron, E. A New pH-Switchable Dimannosyl[c2]Daisy Chain Molecular Machine. *Org. Lett.* **14**, 3741 – 3744 (2008). (b) Romuald, C.; Busseron, E.; Coutrot, F. Very Contracted to Extended co-Conformations with or without Oscillations in Two- and Three-Station [c2]Daisy Chains. *J. Org. Chem.* **75**, 6516–6531 (2010).

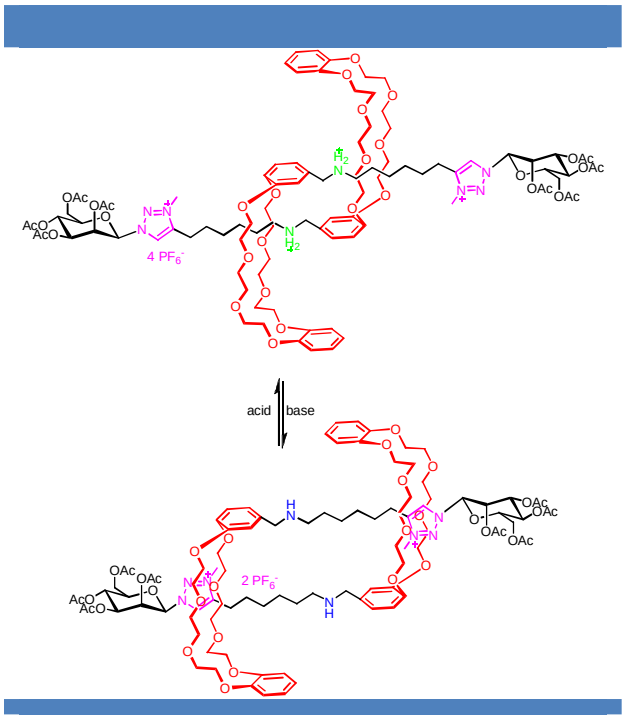

Figure 26 | Acid/base-promoted extension/contracion movements in a bis-mannosyl [2]rotaxane.[64]

Another pH-controlled bistable molecular muscle, based on a doubly threaded Janus-type [2]rotaxane, was obtained using a template-directed self-assembly process (Figure 27). [65]

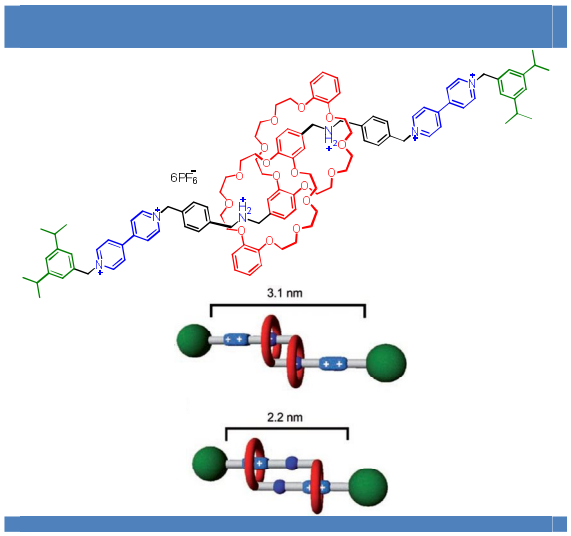

Figure 27 | The anticipated mechanical motions within an acid–base-controlled molecular muscle system based on a [c2]daisy chain. [65]

Under the influence of changes in the pH value, the two identical matching components glide along one another through terminal crown ether moieties, bringing about expansion and

[65] Wu, J. ; Leung, K. C. F. ; Benitez, D. ; Han, J. Y.; Cantrill, S. J. ; Fang, L. ; Stoddart, J. F. An Acid–Base-Controllable [c2]Daisy Chain. *Angew. Chem. Int. Ed.*, **47**, 7470 –7474 (2008).

contraction of the molecule (~0.9 nm). The drawback of this synthesis is the low yields (15-40%) which can be attributed to the propensity of the dimeric superstructures to disassemble during the stoppering reaction at elevated temperatures.

In general, the synthetic strategy to make these acid–base controllable [c2]daisy chains is readily amenable to modification with carefully chosen functional groups, potentially leading to the production of functionalized molecules, which could, for example, be incorporated into liquid crystals or polymeric systems. The material properties of these much larger supramolecular and molecular systems should then be responsible to changes in pH as it will be discussed in the next section.

iii. Attempts to extend bistable rotaxane molecular muscles at the macroscopic level

The molecular systems we mentioned above have been shown to undergo actuation, albeit in an incoherent manner in a solution environment, heralding their potential utilization in mechanical applications including nano- and microrobots for medicine and everyday-life pursuits. Although surprisingly not insurmountable, the harnessing of molecular motion in a cooperative and coherent manner to generate a macroscopic response has yet to be achieved.

The first attempt to produce large-scale mechanical motion triggered by shuttling in a rotaxane was demonstrated using electroactive [3]rotaxane (Figure 28). [66]

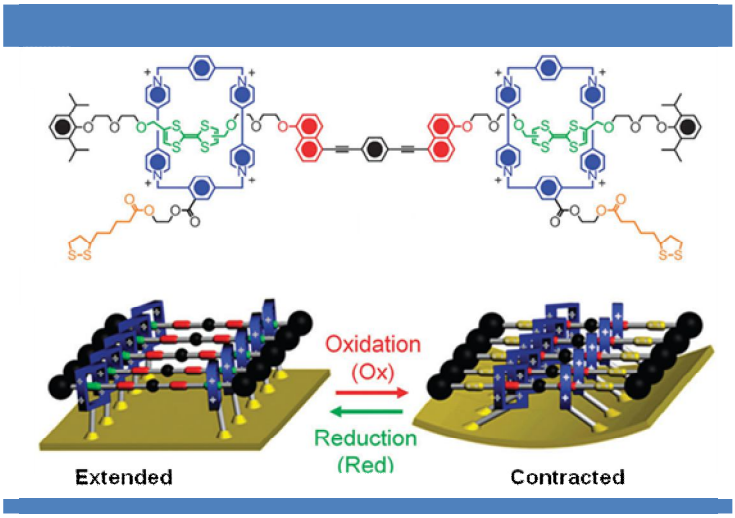

Figure 28 | A molecular muscle based on a self-assembled monolayer of palindromic bistable rotaxanes.[66]

[66] (a) Huang, T.J. ; Brough, B. ; Ho, C. M. ; Liu, Y. ; Flood, A. H. ; Bonvallet, P. A. ; Tseng, H. R.; Stoddart, J. F. ; Ballaer, M. ; Magonov, S. A nanomechanical device based on linear molecular motors. *Appl. Phys. Lett.* **85**, 5391–5393 (2004). (b) Liu, Y.; Flood, A. H.; Bonvallet, P. A.; Vignon, S. A. ;Northrop, B. H.; Tseng, H. R.; Jeppesen, J. A.; Huang, T. J.; Brough, B.; Ballaer, M.; Magonov, S.; Solares, S. D.; Goddard, W. A. ; Ho, C. M.; Stoddart, J. F. Linear artificial molecular muscles. *J. Am. Chem. Soc.* **127**, 9745–9759 (2005). (c) Li, D.; Paxton, W. F.; Baughman, R. H.; Huang, T. J.; Stoddart, J. F.; Weiss, P. S.; Molecular, Supramolecular, and Macromolecular Motors and Artificial Muscles. *MRS Bulletin*. **34**, 671-681(2009).

The investigated system consists of a palindromic bistable rotaxane with two macrocycles and four stations, namely, two tetrathiafulvalene (TTF) and two oxynaphthalene moieties. Tethers attached to each macrocycle are used to anchor the whole rotaxane system as a self-assembled monolayer (SAM) on a gold surface deposited on silicon microcantilever beams. Each microcantilever (500 × 100 × 1 μm) is covered with approximately 6 billions of randomly oriented rotaxane molecules. The setup was then inserted into a fluid cell. Oxidation of the TTF stations (green to pink) results in shuttling the cyclophanes onto the hydroxynaphthalene units (red), significantly shortening the inter-ring separation (from 4.2 nm to 1.4 nm). The chemical oxidant $Fe(ClO_4)_3$ was added to the solution and the combined effect of co-conformational change randomly oriented rotaxanes on each cantilever resulted in an upward bending of the beam by about 35 nm. Reduction with ascorbic acid returned the cantilever to its starting position. The process could be repeated over several cycles, albeit with gradually decreasing amplitude. This important experiment demonstrates the possibility of harnessing cumulative nanoscale movements within surface-bound molecular shuttles to perform larger-scale mechanical work, [67] although the gain of amplitude do not exceed one order of magnitude.

Since [c2]Daisy chains could further serve as special building blocks [65] and be incorporated into discrete or infinite supramolecular assemblies, Stoddart and co-workers prepared some mechanically interlocked supramolecular oligomers from the polymerization of [c2]daisy chains with the purpose of transferring chemical stimuli into amplified mechanical motion (Figure 29). [68]

Functional mechanically interlocked [c2]daisy chain momomers which can undergo reversible extension and contraction movements upon external stimuli were first synthesized. Polymerization of the dialkyne-substituted monomer with a diazide compound resulted in the linear main-chain polymer, the repeating units of which were connected by covalent bonds produced from the ‘click’ reaction. Size exclusion chromatographic analysis of this poorly soluble polymer showed that its number average molecular weight was 33 kDa, indicating that each oligomer chain was only composed of about 11 repeating units.

[67] (a) Eelkema, R.; Pollard, M. M.; Katsonis, N.; Vicario, J.; Broer, D. J.; Feringa, B. L.; Rotational reorganization of doped cholesteric liquid crystalline films. *J. Am. Chem. Soc.* **128**, 14397–14407 (2006). (b) Ferri, V.; Elbing, M.; Pace, G.; Dickey, M.; Zharnikov, M.; Samorì, P.; Mayor, M.; Rampi, M. A. Light-powered electrical switch based on cargo-lifting azobenzene monolayers. *Angew. Chem. Int. Ed.* **47**, 3407–3409 (2008). (c) Percec, V.; Rudick, J. G.; Peterca, M.; Heiney, P. A. Nanomechanical function from self-organizable dendronized helical polyphenylacetylenes. *J. Am. Chem. Soc.* **130**, 7503–7508 (2008).

[68] Fang, L. ; Hmadeh, M.; Wu, J.; Olson, M. A.; Spruell, J. M. ; Trabolsi, A.; Yang, Y. W.; Elhabiri, M.; Albrecht-Gary, A. M.; Stoddart, J. F. Acid-Base Actuation of [c2]Daisy Chains. *J. Am. Chem. Soc*., **131**, 7126–7134 (2009).

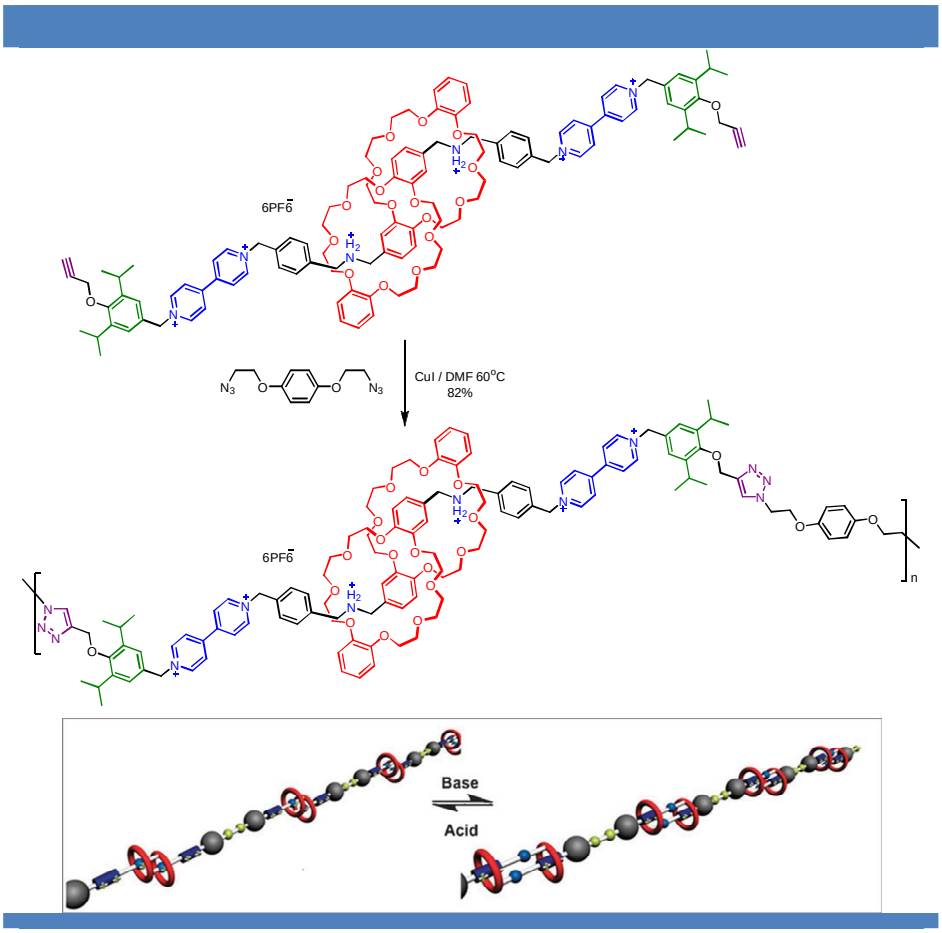

Figure 29 | Oligomerisation of a bisfunctionalised [c2]daisy chain and the acid–base induced switching of the resulting poly[c2]daisy chain developped by Stoddart *et al*. [68]

The acid/base stimulated extension-contraction movements of this oligomer were investigated by ^{1}H NMR spectroscopy and UV/vis absorption spectroscopy. Upon alternated addition of acid or base, the repeating units did undergo muscle-like expansions and contractions as the [c2]daisy chain did. Stop-flow kinetics measurements demonstrated that the extension-contraction movements of polymers are actually faster than those occurring in its monomers.[69] If all repeating units contracted at the same time, the length of the poly[c2]daisy chain would be reduced by roughly 9.9 nm without considering other effects.

In a related system reported by Grubbs *et al.*, a bifunctional [c2]daisy chain was synthesised by employing ring-closing metathesis of a bisolefin-containing polyether templated by a dialkylammonium unit, on account of the strong hydrogen bonds formed between oxygen atoms in the macrocyclic component and the NH_2^+ cationic centre (Figure

[69] Hmadeh, M.; Fang, L.; Trabolsi, A.; Elhabiri, M.; Albrecht-Gary, A. M.; Stoddart, J. F. On the thermodynamic and kinetic investigations of a [c2]daisy chain polymer. *J. Mater. Chem.*, **20**, 3422 (2010).

30). [70]

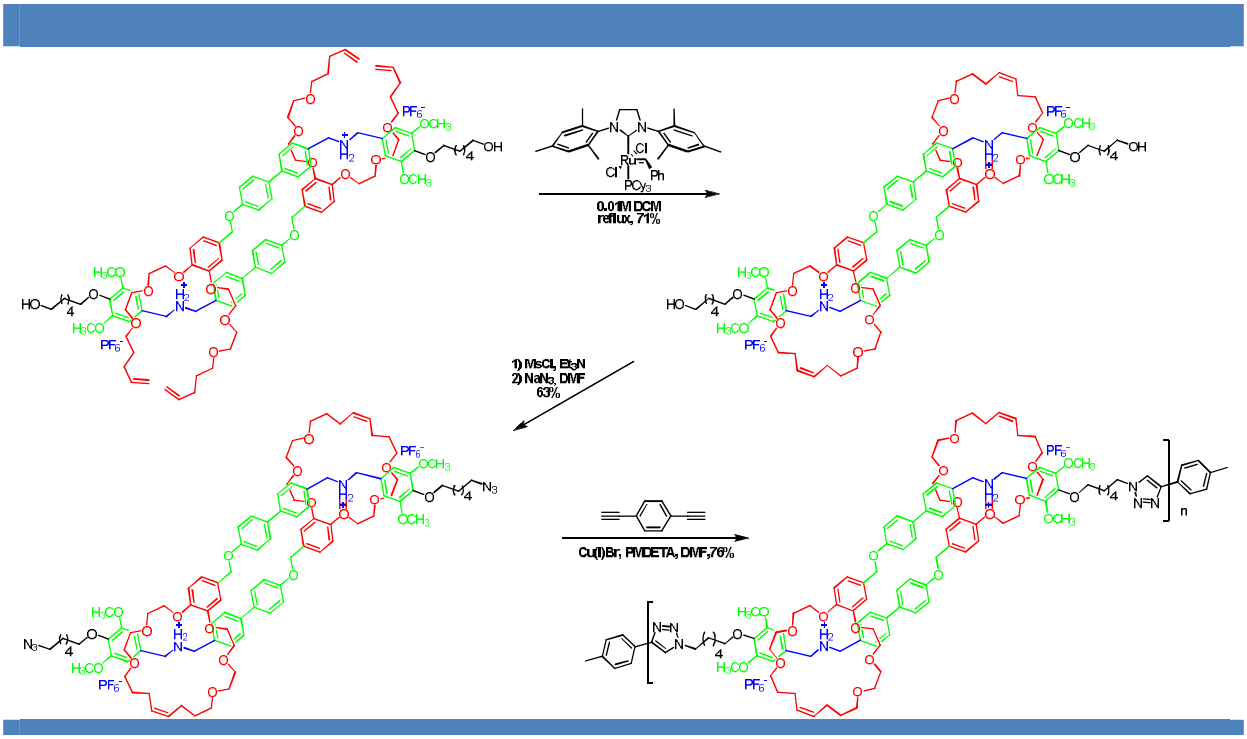

Figure 30 | Chemical structures of bifunctional [c2]daisy chain monomer developped by Grubbs *et al.*[70]

After conversion of the terminal alcohols of the resultant [c2]daisy chain monomers to azide groups, polymerization was carried out by copper-catalyzed ‘‘click’’ reactions, leading to the growth of the oligomer. Gel permeation chromatography revealed that the molecular weight of that polymer was 48 kDa and the degree of polymerization was around 22, a little bit better compared to the previous example. Due to π-π stacking interactions of the dimer aryl rings, the deprotonated polymer remained in the contracted conformation. After increasing the steric bulkiness of the amines (by acylation), the crown rings slipped along the stiff sidearm to give the extended analogue, the size of which increased from 14.8 nm for the contracted analogue to 21.4 nm (48% R_g increase). It should be mentioned that there is only one possible state after acylation reaction.

Thus, in both example by Stoddart and Grubbs, the short length of the oligomers prevents the amplification of the individual motions by several orders of magnitude. In particular, other polymerisation processes could be envisaged to achieve this goal.

[70] Clark, P. G.; Day, M. W.; Grubbs, R. H. Switching and Extension of a [c2]Daisy-Chain Dimer Polymer. *J. Am. Chem. Soc.* **131**, 13631–13633 (2009).

4/ Supramolecular Polymers

a) Definitions and classifications

A supramolecular polymer is a polymer whose monomer repeat units are held together by reversible and highly directional noncovalent bonds, such as hydrogen bonds, coordination, and π-π interactions. The resulting materials therefore maintain their polymeric properties in solution. The directions and strengths of the interactions are precisely tuned so that the array of molecules behaves as a polymer (that is, it behaves in a way that can be described by the theories of polymer physics). The possible reversibility of the non-covalent bonds ensures however that supramolecular polymers are always formed under conditions of thermodynamic equilibrium, and hence the lengths of the chains are directly related to the strength of the non-covalent bond, the concentration of the monomer, and the temperature. [71]

Supramolecular polymerizations can be classified on the basis of three different principles: (1) the physical nature of the non-covalent force that lies at the origin of the reversible interaction (physical origin classification), (2) the type of monomer(s) used (structural monomer classification), and (3) the evolution of the Gibbs free energy of the polymer as a function of conversion (thermodynamical classification). [72] We have chosen to classify different supramolecular polymers on the basis of the physical nature of the various types of interactions that can act as driving forces for the formation of large supramolecular assemblies. Examples of types of polymers in this classification include supramolecular polymers formed by (1) hydrogen bonds, (2) π-π interactions, (3) hydrophobic interactions, or (4) metal-ligand coordinaton bonds.

In this thesis, we will focus on the hydrogen-bonding and metallo-supramolecular (i.e. coordination) polymers.

b) Hydrogen-bonding supramolecular polymers

Hydrogen bonds are very convenient to hold supramolecular polymers together, as they combine high strength with selectivity, and excellent reversibility. Furthermore, because they form bonds only in one direction (and possibly that of the polymer chain), unwanted interactions in other directions are minimized. The strength and reversibility of hydrogen

[71] (a) Aida, T.; Meijer, E. W.; Stupp, S. I.; Functional Supramolecular Polymers. *Science* **335**, 813-817 (2012); (b) De Greef, T. F. A.; Meijer, E. W. Supramolecular polymers. *Nature* **453**, 171-173 (2008).
[72] De Greef, T. F. A.; Smulders, M. M. J.; Wolffs, M.; Schenning, A. P. H. J.; Sijbesma, R. P.; Meijer, E. W. Supramolecular Polymerization. *Chem. Rev.* **109**, 5687 (2009).

bonding between monomers can be precisely tuned by installing an array of hydrogen-bonding groups in the monomers, so allowing several bonds to form. It was shown that the interactions between such strongly bound units can be maintained even when the polymer is dissolved in water, where the solvent molecules compete to form hydrogen bonds with the monomers. [73]

Compounds that have multiple hydrogen bond donor (D) and/or acceptor (A) groups are capable of forming multiple hydrogen-bonding interactions. Rigidity and well-defined geometry of heteroaromatic compounds render them highly interesting as multiple hydrogen-bonding modules featuring highly specific and directional binding properties. Three typical examples of multiple hydrogen-bonding interactions are presented in Figure 31. [74]

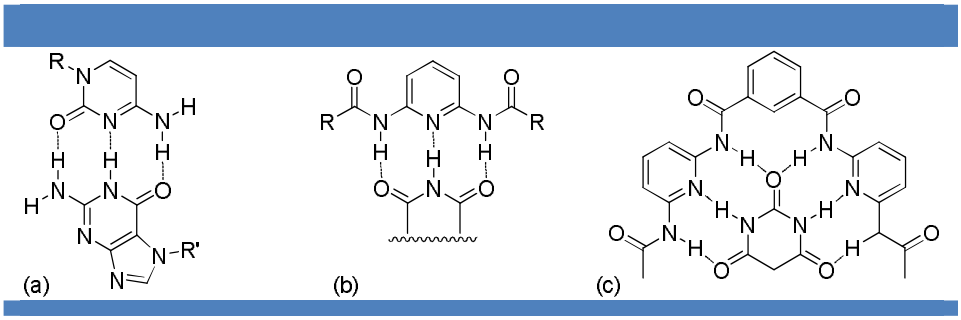

Figure 31 | Examples of multiple hydrogen-bonding interactions between (a) guanine and cytosine modules, (b) acylated diaminopyridine and imide modules and (c) Hamilton-type receptor with barbituric acid module.[74]

For instance, the self-association of 2-ureido-4[1H]-pyrimidinones (UPy) results in the formation of dimers via quadruple hydrogen-bonding and has proven to be one of the most popular motifs in the development of supramolecular polymers. The incorporation of the UPy dimer, which has a large association constant ($K_a > 10^7$ M^{-1} in $CDCl_3$), as a fundamental part of the polymer main chain is an elegant example of how strong supramolecular interactions can affect mechanical properties in the solid state.

Supramolecular materials are inherently thermally sensitive and under continuous equilibrium, thus the ability to reorganize after self-assembly is a property most of these systems share. For example, a low-molecular-weight telechelic polymer, hydroxyl-terminated

[73] Araki, K.; Takasawa, R.; Yoshikawa, I. Design, fabrication, and properties of macroscale supramolecular fibers consisted of fully hydrogen-bonded pseudo-polymer chains. *Chem. Commun*., 1826-1827 (2001).
[74] (a) Lehn, J. M. Supramolecular polymer chemistry—scope and perspectives. *Polym. Int.* **5**, 825-839 (2002). (b) Yagai, S. Supramolecular complexes of functional chromophores based on multiple hydrogen-bonding interactions. *J. Photochem. Photobiol. C: Photochem. Rev.* **7**, 164–182 (2006).

poly(ethylenebutylene), is a viscous liquid at room temperature (Figure 32). [75] However, after functionalizing the material with UPy groups significant chain extension is achieved via UPy dimerization, leading to an apparent high-molecular-weight material that is a mechanically robust, elastic film. The hydrogen bonds can be reversibly disengaged, and at higher temperatures these materials flow like their low-molecular weight constituents. [76]

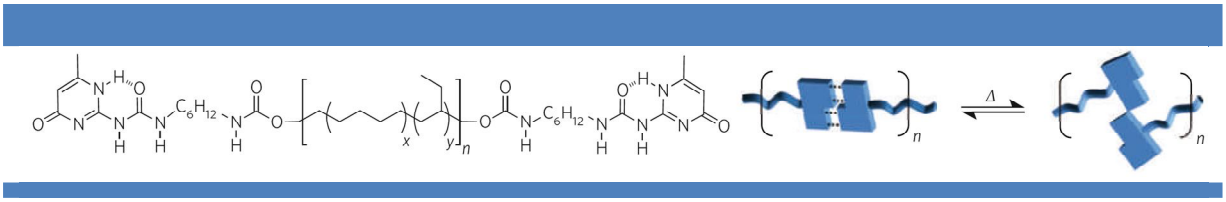

Figure 32 | The quadruple hydrogen-bonding unit UPy incorporated onto the chain ends of low-molecular-weight telechelic polymers as thermally responsive structurally dynamic polymers. [75]

Oligofluorenes have been also functionalized with Upy module at both ends as in Upy-OF3-Upy (Figure 33). [77] Self-aggregation of Upy-OF3-Upy provides supramolecular polymers whose main chains are composed of π-conjugated chromophores. Adding mono-UPy-functionalized oligophenylenevinylenes (Upy-OPV) resulted in end-capped supramolecular polymers with OPV functional moieties, where light-energy harvested by the oligofluorene main chain is efficiently transferred to the terminal OPV moieties. When Upy-OPV was mixed with oligofluorenes lacking UPy modules, incomplete energy transfer was observed, confirming that the observed energy transfer is a result of supramolecular polymerization driven by quadruple hydrogen bonding.

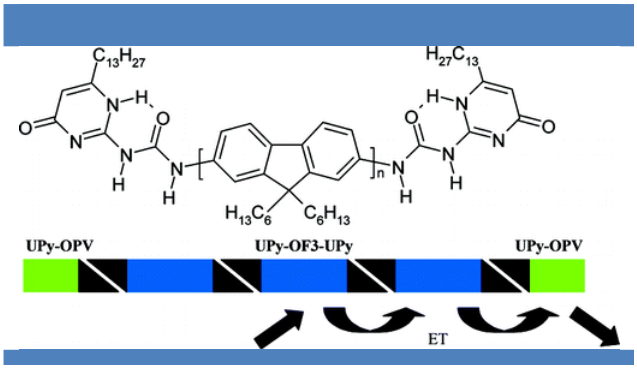

Figure 33 | Energy transfer occurring in a supramolecular polymer of UPy-functionalized oligofluorene, end-capped with UPyfunctionalized OPV. [77]

[75] Sontjens, S. H. M.; Sijbesma, R. P.; vanGenderen, M. H. P.; Meijer, E. W.; Stability and lifetime of quadruply hydrogen bonded 2-ureido-4[1H]-pyrimidinone dimers. *J. Am. Chem. Soc.* **122**, 7487–7493 (2000).
[76] Folmer, B. J. B.; Sijbesma, R. P.; Versteegen, R. M.; van der Rijt, J. A. J.; Meijer, E. W.; Supramolecular polymer materials: chain extension of telechelic polymers using a relative hydrogen-bonding synthon. *Adv. Mater.* **12**, 874–878 (2000).
[77] Dudek, S.P.; Pouderoijen, M.; Abbel, R.; Schenning, A.P.H.J.; Meijer, E.W. Synthesis and Energy-Transfer Properties of Hydrogen-Bonded Oligofluorenes. *J. Am. Chem. Soc.* **127**, 11763-11768 (2005).

c) *Metallo-supramolecular polymers*

There are many advantages of coordination supramolecules: e.g. (1) the presence of metallic elements allows the coordinating supramolecules to offer special optical, electrical, magnetic and mechanical properties; [78] (2) the dynamic nature of the coordinating bonds endows switchability to the system, mimicking the behavior of natural structures; [79] (3) such metal–ligand interactions lies in the large catalogue of accessible ligands, along with applicable metal ions comprising nearly half the periodic table, which means a vast range of metal–ligand complexes can be easily accessed. [80] Therefore, coordinated supramolecules offer a broad platform for the development of smart materials. The architecture of the synthesized metallo-supramolecular polymer structures depends on the localization of the metal ion: main chain or side-chain. When the coordination bond is present in the side chain, the polymeric structures still hold characteristics of covalent polymers, and do not represent a revolutionary change for the polymer properties. In the main chain coordinated supramolecules, metal–ligand coordination bonds are the linking force between repeating units. In this framework, linear, [81] branched, [82] and block copolymers [83] can be formed.

Particularly, terpyridine ligands are highly effective complexing agents and can be used as key building units in metallo-supramolecular polymers. [84] Schubert *et al.* reported a supramolecular polymer where the monomers bearing terpyridine units both at the head and tail were polymerized through coordination with ruthenium(II) (Figure 34). [85] The formation of high molecular weight supramolecular polymers was revealed by GPC analysis. It was found that P2 has a higher molecular weight than P1. Moreover, using a refractive index detector and a linear poly(methyl methacrylate) calibration sample, a number averaged

[78] (a) Marin, V.; Holder, E.; Hoogenboom, R.; Schubert, U. S. Functional ruthenium(II)- and iridium(III)-containing polymers for potential electro-optical applications. *Chem. Rev. Soc.*; **36**, 618-635 (2007); (b) Han, F. S.; Higuchi, M.; Kurth, D. G. Metallosupramolecular Polyelectrolytes Self-Assembled from Various Pyridine Ring-Substituted Bisterpyridines and Metal Ions: Photophysical, Electrochemical, and Electrochromic Properties. *J. Am. Chem. Soc.*; **130**, 2073-2081 (2008); (c) Chow, C. F.; Fujii, S.; Lehn, J. M. Metallodynamers: Neutral Dynamic Metallosupramolecular Polymers Displaying Transformation of Mechanical and Optical Properties on Constitutional Exchange. *Angew. Chem. Int. Ed.*; **46**, 5007-5010 (2007).

[79] Lehn, J. M. From supramolecular chemistry towards constitutional dynamic chemistry and adaptive chemistry. *Chem. Soc. Rev.*; **36**, 151-160 (2007).

[80] Kurth, D. G.; Higuchi, M. Transition metal ions: weak links for strong polymers. *Soft Matter*, **2**, 915-927 (2006).

[81] (a) Wild, A.; Schlutter, F.; Pavlov, G. M.; Friebe, C.; Festag, G.; Winter, A.; Hager, M. D.; Cimrova, V.; Schubert, U. S. π-Conjugated Donor and Donor–Acceptor Metallo-Polymers. *Macromol. Rapid Commun.* **31**, 868–874 (2010); (b) Vermonden, T.; van der Gucht, J.; de Waard, P.; Marcelis, A. T. M.; Besseling, N. A. M. ; Sudholter, E. J. R.; Fleer, G. J.; Stuart, M. A. C. Water-Soluble Reversible Coordination Polymers: Chains and Rings. *Macromolecules* **36**, 7035-7044 (2003).

[82] (a) Vermonden, T.; van Steenbergen, M. J.; Besseling, N. A. M.; Marcelis, A. T. M.; Hennink, W. E.; Sudholter, E. J. R.; Stuart, M. A. C. Linear Rheology of Water-Soluble Reversible Neodymium(III) Coordination Polymers. *J. Am. Chem. Soc.* **126**, 15802-15808 (2004); (b) Zhao, Y.; Beck, J. B.; Rowan, S. J.; Jamieson, A. M.; Rheological Behavior of Shear-Responsive Metallo-Supramolecular Gels. *Macromolecules* **37**, 3529-3531 (2004).

[83] (a) Fustin, C. A.; Guillet, P.; Schubert, U. S.; Gohy, J. F. Metallo-Supramolecular Block Copolymers. *Adv. Mater.* **19**, 1665-1673 (2007); (b) Chiper, M.; Winter, A.; Hoogenboom, R.; Egbe, D. A. M.; Wouters, D.; Hoeppener, S.; Fustin, C. A.; Gohy, J. F.; Schubert, U. S. Synthesis and Micellization of Coil−Rod−Coil Ruthenium(II) Terpyridine Assemblies. *Macromolecules* **41**, 8823-8831 (2008).

[84] (a) Schubert, U. S.; Hofmeier, H.; Newkome, G. R.; *Modern Terpyridine Chemistry*, Wiley-VCH, Weinheim, Germany, 2006; (b) Constable, E. C. 2,2':6',2''-Terpyridines: From chemical obscurity to common supramolecular motifs. *Chem. Soc. Rev.*, **36**, 246–253 (2007).

[85] Meier, M. A. R.; Hofmeier, H.; Abeln, C. H.; Tziatzios, C.; Rasa, M.; Schubert, D.; Schubert, U. S. First GPC results of terpyridine based chain extended supramolecular polymers: comparison with viscosity and analytical ultracentrifugation. *e-Polymer*, **16**, 1-7 (2006).

molecular weight of 1.38×10^5 g/mol and a polydispersity index of 1.55 were reported. This calculated molecular weight of P2 corresponds to 15 monomers (P1).

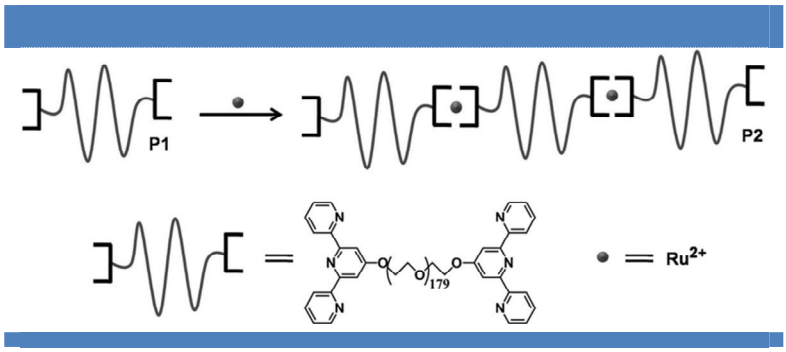

Figure 34 | A bis-terpyridine-functionalized poly(ethylene glycol) (**P1**) was polymerized to form the coordination supramolecular polymer **P2**.[85]

Furthermore, considering the diversity and complexity of biological systems which use a wide variety of noncovalent interactions (such as hydrogen bonding, metal coordination, and hydrophobic interactions) in an orthogonal fashion to introduce function, a multiple-functionalizing methodology (e.g. combining H-bonding and coordination interactions) has been developed. [86] Such systems may open new possibilities for the preparation of dynamic and rapidly optimized ‘‘smart’’ materials.[87]

d) Self-healing

Conceptually, the reversibility of the dynamic bond allows repair to take place at the molecular level to fully restore the original material properties and allows the process which is so-called self-healing behavior to be repeated many times. [88] This could extend the lifetimes of materials used in many applications. For example, metallo-supramolecular polymers that can be mended through exposure to UV light were reported by Weder and co-workers (Figure 35). [89] The polymer is composed of an hydrophobic alkane core carrying 2,6-bis(1’-methylbenzimidazolyl) pyridine (Mebip) ligands at both sites. The Mebip ligands can coordinate to Zn^{2+} and La^{3+} ions to give linear nanoassemblies. The metal coordination can be disrupted by irradiation with UV light, but can subsequently reassemble.

[86] (a) Groger, G.; Meyer-Zaika, W.; Bottcher, C.; Grohn, F.; Ruthard, C.; Schmuck, C.; Switchable Supramolecular Polymers from the Self-Assembly of a Small Monomer with Two Orthogonal Binding Interactions. *J. Am. Chem. Soc.*, **133**, 8961–8971 (2011); (b) Groger, G.; Stepanenko, V.; Wurthnerb, F.; Schmuck, C.; Step-wise self-assembly of a small molecule with two orthogonal binding interactions leads to single stranded linear polymers in DMSO. *Chem. Commun.*, 698–700 (2009) ; (c) Hofmeier, H.; Hoogenboom, R.; Wouters, M. E. L.; Schubert, U. S. High Molecular Weight Supramolecular Polymers Containing Both Terpyridine Metal Complexes and Ureidopyrimidinone Quadruple Hydrogen-Bonding Units in the Main Chain. *J. Am. Chem. Soc.*, **127**, 2913-2921(2005).
[87] Service, R. F. How far can we push chemical self-assembly? *Science* **309**, 95 (2005).
[88] (a) Cordier, P.; Tournilhac, F.; Soulie-Ziakovic, C.; Leibler, L. Self-healing and thermoreversible rubber from supramolecular assembly. *Nature* **51**, 977–980 (2008) ; (b) Mynar, J. L.; Aida, T. Materials science: The gift of healing. *Nature* **451**, 895–896 (2008).
[89] Burnworth, M.; Tang, L.; Kumpfer, J. R.; Duncan, A. J.; Beyer, F. L.; Fiore, G. L.; Rowan, S. J.; Weder, C. Optically healable supramolecular polymers. *Nature* **472**, 334–337 (2011).

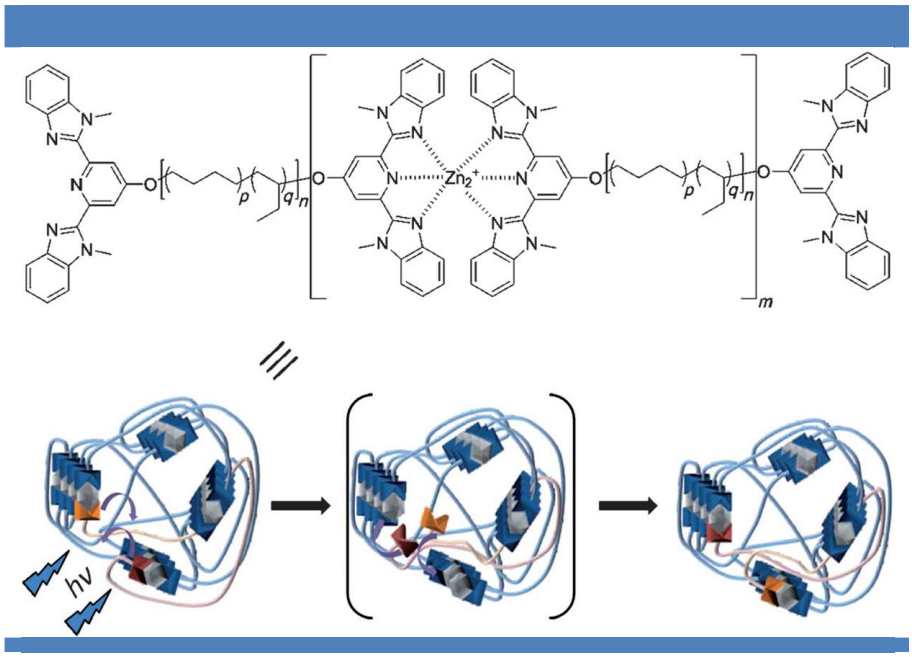

Figure 35 | Chemical structure of the oligomeric zinc complex and schematic representation of its optical self-healing process. [89]

A solution of this polymer is highly viscous, and after evaporation of the solvent, the remaining residue consists of a colorless, elastic film. These films showed a microphase-separated, lamellar morphology in which the metal complexes form a hard phase that physically cross-links the soft alkane domain. Excitation of metal–ligand motifs and conversion of the absorbed energy to heat causes disengagement of the metal–ligand motifs entailing supramolecular recombination and self-healing. This approach towards healable materials, based on supramolecular polymers and on a light–heat conversion step, could be applied to a wide range of supramolecular materials that use various chemistries.

In this bibliographic introduction, we have given an overview of several domains of current interest in chemical sciences and which will be combined in the following parts of this manuscript, namely supramolecular chemistry, molecular machines, and supramolecular polymers. In particular, we have shown that the idea of coupling [c2]daisy chain rotaxanes in polymers has been discussed by the groups of Stoddart and Grubbs. However, due to low polymerization degrees and low solubilities, their systems precluded the actuation and characterization of coupled translational motions towards mesoscopic scales.

Chapter 2 : Synthesis and Characterization of Covalently Polymerized Rotaxanes

In the first chapter we have given a bibliographic overview of the concepts and scientific achievements related to our project. With these ideas in mind, the objective of my PhD work has been to develop a new kind of responsive molecular machine-based material which can contract upon pH modulation over several length scales. For that, we have decided to investigate how well-designed rotaxane-based covalent/supramolecular polymers could lead these structures and combine nanoscopic translation motions in order to translate them to mesoscales and above.

At first, we will start describing the syntheses of a covalent polyrotaxane for comparison with the supramolecular ones. The polyrotaxane consists of a bistable pseudo-rotaxane monomer condensed with a symmetrical bis-oligophenylacetylene-benzyl-N_3 dumbbell. The strategy used to prepare the interwoven target molecules is based on the polymerisation of pseudo[c2]daisy chains by the copper(I)-catalyzed Huisgen alkyne-azide 1,3- dipolar cycloaddition, also called "CuAAC click chemistry". [90] This chapter concerns the synthesis of the covalent polyrotaxane, and the characterization of the molecules needed for the achievement of the project. A combination of ^{1}H NMR, static light scattering, dynamic light scattering and GPC techniques was planned to characterize these polymers, e.g., their molecular weights, as well as the expected pH-triggered contraction/extension process.

1/ Retrosynthetic Approach

The chemical structure of the targeted rotaxane **25** monomer has a bistable nature: one of the recognition sites (station) is a secondary dialkylammonium ($R_2NH_2^+$) center and the other site is a triazolium unit (Scheme 2). The macrocyclic DB24C8 part is known to have a better affinity for the N-benzylammonium template than for the triazolium one, and no affinity at all for the N-benzylamine moiety, thus allowing the two states of the molecular shuttle (contraction and extension) depending on the protonation. The key step of its synthesis was envisioned by the reductive amination between the preliminary synthesized crown ether

[90] Kolb, H. C.; Finn, M. G.; Sharpless, K. B. Click Chemistry: Diverse Chemical Function from a Few Good Reactions. *Angew. Chem., Int. Ed.* **40**, 2004–2021 (2001).

aldehyde **5** and the primary amine linker **9**. The corresponding amine should provide, after protonation, the [c2]daisy chain precursor **11** (Scheme 2).

The syntheses of symmetrical bis-oligophenylacetylene-benzyl-N_3 dumbbell **23** was envisaged from the bis-TMS protected oligophenylacetylene **17**, which could be obtained by iterative sonogashira couplings and silyl groups deprotections.

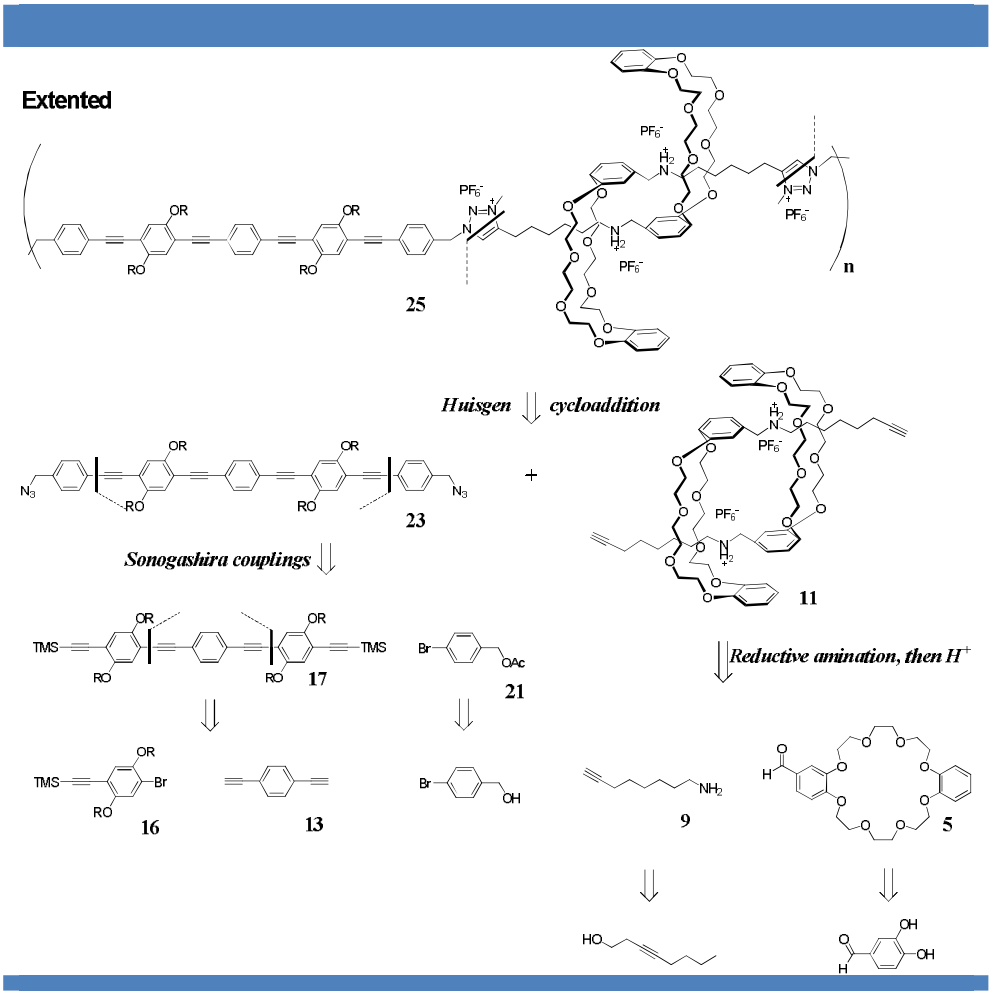

Scheme 2 | Retrosynthesis of polyrotaxane **25** from symmetric dumbbell **23** and pseudo-rotaxane **11**.

2/ Synthesis and characterization of pseudo-rotaxanes

*a) Crown-ether aldehyde **5***

The synthesis of this macrocyclic DB24C8 **5** was first described by Stoddart *et al.* (scheme 3). [91] Alkylation of 3,4-dihydroxybenzaldehyde with commercially available 2-[2-(2-Chloroethoxy) ethoxy] ethanol proceeded under basic conditions in DMF to afford diol **3** in very good yield (93%). Tosylation of diol **3**, under standard conditions, gave ditosylate **4**, which was subsequently reacted with catechol to give the formyl-substituted DB24C8 derivative **5** in reasonable yield (Scheme 3).

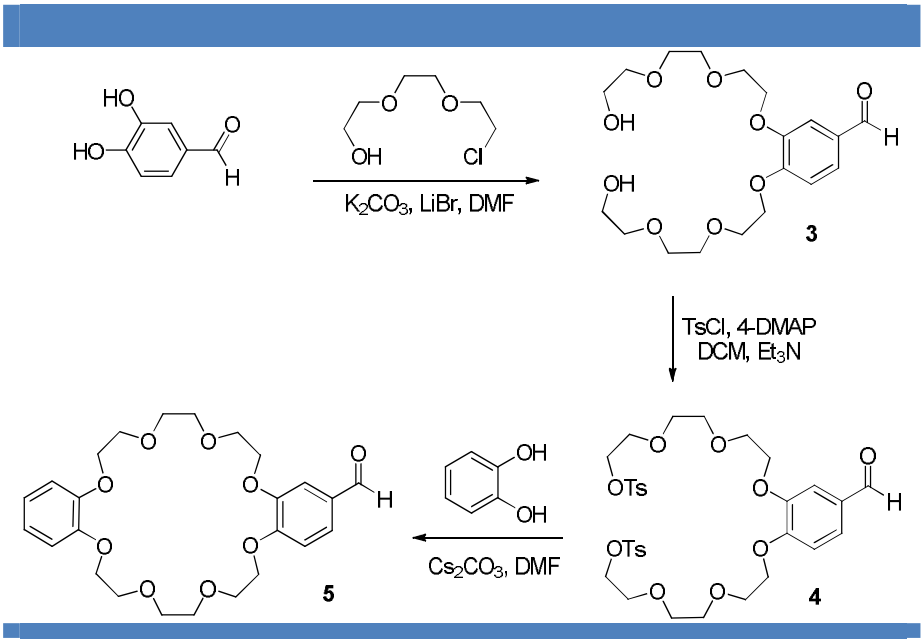

Scheme 3 | Synthesis of the macrocyclic DB24C8 **5**.[91]

Reaction conditions used for Scheme 3:

(a) 3,4-Dihydroxybenzaldehyde (1.0 equiv.), K_2CO_3 (1.0 equiv.), LiBr (1.0 equiv.), 2-[2-(2-Chloroethoxy) ethoxy] ethanol (2.2 equiv.), DMF, 100 °C, 3days, 93%; (b) 3,4-Bis{2-[2-(2-hydroxyethoxy)ethoxy]ethoxy}benzaldehyde (1.0 equiv.), Et_3N (10.0 equiv.), 4-DMAP (1.0 equiv.), TsCl (5.0 equiv.), 0-5°C, 84%; (c) Cs_2CO_3 (5.0 equiv.), ditosylate (1.0 equiv.), cathecol(1.0 equiv.), 100 °C, 8 days, 69%.

[91] Cantrill, S. J.; Youn, G. J.; Stoddart, J. F.; Supramolecular Daisy Chains. *J. Org. Chem.* **66**, 6857-6872 (2001).

*b) Primary amine linker **9***

Oct-7-yn-1-ol **6** was obtained in 81% yield by base-promoted isomerization of internal alkynyl alcohol of the commercially available 3-octyn-1-ol with sodium 2-aminoethylamide generated in situ from sodium hydride and ethylenediamine ("acetylenic zipper" reaction, Scheme 4). [92] 8-bromooct-1-yne **7** was subsequently obtained by the bromination of **6** under mild conditions using triphenylphosphine and carbon tetrachloride which is so called "Appel reaction" with a quantitative yield. [93]

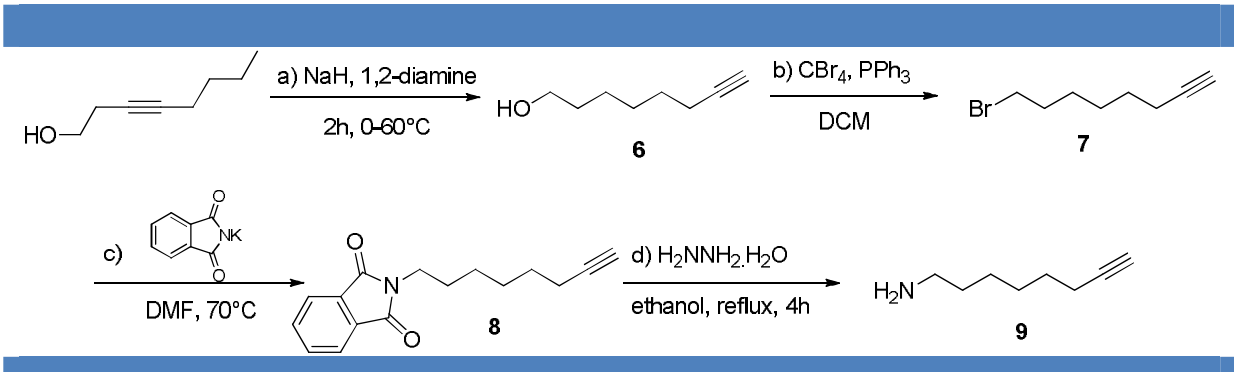

Scheme 4 | Synthesis of 8-aminooct-1-yne **9**.[64]

Reaction conditions used for Scheme 4:

(a) dry ethylene-1,2-diamine (7.0 equiv.), NaH (4.0 equiv.), 3-octyn-1-ol (1.0 equiv.),2h, 81%;(b) **6** (1.0 equiv.), CBr_4 (1.5 equiv.), PPh_3 (2.0 equiv.), reflux, 1hour, quantitative; (c) **7** (1.0 equiv.), potassium phtalimide (1.5 equiv.), 1h, 76%; (d) Hydrazine $hydrate_{aq}$. (3.5 equiv.), **8** (1.0 equiv.), reflux, 87%.

Finally, the 8-aminooct-1-yne **9** was obtained in two steps from **7** which was first treated with potassium phthalimide to produce intermediate **8**. After a deprotection reaction in ethanol using aqueous hydrazine, the corresponding primary amine linker **9** was obtained with a good yield of 87%. [64]

[92] (a) Macaulay,S. R. Isomerization of internal triple bonds of alkyn-1-ols with sodium hydride in 1,3-diaminopropane. *J. Org. Chem.* **45**, 735-737 (1980); (b) Denmark, S. E.; Yang, S. M.; Sequential ring-closing metathesis/Pd-catalyzed, Si-assisted cross-coupling reactions: general synthesis of highly substituted unsaturated alcohols and medium-sized rings containing a 1,3-cis–cis diene unit. *Tetrahedron* **60**, 9695-9708 (2004).
[93] Coutrot, F.; Busseron, E. A New Glycorotaxane Molecular Machine Based on an Anilinium and a Triazolium Station. *Chem. Eur. J.* **14**, 4784 – 4787 (2008).

c) *Synthesis and characterization of pseudo-rotaxanes*

After reductive amination between the previously synthesized crown ether aldehyde **5** and primary amine **9** using sodium borohydride, compound **10** was obtained with a yield of 76%. The subsequent protonation of the secondary amine and counterion exchange enforced the threading of the pseudorotaxane and produced the [c2]daisy chain precursor **11** (Scheme 5).

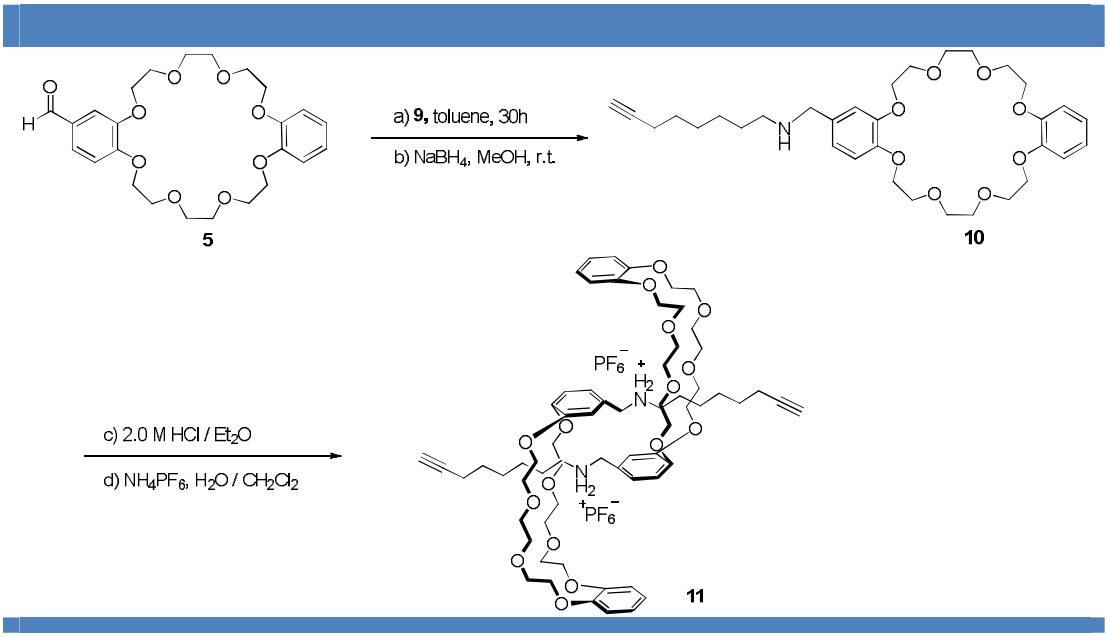

Scheme 5 | Synthesis of pseudo-rotaxane **11**.[93]

Reaction conditions used for Scheme 5:

(a) **5** (1.0 equiv.), **9** (1.1 equiv.), toluene, 30h; (b) $NaBH_4$, MeOH, 4h, 0-5°C, 76%; (c) **10** (1.0 equiv.), HCl 2M (6.2 equiv.); (d) NH_4PF_6 (2.5 equiv.),quantitative.

d) *Pseudo-rotaxanes stereoisomers*

As already mentioned by Stoddart [91] and Coutrot, [64] in compounds such as **11**, there are three possible dimeric interlocked stereoisomers, which arise from the nonsymmetrical substitution of the crown ether by the alkyne ammonium chain. When interlocked into dimers, the alkyne ammonium chain can bind the DB24C8 either by a forward or a backward covalent link, resulting in the formation of a "meso" supramolecular S_2-symmetric stereoisomer **11a** and a "threo" supramolecular racemic C_2-symmetric mixture of **11b**/**11c**. The major

supramolecular stereoisomer was found to be the "meso" supramolecular stereoisomer **11a** (Figure 36).

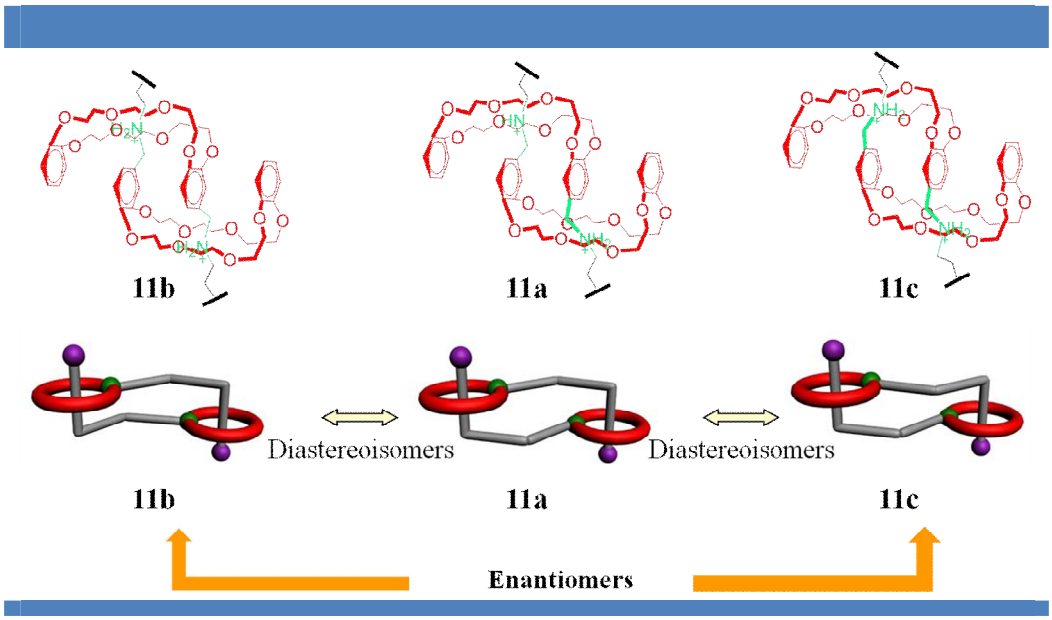

Figure 36 | The three possible [c2]daisy chain stereoisomers **11a-c**.[93]

The self-assembling behavior of compound **11** was studied by ^{1}H NMR in a hydrogen bond promoting solvent $CDCl_3$. After formation of the dimer, the methylene hydrogens H_{14} and H_{16} are dramatically shifted downfield, pointing out that the DB24C8 exclusively resides around the ammonium station (Figure 37) which is consistent with the literature.

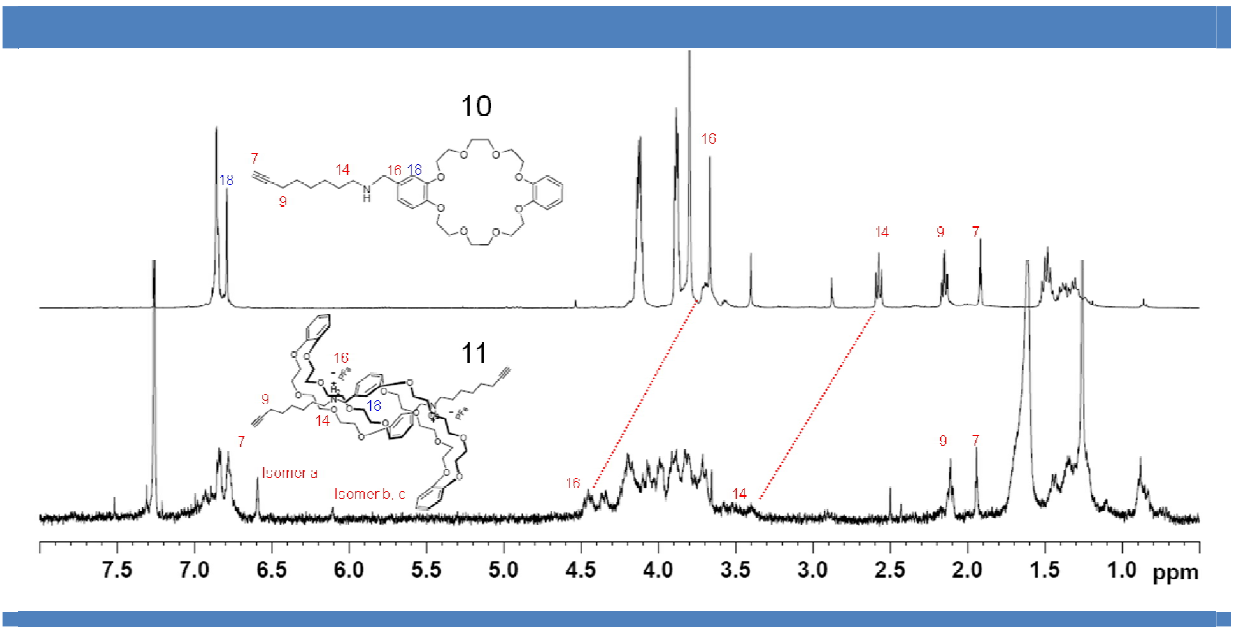

Figure 37 | A comparison of monomer **10** and of its corresponding interlocked dimeric species **11**.

e) Acid-base titration for the switching process

As soon as the pseudo-rotaxane was obtained, an acid-base titration for the threading / unthreading of pseudorotaxane **11** was explored by using CF_3COOD/DABCO (Figure 38). From the ^1H NMR spectra, we can find that the threading process can be controlled by protonation/deprotonation which confirmed the possibility to incorporate this unit in our planned system.

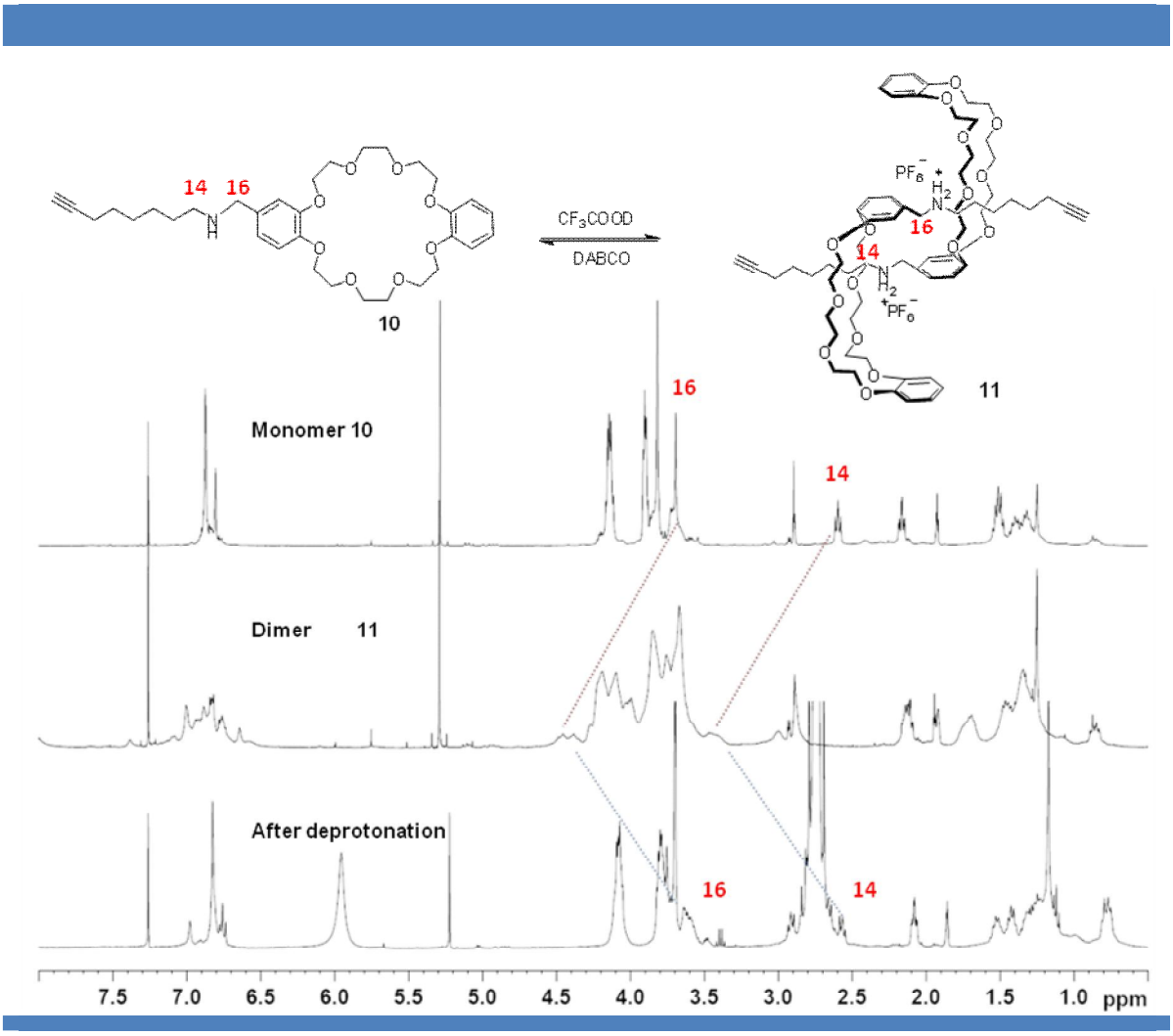

Figure 38 | Acid-base titration for the threading / unthreading of pseudorotaxane **11**.

2/ Synthesis and characterization of symmetric dumbbell 23 (n=1)

In order to introduce ethynyl groups in our planned rigid dumbbells, Hagihara-Sonogashira reactions were applied to our molecular system. [93] Trimethylsilyl-acetylene (TMSA) reacted with 1,4-dibromobenzene in C-C coupling processes catalyzed by palladium(0)/copper(I) iodide in THF. In this manner, the bis((trimethylsilyl)ethynyl)benzene **12** was generated in high yields (Scheme 6).

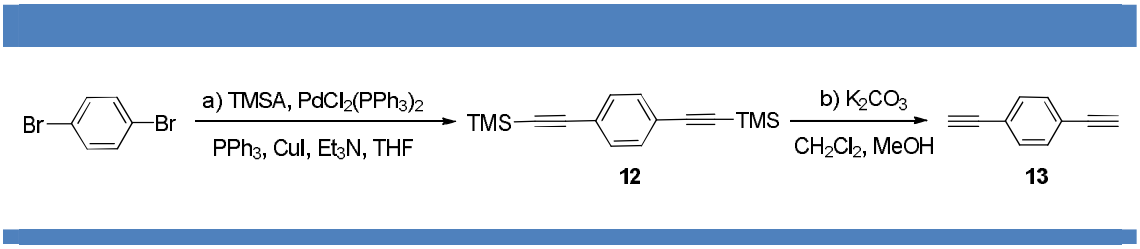

Scheme 6 | Synthesis of 1,4-bis((trimethylsilyl)ethynyl)benzene **13**.

Reaction conditions used for Scheme 6:

(a) 1,4-dibromobenzene (1.0 equiv.), trimethylsilylacetylene (2.2 equiv.), $Pd(PPh_3)_2Cl_2$ (0.1 equiv.), CuI (0.5 equiv.), PPh_3 (0.9 equiv.), TEA, THF, 80°C, overnight, 77%; (b) **12** (1.0 equiv.), K_2CO_3 (10.0 equiv.), CH_2Cl_2/MeOH, r.t., overnight, quantitative.

Deprotection of the alkynes was achieved with potassium carbonate in methanol/CH_2Cl_2 affording the desired compound **13** as a white solid. However this bis free alkyne appeared unstable, its colour turning from white to brown in a few days and this is why it was deprotected immediately prior to use in the next steps of the synthesis.

Bromination of 2-hexyl-1-decanol by Appel reaction gave compound **14**, which then reacted with 2,5-dibromohydroquinone to afford bis-ether **15**. It was found that this reaction could work better by using smaller quantities of the reactants (< 1.0 g each time), which is more convenient for the work-up procedure (Scheme 7).

[93] (a) Sonogashira, K.; Tohda, Y.; Hagihara, N.; A convenient synthesis of acetylenes: catalytic substitutions of acetylenic hydrogen with bromoalkenes, iodoarenes and bromopyridines. *Tetrahedron Lett.* **16**, 4467-4470 (1975); (b) Bull, S. R.; Palmer, L. C.; Fry, N. J.; Greenfield, M. A.; Messmore, B. W.; Meade, T. J.; Stupp, S. I. A Templating Approach for Monodisperse Self-Assembled Organic Nanostructures. *J Am Chem Soc*. **130**, 2742–2743 (2008).

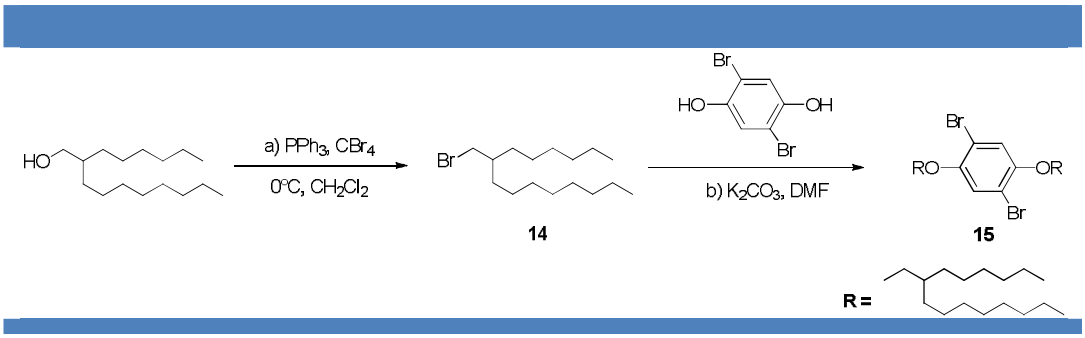

Scheme 7 | Synthesis of bis-ether **15**.

Reaction conditions used for Scheme 7:

(a) 2-hexyl-1-decanol (1.0 equiv.) CBr_4 (1.5 equiv.), PPh_3 (2.0 equiv.), 0°C, 1h; (b) **14** (2.5 equiv.), K_2CO_3 (15.0 equiv.), 2,5-dibromohydroquinone (1.0 equiv.), DMF, 60°C, overnight, 66%.

The bis-ether **15** was then reacted with 1.0 equiv. of TMSA in a coupling reaction catalyzed by palladium(II)/copper(I) iodide in THF/Et_3N affording the mono-bromo compound **16** (Scheme 8). Compound **16** is one of the key intermediates which can be used as a building block to generate large π-conjugated molecules. Unfortunately, the best yield of this mono-bromo compound was only 34% using this procedure. An optimized synthetic pathway will be discussed in the next chapter.

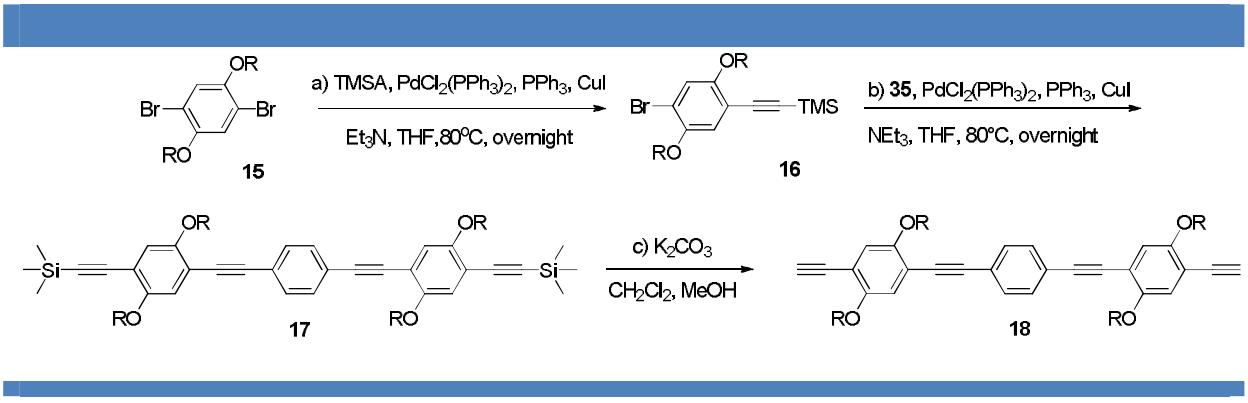

Scheme 8 | Synthesis of bis alkyne **18**.

Reaction conditions used for Scheme 8:

(a) **15** (1.0 equiv.), trimethylsilylacetylene (1.0 equiv.), $Pd(PPh_3)_2Cl_2$ (0.06 equiv.), CuI (0.12 equiv.), PPh_3 (0.12 equiv.), Et_3N, THF, 80°C, overnight, 34%; (b) **13** (1.0 equiv.), **16** (2.2 equiv.), $Pd(PPh_3)_2Cl_2$ (0.1 equiv.), CuI (0.9 equiv.), PPh_3 (1.6 equiv.), Et_3N, THF, 80°C, overnight, 75%; (c) **17** (1.0 equiv.), K_2CO_3 (10.0 equiv.), CH_2Cl_2/MEOH, overnight, r.t., 97%.

Mono-bromo building block **16** was then coupled with free bis alkyne **13** generating bis-TMS trisphenylene acetylene compound **17** by another Sonogashira coupling reaction performed with 75% yield. The lower yield compared with the above coupling reaction could be attributed to the unstability of the free bis alkyne **13**. The deprotection of bis-TMS compound **17** was successfully achieved by cleavage of the trimethylsilyl group with potassium carbonate in methanol/CH_2Cl_2 affording bis free alkyne compound **18**.

In order to synthesize the large bis-oligophenylacetylene-benzyl-alcohol dumbbell **19**, two synthetic routes were explored. The first route was envisioned by reacting free bis-alkyne **18** directly with commecially available 4-bromobenzyl alcohol. However in this case, two kinds of red viscous oils were obtained with low yields after purification, and in addition of expected compound **19**, the major one was the homo-coupling product **20** (Scheme 9).

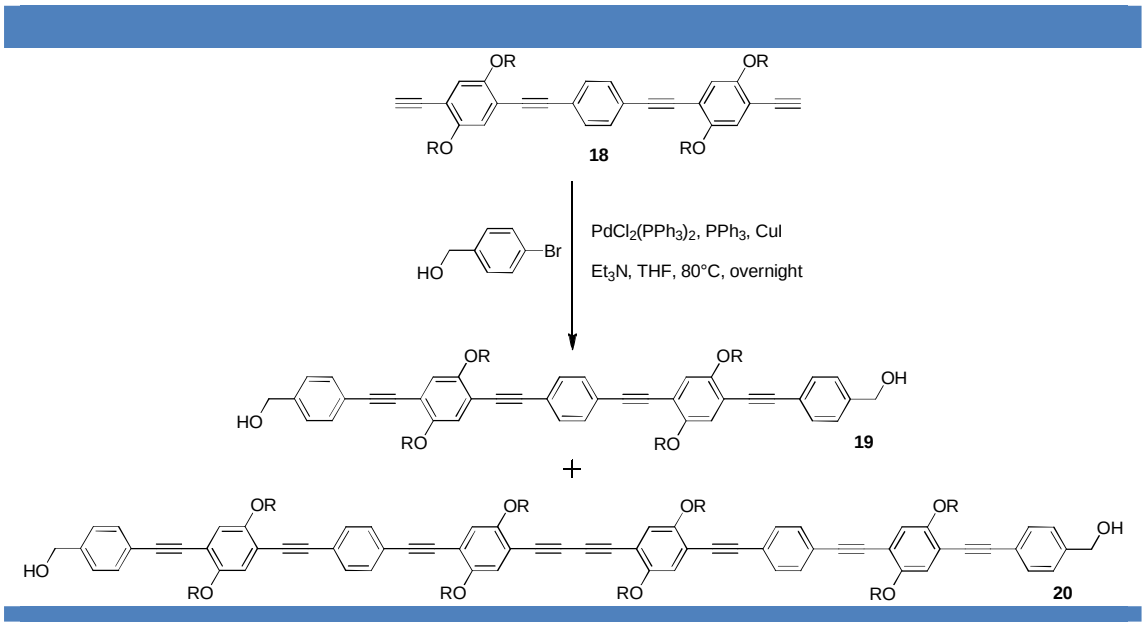

Scheme 9 | An exploration to synthesize bis-oligophenylacetylene-benzyl-alcohol dumbbell **20**.

Reaction conditions used for Scheme 9:

18 (1.0 equiv.), bromobenzyl alcohol (3.0 equiv.), $Pd(PPh_3)_2Cl_2$ (0.1 equiv.), CuI (0.3 equiv.), PPh_3 (1.0 equiv.), Et_3N, THF, 80°C, overnight.

This could be attributed to two problems: *i*. the starting materials (compound **13** and **18**) with two bis free alkynes were unstable; *ii*. as soon as the mono-cross coupling product with benzyl alcohol group formed, the homo-coupling rate between these mono-benzyl alcohol product became higher than that of the cross-coupling rate between the mono-benzyl alcohol

with another bromobenzyl alcohol.[94] Thus, the bromobenzyl alcohol was protected with an acetate group prior to Sonogashira reaction. The bis acetate protected dumbbell **22** was gratifying obtained by using this pathway with a very good yield, (Scheme 10).

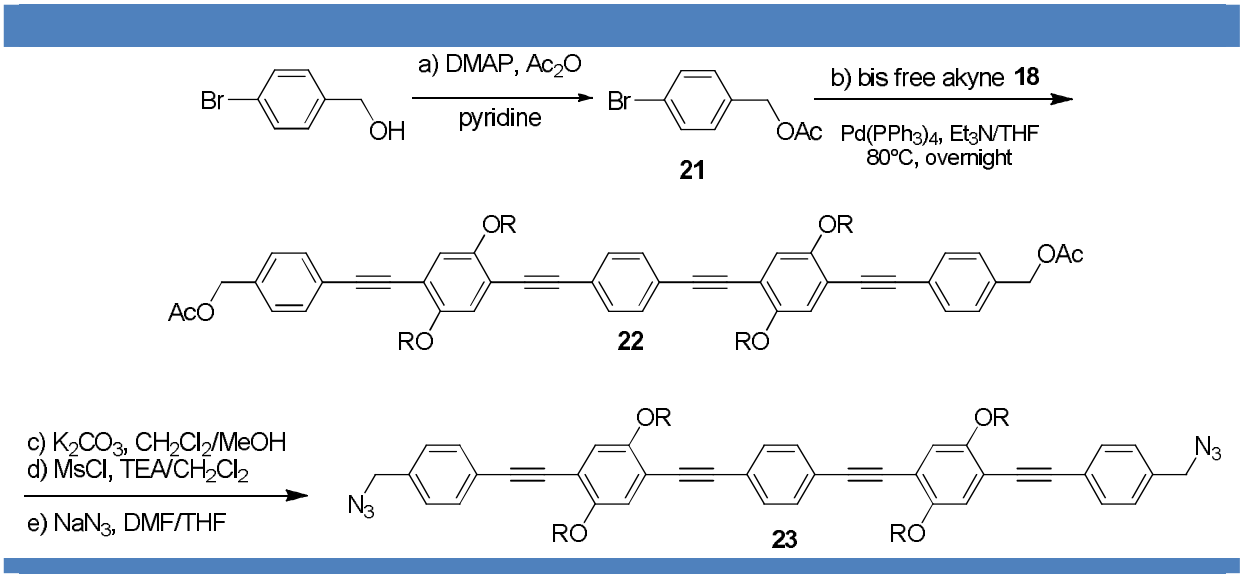

Scheme 10 | Synthesis of bis-oligophenylacetylene-benzyl-azide dumbbell **23**.

Reaction conditions used for Scheme 10:

(a) 4-bromobenzyl alcohol (1.0 equiv.), DMAP (0.1 equiv.), acetic anhydride/pyridine, 91%; [95](b) **18** (1.0 equiv.), **21** (2.2 equiv.), $Pd(PPh_3)_4$ (0.1 equiv.), Et_3N/THF, 70°C, overnight, 85%; (c) **22** (1.0 equiv.), K_2CO_3 (10.0 equiv.), CH_2Cl_2/MeOH (9:1), r.t., overnight; (d) MsCl (6.0 equiv.), Et_3N (6.0 equiv.), CH_2Cl_2, 0°C to r.t., overnight; (e) NaN_3 (10.0 equiv.), DMF/THF (1:1), 50°C, overnight, 58% (3 steps).

Bis-oligophenylacetylene-benzyl-azide **23** was then obtained by performing first the acetate deprotection with K_2CO_3 in a mixture of dichloromethane/methanol thus affording the corresponding bis-benzylic alcohol. Subsequent mesylation with methanesulfonyl chloride at 0°C, and treatment of the crude bis-benzylmesylate with sodium azide afforded the bis-oligophenylacetylene-benzyl-azide dumbbell **23** with an excellent 58% yield over 3 steps.

[94] Batsanov, A. S.; Collings, J. C.; Fairlamb, I. J. S.; Holland, J. P.; Howard, J. A. K.; Lin, Z.; Marder, T. B.; Parsons, A. C.; Ward, R. M.; Zhu, J. Requirement for an Oxidant in Pd/Cu Co-Catalyzed Terminal Alkyne Homocoupling To Give Symmetrical 1,4-Disubstituted 1,3-Diynes. *J. Org. Chem.* **70**, 703-706 (2005).
[95] Bertrand, M. B.; Neukom, J. D.; Wolfe, J. P. Mild Conditions for Pd-Catalyzed Carboamination of N-Protected Hex-4-enylamines and 1-, 3-, and 4-Substituted Pent-4-enylamines. Scope, Limitations, and Mechanism of Pyrrolidine Formation. *J. Org. Chem.*, **73**, 8851–8860 (2008).

4/ Polymerization and characterization of the symmetric dumbbell with pseudo-rotaxane by click chemistry

We have then turned to the synthesis of covalent polyrotaxanes and we first have probed the ability of the unthreaded macrocycle **10** to react with dumbbell **23**. We have thus coupled the symmetric dumbbell **23** with the macrocycle alkyne by "CuAAC click chemistry" producing bis-imidazole **24** in quantitative yield (Scheme 11).

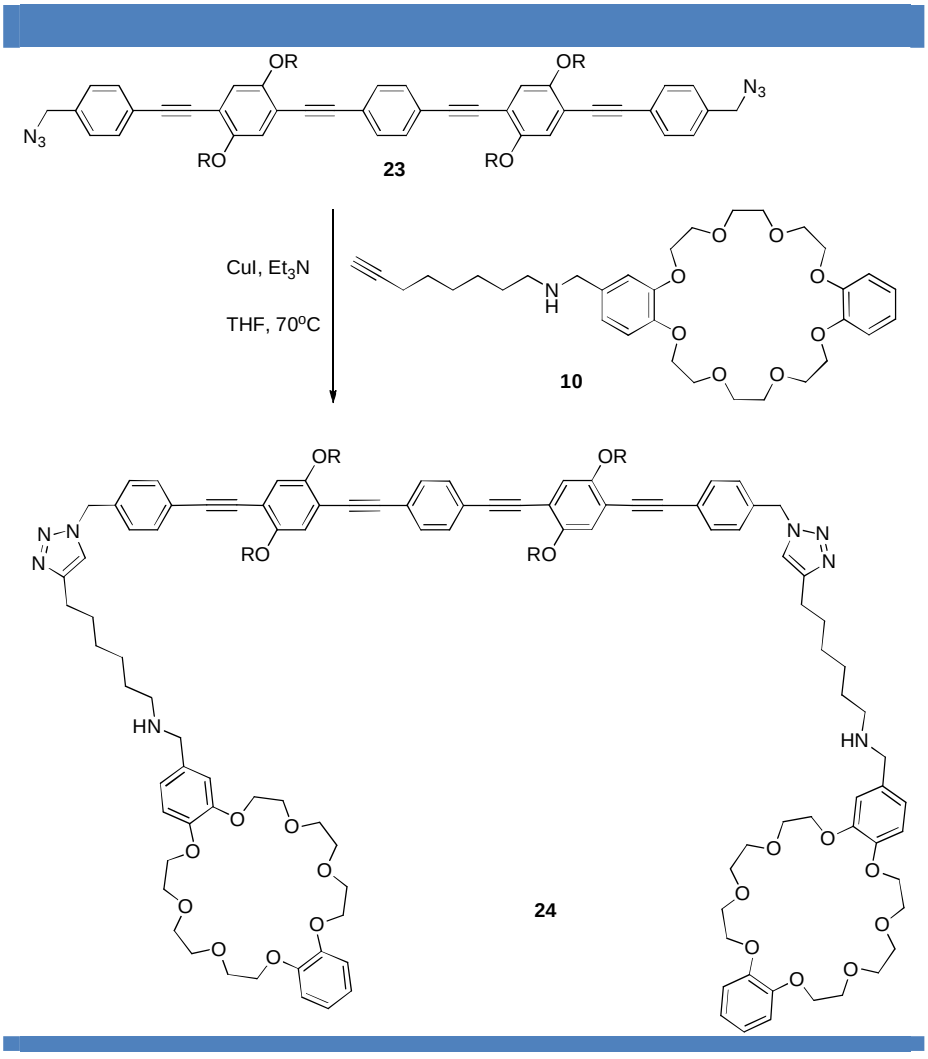

Scheme 11 | Coupling of symmetric bis-azide dumbbell **23** with macrocyclic monomer **10** as a model for the polymerization reaction (See annex 1 for NMR spectra).

Reaction conditions used for Scheme 11:

23 (1.0 equiv.), **10** (2.1 equiv.), CuI (1.0 equiv.), NEt_3/THF (1:1), 70°C, overnight.

Then the polymerisation of symmetric dumbbell **23** with pseudo-rotaxane **11** to form covalent mechanically interlocked polymers was envisaged using different reaction conditions (Scheme 12, Table 1).

Table 1 | Different conditions screened for the polymerization by "CuAAC click chemistry"

[a] DP < 10

Conditions	Observed Product
CuI, NEt_3, THF, $CHCl_3$, 50°C	Short Oligomers [a]
PMDETA, CuBr, CH_2Cl_2	Short Oligomers [a]
$Cu(CH_3CN)_4PF_6$, 2,6-lutidine, CH_2Cl_2, r. t.	Polymer
$Cu(CH_3CN)_4PF_6$, 2,6-lutidine, CH_2Cl_2/CH_3CN, r. t.	Short Oligomers [a]

In most cases, we obtained some short oligomers. This was indicated by the fact that ^1H NMR in $CDCl_3$ in these cases are well defined, showing the characteristic chemical displacement of the benzylic signal from 4.4 ppm for dumbbell **23** up to 5.5 ppm for the "clicked" product. The integration of the two signals confirmed degrees of polymerization lower than 10. The gel permeation chromatography (GPC) was possible as these samples were soluble in THF, however, only low molecular weights of a few monomers were obtained. On the other hand, by using the $Cu(CH_3CN)_4PF_6$ with 2,6-lutidine as catalyst in CH_2Cl_2 at room temperature, it seems that longer polymers were obtained as indicated by the much broader signals observed by ^{1}HNMR. However, the resulting product was poorly soluble in chloroform but more soluble in acetonitrile and this is also why we also attempted a polymerisation in a mixture of CH_2Cl_2/CH_3CN which unfortunately produced again short chains. In addition, attempts to perform GPC in acetonitrile were not succesfull as the compound never went out of the column, probably because of the strong charge interactions with it. Finally, static preliminary light scattering experiments show very high molecular weights (> 10^6 Da) but this might be due to residual aggregations in acetonitrile. Further experiments are still in progress to investigate further these covalent polymers, but we have developed in parallel another strategy using supramolecular polymerization, which has become more promising and thus a priority of this thesis, as discussed in the next chapter.

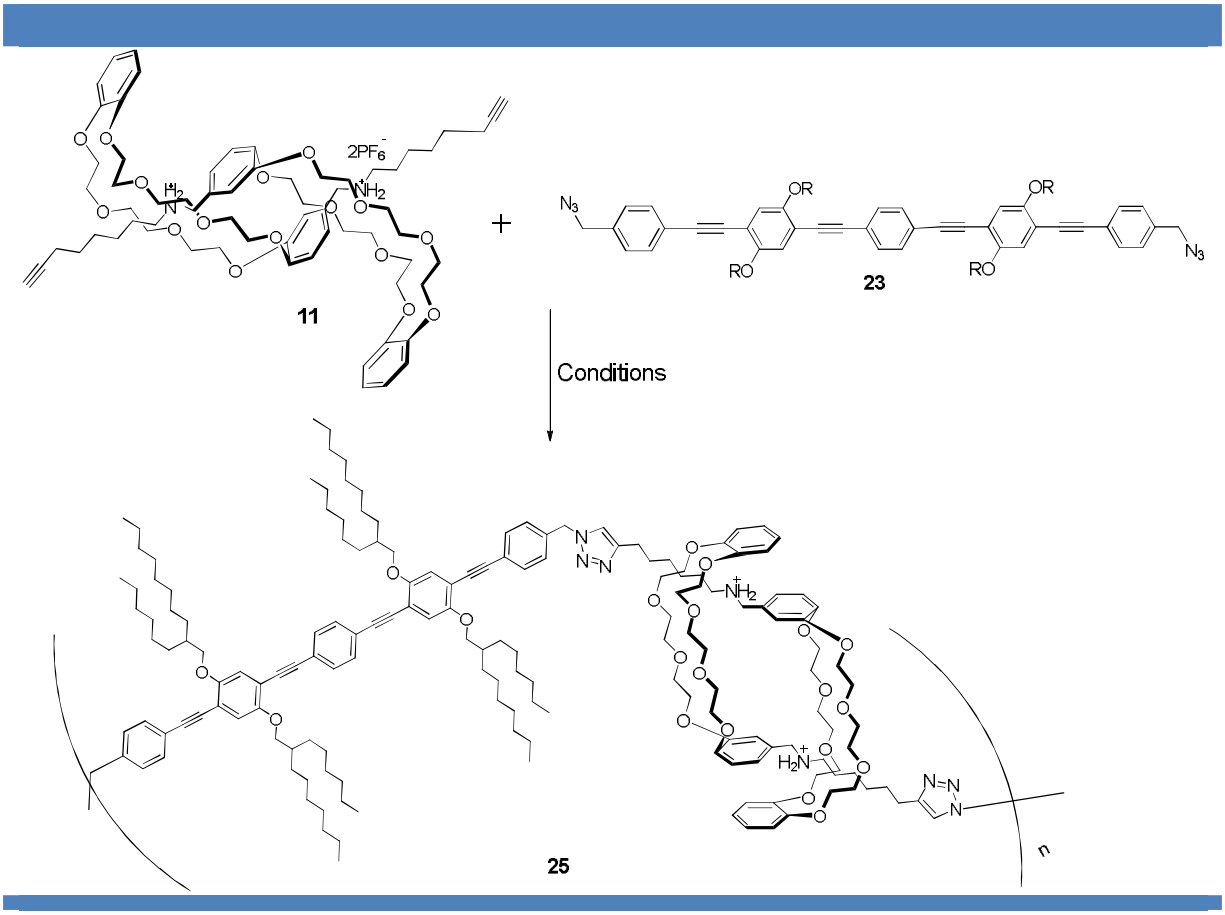

Scheme 12 | Coupling of symmetric bis-azide dumbbell **23** with macrocyclic monomer **11**.

5/ Synthesis of donor-acceptor amphiphilic rotaxane systems (J. J. Cid, A. Wolf, F. Niess)

In another parralel project, in collaboration with J. J. Cid, A. Wolf and F. Niess, pseudorotaxane **11** was used to couple hydrophilic donor triarylamine moiety with a hydrophobic acceptor unit perylene or [60]fullerene covalently linked at both extremities of the pseudo-rotaxane dimer. The amphiphilic interlocked structure presents two molecular stations with different affinities, that allows the occurrence of pH-switchable contraction and stretching movements for optoelectronic modulations (Figure 39).

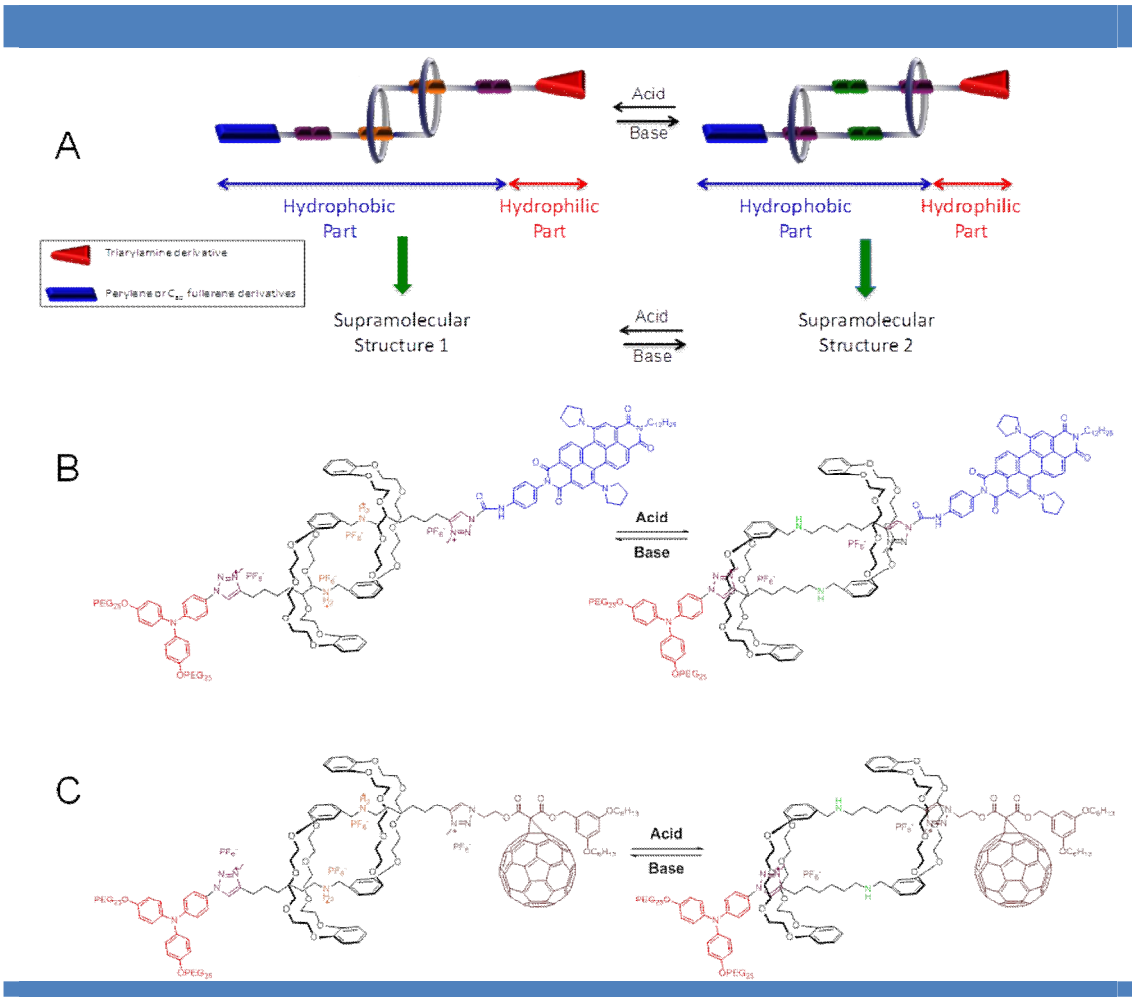

Figure 39 | (**A**) Schematic representation of the pH-dependent stretching movement involving switching in mesophases; pH-switchable donor/acceptor daisy chain-based rotaxanes bearing (**B**) triarylamine/perylene bismide derivatives, (**C**) triarylamine/[60]fullerene derivatives.

However, this project will not be discussed here as it does not constitute the main part of our work.

6/ Conclusion on Covalently Polymerized Rotaxanes

The work of this chapter describes the attempts to synthesize covalent polyrotaxanes which consist of a bistable pseudo-rotaxane monomer condensed with a symmetrical bis-oligophenylacetylene-benzyl-N_3 dumbbell.

The crown ether fragment **10** was synthesized in eight steps. Then the self-assembled dimer pseudo-rotaxane **11** was obtained and its titrations under protonation/deprotonation with d-

TFA/DBCO were studied by ^{1}H NMR in $CDCl_3$ and showed a good threading behavior. In the meantime, the symmetric bis-azide dumbbell **23** (11 steps) was synthesized from bis-TMS protected oligophenylacetylene **18** to prepare the covalent polyrotaxanes for comparison with the supramolecular ones by iterative Sonogashira couplings and silyl groups deprotection.

Polymerization of the symmetric dumbbell with pseudo-rotaxane by click chemistry was envisaged using different reaction conditions and proved to be difficult to achieve. In one case, polymers were possibly obtained as indicated by ^{1}H NMR and static light scattering, although further investigation should be performed which remains difficult due to the poor solubility of the products. However, all the chemistry developed in this part was at the basis of our parallel objective that has focused on the syntheses of metallo-supramolecular polyrotaxane as described in the next chapter.

Chapter 3 : Synthesis and Characterization of Metallo-Supramolecular Polymers

In chapter 2, we have shown that one of the difficulties in obtaining long polymers rests the necessary high yield of the click reaction. To improve this aspect, we envisioned to couple modified rotaxane monomers by supramolecular association and in particular by using coordination chemistry. For that, we planned to attach the ends of each dumbbell to different functional recognition unit, like terpyridine which can complex metal ions. The targeted daisy chain bistable rotaxane monomer consists of terpyridine ended unsymmtric dumbbell with different lengths (n = 0, 1) (Figure 40).

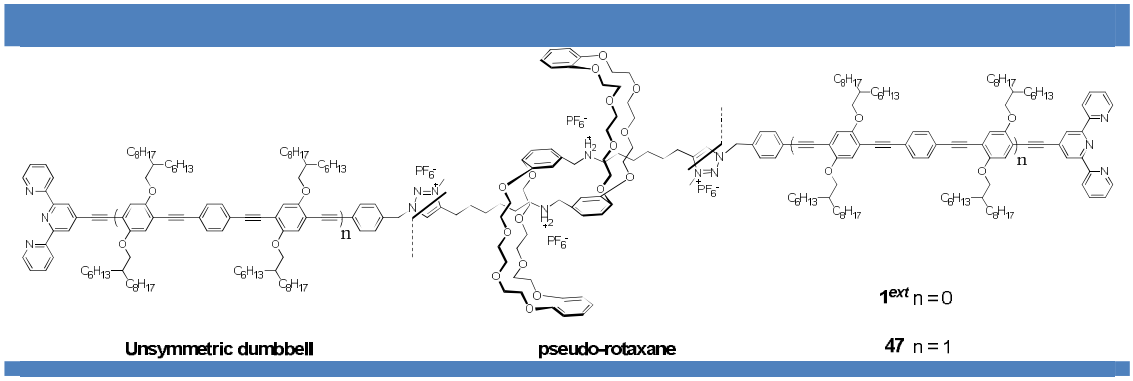

Figure 40 | Target daisy chain bistable rotaxanes **1**^{ext} and **47** which contain terpyridine ends.

These monomers were expected to polymerize by adding metal ions such as Zn(II) and Fe(II). This chapter will describe the synthesis of these metallo-supramolecular polymer rotaxanes. A combination of ^{1}H NMR, UV-Vis spectra, SLS, DLS, and SANS techniques were performed for the study of the supramolecular self-assemblies in order to get structural informations at various length scale and to probe their contraction and extension upon pH modulation.

1/ Retrosynthetic Approach

Compared to what was described in chapter 2 with the synthesis of symmetric dumbbell **23**, we will here focus on the synthesis of unsymmtric dumbbells **48** (n = 0) and **45** (n = 1) with two different lengths (Scheme 13).

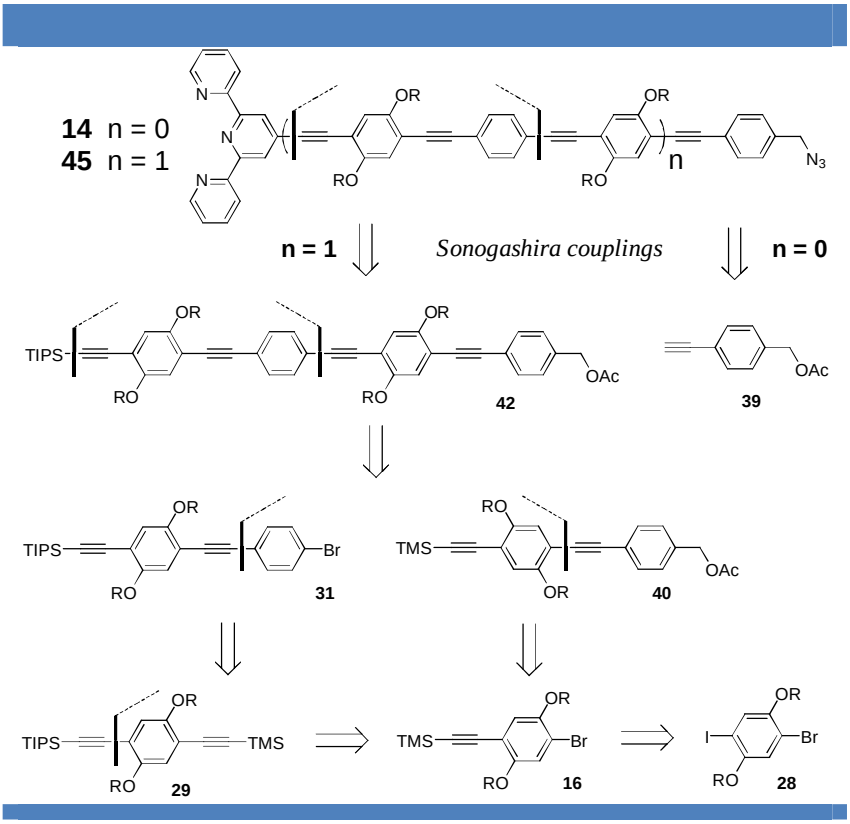

Scheme 13 | Retrosynthesis of unsymmtric dumbbells **48** (n = 0) and **45** (n = 1).

The targeted unsymmtric larger dumbbell **45** consists of two unsymmtric building blocks TIPS-bromo **31** and TMS-benzyl acetate **40** which were synthesized in a parallel procedure. From scheme 13, we can find that mono-bromo compound **16** is one of the key intermediates which serve to generate the large π-conjugated molecules. According to the previous work, the best yield of this compound was only 34%, and another optimized synthetic pathway was developed to improve it.

2/ Synthesis of the unsymmtric dumbbell 45 (n = 1)

For reaching the unsymmtric dumbbell **45**, we decided to start from the mixed bromo-iodo compound **28** in order to have different reactivities for the Sonogashira reaction.The

synthesis of mixed bromo-iodo **28** was performed by two different ways. It was first obtained by treatment of bis-alkylated 2,5-dibromohydroquinone **15** with *n*-BuLi (-80°C) followed by reaction with 1,2-diiodoethane (-60°C). However, only a poor yield of **28** was obtained (10%, Scheme 14).

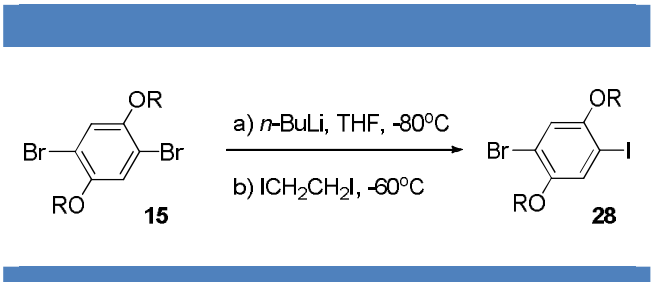

Scheme 14 | Synthesis of the mixed bromo-iodo derivative **28**.

Reaction conditions used for Scheme 14:

(a) **15** (1.0 equiv.), n-BuLi (1.0 equiv)),THF, -80°C; (b) ICH_2CH_2I (1.1 equiv.), -60°C, 10%.

For the other route, a mitsunobu reaction was performed using commercially available hydroquinone and 2-hexyldecanol in the presence of diisopropyl azodicarboxylate (DIAD) to produce 1,4-dialkylbenzene compound **26** (Scheme 15). [96]

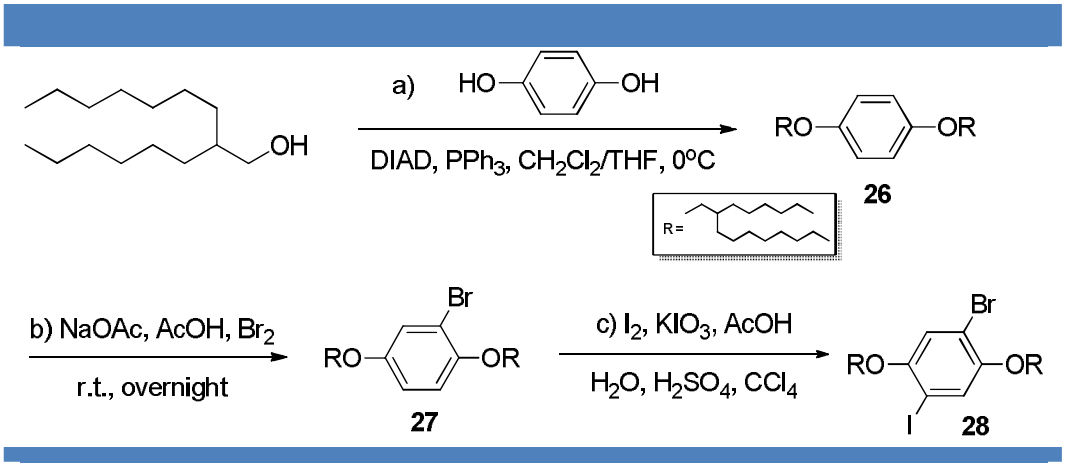

Scheme 15 | Synthesis of the mixed bromo-iodo derivative **28**.

Reaction conditions used for Scheme 15:

(a) Hydroquinone (1.0 equiv.), PPh_3 (2.5 equiv)), DIAD (2.5 equiv.), 2-hexyldecanol (2.5 equiv.), CH_2Cl_2/THF (3:1), 0°C - r.t., overnight, 56%; (b) **26** (1.0 equiv.), NaOAc (1.0

[96] Sparks, S. M.; Chen, C. L.; Martin, S. F. Tandem intramolecular benzyne-furan cycloadditions. Total synthesis of vineomycinone B2 methyl ester. *Tetrahedron* **63**, 8619-8635 (2007).

equiv.), Br_2 (1.0 equiv.), acetic acid, r.t., overnight, 86%; (c) **27** (1.0 equiv.), I_2 (1.0 equiv.), KIO_3 (0.5 equiv.), $AcOH/CCl_4/H_2O/H_2SO_4$, 70°C, overnight, 81%.

Bromination of **26** with equimolar amounts of bromine gave mono-bromo compound **27** with a yield of 86%. The mixed bromo-iodo derivative **28** was then prepared by treatment of compound **27** with $I_2/KIO_3/H_2SO_4$. [98] Compared with the former route, this way is more convenient experimentally because of the mild conditions and because the yield is much better, reaching 70% yield over 2 steps.

Selective coupling of the mixed bromo-iodo derivative **28** with TMSA afforded phenylene acetylene **16** in 88% yield (Scheme 16), which was much better than that of the previous route described in Chapter 2.

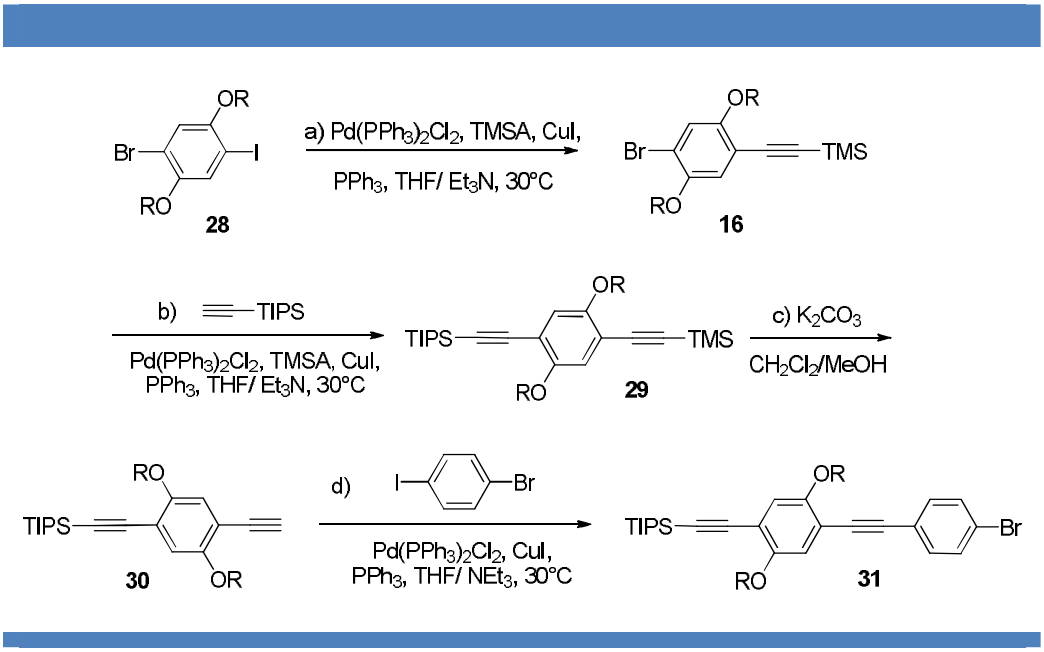

Scheme 16 | Synthesis of unsymmtric compound **31**.

Reaction conditions used for Scheme 16:

(a) **28** (1.0 equiv.), TMSA (1.4 equiv.), $Pd(PPh_3)_2Cl_2$ (0.06 equiv.), CuI (0.2 equiv.), PPh_3 (0.2 equiv.), Et_3N/THF, 30°C, overnight, 88%; (b) mono-bromo compound **16** (1.0 equiv.), (triisopropylsilyl)acetylene (1.5 equiv.), $Pd(PPh_3)_2Cl_2$ (0.06 equiv.), CuI (0.2 equiv.), PPh_3 (0.2 equiv.), Et_3N/THF, 80°C, overnight, 99%; (b) K_2CO_3 (5.0 equiv.), CH_2Cl_2/MeOH, r.t., overnight, 98%; (c) **30** (1.0 equiv.), p-bromoiodobenzene (1.5 equiv.), $Pd(PPh_3)_2Cl_2$ (0.06 equiv.), CuI (0.2 equiv.), PPh_3 (0.2 equiv.), Et_3N/THF, 30°C, overnight, 86%.

[98] (a) Babgi,B.; Rigamonti, L.; Cifuentes, M. P.; Corkery, T. C.; Randles, M. D.; Schwich, T.; Petrie, S.; Stranger, R.; Teshome, A.; Asselberghs, I.; Clays, K.; Samoc, M.; Humphrey, M. G. Length-Dependent Convergence and Saturation Behavior of Electrochemical, Linear Optical, Quadratic Nonlinear Optical, and Cubic Nonlinear Optical Properties of Dipolar Alkynylruthenium Complexes with Oligo(phenyleneethynylene) Bridges. *J. Am. Chem. Soc.* **131**, 10293–10307 (2009); (b) Meier, H.; Ickenroth, D.; Stalmach, U.; Koynov, K.; Bahtiar, A.; Bubeck, C. Preparation and Nonlinear Optics of Monodisperse Oligo(1,4-phenyleneethynylene)s. *Eur. J. Org. Chem.*, 4431-4443 (2001).

We then developed parallel pathways to synthesize the two building blocks **31** and **40**. In a first toute, unsymmtric compound **29** was obtained with 99% yield by treatment of **16** with (triisopropylsilyl)acetylene using palladium cross-coupling chemistry (Scheme 16). Selective deprotection of alkyne **29** was achieved with potassium carbonate in methanol/CH_2Cl_2. [99] Unsymmtric compound **31** was obtained by treatment of the deprotected compoud **30** with *p*-bromoiodobenzene in the presence of $Pd^{II}Cl_2$ and copper iodide with a good yield of 80%.

In the other parallel route, many attempts were tried to reach compound **40**. First, we decided to use 4-ethynylbenzyl alcohol **32** as starting material. This molecule appeared quite sensitive when exposed to air or stored for a long time. However, the free alkyne-benzyl alcohol **34** was obtained by reaction of **32** with mono-bromo compound **16** followed by treatment with K_2CO_3 in THF/CH_3OH (Scheme 17). [100]

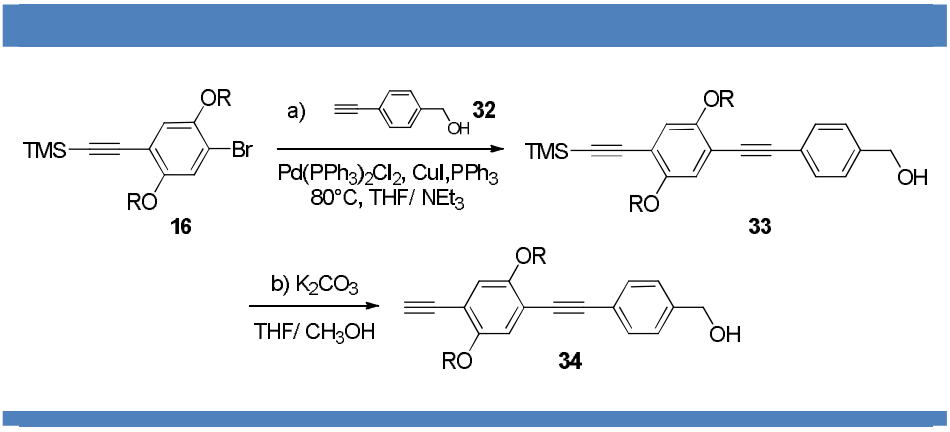

Scheme 17 | Synthesis of alkyne-benzyl alcohol **34**.

Reaction conditions used for Scheme 17:

(a) mono-bromo compound **16** (1.0 equiv.), 4-ethynylbenzyl alcohol **32** (1.2 equiv.), $Pd(PPh_3)_2Cl_2$ (0.1 equiv.), CuI (0.2 equiv.), PPh_3 (0.2 equiv.), TEA/THF, 80°C, overnight, 56%; (b) K_2CO_3 (10.0 equiv.), CH_2Cl_2/MeOH, r.t., overnight, 98%.

The next key coupling reaction was performed between the unsymmtric compounds **31** and **34**. Although this reaction was carried out about 15 times using different procedures, the best yield for compound **36** was only 13%, and the homo-coupling compound **37** was the major product (Scheme 18). This could be attributed to the same reason when we synthesized the bis-benzyl alcohol symmetric dumbbell **19**.

[99] Höger, S.; Bonrad, K.; Mourran, A.; Beginn, U.; Möller, M. Synthesis, Aggregation, and Adsorption Phenomena of Shape-Persistent Macrocycles with Extraannular Polyalkyl Substituents. *J. Am. Chem. Soc.*, **123** , 5651–5659 (2001).
[100] Hiraoka, S.; Hirata, K.; Shionoya, M. A Molecular Ball Bearing Mediated by Multiligand Exchange in Concert. *Angew. Chem. Int. Ed.*, **43**, 3814 –3818 (2004).

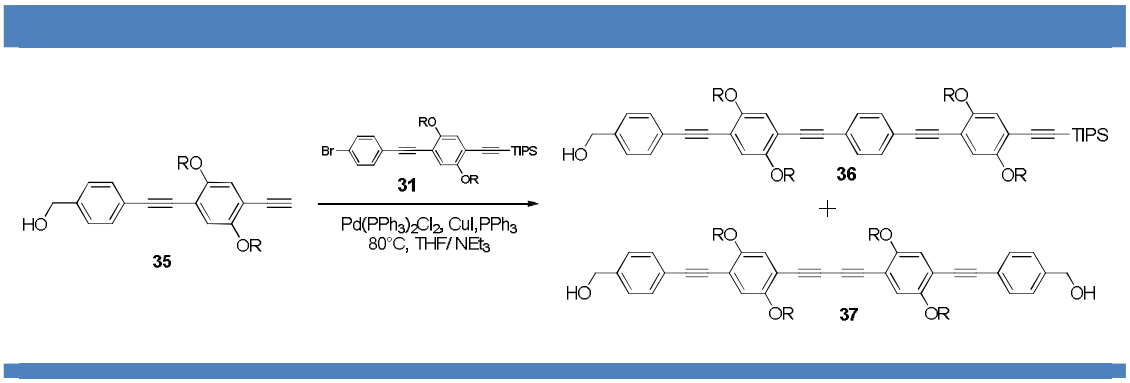

Scheme 18 | Synthesis of TIPS-benzyl alcohol **36**.

Reaction conditions used for Scheme 18:

31 (1.0 equiv.), free alkyne-benzyl alcohol **35** (1.0 equiv.), $Pd(PPh_3)_2Cl_2$ (0.1 equiv.), CuI (0.2 equiv.), PPh_3 (0.2 equiv.), Et_3N/THF, 80°C, overnight, 13%.

As examples of Sonogashira coupling with free benzyl alcohol are scarce in the literature, commercially available 4-bromobenzyl alcohol was protected with an acetate group to produce compound **39** (Scheme 19). After Sonogashira coupling with TMSA, the selective deprotection of the 4-Trimethylsilylbenzyl acetate **39** was achieved with TBAF in THF. Compared to 4-ethynylbenzyl alcohol **32**, 4-ethynylbenzyl acetate **39** can be stored in fridge for several months.

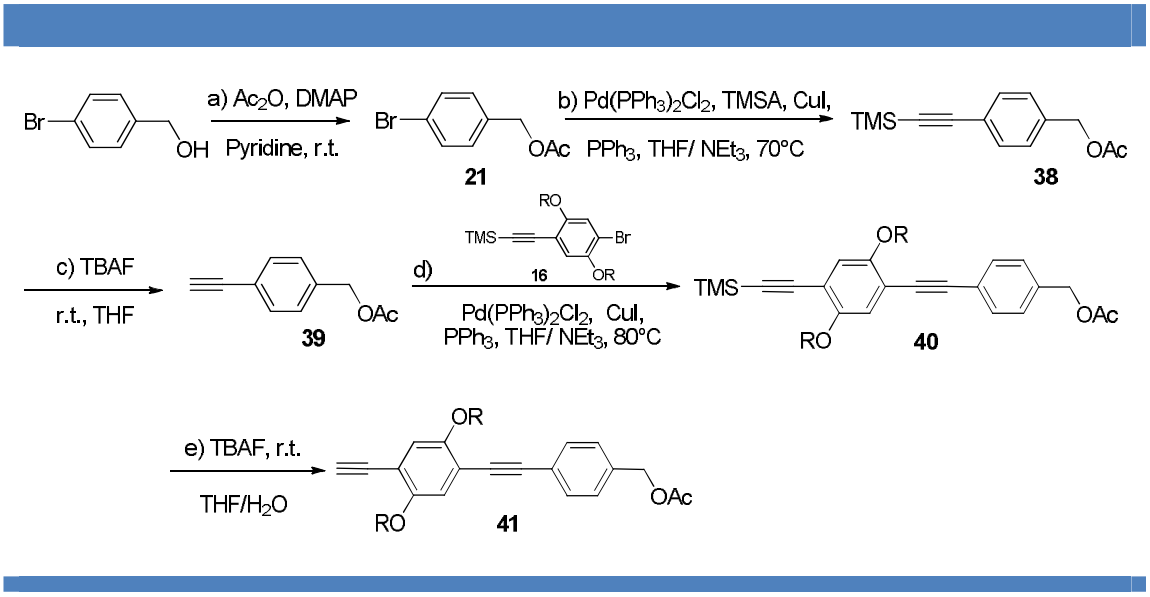

Scheme 19 | Synthesis of the alkyne-benzyl acetate **41**.

Reaction conditions used for Scheme 19:

(a) 4-bromobenzyl alcohol (1.0 equiv.), DMAP (0.1 equiv.), Ac_2O/Pyridine (n=1:1), r.t., 91%; (b) **21** (1.0 equiv.), TMSA (1.2 equiv.), $Pd(PPh_3)_2Cl_2$ (0. 1 equiv.), CuI (0.2 equiv.), PPh_3 (0.2 equiv.), Et_3N/THF, 70°C, 36h, 89%; (c) 4-Trimethylsilylbenzyl acetate (1.0 equiv.), TBAF(0.09 equiv.), THF, r.t., 30min; (d) mono-bromo compound **16** (1.0 equiv.), 4-ethynylbenzyl acetate **39** (1.5 equiv.), $Pd(PPh_3)_2Cl_2$ (0.1 equiv.), CuI (0.2 equiv.), PPh_3 (0.2 equiv.), Et_3N/THF, 80°C, overnight, 87%; (e) TMS-benzyl compound **40** (1.0 eqiv.), TBAF (2.0 equiv.), THF/H_2O, 81%.

Momo-bromo compound **16** was then reacted with 4-ethynylbenzyl acetate **39** to afford TMS-benzyl compound **40** with 87% yield. Selective deprotection of the alkynyl compound **40** was achieved using TBAF in THF to yield **41** with 81%.

The unsymmtric TIPS-benzyl acetate **41** was then obtained by the Pd(0)- catalyzed cross-coupling of alkyne benzyl acetate **41** with compound **31** with 78% yield (Scheme 20).

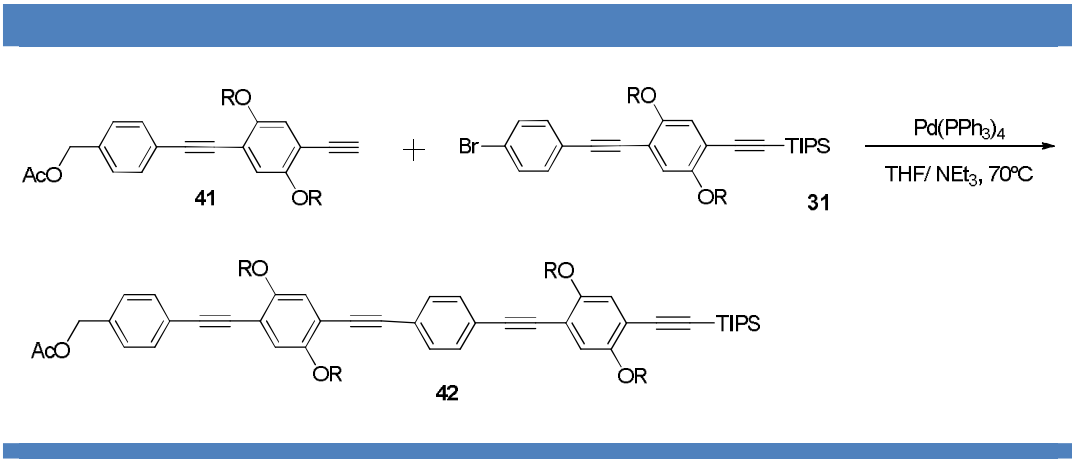

Scheme 20 | Synthesis of the unsymmtric TIPS-benzyl acetate **42**.

Reaction conditions used for Scheme 20:

(a) alkyne benzyl acetate **41** (1.0 equiv.), compound **31** (1.0 equiv.), $Pd(PPh_3)_4$ (0.1 equiv.), Et_3N/THF, 70°C, overnight, 78%.

Terpyridine benzyl acetate **44** was obtained by selective deprotection of the TIPS benzyl acetate **42** with TBAF in THF followed by Sonogashira coupling with 2,2′:6,2″-terpyridine triflate (provided by Dr. Frederic Niess) with a very good yield (Scheme 21).

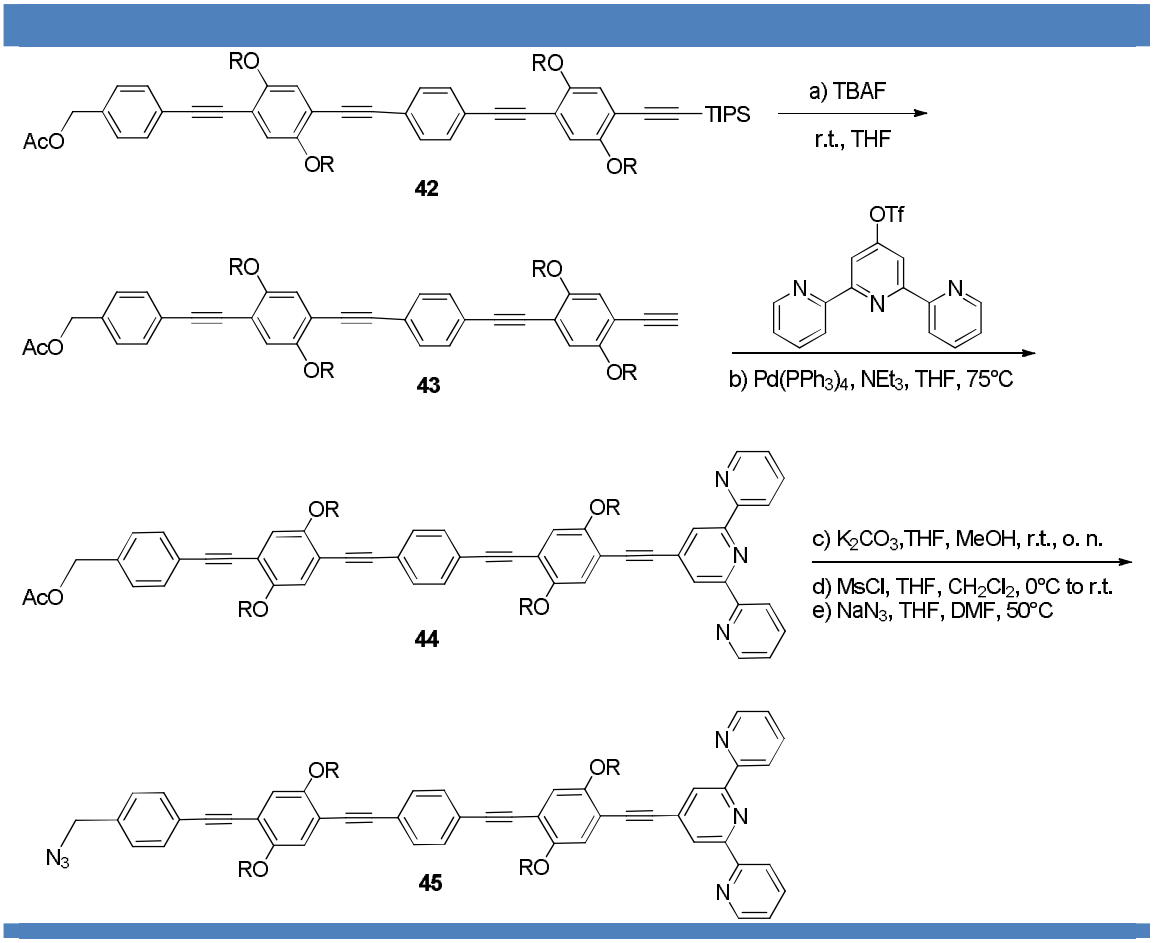

Scheme 21 | Synthesis of the terpyridine-benzyl alcohol **44**.

Reaction conditions used for Scheme 21:

(a) TIPS-benzyl acetate **42** (1.0 equiv.), TBAF (2.0 equiv.), THF, 83%. (b) 2,2′:6,2″-terpyridine triflate (1.2 equiv.), $Pd(PPh_3)_4$ (0.1 equiv.), Et_3N/THF, 60°C, overnight, 85%; (c) **44** (1.0 equiv.), K_2CO_3 (10.0 equiv.), CH_2Cl_2/MeOH (9:1), r.t., overnight; (d) MsCl (6.5 equiv.), Et_3N (6.5 equiv.), CH_2Cl_2, 0°C to r.t., overnight; (e) NaN_3 (10.0 equiv.), DMF/THF (1:1), 50°C, overnight, 60% (3 steps).

Finally the terpyridine benzyl azide **45** was obtained in three steps with 60% overall yield following the already improved sequence described in chapter 2: i) deprotection of the benzyl acetate of compound **44**; ii) followed by mesylation of the resulting benzyl alcohol using methanesulfonyl chloride at 0°C; iii) and nucleophilic substitution with sodium azide at 50°C (See Annex 2 for ^{1}H NMR).

With compound **45** in hands, we envisaged the copper(I)-catalyzed Huisgen alkyne-azide 1,3- dipolar cycloaddition with pseudo-rotaxane **11** and several conditions were tried (Scheme 22, Table 2). Unfortunately, we were not able to obtain the desired bis-terpyridine rotaxane **46**.

Table 2| Different conditions screened for the "CuAAC click chemistry" between compounds **11** and **45**

Conditions
45 (2.1 equiv.), **11** (1.0 equiv.), CuI (3.0 equiv.), CH_2Cl_2, 40°C, 6 days
45 (2.1 equiv.), **11** (1.0 equiv.), $Cu(CH_3CN)_4PF_6$ (4.0 equiv.), 2,6-lutidine (8.4 equiv.), CH_2Cl_2, microwave, 40°C
45 (2.1 equiv.), **11** (1.0 equiv.), $Cu(CH_3CN)_4PF_6$ (4.0 equiv.), 2,6-lutidine (8.4 equiv.), CH_2Cl_2/CH_3CN, r.t.

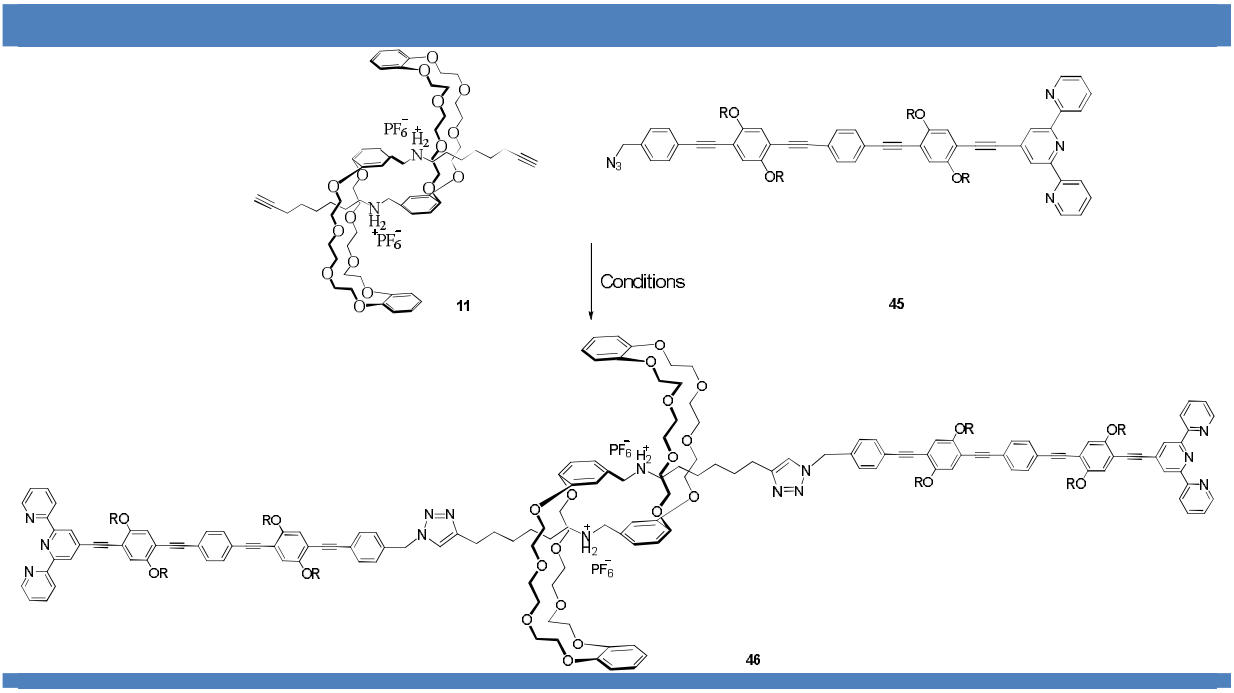

Scheme 22 | Attempted "CuAAC click chemistry" reaction between compounds **11** and **45**

Further attempts to synthesize compound **46** will be made in the next future but we decided to focus first on the synthesis of a short dumbbell **49** to produce a model rotaxane for metallo-supramolecular polymerization (see paragraph 3).

3/ Synthesis and characterization of model rotaxane (n=0)

In parallel with the synthesis of the dumbbell rotaxane **46**, we also explored the less complex model system leading to compound $\mathbf{1}^{ext}$ (n = 0, Figure 40, **p75**).

To access compound $\mathbf{1}^{ext}$, compound **48** was first obtained by the reaction of 2,2′:6,2″-terpyridine triflate with 4-ethynylbenzyl acetate **39** with 71% yield (Scheme 23). The terpyridine benzyl azide **49** was obtained in 66% overall yield using the classical three steps sequence: i). deprotection of the benzyl acetate; ii) followed by treatment with methanesulfonyl chloride at 0°C; iii) and reaction with sodium azide at 50°C.

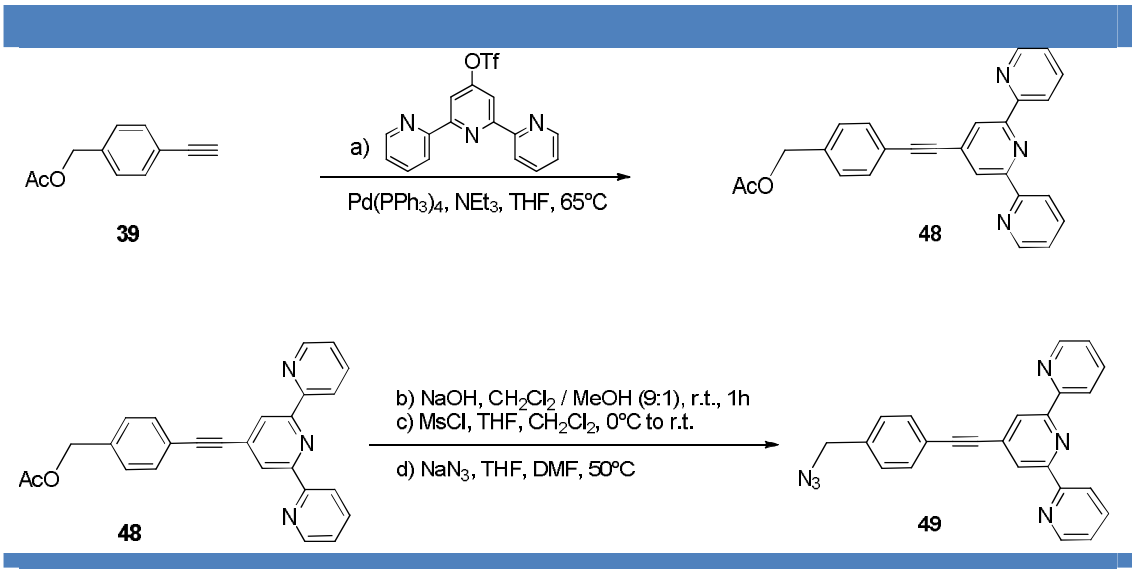

Scheme 23 | Synthesis of model terpyridine-benzyl azide **49**.

Reaction conditions used for Scheme 23:

(a) 2,2′:6,2″-terpyridine triflate (1.0 equiv.), 4-ethynylbenzyl acetate **39** (1.3 equiv.), $Pd(PPh_3)_4$ (0.1 equiv.), Et_3N/THF, 65°C, overnight, 71%; (b) **49** (1.0 equiv.), NaOH (10.0 equiv.), CH_2Cl_2/MeOH (9:1), r.t., 1h; (c) MsCl (3.3 equiv.), Et_3N (3.3 equiv.), CH_2Cl_2, 0°C to r.t., overnight; (d) NaN_3 (5.9 equiv.), DMF/THF (1:1), 50°C, overnight, 66% (3 steps).

Gratifyingly, the reaction between terpyridine azide **49** and pseudo-rotaxane **11** was efficiently carried out by microwave irradiation in a mixture of CH_2Cl_2/CH_3CN, and in the presence of $Cu(MeCN)_4PF_6$. For the methylation of the triazolium, $Cu(OTf)_2$ was introduced to first protect the terpyridine unit, followed by the addition of iodomethane. The final model terpyridine rotaxane $\mathbf{1}^{ext}$ was obtained by a series of extraction and counter ion exchange procedure with 92% yield (Scheme 24).

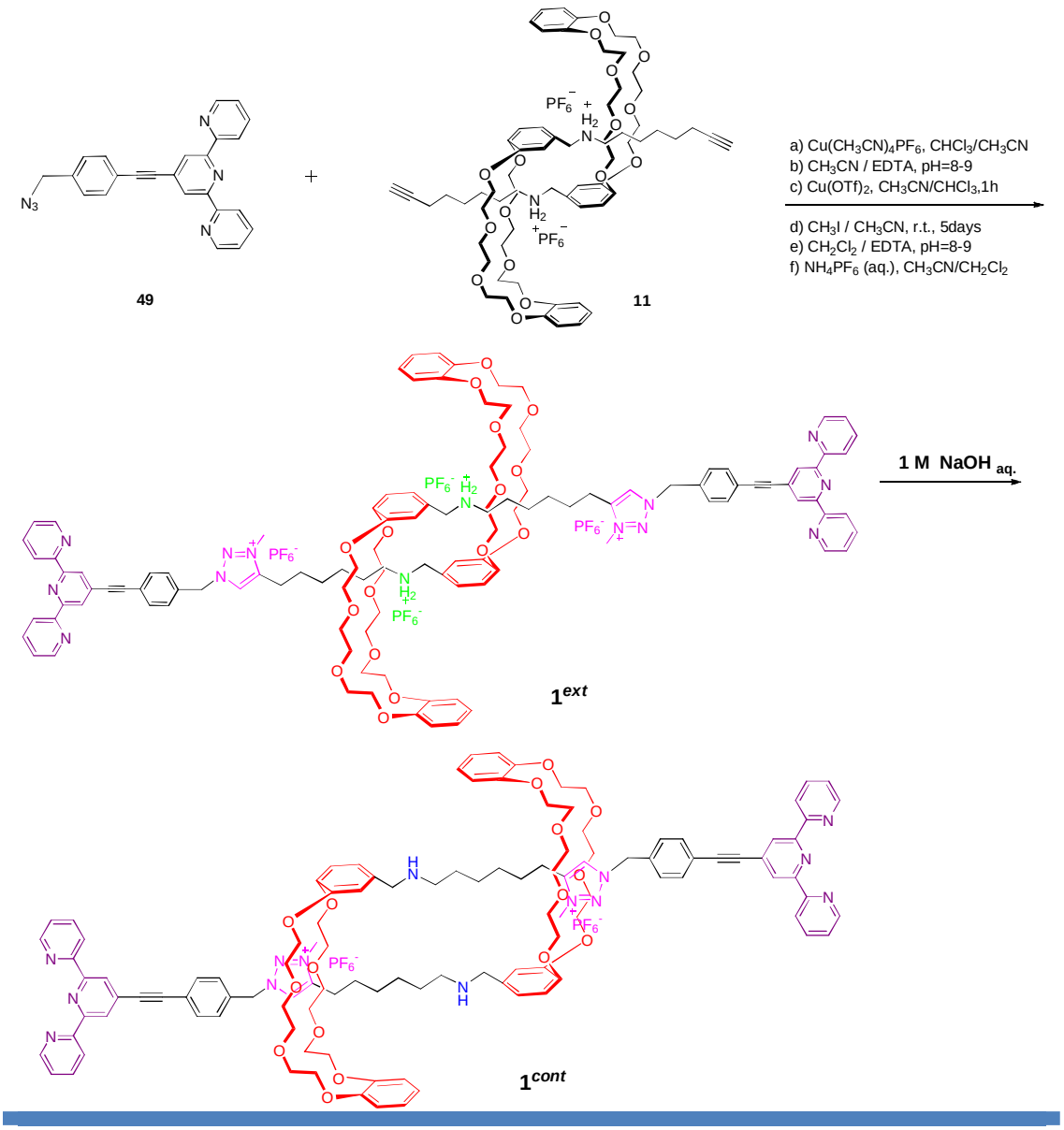

Scheme 24 | Synthesis of the protonated and deprotonated model terpyridine rotaxanes **1**^{ext} and **1**^{cont}.

Reaction conditions used for Scheme 24:

(a) pseudo-rotaxane **11** (1.0 equiv.), teypyridine azide **49** (2.1 equiv.), $Cu(CH_3CN)_4PF_6$ (8.3 equiv.), 2,6-lutidine (8.3 equiv.), $CHCl_3/CH_3CN$, 1h, 30°C; (b) EDTA aq.(pH ≈ 8-9), CH_3CN, 2h, 72% (2 steps); (c)$Cu(OTf)_2$ (3.0 equiv.), CH_3CN, 30°C, 1h; (d) CH_3I/CH_3CN (1:1), r.t., 5days; (e) EDTA aq.(pH ≈ 8-9), $CHCl_3$, overnight; (f) NH_4PF_6 aq. (8.0 eqiuv.), $CHCl_3/CH_3CN$, 92%.

The deprotonated terpyridine rotaxane **1**^{cont} was then easily obtained by washing protonated rotaxane **1**^{ext} with 1M $NaOH_{aq}$.

The bistable nature of this rotaxane is provided by the two binding sites on its axle, i.e. the secondary ammonium and the triazolium, which are known in the literature to present

different binding constants with the dibenzo-24-crown-8 ether. In its protonated form, the ammonium binds to the macrocycle (extended $\mathbf{1}^{ext}$), whereas, in its deprotonated one, the crown ether moves to the triazolium site (contracted $\mathbf{1}^{cont}$), as confirmed by ^{1}H NMR titrations in both directions using either trifluoroacetic acid or sodium hydroxide (Figure 40).

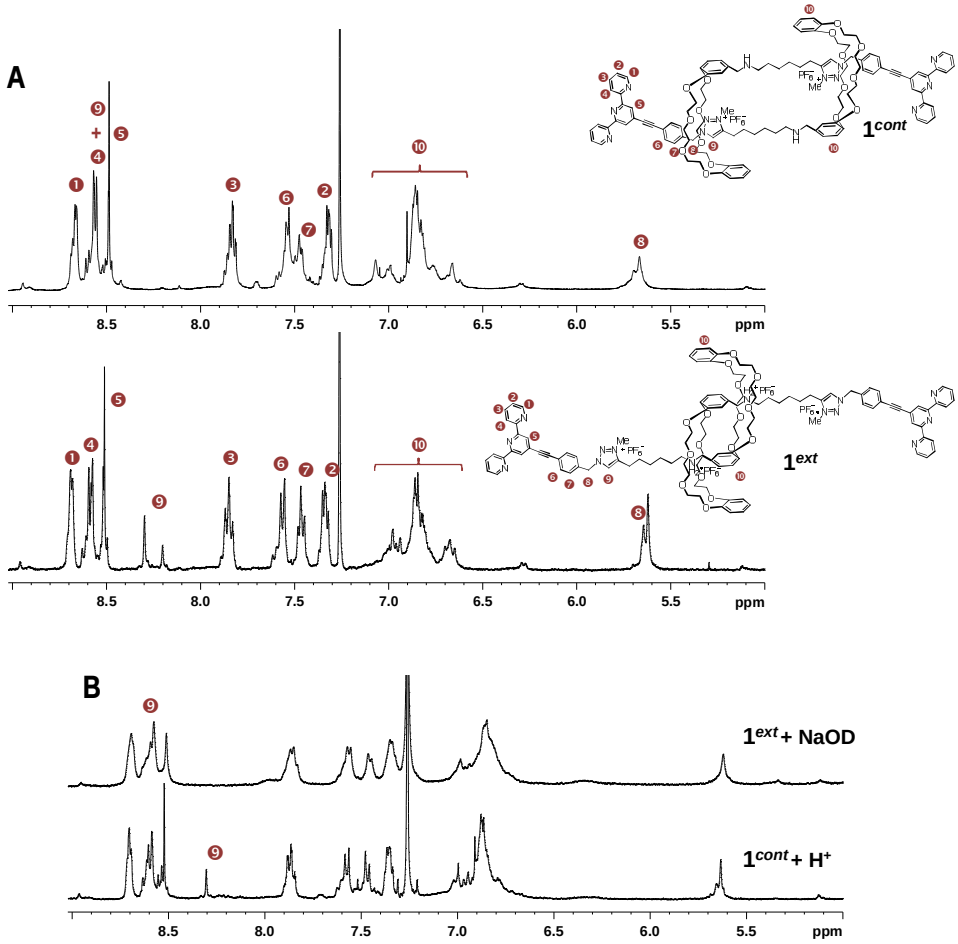

Figure 40 | (**A**) Characteristic ^{1}H NMR shifts of the imidazolium proton *number 9* in compounds $\mathbf{1}^{cont}$ and $\mathbf{1}^{ext}$, together with (**B**) the superimposed spectra of $\mathbf{1}^{ext}$ + 2.2 eq. NaOD (leading to $\mathbf{1}^{cont}$), and $\mathbf{1}^{cont}$ + 2.2 eq. *d*-TFA (leading to $\mathbf{1}^{ext}$).

4/ Characterization of the metallo-supramolecular polymers

a) ^{1}H NMR experiments

We then turned to the supramolecular polymerizations of **1**^{cont} and **1**^{ext} using one equivalent of either $Zn(OTf)_2$ or $FeCl_2$ as metal ions in a 1:1 mixture of $CDCl_3/CD_3CN$ ([**1**] = 10 mM). Upon the addition of 1.0 molar equivalent of **1**^{ext} to the solution of $FeCl_2$, the solution immediately turned purple as a characteristic of complex formation (Figure 41). [101] As expected, the ^{1}H NMR spectra of the four resulting products (namely **Zn1**^{cont}, **Zn1**^{ext}, **Fe1**^{cont}, and **Fe1**^{ext}) were too broad to be informative although strong shifts could be identified in the terpyridine region, indicating a probable binding of the metal ions. [102]

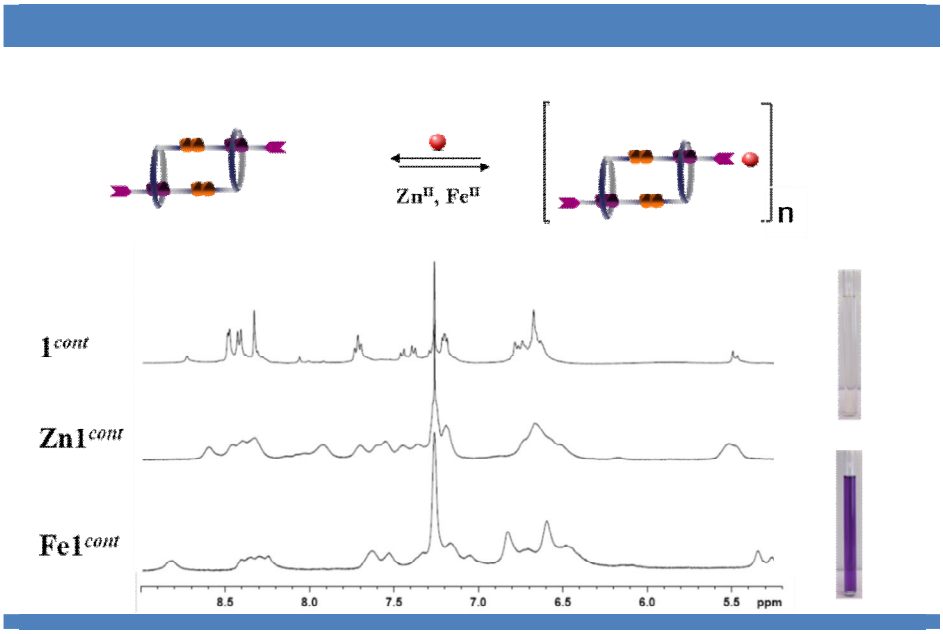

Figure 41| Polymerisation of **1**^{cont} with Zn(II) or Fe(II) ions.

b) UV-Vis experiments

This coordination was however unambiguously confirmed by UV-Vis analyzes (**Fe1**^{cont} and **Fe1**^{ext}). The absorption spectrum showed a typical metal-to-ligand charge transfer band (MLCT) at λ = 580 nm and a new band around λ = 340 nm, which increased upon addition of the Fe(II) ion, whereas the ligand band around λ = 287 nm decreased (Figure 42). [103] The

[101] (a) Groger, G.; Stepanenko, V.; Wurthner, F.; Schmuck, C. Step-wise self-assembly of a small molecule with two orthogonal binding interactions leads to single stranded linear polymers in DMSO. *Chem. Commun.*, 698–700 (2009); (b) Groger, G.; Zaika, W. M.; Bottcher, C.; Grohn, C.; Ruthard, C.; Schmuck, C. Switchable Supramolecular Polymers from the Self-Assembly of a Small Monomer with Two Orthogonal Binding Interactions. *J. Am. Chem. Soc.*, **133**, 8961–8971 (2011).

[102] (a) Elsbernd, H.; Beattie, J. K. The NMR spectra of terpyridine and the bis-terpyridine complexes of cobalt(III) and iron(II). *J. Inorg. Nucl. Chem.*, **34**, 771-774 (1972); (b) Hofmeier, H.; Schubert, U. S. Recent developments in the supramolecular chemistry of terpyridine–metal complexes. *Chem. Soc. Rev.*, **33**, 373-399 (2004); (c) Constable, E. C. 2,2′:6′,2″-Terpyridines: From chemical obscurity to common supramolecular motifs. *Chem. Soc. Rev.*, **36**, 246-253 (2007).

[103] (a) Wild, A.; Schlutter, F.; Pavlov, G. M.; Friebe, C.; Festag, G.; Winter, A.; Hager, M. D.; Cimrova´, V.; Schubert, U. S. π-Conjugated Donor and Donor–Acceptor Metallo-Polymers. *Macromol. Rapid Commun.*, **31**, 868–874 (2010). (b) Grimm, F.; Ulm, N.; Grçhn, F.; During,

Zn(II) spectra show no absorbance at wavelengths higher than 400 nm, in contrast to the titration bands of Fe(II).

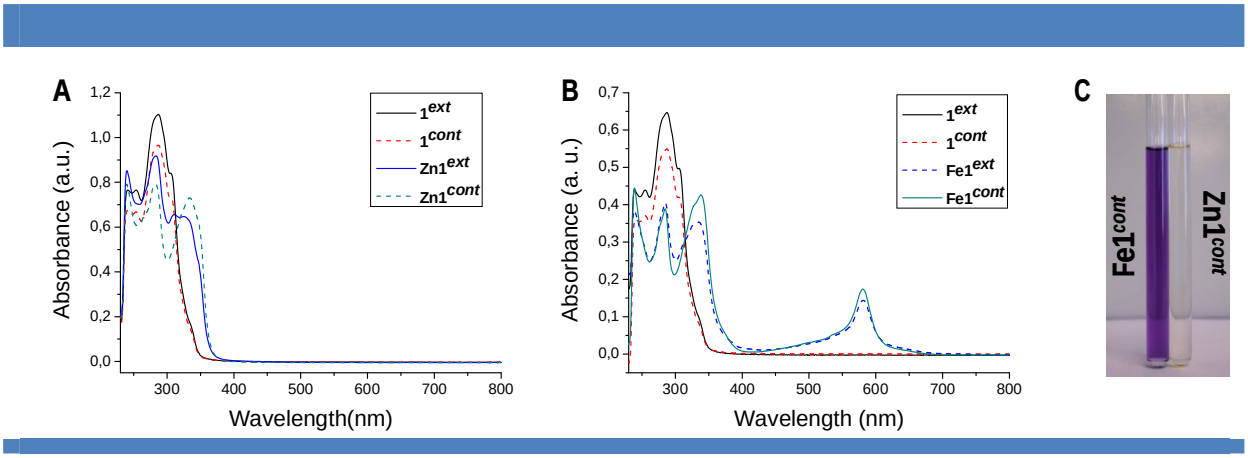

Figure 42│ UV-Vis spectra comparison between monomers **1**^{ext} / **1**^{cont} and (**A**) polymers **Zn1**^{ext} / **Zn1**^{cont} (2.10^{-2} mM in 1:1 $CDCl_3/CD_3CN$) and (**B**) polymers **Fe1**^{ext} / **Fe1**^{cont} (1.10^{-2} mM in 1:1 $CDCl_3/CD_3CN$); (C) Image of two polymer solutions (**Fe1**^{cont} and **Zn1**^{cont}) at a concentration of 10 mM in a 1:1 $CDCl_3/CD_3CN$ solvent mixture.

The occurrence of the MLCT band and the shift of the terpyridine π-π* transitions confirmed metal ion coordination and formation of metallo-supramolecular polymers.

c) *Light and neutron scattering experiments*

This part can be followed with further details with the help of the experimental part describing the theory and equations used.

To probe further the length of the expected supramolecular polymers, as well as their conformation, we have combined a series of light and small-angle neutron scattering (SANS) experiments and extracted key structural parameters grouped in Table 3.

J.; Hirsch, A. Self-Assembly of Supramolecular Architectures and Polymers by Orthogonal Metal Complexation and Hydrogen-Bonding Motifs. *Chem. Eur. J.*, **17**, 9478-9488 (2011).

Table 3 | Characteristic structural parameters obtained from the DLS, SLS, and SANS experiments for polymers **Zn1**^{cont}, **Fe1**^{cont}, and **Fe1**^{ext}. (**A**) Theoretical values; (**B**) Experimental parameters obtained from the fitting procedure. According to the optimization of the fitting procedures, the calculation of the contrast and the measurement of the monomer density, we estimate an absolute error within 10% on the characteristic structural parameters of Table 1B.

A

	M° (g/mol)	a_{theo} (nm)	M_{Ltheo} (g/mol/nm)	Φ
Zn1^{cont}	2334	3.6	648	0.0202
Fe1^{cont}	2395	3.6	665	0.0184
Fe1^{ext}	2687	4.8	559	0.0190

B

	$M_{w\ fit}$ (x10^6 g/mol)	DP	L_c (nm)	L_{ctheo}=DP*a_{theo}	$M_{l\ exp}$ (g/mol/nm)	L_p (nm)
Zn1^{cont}	5.179	1967	8854	8261	585	15.5
Fe1^{cont}	7.030	2937	9398	10573	748	12.8
Fe1^{ext}	7.890	2937	15861	14097	498	17.6

	$R_{g\ Benoît-Doty}$ (nm)	a_{exp} (nm)	R_c (nm)	S (nm²)	R_h (nm)
Zn1^{cont}	213	4.5	0.30	1.412	206
Fe1^{cont}	200	3.2	0.45	1.791	167
Fe1^{ext}	305	5.4	0.40	1.596	189

SANS is the most powerful method to determine characteristic sizes and shapes of objects in solution over the range of 1-300 nm. The scattering pattern for a 10 mM solution of **Zn1**^{cont} that is below the overlap concentration is displayed in Figure 43A. The product $M_wP(q)$ as a

function of the scattered wave-vector q [104] has been obtained by coupling low-q static light scattering (SLS) and SANS measurements, where M_w is the weight-average molecular weight of the scattered species and P(q) the form factor.

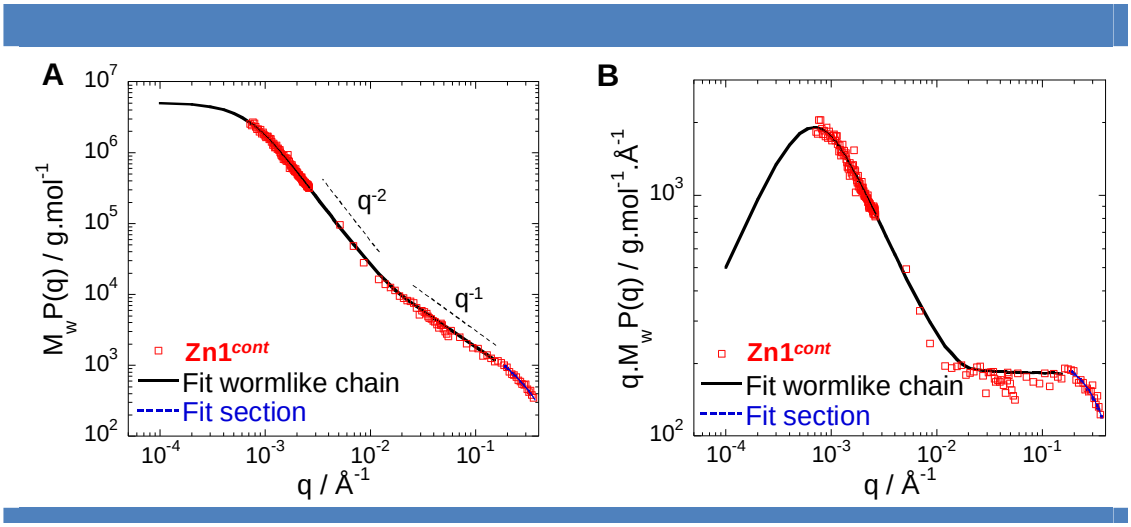

Figure 43 | (**A**) Log-Log plot of combined SLS and SANS measurements for a solution of **Zn1**^{cont} (10 mM in 1:1 $CDCl_3/CD_3CN$ at T=20°C); (**B**) corresponding Holtzer plot. The continuous line represents the data fit by the wormlike chain model (eq. S10, see experimental part) and the dashed line represents the data fit at high-q by a Guinier expression for the form factor of the section (eq. S11, see experimental part).

The scattering curve exhibits an overall behavior characterized by the following sequence: *i*) an onset of a smooth variation analogous to a Guinier regime at very low-q, associated with the finite size and mass of the objects; *ii*) a low-q regime in which the q-dependence of the data can be described by a power law with exponent close to -2, like in Gaussian coils; *iii*) a q^{-1} domain at intermediate q characteristic of a rigid rod-like behavior for distances smaller than the persistence length L_p, followed by *iv*) another Guinier regime associated with the cross-section of the polymers. This ensemble of variations is characteristic of worm-like chain behavior. [105] In such case, one usually represents scattering data by a "Holtzer plot" [106] of the product $M_wP(q)\times q$ as a function of q as is shown in Figure 43B, which directly demonstrates the crossover from a rigid rod-like to a coil-like behavior at a length scale of L_p.

[104] J. Appell, G. Porte, E. Buhler, Self-diffusion and Collective Diffusion of Charged Colloids Studied by Dynamic Light Scattering. *J. Phys. Chem. B* **109**, 13186-13194 (2005).

[105] E. Buhler, F. Boué, Persistence length for a model semirigid polyelectrolyte as seen by small angle neutron scattering: a relevant variation of the lower bound with ionic strength. *Eur. Phys. J. E* **10**, 89-92 (2003).
[106] M. Rawiso, De l'intensité diffusée à la structure en physico-chimie des polymères. *J. Phys. IV* **9** (Pr1), 147-195 (1999).

The ensemble of variations shown in Figure 43A,B can be considered as a form factor and fitted satisfactorily by a wormlike chain model, yielding persistence length L_p=15.5±1.6 nm, linear mass density $M_L=M_W/L_c$ =585±110 g/mol/nm, and contour length L_c=8854±900 nm. From the data at q=0, one obtains a polymerization degree (DP) of 1967±190. The level of the intermediate q^{-1}-regime is controlled by the M_L value, which is in excellent agreement with that of a single-strand polymer chain (linear mass density of deprotonated monomer **1**^{cont} is m/a=2632/3.6=731 g/mol/nm, where m and a represent the mass and the length of a monomer unit respectively (Figure 44 and Table 4). The high-q data has been fitted by a Guinier expression for the form factor of the polymer section, determining the cross-section, S=1.42±0.15 nm^2, and the radius of gyration of the cross-section, R_c=0.3±0.03 nm, values in agreement with monomers section.

Table 4 | Values of key parameters used in this study and determined from SANS on monomers **1**^{ext} and **1**^{cont} (solutions in 1:1 $CDCl_3/CD_3CN$ at T=20°C). *Here the M^O term is different from Table 1 because it does not include metal ions in the monomeric form.*

	C (mM)	M° (g/mol)	I_0 (cm^{-1})	R_g (nm)	$\frac{CM^{\circ 2}}{I_0 N_a}$ (x 10^{-21} g^2/cm^2)	*d* (g/cm^3)	Scattering length density (x 10^{10} cm^{-2})	$\Delta\rho^2$ (x 10^{20} cm^{-4})
1^{ext}	10	2560	0.0185	0.89 +/-0.1	5.88	1.42 +/-0.14	2.17	3.4596
1^{cont}	10	2268	0.0210	0.89 +/-0.1	5	1.30 +/-0.13	1.99	4.1616

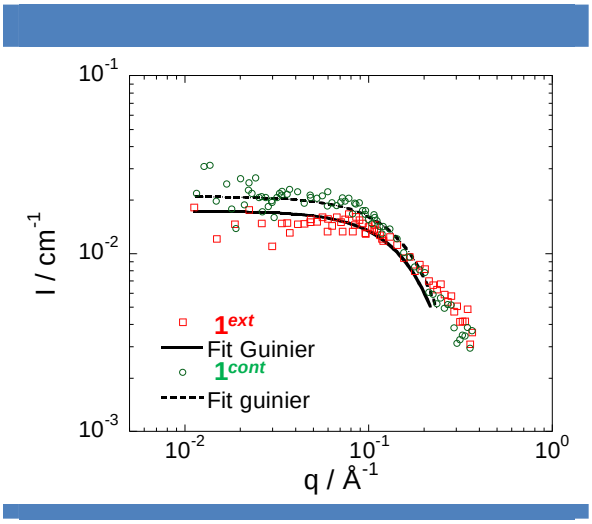

Figure 44| SANS data for solutions of **1**^{ext} and **1**^{cont} (10 mM in 1:1 $CDCl_3/CD_3CN$ at T=20°C). The dashed lines represent the best fits of the data obtained using a classical Guinier expression (eq. S14, see experimental part).

As shown by the dynamic light scattering (DLS) experiments presented in Figure 45A, **Zn1**^{ext} samples present a partial depolymerization. The size distribution obtained by applying the Contin analysis to our data shows two populations, one around 2-3 nm corresponding to monomers and another one around 200 nm corresponding to polymers.

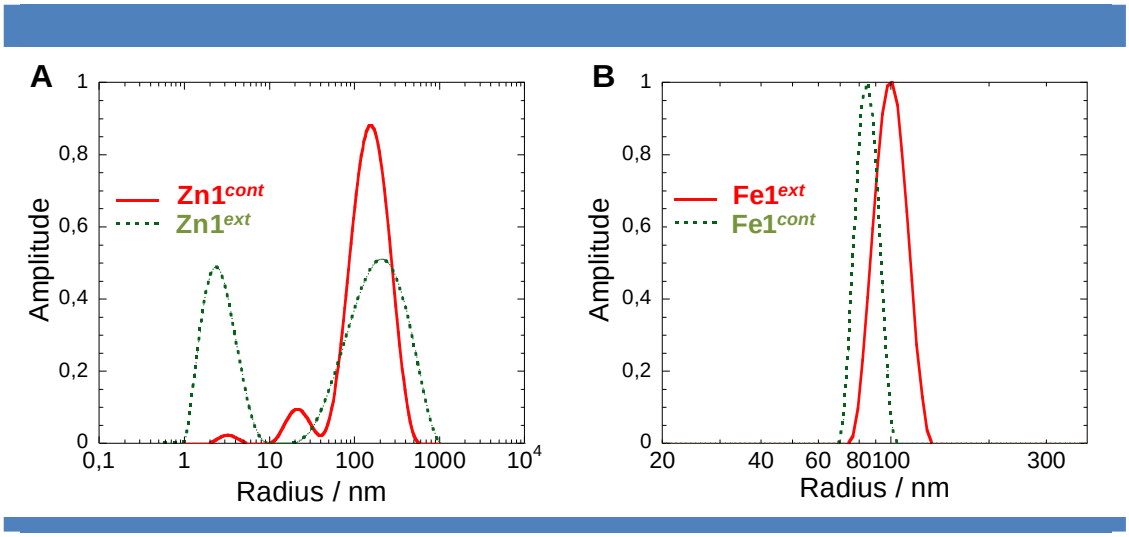

Figure 45| Distribution of the scattering intensity with the hydrodynamic radii (RH) obtained by applying the Contin method to our data at θ=90° for (**A**) Zn-based supramolecular polymers and (**B**) Fe-based supramolecular polymers.

The hydrodynamic radius of the **Zn1**^{cont} sample obtained from extrapolation of the data at zero-q is R_H=206±20 nm. This observation was confirmed by starting with the preformed polymer and by adding increasing amounts of trifluoroacetic acid, revealing a competition between protonation and coordination with the zinc ions. To avoid such drawback, we turned to Fe(II) ions as coordination metal which is known to bind even more strongly with terpyridine ligands (log β =20.9 M^{-2} in water) [107] Gratifyingly, DLS measurements performed on iron systems indicate the presence of a single polymer population for all deprotonated and protonated samples at various temperatures (Figure 45B and 46). We have determined after extrapolation of the data at q=0 a R_H=167±17 nm for **Fe1**^{cont} and a R_H=189±19 nm for **Fe1**^{ext}.

[107] A. E. Martell, R. M. Smith, Critical Stability Constants, Plenum Press, New York (1974).

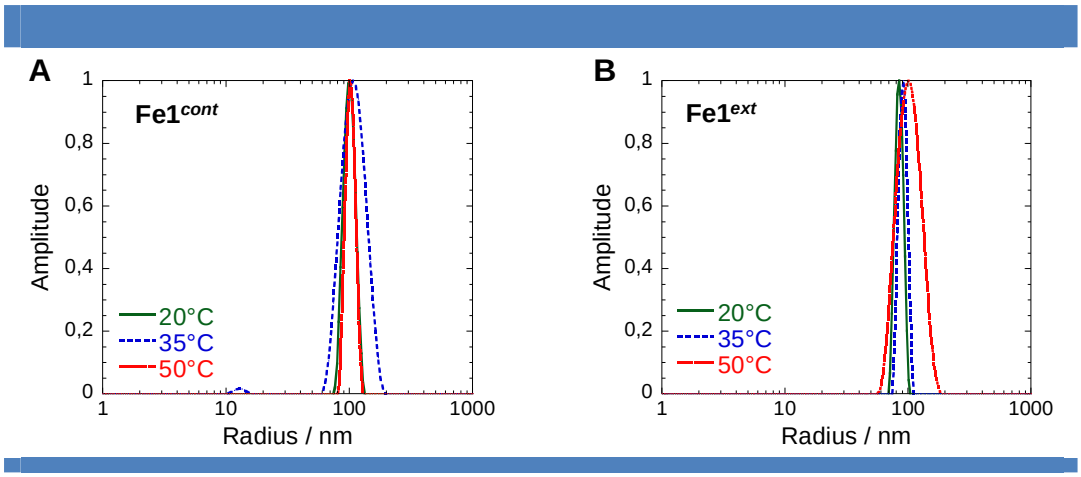

Figure 46| Hydrodynamic radii (R_H) distribution obtained using the Contin method in DLS at θ=90° for (**A**) **Fe1**^{cont} and (**B**) **Fe1**^{ext} (in both case, c=10 mM in 1:1 $CDCl_3/CD_3CN$).

The scattering patterns of **Fe1**^{cont} and **Fe1**^{ext} in 10 mM solutions are displayed in Figure 47A and at various temperatures in Figure 48.

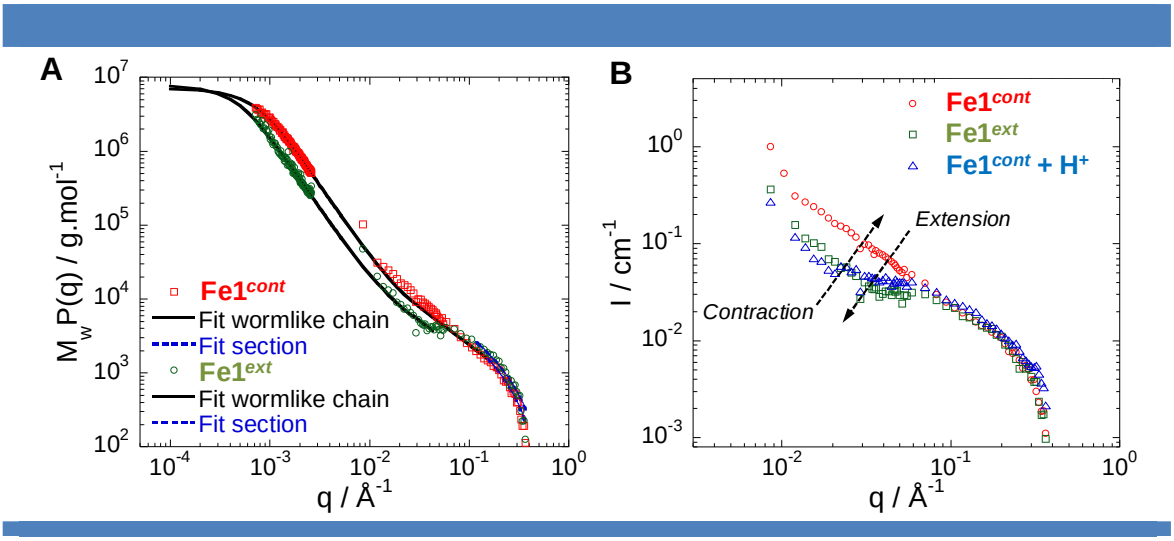

Figure 47| (**A**) SLS and SANS data for **Fe1**^{ext} and **Fe1**^{cont} (10 mM in 1:1 $CDCl_3/CD_3CN$ at T=20°C). The continuous lines represent the best fit of the data by a wormlike chain model (eq. S10) and the dashed line represents the data fit at high-q by a Guinier expression for the form factor of the cross-section (eq. S11). (**B**) SANS only showing the effect of in situ protonation (2 equiv. of CF_3CO_2D) starting from Fe1cont and leading to **Fe1**^{ext} as compared with the reference of **Fe1**^{ext} polymerized from already extended monomer.

Both samples exhibit the same wormlike-chain behavior, characterized by the sequence described above for **Zn1**^{cont}. Scattering variations are fitted satisfactorily by the wormlike-chain model and one obtains respectively L_p=12.8±1.3 nm, M_L=748±150 g/mol/nm,

L_c=9398±1000 nm, and DP=2937±290 for **Fe1**^{cont} and L_p=17.6±1.8 nm, M_L=498±100 g/mol/nm, L_c=15861±1500 nm, and DP=2937±290 for **Fe1**^{ext}. The contraction-extension process is clearly demonstrated by these results as for the **Fe1**^{ext} sample we observe *i*) an increase of the contour length of the chain, and *ii*) a reduction of the linear density. The values of the experimental linear mass densities are in agreement with that calculated for a single-strand contracted chain (m/a=665 g/mol/nm) and for a single-strand extended chain (m/a=559 g/mol/nm). Cross-section dimensions for both iron samples correspond to that of a monomer section, confirming that no lateral aggregation occurs: R_c=0.42±0.04 nm and S=1.7±0.15 nm^2. We have also checked by using SANS the effect of the *in situ* protonation of **Fe1**^{cont} which confirms the extension of the supramolecular polymer because, in the q^{-1} regime, the intensity of **Fe1**^{cont} + H^+ overlaps with the one measured for the sample **Fe1**^{ext} prepared by the supramolecular polymerization from already protonated monomer **1**^{ext} (see Figure 47B).

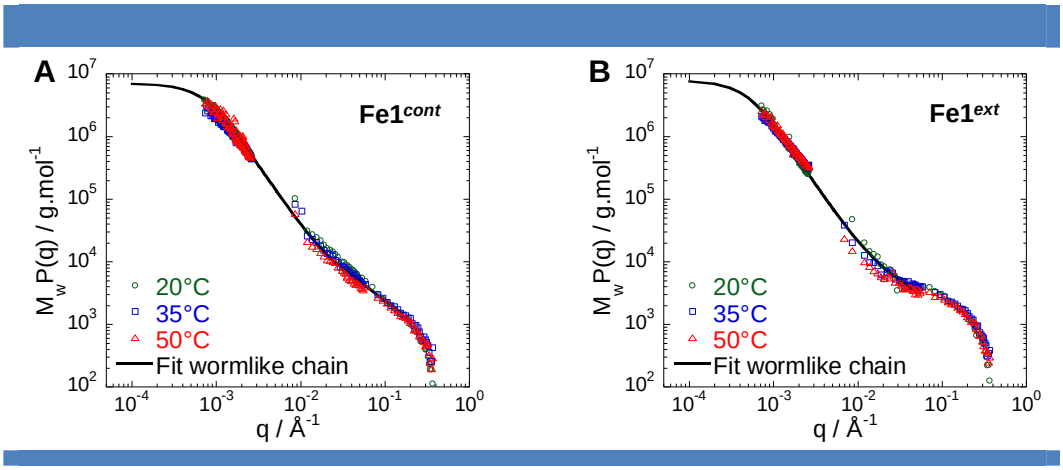

Figure 48| Combined SLS and SANS measurements as a function of the temperature for solutions of (**A**) **Fe1**^{cont} and (**B**) **Fe1**^{ext} (10 mM in 1:1 $CDCl_3/CD_3CN$). The continuous line represents the data fit by the wormlike chain model (eq. S10, see experimental part).

d) Conclusions

This work shows, through a number of experimental evidences, that the coupling of thousands of molecular machines along a single polymer chain provides a pathway to integrate their single motions at mesoscale. The key features of the present system rests on a very efficient metallo-supramolecular polymerization of highly functional and bistable [c2]daisy chains which produce perfect worm-like chains. This crucial experimental aspect allows a clear and precise determination of the occurring one-dimensional contraction

process, and avoids parasitic effects that would be necessarily brought by cross-chain interactions. By looking at **Fe1**^{ext} and **Fe1**^{cont}, the shift between the two SANS curves is the signature of the relative change in linear mass density between the two samples and one can quantify it with an excellent precision (ΔM_L=250±25 g/mol/nm). This local change of the polymer chain is directly correlated with the global change of the polymer contour length (ΔL_c=6.4±0.7 µm; a value which is, by analogy, in the range of the contraction observed in sarcomeres). The measured effect is in good agreement with the expected theoretical value based on the distance between the two stations and on the degree of polymerization. They also perfectly fit with the experimental SANS values measured on both monomers as references. Thus, this amplification by four orders of magnitude of the mechanical output of thousands of molecular machines linked within a single-strand macromolecular chain, going from the low nanometer scale to the ten of micrometers, is accessible by combining molecular synthesis, supramolecular engineering, and polymerization processes. The next challenge in this direction will consist in bundling such fibers, and possibly in orienting them, to access macroscopic responses just as myofibrils do in muscles.

5/ Self-healing behavior of the metallo-supramolecular polymers connected by tristerpyridine

Previous studies have proved that the metallo-supramolecular polymers exhibit a characteristic of wormlike-chain behavior with microscopic extension/contraction. Then the polymers were tested for macroscopic motions in “muscle-like” films and gels. For that, we decided to use cross-linking agent.

When three-head telechelic ligand molecules are used, branched coordination supramolecules can be formed, as illustrated in Figure 49. [109]

[109] Sievers,T.K.; Vergin, A.; Möhwald, H.; Kurth, D. G. Thin Films of Cross-Linked Metallo-Supramolecular Coordination Polyelectrolytes. *Langmuir*, **23**, 12179-12184 (2007).

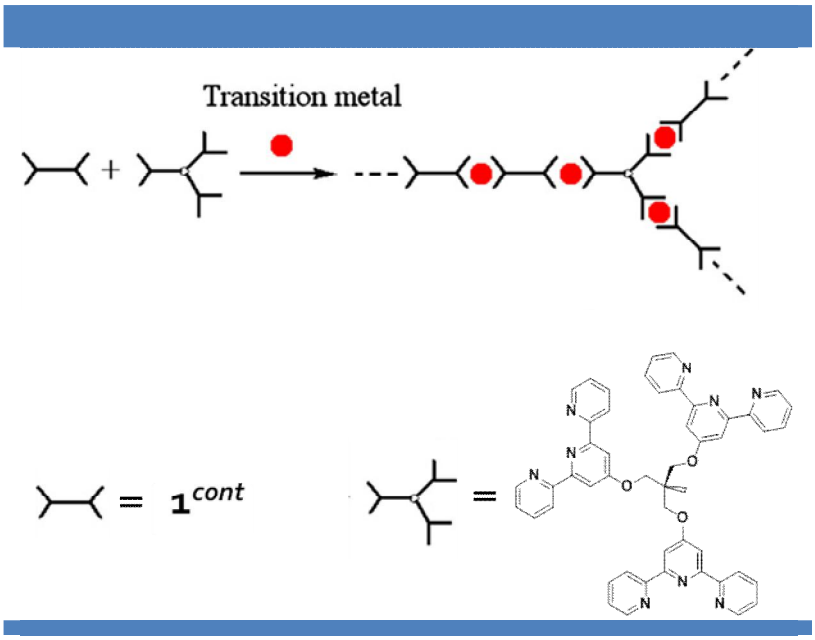

Figure 49| Illustration of branched coordination supramolecules.[109]

The three-head telechelic ligand 1,1,1-Tris(2,2':6',2''-terpyridinyl-4'-oxymethyl)ethane (tritpy) was obtained by a condensation of 1,1,1-Tris(hydroxymethyl)ethane with commercially available 4'-Chloro-2,2':6',2''-terpyridine in DMSO in basic condition (Scheme 25).

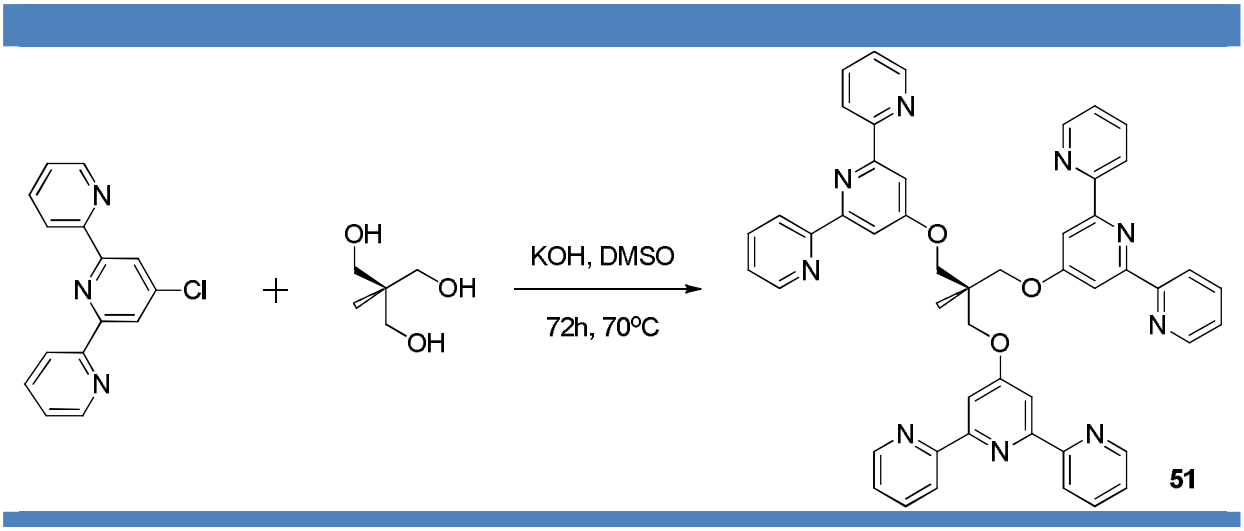

Scheme 25 | Synthesis of the 1,1,1-Tris(2,2':6',2''-terpyridinyl-4'-oxymethyl)ethane **51**.

Reaction conditions used for Scheme 25:

1,1,1-Tris(hydroxymethyl)ethane (1.0 equiv.), KOH (15.0 equiv.), 4'-Chloro-2,2':6',2''-terpyridine (4.0 equiv.), DMSO, 70°C, 72 h, 42%.

Then we synthesized coordination networks with different percentages of cross-linking agent (Table 5). To specify the network, we use the cross-linking degree expressed in percent, which is defined as $z = n_{tritpy}/(n_{tritpy} + n_{rotaxane}) \times 100\%$, where n_{tritpy} is the molar amount of the tritopic ligand tritpy used for cross-linking and $n_{rotaxane}$ the molar amount of the terpyridine rotaxane.

Table 5 | Different percentage of cross-linking agent **51** used for the formation of films

n_{tritpy} / × 10^{-3} mmol	$n_{Fe(II)}$ / × 10^{-3} mmol	$n_{rotaxane}$ / × 10^{-3} mmol	z
0.51	25.0	25.0	2%
0.53	25.0	25.0	5%
0.56	25.0	25.0	10%

A series of networks containing between 2% and 10% of cross-linking terpyridine and films were made by evaporation of the solvent. Then we found these supramolecular materials behaved a self-healing property after broken, as shown in figure 50. This behavior can be repeated many times.

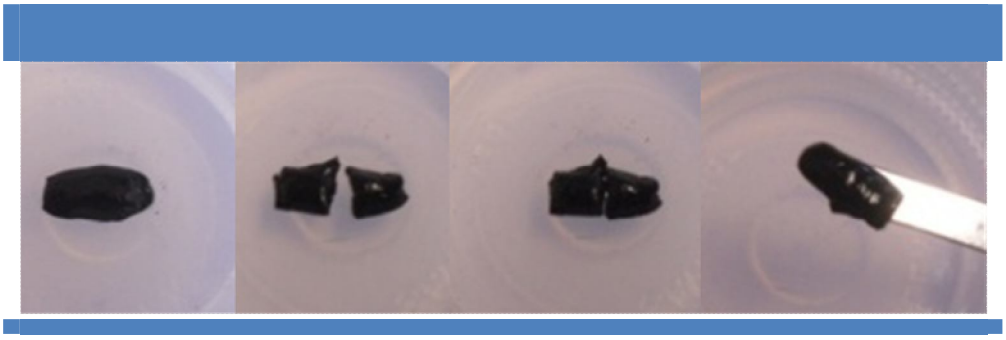

Figure 50 | Self – healing property of the polymer (**1**^{ext} + Fe(II) + 2% **51**). After cutting the material, the simple contact of the two pieces under vapors of solvent resulted in their soldering after two hours.

As we mentioned in chapter 1, the reversibility of the dynamic bond allows repair to take place at the molecular level to fully restore the original material properties.

6/ Oligophenylacetylene dumbbell functionalied triarylamine-fullerene dyads

In a parallel project of the laboratoray and in collaboration with Dr. E. Busseron and J.-J. Cid, we also used our dumbbell **42** to synthesize donor-acceptor (D-A) molecules. These D-A systems are based on recently discovered light-responsive triarylamine derivatives[110] as electron donor, oligo(p-phenylene ethynylene) (OPE) as π-conjugated linkers of variable lengths and on fullerene (C_{60}) as electron acceptor (Figure 51).

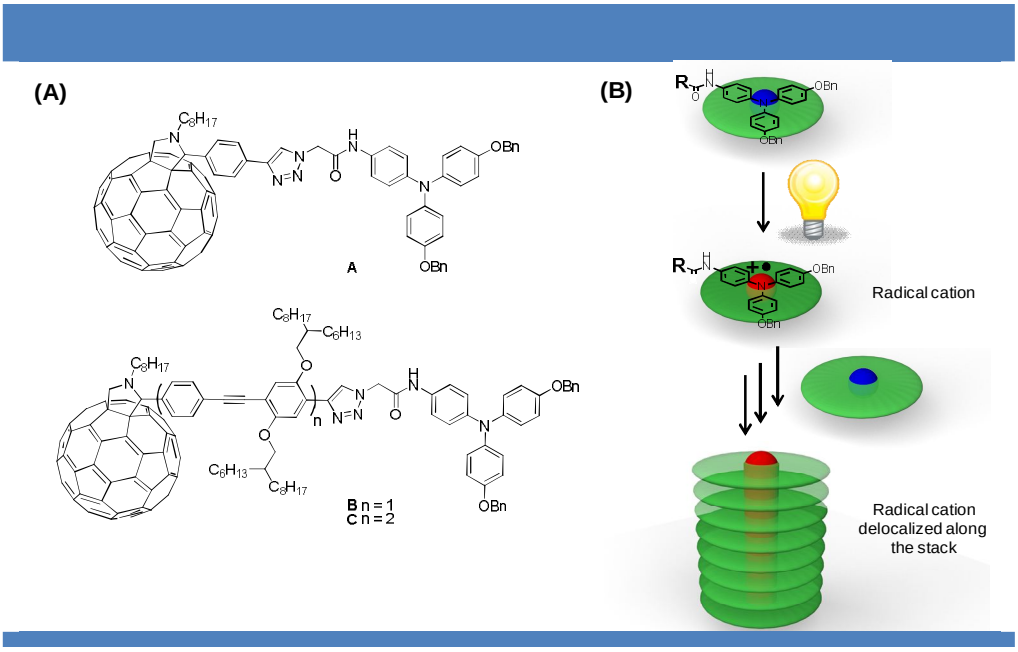

Figure 51| (**A**) Structures of three pyrrolidinofullerene-triarylamine dyads **A**-**C**; (**B**) Principle of the self-assembly of the triarylamine unit upon photo-irradiation with visible light.

These molecules are able to self-assemble in highly ordered supramolecular nanostructures and are promising candidates for application in organic optoelectronic devices, where a well-defined morphology of the photo-active layer is of great importance for improved performances. However, this will not be described in details here because it was not related to the main topic of this PhD.

7/ Conclusions

[110](a) Moulin, E.; Niess, F.; Maaloum, M.; Buhler, E.; Nyrkova, I.; Giuseppone, N. The Hierarchical Self-Assembly of Charge Nanocarriers : A Highly Cooperative Process Promoted by Visible Light. *Angew. Chem. Int. Ed.*, **49**, 6974-6978 (2010). (b) Faramarzi, V.; Niess, F.; Moulin, E.; Maaloum, M.; Dayen, J.-F.; Beaufrand, J.-B.; Zanettini, S.; Doudin, B.; Giuseppone, N. Light triggered self-fabrication of supramolecular organic nanowires as metallic interconnects. *Nature Chem.*, **4**, 485-490 (2012).

The work of this chapter describes the syntheses of metallo-supramolecular polymer rotaxanes. The unsymmtric dumbbell **45** was synthesized by using a selective substitution of the building block **26** under an iterative Sonogashira couplings and silyl groups deprotection conditions. Then the model rotaxane was synthesized and polymerized. Two metal ions were studied and perfect wormlike chain supramolecular polymers were obtained. Characterizations by a combination of scattering techniques in solution reveal the formation of single-strand supramolecular polymer chains with very high molecular weights (up to 8.10^6 g.mol-1). The subsequent pH modulation triggers cooperative nano-contractions (or extensions) of the individual rotaxanes resulting in an amplified motion of the muscle-like supramolecular chains with changes of their contour lengths by several micrometers.

In the first attempts to create contractile films at the macroscopic level, we were able to cross-link these polymer chains and we noticed the self-healing behavior of the material, a behavior which should be investigated further in the future.

After a description of the synthesis of metallo-supramolecular polymer rotaxanes, we will now focus on the syntheses of H-bonding supramolecular polyrotaxanes.

Chapter 4 : Synthesis and Characterization of Hydrogen-Bonding Supramolecular Polymers

After the full characterizatin of the microscopic contraction /extension process determined as a monodimensional event in the single-strand metallo-supramolecular polymers we tried to investigate the buildling of such fibers to access macroscopic motions. With this idea in mind, the fourth chapter deals with the synthesis of two types of H-bonding units donor-acceptor-donor (DAD) or acceptor-donor-acceptor (ADA) ended rotaxane. These rotaxane were designed to polymerize with appropriate connectors by complementary hydrogen-bonding interactions (Figure 52).

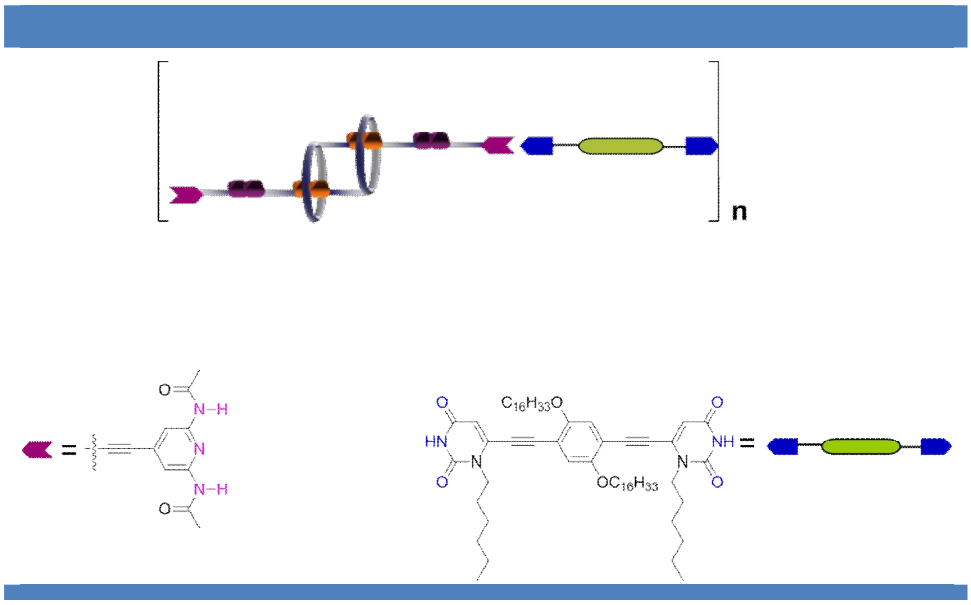

Figure 52 | General representation of the bistable rotaxane based H-bonding supramolecular polymers.

1/ Synthesis of a model hydrogen-bonding rotaxane (DAD type)

a) Synthesis of the rotaxanes 2^{ext} *and* 2^{cont}

4-bromo-2,6-diaminopyridine[111] (synthesized by Dr. F. Niess) was prepared in five steps starting from commercially available chelidamic acid monohydrate, which was subsequently

[111] Nettekovan, M.; Jenny, C. The development of a practical and reliable large-scale synthesis of 2,6-diamino-4-bromopyridine. *Org. Process Res. Dev.*, **7**, 38-43 (2003).

acetylated with acetic anhydride in pyridine yielding 4-bromo-2,6-diacetylaminopyridine (Scheme 26).

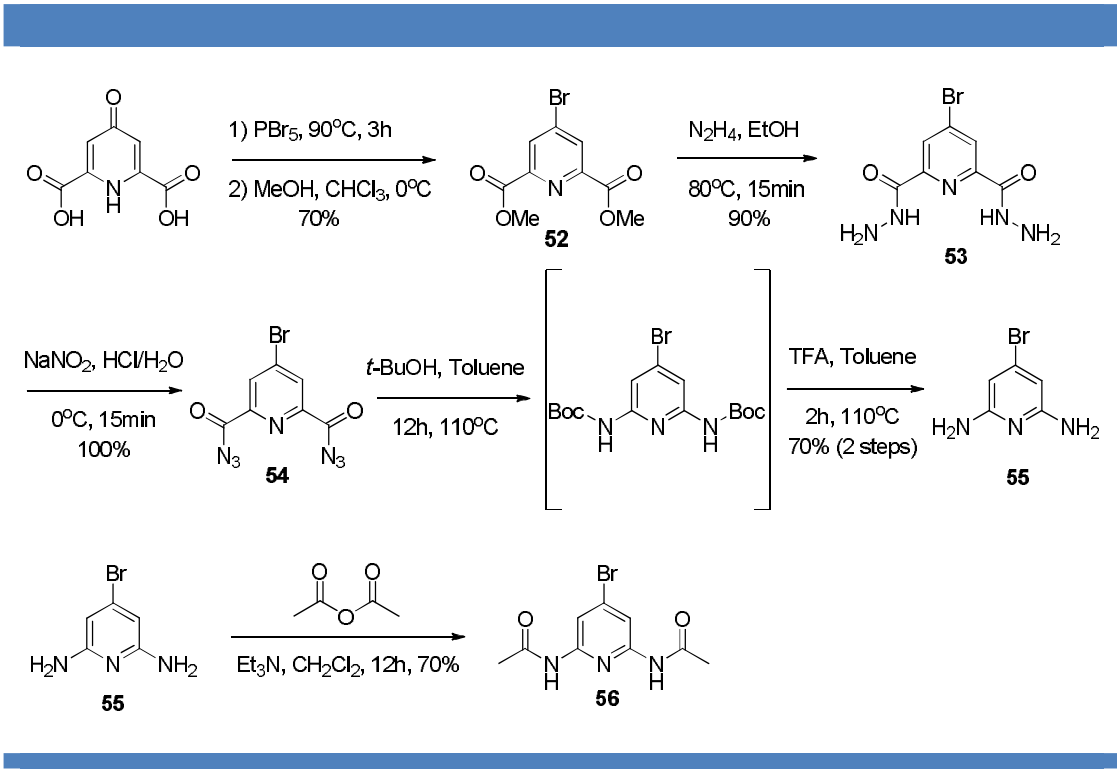

Scheme 26 | Synthesis of 4-bromo-2,6-diacetylaminopyridine **57**.

Reaction conditions used for Scheme 26:

(a) chelidamic acid monohydrate (1.0 equiv.), PBr_5 (1.8 equiv.), 90°C, 3h; (b) MeOH, $CHCl_3$, 0°C to r.t., 30min, 70%; (c) **52** (1.0equiv.), hydrazine monohydrate (65%), ethanol, reflux, 15min, 90%; (d) **53** (1.0 equiv.), HCl (37%), $NaNO_2$, 0°C, 15 min; (e) tert-butanol, toluene, reflux, 12h; (f) TFA, toluene, reflux, 2h, 74% (3 steps); (g) **55** (1.0 equiv.), acetic anhydride (12.6 equiv.), pyridine, r.t., 12h, 68%.

Sonogashira coupling between 4-bromo-2,6-diacetylaminopyridine **57** and 4-ethynylbenzyl acetate **39** followed by acetate deprotection using CH_3ONa in MeOH afforded compound **56** (Scheme 27). [112]

[112] Llanes-Pallas, A.; Palma, C. A.; Piot, L.; Belbakra, A.; Listorti, A.; Prato, M.; Samorì, P.; Armaroli, N.; Bonifazi, D. Engineering of supramolecular H-bonded nanopolygons via self-assembly of programmed molecular modules. *J. Am. Chem. Soc.*, **131**, 509–520 (2009).

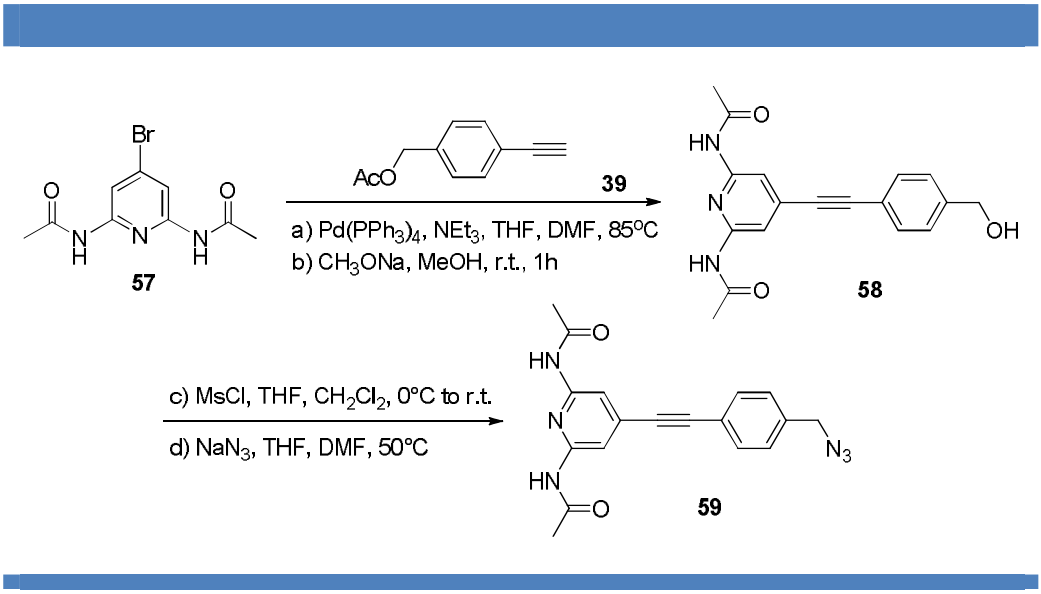

Scheme 27 | Synthesis of compound **59**.

Reaction conditions used for Scheme 35:

(a) 4-bromo-2,6-diacetylaminopyridine (1.0 equiv.), 4-ethynylbenzyl acetate (1.3 equiv.), $Pd(PPh_3)_4$ (0.4 equiv.), CuI (0.8 equiv.), NEt_3/THF/DMF, 85°C, overnight; (b) CH_3ONa (2.0 equiv.), MeOH, r.t., 1h, 62% (2 steps); (c) compound **58** (1.0 equiv.), MsCl (1.3 equiv.), TEA (1.3 equiv.), CH_2Cl_2, 0°C to r.t., overnight; (d) NaN_3 (10.0 equiv.), DMF/THF (1:1), 50°C, overnight, quantitative (2 steps).

Benzyl azide **59** was then obtained quantitatively in two steps after treatment of product **58** with methanesulfonyl chloride at 0°C and subsequent reaction with sodium azide at 50°C.

The introduction of the hydrogen-bonding benzyl azide **59** stopper on the pseudorotaxane **11** was efficiently carried out by microwave irradiation in a mixture solvent of CH_2Cl_2/CH_3CN in the presence of $Cu(MeCN)_4PF_6$. The final H-bonding rotaxane $\mathbf{2}^{ext}$ was obtained by methylation and the subsequent extraction and counter ion exchange procedure (Scheme 28). The deprotonated rotaxane $\mathbf{2}^{cont}$ was then easily obtained by washing the protonated rotaxane $\mathbf{2}^{ext}$ with 1M $NaOH_{aq.}$.

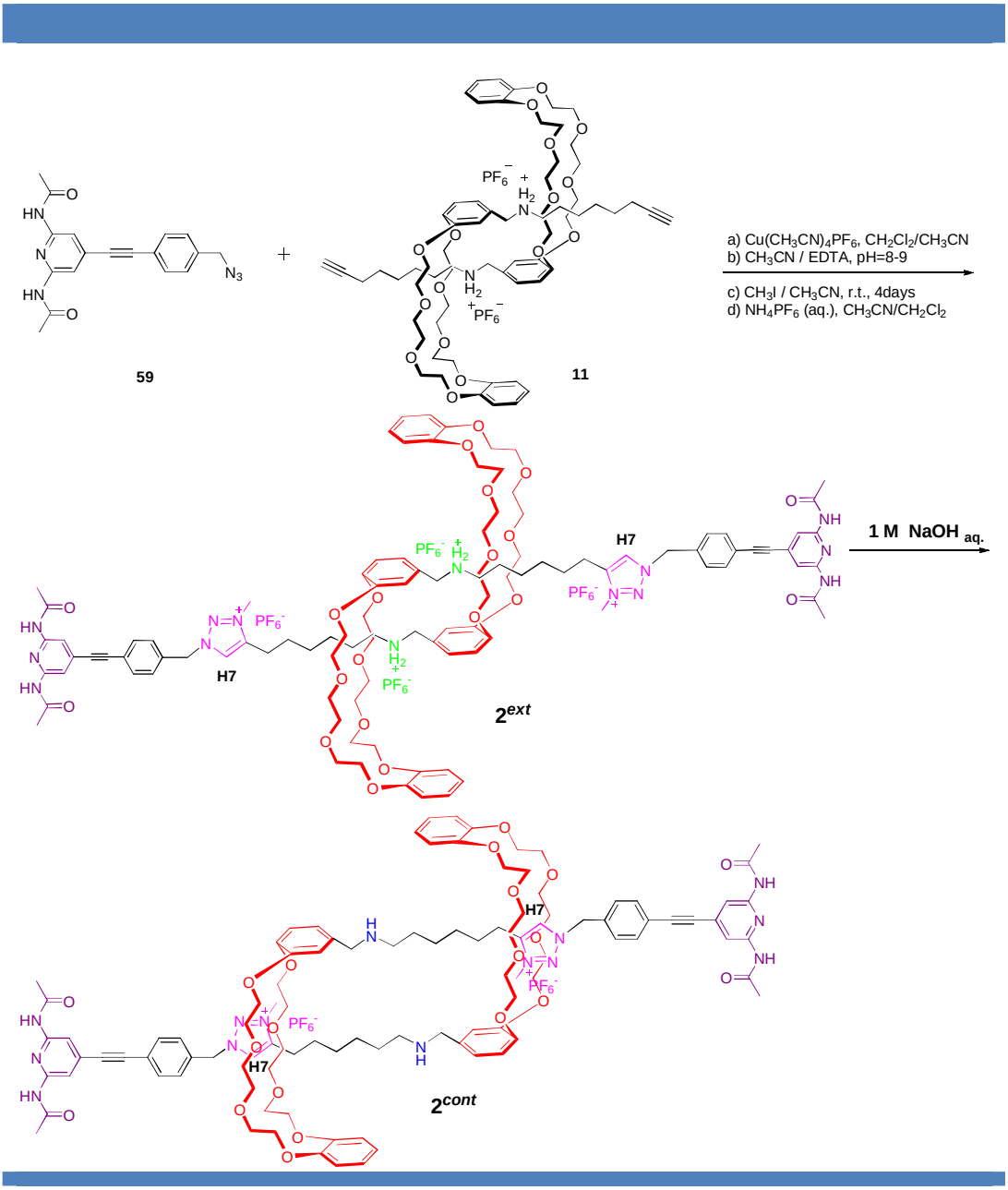

Scheme 28 | Synthesis of protonated and deprotonated rotaxanes **2**^{ext} and **2**^{cont}.

Reaction conditions used for Scheme 28:

(a) pseudo-rotaxane **11** (1.0 equiv.), benzyl azide **59** (2.1 equiv.), $Cu(CH_3CN)_4PF_6$ (2.0 equiv.), 2,6-lutidine (2.0 equiv.), CH_2Cl_2/CH_3CN, 2h, 30°C; (b) EDTA aq.(pH ≈ 8-9), CH_3CN, 2h; (c) $CH_3ICHCl_3//CH_3CN$ (1:1), r.t., 4days; (d) NH_4PF_6 (aq.), CH_2Cl_2/CH_3CN, 75% (overall steps).

As already shown in the case of the terpyridine bistable rotaxane, the ammonium station proved to have a better affinity for the DB24C8 than for the triazolium. It follows that both the stretched and the contracted state could be obtained upon protonation or deprotonation.

Deprotonation of the ammonium caused the displacement of the DB24C8 part around the triazolium station, whereas the macrocycle shuttled back around the ammonium station upon protonation of the amine.

As it is based on the comparison of the protonated with the deprotonated [c2]daisy chains, the ^{1}HNMR titration from $\mathbf{2}^{cont}$ to $\mathbf{2}^{ext}$ has been performed. Solutions of $\mathbf{2}^{cont}$ (5×10^{-3} mmol) monomer in $CDCl_3$ and *d*-TFA (0.2 mol/L) in $CDCl_3$ for the pH-^{1}HNMR titration were prepared respectively. Then 2µL of *d*-TFA solution was added to the $\mathbf{2}^{cont}$ solution for each titration. The complete titration was finished after 22 times (up to 2.2 equiv.). The ^{1}H NMR spectroscopy evidence of the localization of the DB24C8 part around the two molecular stations is reported in Figure 53.

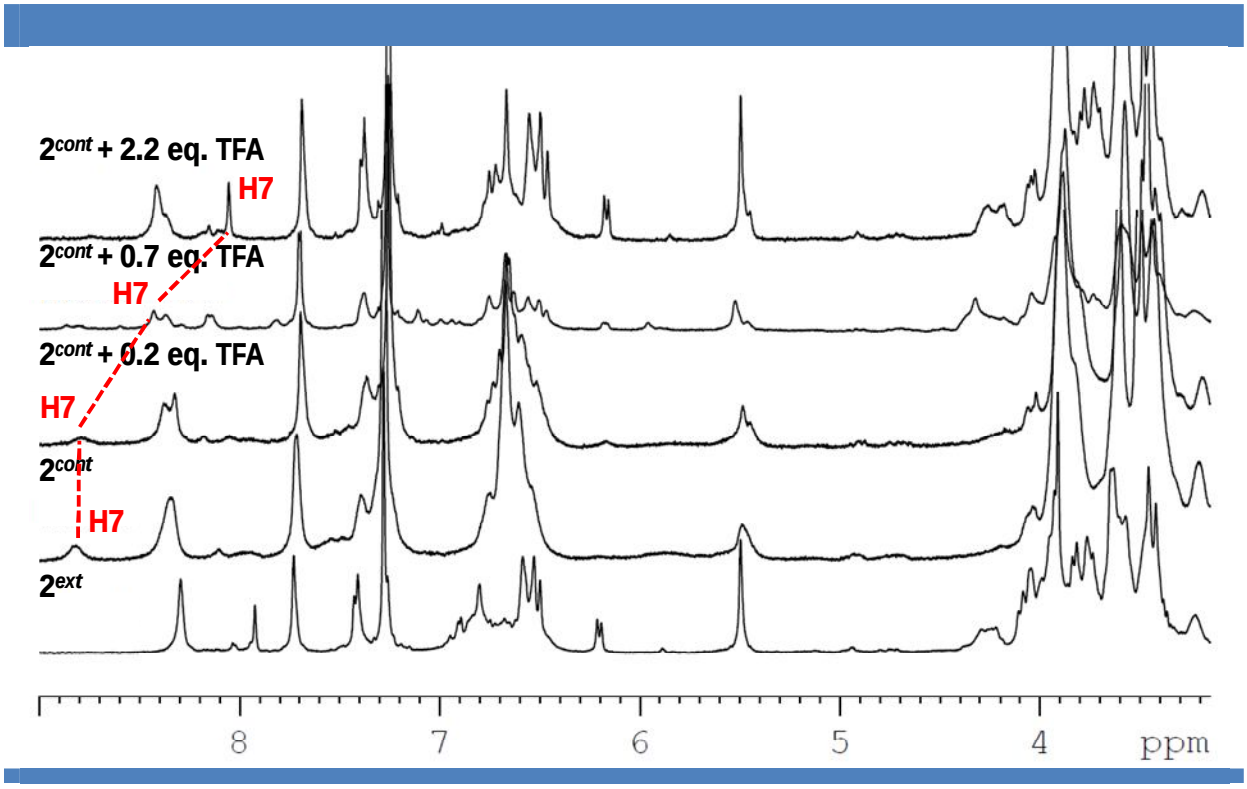

Figure 53 | ^{1}H NMR titration from $\mathbf{2}^{cont}$ to $\mathbf{2}^{ext}$ monomer by adding *d*-TFA.

As shown on Scheme 28, when the amine moiety was protonated, the DB24C8 part moved toward the ammonium station. By comparing the [c2]daisy chains $\mathbf{2}^{cont}$ and $\mathbf{2}^{ext}$, dramatically upfield shifts are observed for the triazolium protons H7 ($\Delta\delta \sim 0.75$ ppm) due to the uncomplexation of the crown ether to triazolium station. The slight chemical shift changes of CH_2 protons close to the ammonium and of the aromatic protons from the crown ether can also be observed as a result of both the protonation of the neighboring ammonium and the

shuttling of the macrocycle. It should be pointed out that, after the protonation process, 2.2 equivalents of $CF_3CO_2^-$ were introduced. Therefore, there are slight shifts in the NMR spectrum with respect to the original spectrum.

b) Synthesis of the complementary hydrogen-bonding dumbbell **64**

To produce the complementary hydrogen-bonding dumbbell, 1-Hexyluracil **61** was obtained by reaction of commercially available unsubstituted uracil with 1-bromohexane in the presence of K_2CO_3 and DMSO. Subsequent deprotonation of **61** with Lithium diisopropylamine (LDA) and addition of I_2 afforded the C6-iodinated derivative **62** (Scheme 29).

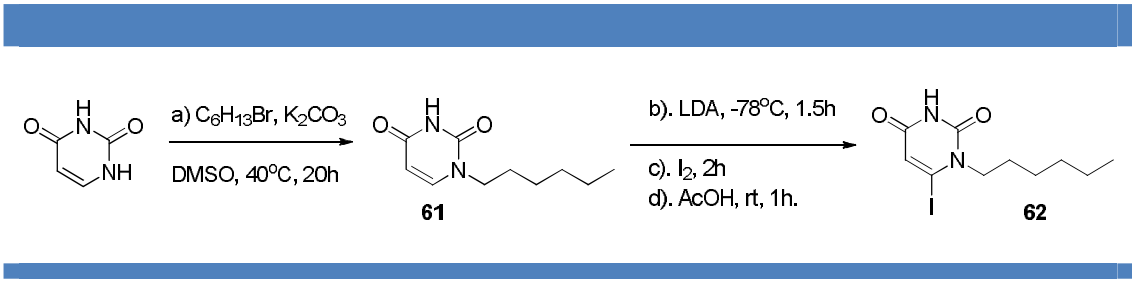

Scheme 29 | Synthesis of compound **62**.

Reaction conditions used for Scheme 29:

(a) uracil (1.0 equiv.), K_2CO_3 (1.1 equiv.), 1-bromohexane (1.0 equiv.), DMSO, 40°C, 20h, 71%; (b) 1-hexyluracil **61** (1.0 equiv.), LDA (2.2 equiv.), THF, -78°C, 1.5h; (c) I_2 (4.8 equiv.), 2h; (d) acetic acid, 1h, 78% (3 steps).

Then complementary hydrogen bonding dumbbell **64** was synthesized following a similar approach to that utilized for the unsymmtric dumbbell terpyridine in the previous chapter, using the Pd-catalyzed cross-coupling reaction. Treatment of the unsymmtric compound **29** with aqueous TBAF in THF afforded **63**, which was coupled to 1-Hexyl-6-iodouracil **62** via Sonogashira reaction (Scheme 30). [113]

[113] Yoosaf, K.; Llanes-Pallas, A.; Marangoni, T.; Belbakra, A.; Marega, R.; Botek, E.; Champagne, B.; Bonifazi, D.; Armaroli, N. From Molecular to Macroscopic Engineering: Shaping Hydrogen-Bonded Organic Nanomaterials. *Chem. Eur. J.*, **17**, 3262-3273 (2011).

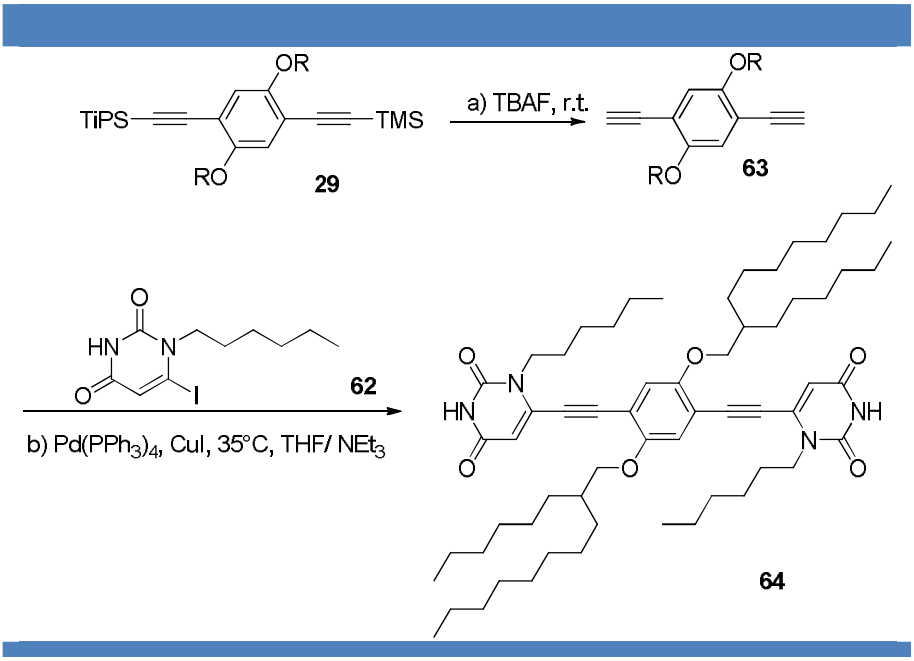

Scheme 30 | Synthesis of complementary Hydrogen-bonding dumbbell **64**.

Reaction conditions used for Scheme 30:

(a) compound **29** (1.0 equiv.), TBAF (1.0 equiv.), THF, r.t., 1h; (b) compound **63** (1.0 equiv.), 1-Hexyl-6-iodouracil (2.2 equiv.), $Pd(PPh_3)_4$ (0.08 equiv.), CuI (0.16 equiv.), Et_3N/THF, 35°C, overnight, 40% (2 steps).

2/ Characterization of the model hydrogen-bonding polymeric rotaxanes

Due to strong propensity for π-stacking, linear π-conjugated systems when functionalized with H-bonding moieties are known to form diverse supramolecular architectures. Two dumbbell connectors with complementary H-binding were probed with the deprotonated monomer $\mathbf{2}^{cont}$ in the aim of polymerisation (Figure 54).

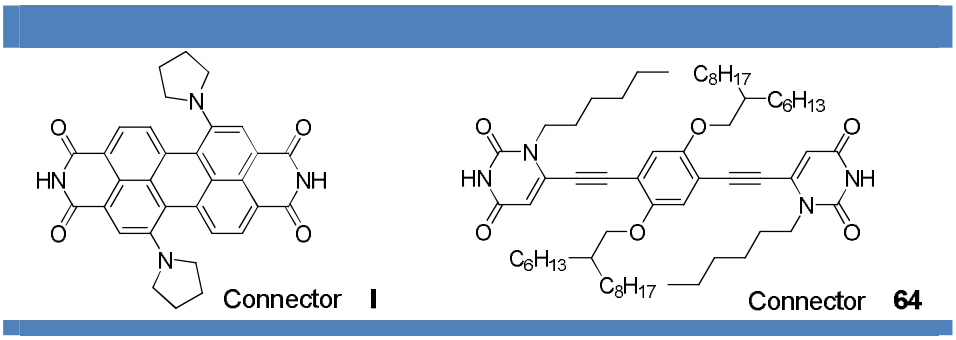

Figure 54 | Two kinds of connectors used for the hydrogen-bonding polymerisation.

a) ^{1}H NMR experiments

Conceptually, the H-bonding molecular recognition process between rotaxane monomer $\mathbf{2}^{cont}$ and connectors (**I** or **64**) can be monitored in solution. This turned out to be particularly challenging because of the poor solubility of perylene connector **I** in our solvent system. Attempts made in mixture of $CDCl_3/CH_3CN$, in which the rotaxane $\mathbf{2}^{cont}$ is soluble, gave no evidence of association. ^{1}H NMR spectra showed there are no significant splitting and shift changes of the rotaxane and perylene, which could be attributed to the insolubility of the perylene. However, a clear proof of molecular recognition was obtained by using **64** as connector. Upon addition 1.0 molar equivalent of the uracil connector **64** to the solution of $\mathbf{2}^{cont}$ in $CHCl_3/CH_3CN$, a significant downfield shift with a $\Delta\delta$ of about 0.40 ppm of the imidic protons due to the complexation of the uracil was observed, which means the formation of supramolecualr polymers $\mathbf{[64•2]}^{cont}$. [114] The protonation-deprotonation switch process can also be monitored by the acid –base titration for the supramolecular polymers, as shown in Figure 55.

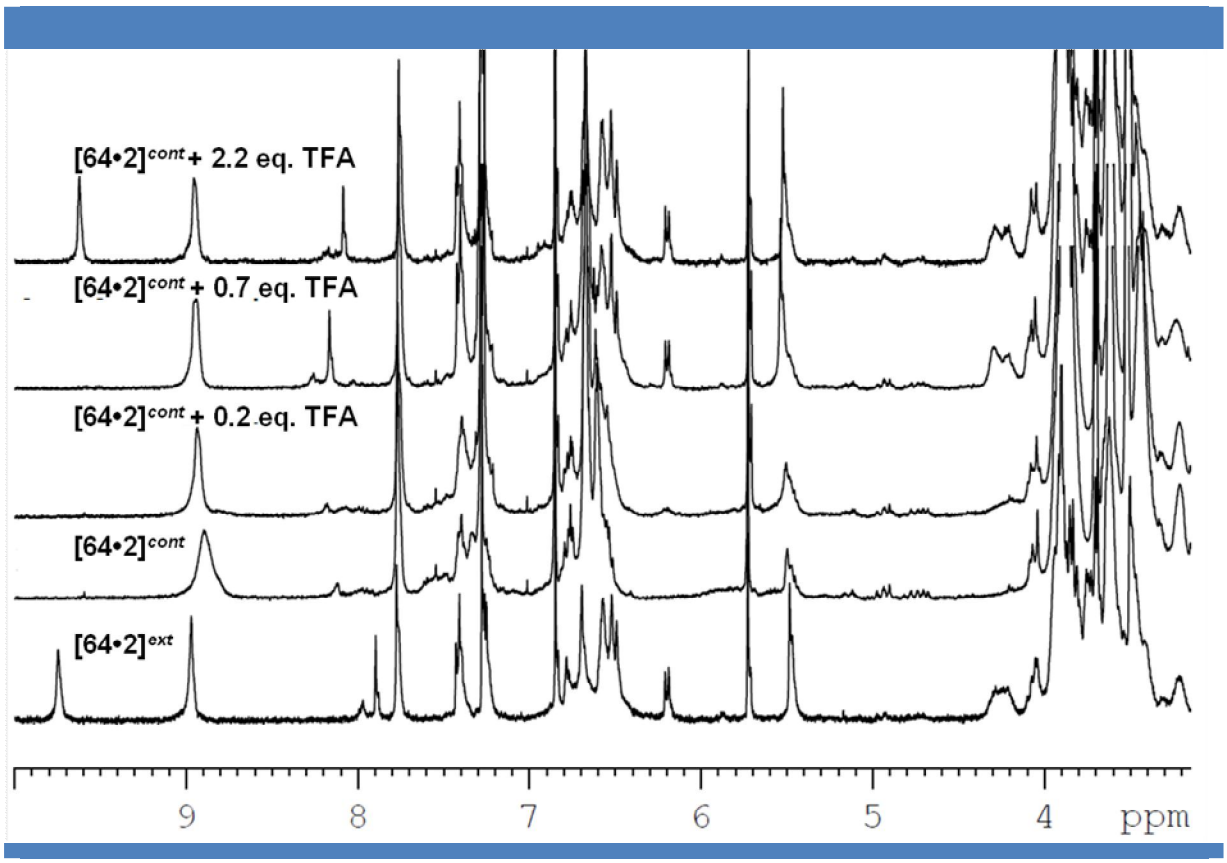

Figure 55 | ^{1}H NMR titration from $\mathbf{[64•2]}^{cont}$ to $\mathbf{[64•2]}^{ext}$ supramolecular polymers by adding *d*-TFA.

[114] Piot, L.; Palma, C. A.; Llanes-Pallas, A.; Prato, M.; Szekre´nyes, Z.; Kamara´s, K.; Bonifazi, D.; Samorı`, P. Selective Formation of Bi-Component Arrays Through H-Bonding of Multivalent Molecular Modules. *Adv. Funct. Mater.*, **19**, 1207–1214 (2009).

As shown in Figure 55, we can find a similar chemical shift changes for the **[64•2]**^{cont} to **[64•2]**^{ext} polymers as we found from the **2**^{cont} to **2**^{ext} monomer. When the amine moiety was protonated, the DB24C8 part moved toward the ammonium station. By comparing the [c2]daisy chains **[64•2]**^{cont} and **[64•2]**^{ext}, dramatically upfield shifts are observed for the triazolium protons H7 due to the uncomplexation of the crown ether to triazolium station.

b) Light and neutron scattering experiments

We have performed a series of neutron experiments to characterize further the polymerization of compound **2** with the two connectors described above. In the case of connector **I** alone, precipitation during experiment precluded a clear analysis of the monomer. For the second connector **64**, a clear characterization was obtained (Figure 56) indicating that no aggregation occurs at this concentration with the obtention a plateau at low q. The high-q data has been fitted by a Guinier expression for the form factor of the polymer section, determining the cross-section, S=5.12 Å^2, and the radius of gyration of the cross-section, R_c=0.4±0.05 Å, values in agreement with monomers section.

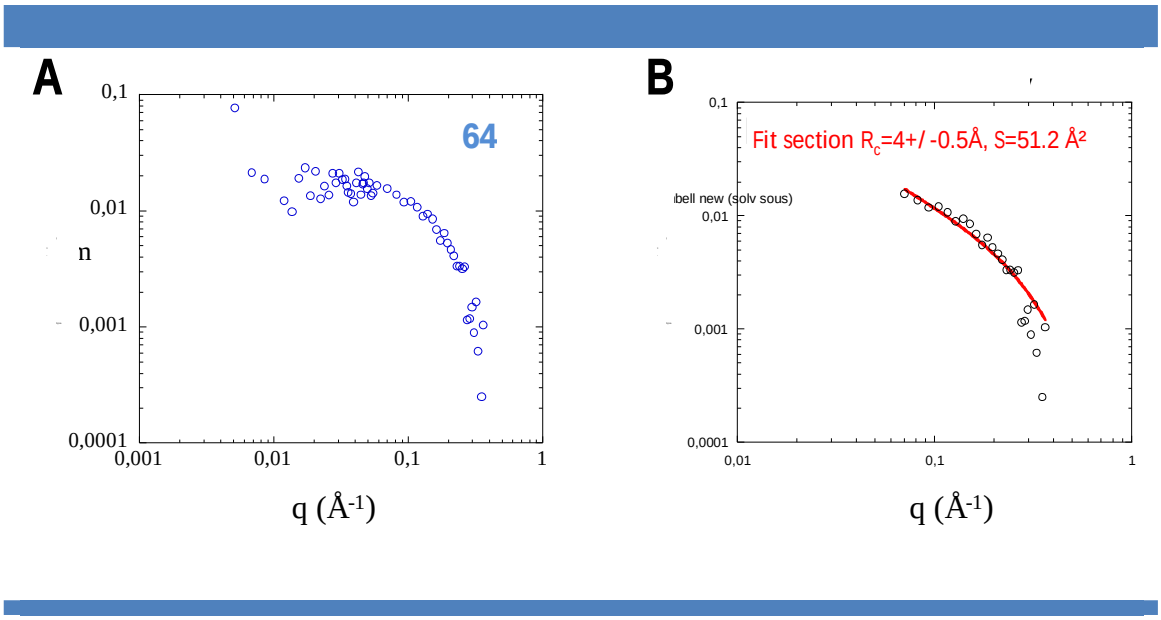

Figure 56 | SANS data (**A**) and corresponding fit (**B**) for a solution of **64** (10 mM in 1:1 $CDCl_3/CD_3CN$ at T=20°C). The red line represents the best fit of the data obtained using a classical Guinier expression (eq. S14, see experimental part).

In the same configuration, monomers **2**^{ext} and **2**^{cont} were analyzed by SANS and statisfyingly revealed no aggregation at this concentration (Figure 57, A and B). Interestingly, when **2**^{cont} is mixed with **64** in an equimolar ratio (Figure 57 C), an increase at small angles with a q^{-4} slope indicates either an aggregation of the monomer or a collapse of several polymer chains. However, it can be seen from the intensity of the plateau at higher q values (I_0=0.053 cm^{-1}, that the experimental molecular weight is M_w=3291 $g.mol^{-1}$, which exactly corresponds to the theoretical mass of the association between **2** and **64** ($C_{166}H_{230}F_{12}N_{18}O_{26}P_2$, 3180 g.mol-1), thus proving the supramolecular polymerization of our system, which then aggregates several single chains together. In the case of connector I however, if the same q-4 slope is observed at low values of q, we can see from the intensity of the plateau that no polymer is formed, and that the aggregation comes from connector **I** itself as also observed when measured alone, and because of its low solubilty. Finally, in Figure 57 D, **[64•2]**^{cont}.and **[64•2]**^{ext}.were compared and revealed a change in their aggregation state and their linear mass density, going as expected to a less dense extended form.

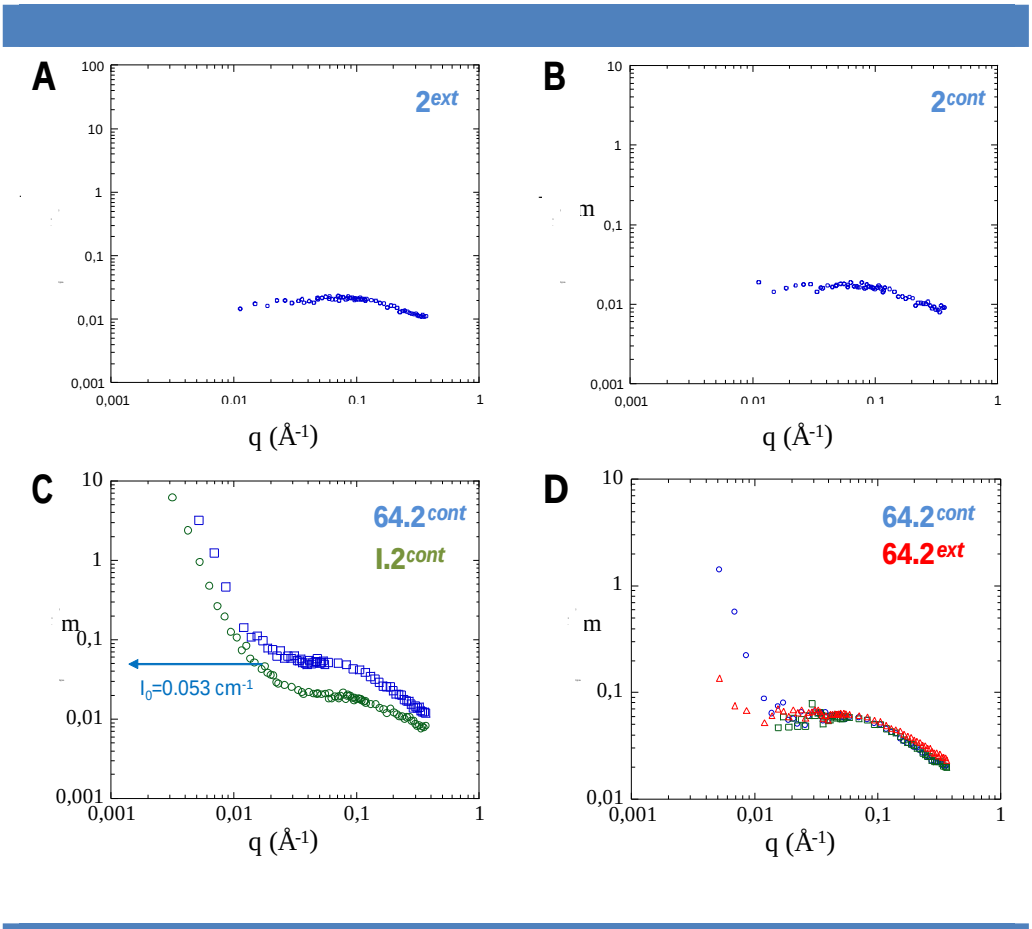

Figure 57 | SANS data of (**A**) monomer **2**^{ext}; (**B**) monomer **2**^{cont}; (**C**) H-bonding polymers **[64•2]**^{cont} and **[I•2]**^{cont} ; and (**D**) H-bonding polymers **[64•2]**^{cont} and **[64•2]**^{ext} (10 mM in 1:1 $CDCl_3/CD_3CN$ at T=20°C).

c) TEM microscopy

Interestingly, TEM imaging of **[64•2]**^{cont}.and **[64•2]**^{ext}.confirmed the formation of beautiful bundles of fibers (Figure 58). Just as described by neutrons in solution, single chain H-bonding polymers forms larger and stiffer fibbers by lateral aggregations which combine in dense networks of several micrometers. Although it is difficult to asses precisely the differences between the extended and contracted form of the polymer, we can notice some changes in the aspect and the density of the bundling. In sum, from this set of experiments, we can conclude that our objective to bring together several contractile sigle chains of polymers in larger aggregates by hydrogen bondings was successful. This kind of materials present high potential to amplify the nanoscopic motion above mesoscale in gels of films, and numerous experiments will be pursued in this direction.

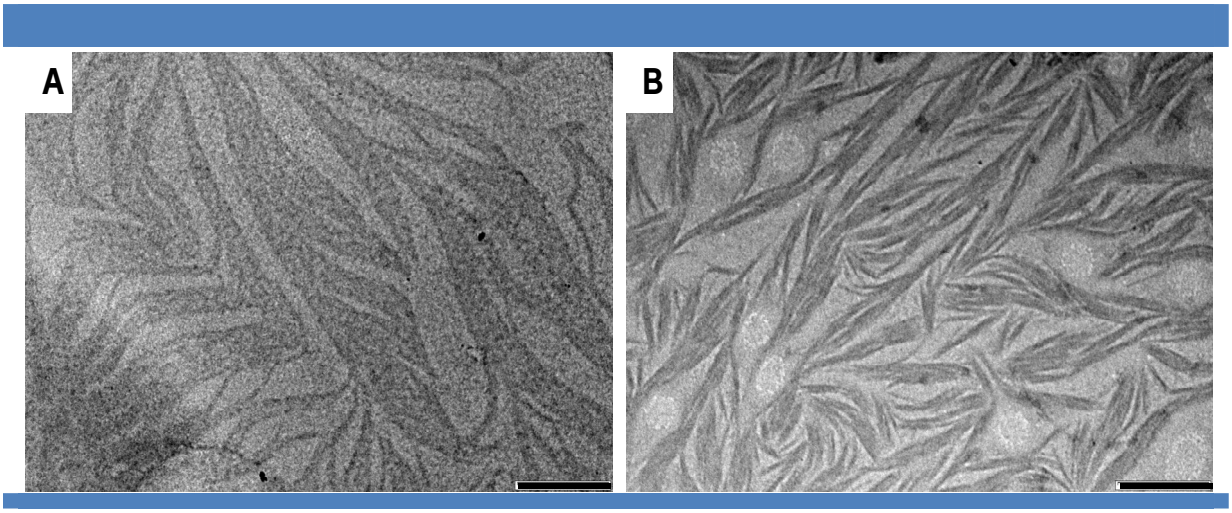

Figure 58 | TEM images of (**A**) **[64•2]**^{cont} and (**B**) **[64•2]**^{ext} (bar scales: 500nm).

3/ Synthesis of a model hydrogen-bonding rotaxane (ADA type)

We have also envisioned the synthesis of other types of hydrogen-bonding units such as acceptor-donor-acceptor (ADA)-ended rotaxane. This rotaxane was designed to polymerize with a DAD-type rotaxane and without dumbbell (Figure 59).

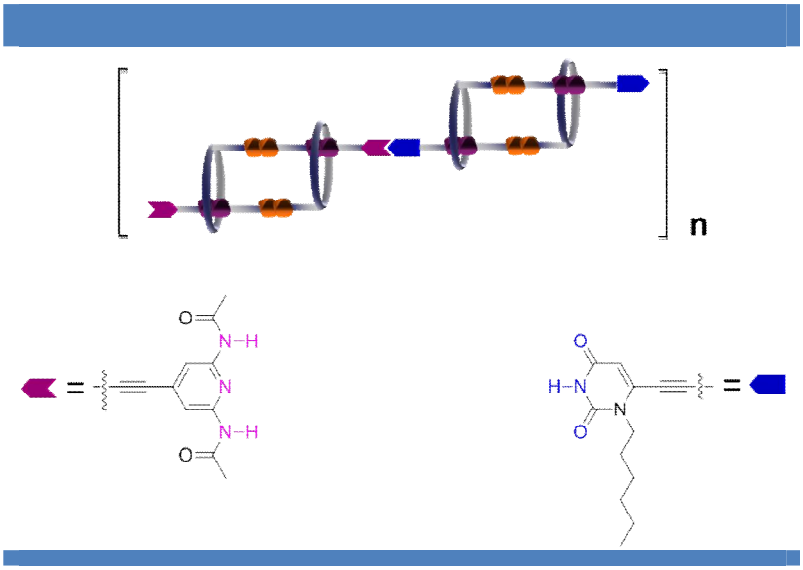

Figure 59 | General representation of two complementary H-bonding bistable rotaxane based supramolecular polymers.

Reaction of 4-ethynylbenzyl acetate **39** with **62** in the presence of CuI and $Pd(PPh_3)_4$ afforded the benzyl acetate **65** as a a brown powder, which was subsequently deprotected by KOH in MeOH with a relatively low yield (Scheme 31).

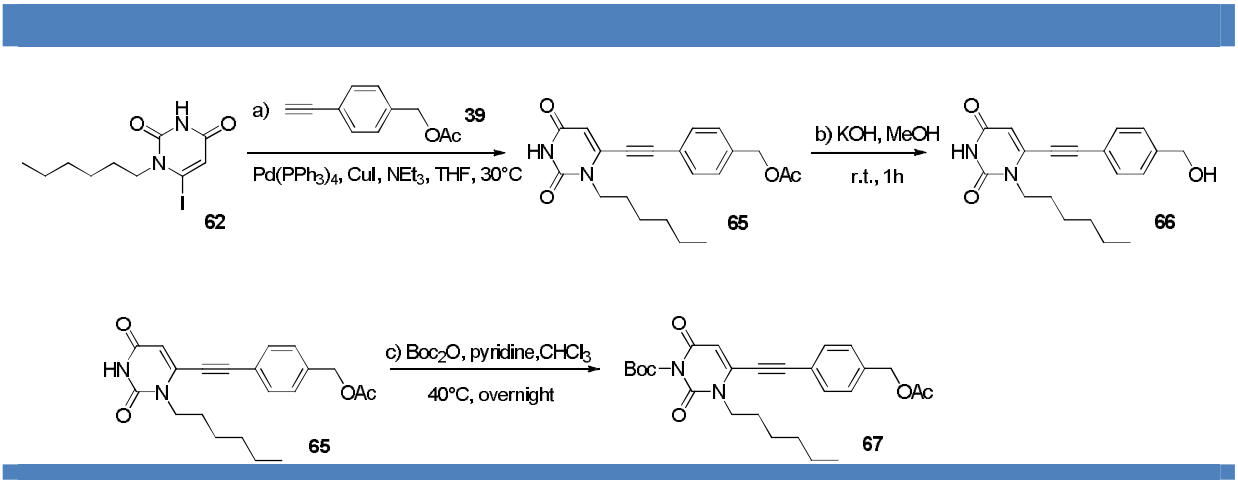

Scheme 31 | Synthesis of compound **67**.

Reaction conditions used for Scheme 31:

(a) **62** (1.0 equiv.), 4-ethynylbenzyl acetate **39** (1.2 equiv.), $Pd(PPh_3)_4$ (0.05 equiv.), CuI (0.07 equiv.), Et_3N/THF, 45°C, overnight, 86%; (b) KOH (5.0 equiv.), MeOH, r.t., 1h, 47%; (c) **65** (1.0 equiv.), Boc_2O (3.0 equiv.), pyridine, $CHCl_3$, 40°C, overnight, 88%.

The uracil unit was then protected using Boc_2O in pyridine before its introduction on the rotaxane which should be further mesylated on its triazole moiety.

In the meantime, another synthetic pathway was developed by protecting of the uracil group from 1-Hexyl-6-iodouracil in the presence of Boc_2O in pyridine (Scheme 32). Sonogashira reaction between 4-ethynylbenzyl acetate **39** and compound **68** in the presence of CuI and $Pd(PPh_3)_4$ afforded the benzl acetate **67** as a brown powder, which was subsequently deprotected by K_2CO_3 in a (2:1) mixture solvent of $MeOH/CH_2Cl_2$ with a much better yield compared with the previous pathway.

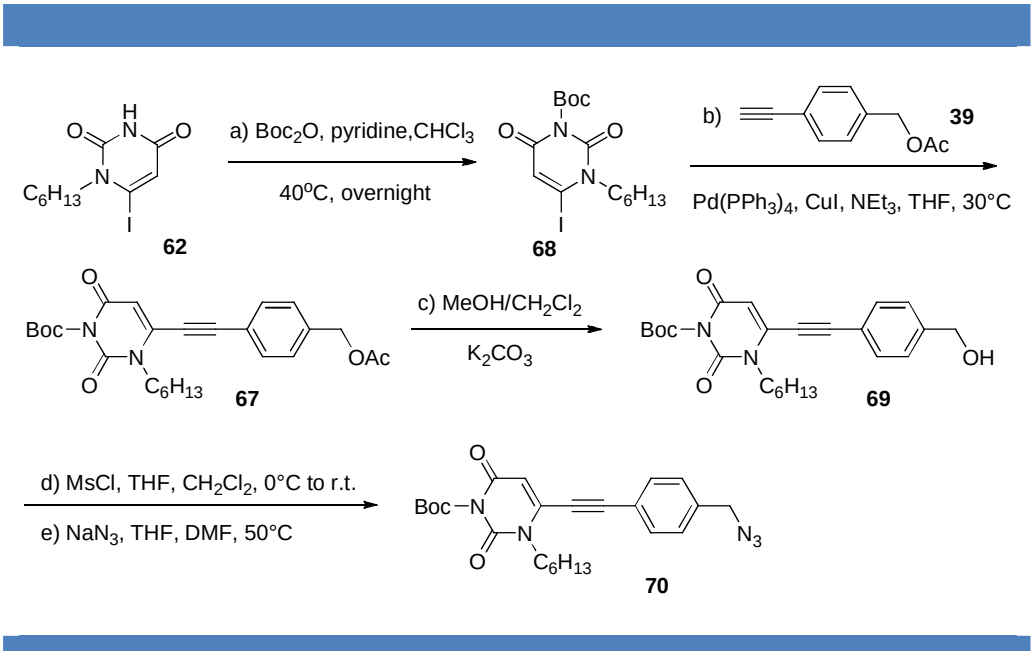

Scheme 32 | Synthesis of compound **70**.

Reaction conditions used for Scheme 32:

(a) **58** (1.0 equiv.), Boc_2O (3.0 equiv.), pyridine, $CHCl_3$, 40°C, overnight, 89%; (b) **68** (1.0 equiv.), 4-ethynylbenzyl acetate **39** (1.2 equiv.), $Pd(PPh_3)_4$ (0.04 equiv.), CuI (0.08 equiv.), NEt_3/THF, 45°C, overnight, 86%; (c) K_2CO_3 (12.0 equiv.), $MeOH/CH_2Cl_2$ (2:1), r.t., overnight, 88%. overnight, 89%; (d) compound **69** (1.0 equiv.), MsCl (1.3 equiv.), Et_3N (1.3 equiv.), CH_2Cl_2, 0°C to r.t., overnight; (e) NaN_3 (5.0 equiv.), DMF/THF (1:1), 50°C, overnight, 37% (2 steps).

The benzyl azide **70** was then obtained in two steps by treatment with methanesulfonyl chloride at 0°C affording the crude mesylated compound, which was then reacted with sodium azide at 50°C.

The introduction of the complementary hydrogen-bonding uracil stopper **70** on the pseudorotaxane **11** was carried out by microwave irradiation in a mixture solvent of CH_2Cl_2/CH_3CN in the presence of $Cu(MeCN)_4PF_6$, but was not purified further and characterizations are currently performed (Scheme 33).

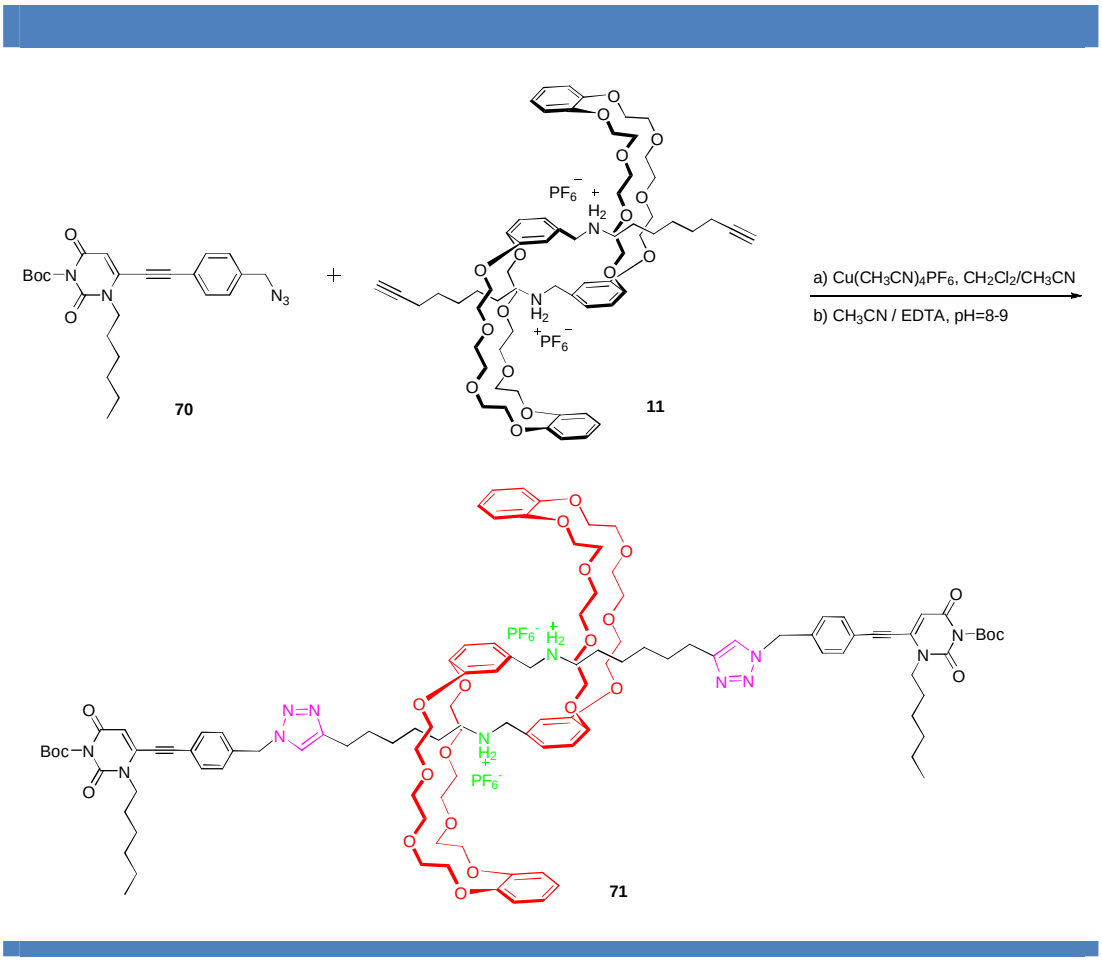

Scheme 33 | Synthesis of compound **71**.

Reaction conditions used for Scheme 33:

(a) pseudo-rotaxane **11** (1.0 equiv.), benzyl azide **70** (2.1 equiv.), $Cu(CH_3CN)_4PF_6$ (2.0 equiv.), 2,6-lutidine (2.0 equiv.), CH_2Cl_2/CH_3CN, 2h, 30°C; (b) EDTA aq.(pH ≈ 8-9), CH_3CN, 2h.

4/ Conclusions

The work of this chapter describes the syntheses of two types of hydrogen-bonding supramolecular polymer rotaxanes. A DAD-type hydrogen-bonding rotaxane **2** was first synthesized and polymerized by connector **64** having complementary hydrogen-bonds. The pH modulation of contraction/extension was demonstrated for both of the monomer and polymers. SANS and TEM studies showed that bundles of fibers were formed after polymerization. This systems seems promising to generate macroscopic contractions and extensions in gels or films by the coordinated motions of molecular machines and and the project will be pursued in the next future.

The syntheses of another ADA type hydrogen-bonding rotaxane was envisioned, and further works are in progress to characterize it.

Conclusion and Perspectives

One of the current challenges in nanotechnologies consists in coupling together well-defined molecular machines, individually producing translational or rotational motions, in order to amplify their mechanical output by several orders of magnitude. In particular, recent example by Stoddart and Grubbs attempted to polymerize bistable [2] rotaxane monomers by click chemistry but without showing high degrees of condensation, thus precluding the production and characterization of amplified motion along the polymer chains.

The main objective of my PhD work was to develop well-soluble supramolecular polymers with high degrees of polymerization based on bistable [2] rotaxane monomers and which can contract and extend upon pH modulation. We have described the synthesis and characterization of a series of bistable polyrotaxanes which were polymerized by either covalent bonds, or metallo-supramolecular connections, or hydrogen-bonds.

If in the case of the covalent polyrotaxanes mainly low DP were obtained and for longer polymers, problems of solubility were encountered. However, supramolecular polymers were revealed as very interesting candidates for this study. First, the formation of high molecular weight single chain polymers (up to 8×10^6 $g.mol^{-1}$) were obtained through the metallo-polymerization approach with the terpyridine ended rotaxane monomer. We have shown that their molecular motions based on each monomer have been successfully translated from the nanometer to the tens of the micrometers through a number of experimental evidences. Thus, we have shown that an amplification by four orders of magnitude of the mechanical output of thousands of molecular machines linked within a single-strand macromolecular chain, going from the low nanometer scale to the ten of micrometers, is accessible by combining molecular synthesis, supramolecular engineering, and polymerization processes.

In another example, consisting in a rotaxane monomer ended by pyridine bis-imide units which can form donor-acceptor-donor type hydrogen-bonding with a complementary connector, we have been able to combine several level of hierarchical organization by bundling the contractile single chains in larger fibers. The translational motion of the rotaxane and of the corresponding polymer with the connector was studied by ^1H NMR and neutron scattering. TEM studies showed the formation of bundles of fibers, a promissing structuring to cross the scales up to macroscopic motions in films or gels. Yet, the macroscopic response of these later systems should be investigated further.

Overall, the results presented in chapter 3 are the most significant because they represent the first example in the literature showing this synchronization of thousands of linear molecular machines to cross several length scales and as such, it is considered as a major step in supramolecular chemistry at its interface with nanotechnologies. However, we believe that the structures using branched terpyridine units and H-bonded systems should be studied further to probe their contractile behavior at the macroscopic scale, in films or gels. As we have now defined efficient synthetic pathways to produce them in large quantities, physical chemistry can be envisaged to find the good conditions to probe the hierarchical dynamic of these materials.

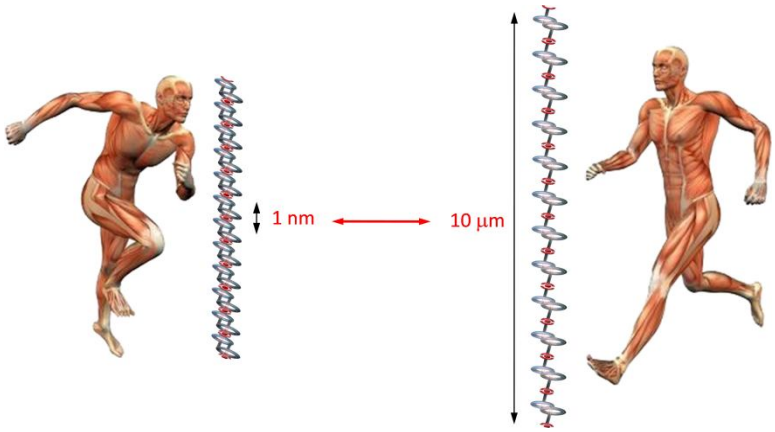

EXPERIMENTAL PART

Synthesis and characterization of organic compounds

1/ General Procedures

a) *Solvent and chemical reagents*

All reagents and solvents were purchased at the highest commercial quality and used without further purification unless otherwise noted. Dry solvents were obtained using a double column SolvTech purification system. Water was deionized by using a milli-gradient system (Millipore, Molsheim, France). All reactions were carried out under argon atmosphere. Microwave reactions were carried out with a single mode cavity Discover Microwave Synthesizer (CEM Corporation, NC, USA), producing continuous irradiation at 2455 MHz and equipped with simultaneous external air-cooling system. Yields refer to spectroscopically purified (^{1}H NMR) homogeneous materials.

b) *Chromatographic methods*

Thin Layer Chromatographies were performed using TLC silica plastic sheets (Polygram SIL G/UV254, Macherey-Nagel) or TLC alox plastic sheets (Polygram Alox N/UV254, Macherey-Nagel). In most cases, irradiation using a *Bioblock VL-4C* UV-Lamp (6 W, 254 nm and/or 365 nm) as well as *p*-anisaldehyde and Ce-molybdate stainings were used for visualization. *Preparative Adsorption Flash Column Chromatographies* were performed using silica gel (Geduran, silica gel 60 (230 – 400 mesh, 40 – 63 μm, Merck)) or aluminium oxide 90 (standardized activity II, 70 – 230 mesh, Merck).

c) *Analytical methods and instruments*

i) Nuclear Magnetic Resonance (NMR).

^{1}H NMR spectra were recorded on a *Bruker Avance 400* spectrometer at 400 MHz and ^{13}C spectra at 100 MHz. The spectra were internally referenced to the residual proton solvent signal. Residual solvent peaks were taken as reference ($CDCl_3$: 7.26 ppm, d_6-dmso: 2.50 ppm,

CD_3OD: 3.31 ppm). For ^1H NMR assignments, the chemical shifts are given in ppm. Coupling constants *J* are given in Hz. Peaks are described as singlet (s), doublet (d), triplet (t), quartet (q), multiplet (m) and broad (br).

ii) Mass spectrometry.

Ultra Performance Liquid Chromatographies coupled to Mass Spectroscopy (UPLC-MS) were carried out on a *Waters Acquity UPLC-SQD* apparatus equipped with a PDA detector (190–500 nm, 80Hz), using a reverse phase column (Waters, BEH C_{18} 1.7 µm, 2.1 x 50 mm), the MassLynx 4.1 – XP software and a gradient (water-acetonitrile + 0.1% TFA) as eluent.

MALDI-TOF mass spectra were recorded on a Bruker Daltonics AutoflexII TOF spectrometer.

iii) Elemental analyses.

Elemental analyses were performed by the Service de Microanalyse, Institut Charles Sadron, CNRS.

iv) Small angle neutron scattering (SANS)

SANS spectra were performed on the PAXE and PACE spectrometers at the Laboratoire Leon Brillouin (LLB, CEA Saclay).

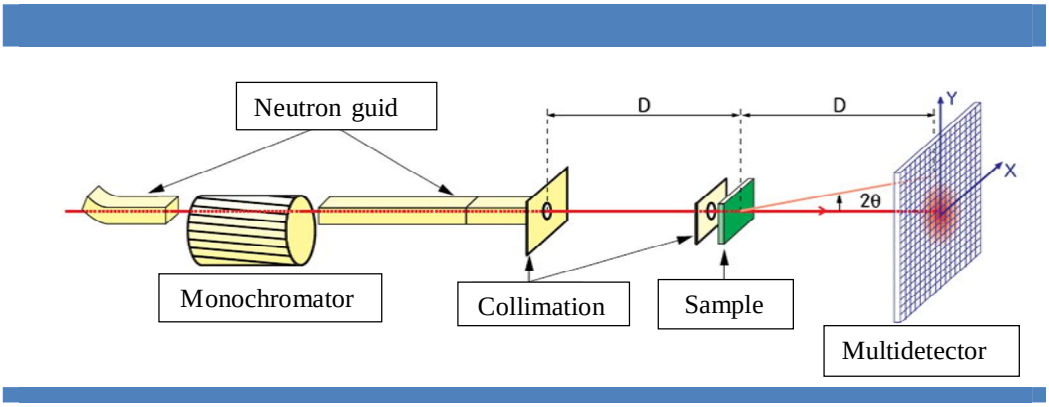

Figure 53 | General scheme of the small angle neutron scattering principle

The chosen incident wavelength, λ, depends on the set of experiments, as follows. For a given wavelength, the range of the amplitude of the transfer wave vector *q* was selected by changing the detector distance, D. Two sets of sample-to-detector distances and wavelengths

were chosen (D = 1.2 m, λ = 5 ± 0.5 Å; and D = 4.7 m, λ = 8± 0.5 Å) so that the following q-ranges were respectively available: $3.54\times10^{-2} \leq q$ (Å^{-1}) $\leq 3.65\times10^{-1}$, and $5.2\times10^{-3} \leq q$ (Å^{-1}) $\leq 5.5\times10^{-2}$. Measured intensities were calibrated to absolute values (cm^{-1}) using normalization by the attenuated direct beam classical method. Standard procedures to correct the data for the transmission, detector efficiency, and backgrounds (solvent, empty cell, electronic, and neutronic background) were carried out. The scattered wave vector, q, is defined by equation 1, where θ is the scattering angle:

$$q = \frac{4\pi}{\lambda}\sin\frac{\theta}{2} \qquad \text{(S1)}$$

The usual equation for absolute neutron scattering combines the intraparticle scattering $S_1(q) = V_{chain}\phi_{vol}P(q)$ form factor with the interparticle scattering $S_2(q)$ factor

$$I(q)(cm^{-1}) = (\Delta\rho)^2\left(S_1(q) + S_2(q)\right) = (\Delta\rho)^2\left(V_{chain}\phi_{vol}P(q) + S_2(q)\right) \qquad \text{(S2)}$$

where $(\Delta\rho)^2=(\rho_{monomer}-\rho_{solvent})^2$ is a contrast per unit volume between the polymer and the solvent and was determined from the known chemical composition. $\rho = \Sigma n_i b_i/(\Sigma n_i m_i v\times1.66\times10^{-24})$ represents the scattering length per unit volume, b_i is the neutron scattering length of the species i, m_i the mass of species i, and v the specific volume of the monomer (which was measured and been taken to be equal to 0.704 cm^{3}g^{-1}) or the solvent (i.e., 0.77 cm^{3}g^{-1} for 50/50 $CDCl_3$/CD_3CN). $P(q)$ is the form factor, $V_{chain}=Nvm\times1.66\times10^{-24}$ is the volume of the N monomers (of mass m) in a chain and ϕ_{vol} is the volume fraction of monomer. In the high q-range, the scattering is assumed to arise from isolated chains; i.e., $S_2(q) = 0$, and thus $I(q) \propto P(q)$.

v) Dynamic and Static light scattering experiments (DLS and SLS)

DLS and SLS spectra were performed at the University Paris Diderot on the 3D DLS spectrometer (LS Instruments, Fribourg, Switzerland) equipped with a 25mW HeNe laser (JDS uniphase) operating at λ=632.8 nm, a two channel multiple tau correlator (1088 channels in autocorrelation), a variable-angle detection system, and a temperature-controlled index matching vat (LS Instruments). The scattering spectrum was measured using two single mode fibre detections and two high sensitivity APD detectors (Perkin Elmer, model SPCM-

AQR-13-FC). Solutions were directly filtered through 0.22 μm Millipore filter into the scattering cell.

In the dynamic light scattering experiments (DLS), the normalized time autocorrelation function, $g^{(2)}(q,t)$, is measured as a function of the scattered wave-vector, q, given by $q=(4\pi n/\lambda)\sin(\theta/2)$, where n is the refractive index of the solvent (1.39 for 50/50 $CDCl_3/CD_3CN$ at 20 °C), and θ is the scattering angle. In our experiments, θ was varied between 30° and 140°, which corresponds to scattering wave vectors, q, in the range from 7.2×10^{-3} to 2.6×10^{-2} nm^{-1}. The measurements used a 3D DLS spectrometer (LS Instruments, Fribourg, Swiss) equipped with a 25mW HeNe laser (JDS uniphase) operating at λ=632.8 nm, a two channel multiple tau correlator (1088 channels in autocorrelation), a variable-angle detection system, and a temperature-controlled index matching vat (LS Instruments). The scattering spectrum was measured using two single mode fibre detections and two high sensitivity APD detectors (Perkin Elmer, model SPCM-AQR-13-FC). Solutions were filtered through 0.2 μm PTFE Millipore filter into the cylindrical scattering cell.

In Static Light Scattering (SLS) experiments, the excess of scattered intensity is measured with respect to the solvent. The absolute scattering intensity (i.e., the excess Rayleigh ratio in cm^{-1}) can be deduced by using a toluene sample reference for which the excess Rayleigh ratio is well-known ($R_{toluene}=1.3522\times10^{-5}$ cm^{-1} at 633 nm):

$$R_{solute}(cm^{-1}) = \frac{I_{solution} - I_{solvent}}{I_{toluene}} \times \left(\frac{n}{n_{toluene}}\right)^2 \times R_{toluene}(cm^{-1}) \qquad \text{(S3)}$$

The usual equation for absolute light scattering combines the form factor P(q), the structure factor S(q) and the weight-average molecular weight M_W of the scattered objects:

$$R(q) = \frac{4\pi^2 n^2}{N_A \lambda^4}\left(\frac{dn}{dc}\right)^2 C M_W P(q) S(q) \qquad \text{(S4)}$$

C is the solute concentration in g/cm^3. The scattering constant is $K=4\pi^2n^2(dn/dC)^2/N_A\lambda^4$ where dn/dC is the refractive index increment (measured using a Mettler Toledo PortableLab refractometer) and N_A is Avogadro's number ($K=3.23\text{x}10^{-8}$, $5.54\text{x}10^{-6}$, and $3.53\text{x}10^{-6}$ $cm^2.g^{-2}.mol$ respectively for **Zn1**^{cont}, **Fe1**^{cont}, and **Fe1**^{ext}).

In DLS the experimental signal is the normalized time autocorrelation function of the scattered intensity:

$$g^{(2)}(q,t) = \frac{\langle I(q,0)I(q,t)\rangle}{\langle I(q,0)\rangle^2} \qquad \text{(S5)}$$

The latter can be expressed in terms of the field autocorrelation function or equivalently in terms of the autocorrelation function of the concentration fluctuations, $g^{(1)}(q,t)$, through:

$$g^{(2)}(q,t) - 1 = \alpha + \beta\left|g^{(1)}(q,t)\right|^2 \qquad \text{(S6)}$$

Where α is the baseline (varying between 1×10^{-4} and 2×10^{-4} depending on the scattering angle and/or the system) and β the coherence factor, which in our experiments is varying between 0.7 and 0.9 depending on the samples. The normalized dynamical correlation function, $g^{(1)}(q,t)$, of polymer concentration fluctuations is defined as:

$$g^{(1)}(q,t) = \frac{\langle \delta c(q,0)\delta c(q,t)\rangle}{\langle \delta c(q,0)^2\rangle} \qquad \text{(S7)}$$

Where $\delta c(q,t)$ and $\delta c(q,0)$ represent fluctuations of the polymer concentration at time t and zero, respectively.

In our experiments, some of our solutions were characterized by a single relaxation mechanism with a characteristic relaxation time inversely proportional to q^2. The extrapolation of $(\tau_c q^2)^{-1}$ to q=0, where τ_c is the average relaxation time of $g^{(1)}(q,t)$, yields the mutual diffusion coefficient D. The latter is related to the average apparent hydrodynamic radius, R_H, of the species through the Stokes-Einstein relation:

$$D = \frac{k_B T}{6\pi\eta_s R_H} \qquad \text{(S8)}$$

Where k_B is the Boltzmann constant, η_s the solvent viscosity (0.444 cP for 50/50 $CDCl_3/CD_3CN$ at T=20°C), and T the absolute temperature.

To determine the sizes as well as the size distributions, especially when solutions were characterized by several relaxation mechanisms (e.g. monomers and polymers), we have used the Contin method based on the inverse Laplace transform of $g^{(1)}(q,t)$. If the spectral profile of

the scattered light can be described by a multi-Lorentzian curve, then $g^{(1)}(q,t)$ can be written as:

$$g^{(1)}(q,t) = \int_0^\infty G(\Gamma)\exp(-\Gamma t)d\Gamma \qquad \text{(S9)}$$

Where G(Γ) is the normalized decay constant distribution.

Worm-like chain model:

To interpret the scattering and extract the structural parameters, it is also very useful to have a correct expression of the scattering of an individual chain, P(q). We have used an expression *(4, 5)* based on the expressions derived by Burchard and Kajiwara for rodlike structure *(6)* in which the form factor calculated by Sharp and Bloomfield *(7)* for finite wormlike chains of contour length L_c is used at low q.

$$P(q) = \left(\frac{2[\exp(-x)+x-1]}{x^2} + \left[\frac{4}{15}+\frac{7}{15x} - \left(\frac{11}{15}+\frac{7}{15x}\right)\exp(-x)\right]\frac{2L_p}{L_c}\right)\times\exp\left[-\left(\frac{2qL_p}{\alpha}\right)^\beta\right] \qquad \text{(S10)}$$
$$+\left(\frac{1}{2L_cL_pq^2}+\frac{\pi}{qL_c}\right)\times\left(1-\exp\left[-\left(\frac{2qL_p}{\alpha}\right)^\beta\right]\right)$$

With $x=L_cL_pq^2/3$ and valid for $L_c>4L_p$. Values of the empirical parameters $\alpha=5.53$ and $\beta=5.33$, which contribute to the balance between the low-q and large-q terms, have been optimized in ref. 4. Polydispersity and excluded volume effects can be neglected in the regime $qR_G>1$ where the scattering experiments were performed *(ref. 25 of the main text)*; with R_G being the radius of gyration of the chains.

High-q data can be fitted by a Guinier expression for the form factor of the polymer section:

$$V_{chain}P(q) = \frac{\pi S}{q}\exp\left(-\frac{q^2R_c^2}{2}\right) \qquad \text{(S11)}$$

Determination of the density of the monomers:

To determine the density *d* of the compounds we used the SANS measurements of the monomer solutions (without metals) as shown in Figure 44. Indeed the scattering intensity extrapolated to q=0 can be expressed as follows:

$$I_0 = \frac{\phi \Delta\rho^2 M^\circ}{dN_a} = \frac{C\Delta\rho^2 M^{\circ 2}}{d^2 N_a} \qquad \text{(eq. S12)}$$

With C being the monomer concentration, $\Delta\rho^2=(\rho-\rho_{solvent})^2$ the contrast term, M° the molar mass of the monomer, N_a the Avogadro number and *d* the density.

As the density is also present in the calculation of the contrast term we have to determine *d* which satisfies the following relation:

$$\frac{d^2}{\Delta\rho^2} = \frac{CM^{\circ 2}}{I_0 N_a} \qquad \text{(eq. S13)}$$

Hence, the extrapolation of the intensities to q=0 gives I_0=0.0185cm^{-1} for **1**^{ext} and I_0=0.021 cm^{-1} for **1**^{cont}. Using these values and the relation S13 we thus obtained a density of 1.42g/cm^3 and 1.30 g/cm^3 for respectively **1**^{ext} and **1**^{cont}.

Finally we can also determine the radius of gyration R_g of the monomers using the Guinier relation:

$$I(q) = I_0 \exp(\frac{-q^2 R_g{}^2}{3}) \qquad \text{(eq. S14)}$$

We obtained R_g=8.9+/-0.1Å for both monomers.

vi) Transmission Electron Microscopy (TEM) experiments

TEM experiments were performed using a CM12 Philips microscope equipped with a MVIII (SoftImaging System) CCD camera. Samples were analyzed in Bright Field Mode with a LaB6 cathode and 120 kV tension. Image treatments were performed by using analySIS (Soft Imaging System) software. For the sample preparation, a carbon-coated copper grid was placed on a Whatman filter paper. Then, a 5 µL drop was casted on the grid and the grid was left to dry at air before analysis.

2 / Synthesis of compounds

Compound 3

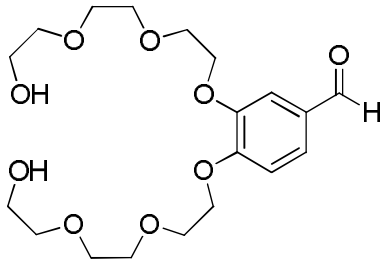

3

3,4-Bis{2-[2-(2-hydroxyethoxy)ethoxy]ethoxy}benz-aldehyde: 3,4-Dihydroxybenzaldehyde (0.50 g, 0.36 mmol), K_2CO_3 (1.24 g, 0.90 mmol) and LiBr (0.32 g, 0.36 mmol) were placed in a 50 mL round-bottomed flask fitted with a condenser and a pressure-equalized dropping funnel, and anhydrous DMF (25 mL) was added. 2-[2-(2-Chloroethoxy) ethoxy] ethanol (1.35 g, 0.80 mmol) was dissolved in DMF (3.5 mL) and added to the dropping funnel, through a flow of nitrogen. The suspension in the flask was heated to 100 °C while stirring and the 2-[2-(2-Chloroethoxy) ethoxy] ethanol solution was added dropwise over 1 hour. The reaction mixture was stirred at 100 °C for 3 days. After this time, the reaction mixture was filtered (in order to remove inorganic salts) and evaporated to dryness, and the residue was partitioned between CH_2Cl_2 (10 mL) and 10% w/v K_2CO_3 (10 mL) solution. The organic layer was further washed with 10% w/v K_2CO_3 solution (3 × 5 mL), dried over Na_2SO_4 and concentrated. The crude was purified by column chromatography (SiO_2, CH_2Cl_2 → CH_2Cl_2/MeOH 96/4) to give compound **3** (1.40 g, 93%) as a pale yellow oil. R_f = 0.1 (CH_3OH/CH_2Cl_2: 1/99); ^{1}H NMR ($CDCl_3$, 400 MHz, 25°C): δ = 9.83 (s, 1H), 7.46-7.43 (m, 2H), 6.98 (d, J = 8.6 Hz, 1H), 4.27-4.22 (m, 4H), 3.94-3.89 (m, 4H), 3.78-3.62 (m, 16H), 3.60 (br s, 2H); ^{13}C NMR ($CDCl_3$, 100 MHz, 25°C): δ = 190.8, 154.0, 148.9, 130.1, 126.7, 112.2, 111.5, 72.6, 70.8, 70.7, 70.2, 69.3, 69.2, 68.5, 61.5.

Compound 4

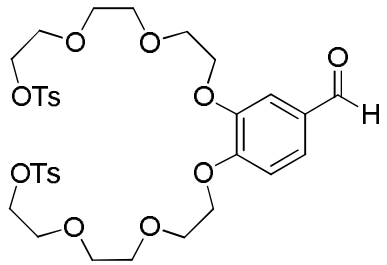

4

3,4-Bis(2-{2-[2-(p-toluenesulfonyloxy)ethoxy]ethoxy}-ethoxy)benzaldehyde: 3,4-Bis{2-[2-(2-hydroxyethoxy)ethoxy]ethoxy}benzaldehyde (1.89 g, 4.7 mmol), Et_3N (4.76 g, 47.0 mmol) and a catalytic amount of 4-(dimethylamino)pyridine were dissolved in CH_2Cl_2 (28.7 mL), and this solution was cooled to 0-5°C. A solution of *p*-toluenesulfonyl chloride (4.48 g, 23.5 mmol) in CH_2Cl_2 (14.7 mL) was then added dropwise over a period of 1 hour while maintaining the reaction temperature below 5°C. The reaction mixture was then stirred for 8 hours at 5°C and finally acidified with HCl 5M solution (18 mL). Tthe organic layer was washed with 2M HCl solution (15 mL) and saturated brine (2 × 15 mL), dried over Na_2SO_4, and the solvents were removed in vacuo. The residue was purified by column chromatography (SiO_2, EtOAc/n-hexane: 1/1 → EtOAc/n-hexane: 4/1) to yield compound **4** (2.77 g, 84%) as a pale yellow oil. R_f = 0.2 (EtOAc/n-hexane: 2/1); ^{1}H NMR ($CDCl_3$, 400 MHz, 25°C): δ = 9.84 (s, 1H), 7.78 (d, *J* = 8.2 Hz, 4H), 7.45-7.41 (m, 2H), 7.32 (d, *J* = 8.2 Hz, 4H), 6.99 (d, *J* = 8.2 Hz, 1H), 4.24-4.13 (m, 8H), 3.86 (m, 4H), 3.70-3.59 (m, 12H), 2.42 (s, 6H); ^{13}C NMR ($CDCl_3$, 100 MHz, 25°C): δ = 190.9, 154.3, 149.2, 144.8, 133.0, 130.3, 129.9, 128.0, 126.8, 112.5, 111.8, 111.3, 70.8, 69.6, 69.5, 69.3, 69.2, 68.7, 21.6.

Compound 5

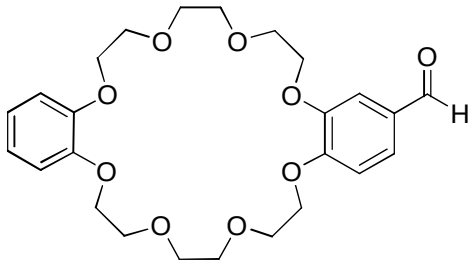

5

(2-Formyl)dibenzo[24]crown-8: Cesium carbonate (2.29 g, 7.03 mmol) was placed in a 150 mL round-bottomed flask fitted with a condenser and a pressure-equalized dropping funnel and anhydrous DMF (24 mL) was added. The ditosylate **4** (1.00 g, 1.41 mmol) and cathecol (155 mg, 1.41 mmol) were dissolved in DMF (60 mL) and added to the dropping funnel. The suspension in the flask was heated to 100°C while stirring and the ditosylate /catechol solution was added dropwise over 8 hours. The mixture was stirred at 100°C during 7 days. Subsequently, the solvent was removed in vacuo and the residue partitioned between toluene (35 mL) and 10% w/v K_2CO_3 (35 mL). The aqueous layer was further extracted with toluene (3 × 25 mL) and the combined organic layers were washed with 10% w/v K_2CO_3 (35 mL). The organic phase was dried over Na_2SO_4 and the solvents were removed in vacuo. The residue was purified by column chromatography (SiO_2, EtOAc → EtOAc/MeOH 99/1) to

yield compound **5** (460 mg, 69%) as a white solid. R_f = 0.35 (EtOAc); ^{1}H NMR ($CDCl_3$, 400 MHz, 25°C): δ = 9.81 (s, 1H), 7.41 (dd, 2H), 7.37 (d, *J* = 8.2 Hz, 1H), 6.94 (d, *J* = 8.2 Hz, 1H), 6.89-6.86 (m, 4H), 4.22-4.18 (m, 8H), 3.96-3.92 (m, 8H), 3.84-3.82 (m, 8H); ^{13}C NMR ($CDCl_3$, 100 MHz, 25°C): δ = 190.9, 154.4, 149.3, 149.0, 130.3, 126.9, 121.5, 114.2, 112.0, 111.2, 71.7, 71.5, 71.4, 70.1, 69.7, 69.8, 69.7. ESI-MS: calcd. for $C_{25}H_{32}O_9$: 499.20 $[M+Na]^+$, found: 499.16.

Compound 6

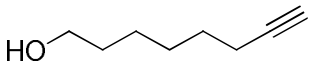

6

Oct-7-yn-1-ol: To dry ethylene-1,2-diamine (60 mL) at 0°C was added NaH (5.07 g, 126.1 mmol, 60% in oil) in one portion. The white mixture was allowed to warm slowly to 60°C and stirred for 1 hour to give a deep blue mixture. It was then cooled to 45°C and 3-octyn-1-ol (3.79 g, 31.7 mmol) was added dropwise. The solution was stirred at 60°C for 1 hour and cooled to 0°C to provide a purple solution. Water (100 mL) and Et_2O (100 mL) were then added slowly and HCl 12M was added very slowly until pH 1. The aqueous layer was extracted with Et_2O (4 x 100 mL) and the organic layers were combined, dried over Na_2SO_4 and concentrated. The crude oil was then purified by column chromatography (SiO_2, n-hexane → n-hexane/EtOAc 1/1) to provide product **6** (3.06 g, 81 %) as a yellow oil. R_f = 0.3 (n-hexane/EtOAc: 3/1); ^{1}H NMR ($CDCl_3$, 400 MHz, 25°C): δ = 3.63 (t, *J* = 6.7 Hz, 2H), 2.19 (td, *J* = 7.0, 2.7 Hz, 2H), 1.91 (t, *J* = 2.6 Hz, 1H), 1.61-1.51 (m, 4H), 1.49-1.33 (m, 4H); ^{13}C NMR ($CDCl_3$, 100 MHz, 25°C): δ = 84.7, 68.3, 63.0, 32.7, 28.6, 28.5, 25.4, 18.5; ESI-MS: calcd. for $C_8H_{14}O$: 127.11 $[M+H]^+$, found: 127.18.

Compound 7

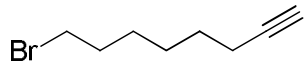

7

1-bromooct-7-yne: To a solution of oct-7-yn-1-ol (2.35 g, 18.6 mmol) in dry CH_2Cl_2 (77 mL) were added CBr_4 (9.28 g, 28 mmol) and PPh_3 (9.55 g, 36.4 mmol). The mixture was stirred at reflux for 1 hour. A solution of EtOAc/n-hexane (100 mL, 10/90) was then added and the resulting precipitate was filtered and washed abundantly with pentane. The filtrate was evaporated and the crude mixture was purified by by column chromatography (SiO_2, n-hexane → n-hexane/EtOAc 9/1) to give compound **7** (2.12 g) in a quantitative yield as a colorless oil. R_f = 0.23 (n-hexane/EtOAc: 9/1); ^{1}H NMR ($CDCl_3$, 400 MHz, 25°C): δ = 3.39 (t, *J* = 6.8 Hz,

2H), 2.18 (td, *J* =6.8, 2.7 Hz, 2H), 1.92 (t, *J* = 2.6 Hz, 1H), 1.89-1.82 (m, 2H), 1.56-1.47 (m, 2H), 1.46-1.34 (m, 4H); ^{13}C NMR ($CDCl_3$,100 MHz, 25°C): δ = 84.5, 68.5, 33.9, 32.8, 28.3, 27.9, 27.8, 18.5.

Compound 8

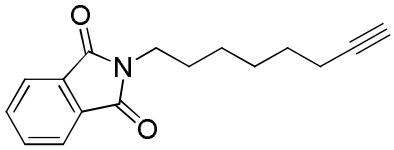

8

8-phtalimidooct-1-yne: Potassium phtalimide (1.80 g, 9.77 mmol) was added to a solution of 8-bromooct-1-yne (1.23 g, 6.49 mmol) in DMF (20 mL). After stirring for 1 hour at 70°C, the solvent was removed in vacuo. The solid residue was suspended in CH_2Cl_2 (30 mL) and filtered through a pad of silica gel. The filtrate was evaporated to give compound **8** (1.29 g, 78%) as a colorless oil. R_f = 0.6 (n-hexane/EtOAc: 3/1); ^{1}H NMR ($CDCl_3$, 400 MHz, 25°C): δ = 7.85-7.83 (m, 2H), 7.71-7.69 (m, 2H), 3.68 (t, *J* = 7.3 Hz, 2H), 2.17 (td, *J* = 6.8, 2.6 Hz, 2H), 1.92 (t, *J* = 2.7 Hz, 1H,), 1.69 (tt, *J* = 7.5, 7.5 Hz, 2H), 1.54-1.34 (m, 6H); ^{13}C NMR ($CDCl_3$, 100 MHz, 25°C): δ = 168.6, 134.0, 132.4, 123.3, 84.6, 68.4, 38.1, 28.6, 28.5, 28.4, 26.5, 18.5; ESI-MS: calcd. for $C_{16}H_{17}NO_2$: 256.13 $[M+H]^+$, found: 256.26.

Compound 9

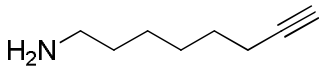

9

8-aminooct-1-yne: Hydrazine hydrate (2.50 mL, 58.4 mmol) was added to a solution of 8-phtalimidooct-1-yne (4.26 g, 16.7 mmol) in ethanol (160 mL). The mixture was stirred at reflux for 4 hours (after 1 hour, a white precipitate appears) and then cooled to room temperature. The solvent was removed in vacuo and an aqueous solution of KOH 1N (80 mL) was added. The solution was extracted three times with CH_2Cl_2 (80 mL) and then the organic layers were combined, dried over Na_2SO_4 and concentrated to provide the desired product **9** (1.82 g, 87%) as a yellow oil. R_f = 0.6 (CH_3OH/CH_2Cl_2: 1/9); ^{1}H NMR ($CDCl_3$, 400 MHz, 25°C): δ = 2.69 (t, *J* = 7.0 Hz, 2H), 2.19 (td, *J* = 7.2, 2.7 Hz, 2H), 1.93 (t, *J* = 2.7 Hz, 1H), 1.56-1.46 (m, 2H), 1.40-1.26 (m, 6H); ^{13}C NMR ($CDCl_3$, 100 MHz, 25°C): δ = 84.6, 68.1, 41.9, 33.6, 28.5, 28.4, 26.4, 18.4.

Compound 10

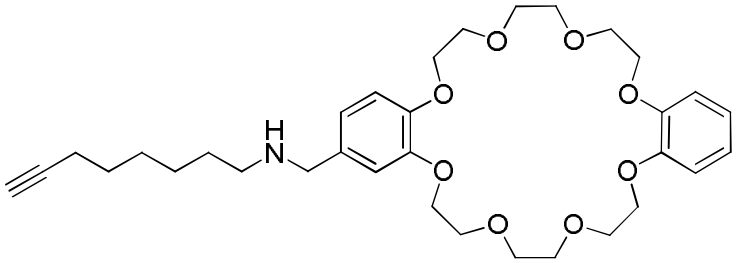

10

A solution of the formyl crown ether **7** (289 mg, 0.62 mmol) and 8-aminooct-1-yne **9** (84.7 mg, 0.67 mmol) in toluene (18 mL) was heated up to reflux for 30 hours using a Dean-Stark apparatus. The solvent was then evaporated, giving a yellow oil. The mixture was diluted with MeOH (13.5 mL), and then $NaBH_4$ (233 mg, 6.2 mmol) was added portionwise at 0-5°C. Stirring was maintained at room temperature for further 4 hours, then an aqueous solution of HCl 5M (15 mL) was added to the reaction mixture. Methanol was evaporated, and the residue was diluted with CH_2Cl_2 (15 mL) and washed with an aqueous solution of NaOH 5M (15 mL). The aqueous layer was extracted with CH_2Cl_2 (2 x 15 mL) and the organic layers were combined, dried over Na_2SO_4 and concentrated. The crude was purified by column chromatography (SiO_2, MeOH/CH_2Cl_2/NH_4OH 19/80/1) to yield compound **10** (270 mg, 76 %) as a pale yellow oil.

R_f = 0.8 (MeOH/CH_2Cl_2/NH_4OH: 19/80/1); ^{1}H NMR ($CDCl_3$, 400 MHz, 25°C): δ = 6.91-6.74 (m, 7H), 4.18-4.08 (m, 8H), 3.96-3.84 (m, 8H), 3.84-3.77 (m, 8H), 3.67 (s, 2H), 2.58 (t, *J* = 7.0 Hz, 2H), 2.15 (t, *J* = 7.2 Hz, 2H), 1.92 (brs, 1H), 1.54-1.24 (m, 8H); ^{13}C NMR ($CDCl_3$, 100 MHz, 25°C): δ = 149.0, 148.9, 147.9, 133.9, 121.5, 120.9, 114.2, 114.2, 114.0, 114.0, 84.7, 71.3, 70.0, 69.6, 69.5, 68.3, 53.8, 49.4, 30.0, 28.7, 28.4, 26.9, 18.4; ESI-MS: calcd. for $C_{33}H_{47}NO_8$: 586.338 $[M+H]^+$, found: 586.34.

Compound 11

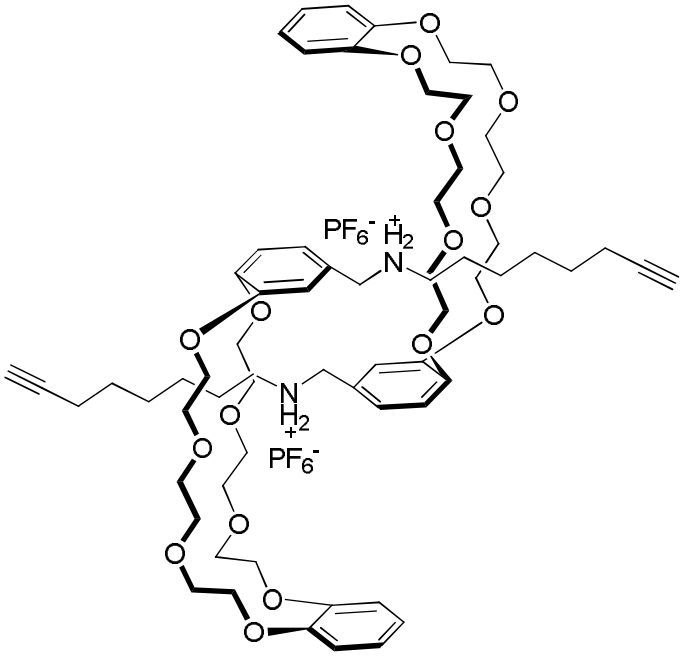

11

To a solution of compound **10** (1.00 g, 1.63 mmol) in Et_2O (18 mL) was added HCl 2M in Et_2O (5.0 mL, 10.1 mmol). The mixture was stirred for 30 min and then Et_2O was evaporated. To a solution of the resulting solid in H_2O (27 mL) was added NH_4PF_6 (0.66 g, 4.03 mmol) and CH_2Cl_2 (27 mL). The biphasic solution was stirred vigorously for 1 hour. The aqueous layer was extracted with CH_2Cl_2 (3 x 30 mL). The organic layers were combined, dried over Na_2SO_4 and concentrated to give compound **11** (1.16 g, 96%) as a white solid. ^{1}H NMR ($CDCl_3$, 400 MHz, 25°C): δ = 6.91 (d, *J* = 8.3 Hz, 2H), 6.84-6.71 (m, 10H), 6.57 (s, 2H), 4.44-4.38 (m, 2H), 4.35-4.29 (m, 2H), 4.23-3.63 (m, 48H), 3.56-3.36 (m, 4H), 2.09 (td, *J* = 6.9, 1.8 Hz, 4H), 1.92 (brs, 2H), 1.48-1.14 (m, 16H); ^{13}C NMR ($CDCl_3$, 100 MHz, 25°C): δ = 147.9, 147.8, 147.8, 147.0, 146.5, 146.3, 124.8, 123.2, 121.4, 121.2, 113.4, 112.7, 112.1, 112.0, 84.4, 72.6, 72.0, 71.3, 71.0 (x3), 70.6, 70.5, 68.8, 68.7, 67.8, 67.2, 67.1 (x2), 66.9, 52.4, 49.0, 28.2, 26.8, 26.4, 18.4; ESI-MS: calcd. for $C_{66}H_{96}N_2O_{16}$: 586.84 $[M\text{-}2PF_6]^{2+}$, found: 586.45.

Compound 12

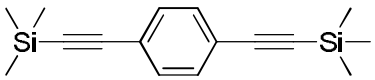

12

1,4-bis((trimethylsilyl)ethynyl)benzene: 1,4-dibromobenzene (1.0 g, 4.24 mmol), trimethylsilylacetylene (1.32 mL, 9.33 mmol), $Pd(PPh_3)_2Cl_2$ (325 mg, 0.42 mmol), copper

iodide (400 mg, 2.1 mmol), triphenylphosphine (980 mg, 3.74 mmol), triethylamine (5 mL) and dry THF (20 mL) were added to an oven-dried Schlenk. The solution was degassed using freeze-thaw cycles. The reaction mixture was heated at 80 ^{o}C overnight. The reaction was quenched with $NH_4Cl_{\ sat.}$ (20 mL) and extracted with diethyl ether (3 × 20 mL). The organic phase was washed with $NH_4Cl_{\ sat.}$ (20 mL), water (20 mL) and dried over $Na_2SO_{4\ anhydrous}$. Removal of the solvent and purification by column chromatography (SiO_2, n-hexane/4% CH_2Cl_2) provide compound **12** (887 mg, 77%) as a colorless solid. R_f = 0.25 (n-hexane); ^{1}H NMR ($CDCl_3$, 400 MHz, 25°C): δ = 7.38 (s, 4H), 0.25 (s, 18H); ^{13}C NMR ($CDCl_3$, 100 MHz, 25°C): δ = 131.9, 123.3, 104.7, 96.5, 0.06; ESI-MS: calcd for $C_{16}H_{22}Si_2$ 271.13 $[M+H]^+$, found: 271.15.

Compound 13

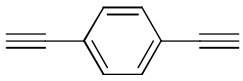

13

1,4-diethynylbenzene: To a solution of 1,4-bis((trimethylsilyl)ethynyl)benzene **12** (876 mg, 3.24 mmol) in a 1:1 mixture of CH_2Cl_2 and MeOH (20 mL), K_2CO_3 (4.46 g, 32.3 mmol) was added and the reaction mixture was stirred overnight at room temperature. The reaction mixture was then washed with water (3 × 20 mL) and dried over Na_2SO_4. Further evaporation of the solvent provided bis-alkyne **13** (408 mg, quantitative) as a white solid, which turned brown in few days. ^{1}H NMR ($CDCl_3$, 400 MHz, 25°C): δ = 7.44 (s, 4H), 3.17 (s, 2H); ^{13}C NMR ($CDCl_3$, 100 MHz, 25°C): δ = 132.2, 122.7, 83.2, 79.2; ESI-MS: calcd for $C_{10}H_6$ 127.05 $[M+H]^+$, found: 127.11.

Compound 14

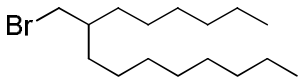

14

1-bromo-2-hexyldecane: A solution of 2-hexyl-1-decanol (5.0 g, 20.6 mmol) and carbon tetrabromide (10.3 g, 30.9 mmol) in CH_2Cl_2 (300 mL) was cooled to 0 ^{o}C. PPh_3 (10.8 g, 41.2 mmol) was added in portions over 30 min at 0 ^{o}C and stirring was continued overnight at room temperature. CH_2Cl_2 (200 mL) was added to the reaction mixture and the organic phase was washed with water (3 × 400 mL), and dried over Na_2SO_4. Further evaporation of the

solvent and purification by column chromatography (SiO_2, n-hexane) yielded compound **14** as a colorless oil. Unfortunately, this compound could not be obtained as chemically pure but, the purity was sufficient for the next reaction. ^{1}H NMR ($CDCl_3$, 400 MHz, 25°C): δ = 3.45 (d, *J* = 4.8Hz, 2H), 1.61-1.57 (m, 1H), 1.45-1.18 (m, 24H), 0.89 (t, *J* = 6.8Hz, 6H); ^{13}C NMR ($CDCl_3$, 400 MHz, 25°C): δ = 39.9, 39.7, 32.8, 32.7, 32.1, 32.0, 29.9, 29.7, 29.6, 29.5, 26.7, 26.7, 22.8, 22.8, 14.3, 14.24.

Compound 15

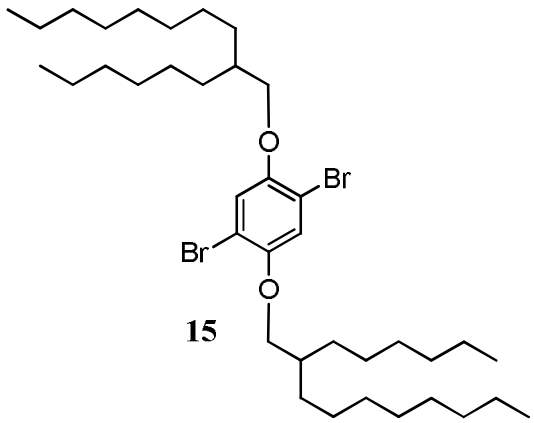

15

To a solution of 1-bromo-2-hexyldecane **14** (2.52 g, 8.25 mmol) in DMF (60 mL) was added K_2CO_3 (6.84 g, 49.5 mmol), 2,5-dibromohydroquinone (884 mg, 3.3 mmol) in DMF (50 mL) was then added dropwise over 1 hour and the dark brown solution was stirred overnight at 60 ^{o}C. Diethyl ether (120 mL) was added to the reaction mixture and the organic phase was washed with 5% citric acid in water (3 × 120 mL) and dried over Na_2SO_4. Evaporation of the solvent and further purification by column chromatography (SiO_2, n-hexane) provide compound **15** (1.55 g, 66%) as a colorless oil. R_f = 0.25 (n-hexane); ^{1}H NMR ($CDCl_3$, 400 MHz, 25°C): δ = 7.07 (s, 2H), 3.82 (d, *J* = 5.6Hz, 4H), 1.82-1.78 (m, 2H), 1.56-1.19 (m, 48H), 0.89-0.86 (m, 12H); ^{13}C NMR ($CDCl_3$, 400 MHz, 25°C): δ = 150.3, 118.3, 111.2, 73.1, 38.1, 32.1, 32.0, 31.5, 31.5, 30.1, 29.8, 29.7, 29.5, 27.0, 26.9, 22.8, 14.3; Anal. calcd. for $C_{38}H_{68}Br_2O_2$: C 63.68, H 9.56, O 4.46, found: C 63.76, H 9.78, O 4.5.

Compound 16

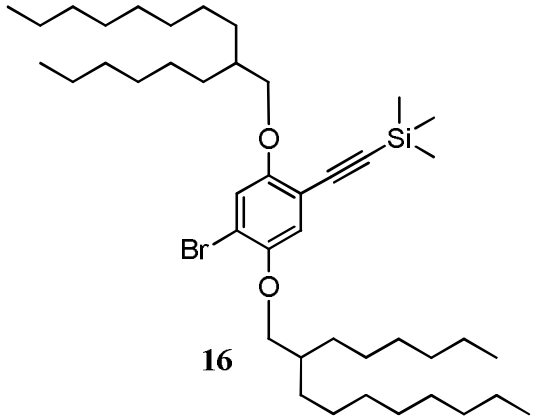

16

Route 1: To an oven-dried Schlenk were added compound **15** (2.71 g, 3.78 mmol), 3-trimethylsilylacetylene (523 µL, 3.78 mmol), $Pd(PPh_3)_2Cl_2$ (159 mg, 0.23 mmol), copper iodide (86 mg, 0.46 mmol), triphenylphosphine (119 mg, 0.46 mmol), triethylamine (10 mL) and dry THF (15 mL) and the solution was degassed using freeze-thaw cycles. The reaction mixture was stirred at 80 °C overnight. After cooling down to room temperature, the reaction mixture was quenched with $NH_4Cl_{\ sat.}$ (20 mL) and extracted with diethyl ether (40 mL). The organic phase was washed with $NH_4Cl_{\ sat.}$ (20 mL), water (20 mL) and dried over Na_2SO_4. After removing the solvent, the product was treated with pentane and filtered. Evaporation of the filtrate and further purification by column chromatography (SiO_2, n-hexane/3% CH_2Cl_2) provide compound **16** (949 mg, 34%) as a light yellow oil. R_f = 0.3 (n-hexane/3% CH_2Cl_2); ^{1}H NMR ($CDCl_3$, 400 MHz, 25°C): δ = 7.03 (s, 1H), 6.92 (s, 1H), 3.82 (d, *J* = 5.5Hz, 4H), 1.82-1.78 (m, 2H), 1.54-1.19 (m, 48H), 0.88-0.85 (m, 12H), 0.25 (s, 9H); ^{13}C NMR ($CDCl_3$, 100 MHz, 25°C): δ = 155, 149.5, 117.7, 117.5, 113.7, 112.3, 100.8, 99.1, 77.2, 72.9, 72.2, 38.3, 38.1, 32.1, 32.1, 32.0, 32.0, 31.5, 31.4, 31.4, 30.2, 30.2, 29.9, 29.8, 29.8, 29.7, 29.5, 29.5, 27.0, 27.0, 27.0, 26.9, 22.8, 14.3, 0.1; Anal. calcd for $C_{43}H_{77}BrO_2Si$: C 70.36, H 10.57, Si 3.83, found: C 70.58, H 10.9, Si 3.3.

Compound 17

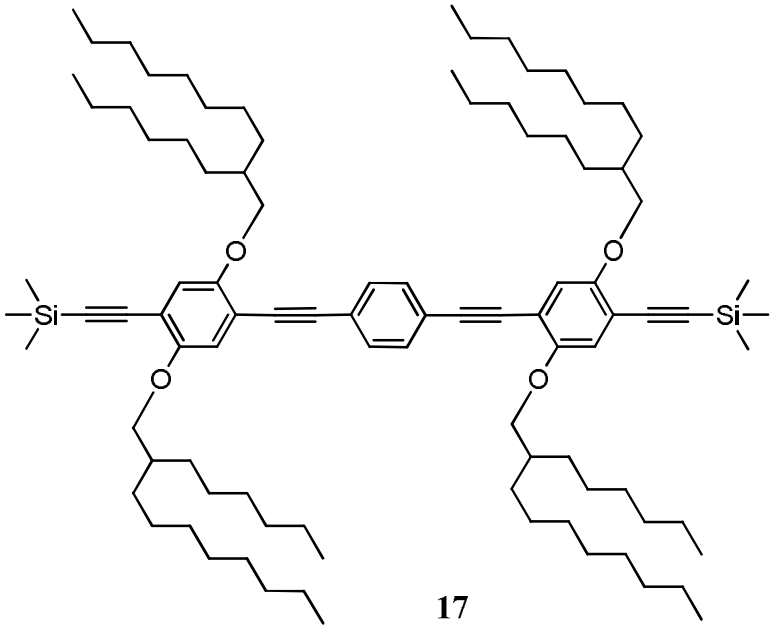

17

To an oven-dried Schlenk were added compound **16** (1.2 g, 1.65 mmol), compound **13** (95 mg, 0.75 mmol), $Pd(PPh_3)_2Cl_2$ (53 mg, 0.075 mmol), copper iodide (129 mg, 0.67 mmol), triphenylphosphine (316 mg, 1.2 mmol), triethylamine (15 mL) and dry THF (7 mL) and the solution was degassed using freeze-thaw cycles. The reaction mixture was stirred at 80 °C overnight. After cooling down to room temperature, the reaction mixture was quenched with $NH_4Cl_{\ sat.}$ (20 mL) and extracted with diethyl ether (40 mL). The organic phase was washed with $NH_4Cl_{\ sat.}$ (20 mL), water (20 mL) and dried over Na_2SO_4. After removing the solvent, the product was treated with pentane and filtered. Evaporation of the filtrate and further purification by column chromatography (SiO_2, n-hexane/10-15% CH_2Cl_2) provide compound **17** (811 mg, 75%) as a light yellow oil, which solidifies in few days. R_f = 0.1 (n-hexane/10% CH_2Cl_2); ^{1}H NMR ($CDCl_3$, 400 MHz, 25°C): δ = 7.47 (s, 4H), 6.93 (s, 4H), 3.86 (2d, *J* = 6.0Hz, 8H), 1.83-1.78 (m, 4H), 1.60-1.16 (m, 96H), 0.89-0.85 (m, 24H), 0.26 (s, 18H); ^{13}C NMR ($CDCl_3$, 100 MHz, 25°C): δ = 154.5, 153.8, 131.5, 123.4, 117.1, 116.4, 114.0, 113.8, 101.3, 100.2, 94.7, 88.1, 77.2, 72.4, 72.0, 38.3, 38.3, 32.1, 32.0, 31.6, 31.4, 30.3, 30.2, 29.9, 29.9, 29.8, 29.8, 29.5, 27.1, 27.0, 27.0, 22.8, 14.3, 0.15; Anal. calcd for $C_{96}H_{158}O_4Si_2$: C 80.49, H 11.12, Si 3.92; found: C 80.37, H 11.44, Si 3.73.

Compound 18

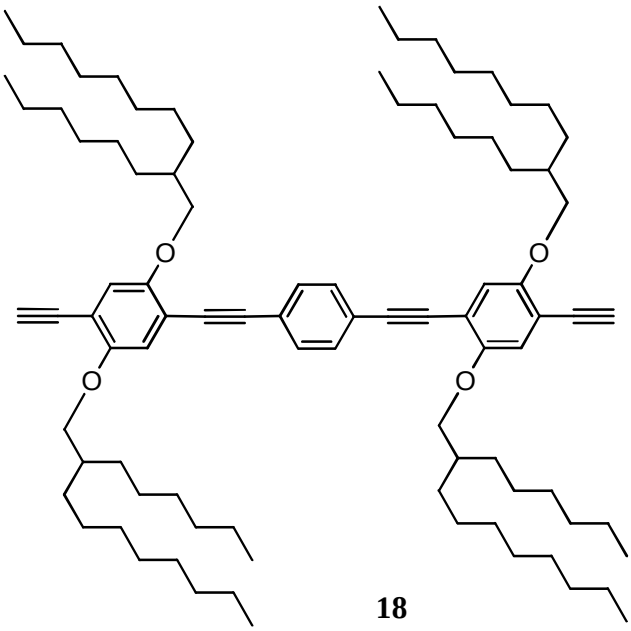

18

To a solution of compound **16** (329 mg, 0.23 mmol) in a 1:1 mixture of CH_2Cl_2 and MeOH (16 mL), K_2CO_3 (317 mg, 2.3 mmol) was added and the mixture was stirred overnight at room temperature. The reaction mixture was then washed with water (3 × 20 mL), dried over Na_2SO_4. Removal of the solvent afford compound **18** (288 mg, 97%) as a red viscous oil. ^{1}H NMR ($CDCl_3$, 400 MHz, 25°C): δ = 7.48 (s, 4H), 6.98 (s, 2H), 6.97 (s, 2H), 3.87 (d, *J* = 5.7Hz, 8H), 3.32 (s, 2H), 1.83-1.78 (m, 4H), 1.62-1.15 (m, 96H), 0.89-0.85 (m, 24H); ^{13}C NMR ($CDCl_3$, 400 MHz, 25°C): δ = 154.4, 153.7, 131.4, 123.3, 117.4, 116.8, 114.3, 112.9, 94.6, 87.8, 82.3, 80.0, 77.2, 72.6, 72.4, 38.2, 38.0, 31.9, 31.9, 31.9, 31.8, 31.5, 31.5, 31.4, 30.1, 30.0, 29.7, 29.7, 29.6, 29.4, 26.9, 26.9, 26.8, 26.8, 22.7, 14.1, 14.1; Anal. calcd for $C_{90}H_{142}O_4$: C 83.92, H 11.11, found: C 83.6, H 11.37.

Compound 21

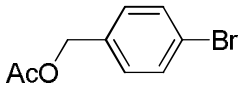

21

4-Bromobenzyl acetate. A solution of 4-bromobenzyl alcohol (4.00 g, 21.4 mmol) and DMAP (268 mg, 2.14 mmol) in a 1:1 mixture of acetic anhydride/pyridine (40 mL) was stirred at room temperature for 22 hours until the starting material had been consumed as determined by TLC analysis. Water (10 mL) and ethyl acetate (10 mL) were then added, and the layers were separated. The organic layer was washed with $HCl_{aq.}$ (10 mL, 1 M) and brine (10 mL). The organic layer was then dried over Na_2SO_4, filtered, and concentrated in vacuo.

Further purification by flash chromatography (SiO_2, n-hexane/EtOAc: 5/95) afforded compound **21** (4.45 g, 91%) as a pale yellow solid. R_f = 0.45 (n-hexane/EtOAc: 20/1); ^{1}H NMR ($CDCl_3$, 400 MHz, 25°C): δ = 7.48 (d, *J* = 8.4Hz, 2H), 7.23 (d, *J* = 8.3Hz, 2H), 5.05 (s, 2H), 2.10 (s, 3H); ^{13}C NMR ($CDCl_3$, 100 MHz, 25°C): δ = 170.9, 135.1, 131.8, 130.1, 122.4, 65.6, 21.1; ESI-MS: calcd. for $C_9H_9BrO_2$: 228.99 $[M+H]^+$, found: 229.13.

Compound 22

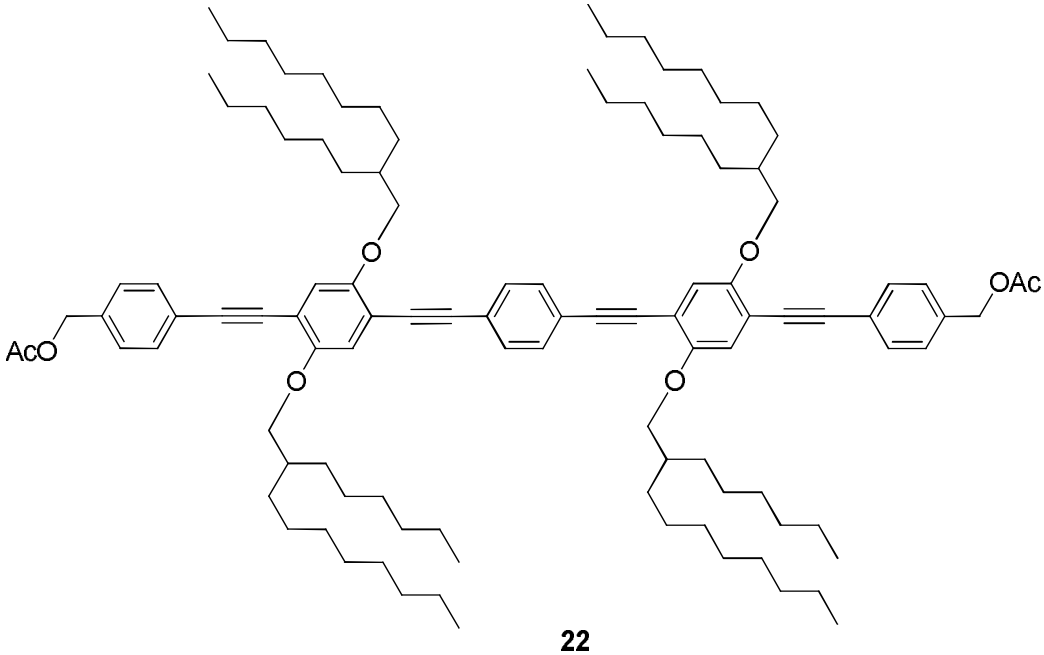

22

To an oven-dried Schlenk were added compound **18** (340 mg, 0.26 mmol), *p*-bromobenzyl acetate (133 mg, 0.58 mmol) in a 1:1 mixture of triethylamine and tetrahydrofuran (2.5 mL). The mixture was degassed by using freeze-thaw cycles and $Pd(PPh_3)_4$ (31 mg, 0.026 mmol) was added. The mixture was degassed once more by using freeze-thaw cycles and then heated up to 70°C overnight. The resulting dark brown mixture was filtered and the solvent was removed in vacuo. Further purification by column chromatography (SiO_2, n-hexane/CH_2Cl_2: 10/1) provided compound **22** (350 mg, 85%) as a yellow oil. R_f = 0.15 (n-hexane/CH_2Cl_2: 10/1); ^{1}H NMR ($CDCl_3$, 400 MHz, 25°C): δ = 7.53 (d, *J* = 7.8Hz, 4H), 7.49 (s, 4H), 7.35 (d, *J* = 7.8Hz, 4H), 7.01 (s, 4H), 7.00 (s, 2H), 4.73 (s, 4H), 3.90 (d, *J* = 5.7Hz, 8H), 1.92-1.88 (m, 4H), 1.62-1.15 (m, 96H), 0.89-0.86 (m, 24H); ^{13}C NMR($CDCl_3$, 100 MHz, 25°C): δ = 170.8, 153.9, 135.9，131.7, 131.4，128.0, 123.5, 123.3, 116.6，113.9, 113.8, 94.6, 94.5, 88.0, 86.5, 72.4, 65.9, 38.2, 31.9, 31.9, 31.8, 30.1, 29.8, 29.6, 29.4, 26.9, 26.9, 22.7, 21.0, 14.1, 14.1, 14.1.

Compound 23

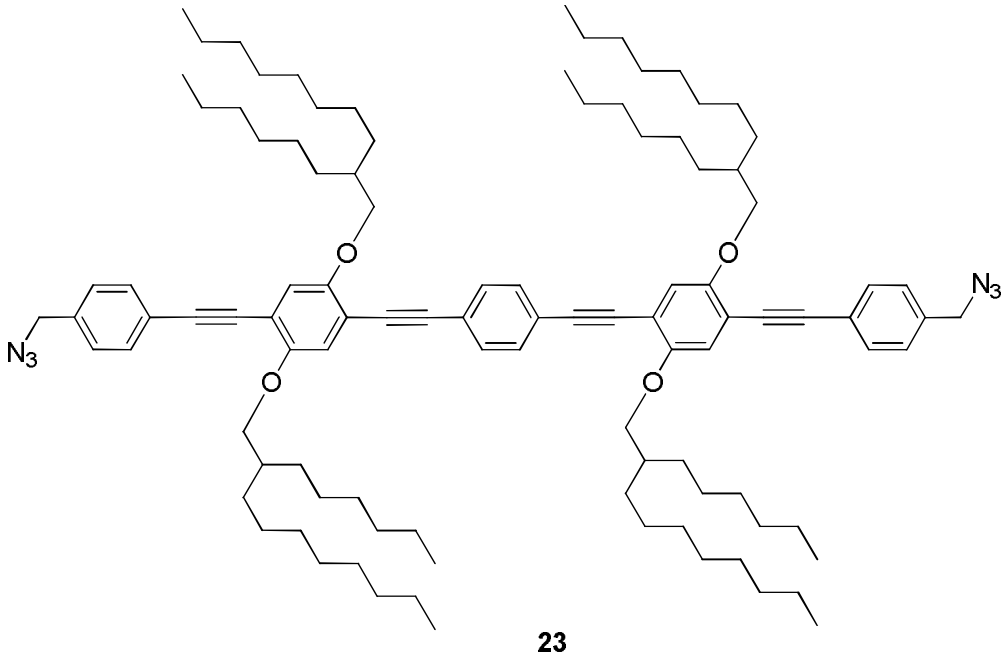

23

A solution of compound **22** (350 mg, 0.22 mmol) in a 9:1 mixture of dichloromethane/methanol (10 mL) was treated with K_2CO_3 (305 mg, 2.2 mmol) and the solution was stirred at room temperature for overnight. The solvent was then removed in vacuo, and the resulting mixture was dissolved with a mixture of CH_2Cl_2 (20 mL) and water (20 mL), and the aqueous phase was extracted with CH_2Cl_2 (3 × 20 mL). The organic phases were combined, dried over Na_2SO_4, and evaporated in vacuo to give the resulting bis-benzyl alcohols, which was pure enough to be used as such in the next step. ^{1}H NMR ($CDCl_3$, 400 MHz, 25°C): δ = 7.53 (d, *J* = 7.8Hz, 4H), 7.49 (s, 4H), 7.35 (d, *J* = 7.5Hz, 4H), 7.01 (s, 2H), 7.00 (S, 2H), 4.73 (s, 4H), 3.90 (d, *J* = 5.7 Hz, 8H), 1.92-1.89 (m, 4H), 1.62-1.15 (m, 96H), 0.89-0.86 (m, 24H).

A solution of the crude bis-benzyl alcohol in CH_2Cl_2 (10 mL) was cooled down to 0°C and triethylamine (190 µL, 1.32 mmol) and methanesulfonyl chloride (110 µL, 1.32 mmol) were added. The reaction mixture was then stirred overnight at room temperature. The organic phase was then extracted with water (10 mL) and NH_4Cl sat. (10 mL), dried over Na_2SO_4 and concentrated in vacuo to provide the mesylated derivative, which was pure enough to be used as such in the next step.

A solution of this crude mesylate in a 1:1 mixture of DMF and THF (0.9 mL) was treated with sodium azide (172 mg, 2.65 mmol) and heated up overnight to 50°C. After cooling down to room temperature, the reaction mixture was diluted with CH_2Cl_2 (10 mL). The organic phase

was then extracted with water (10 mL) and NH_4Cl sat. (10 mL), dried over Na_2SO_4 and concentrated in vacuo. Further purification by column chromatography (SiO_2, n-hexane/CH_2Cl_2: 10/1) provided compound **23** (199 mg, 58% over 3 steps) as a yellow oil. R_f = 0.1 (n-hexane/CH_2Cl_2: 10/1)); ^{1}H NMR ($CDCl_3$, 400 MHz, 25°C): δ = 7.55 (d, *J* = 8.2Hz, 4H), 7.50 (s, 4H), 7.30 (d, *J* = 8.4Hz, 4H), 7.01 (s, 2H), 7.00 (s, 2H), 4.37 (s, 4H), 3.92 (d, *J* = 5.8Hz, 8H), 1.90-1.80 (m, 4H), 1.64-1.14 (m, 96H), 0.91-0.81 (m, 24H); ^{13}C NMR (100 MHz, $CDCl_3$, 25°C): δ = 153.9, 135.4, 132.0, 131.4, 128.1, 123.6, 123.3, 116.6, 113.9, 113.8, 94.6 , 94.3, 88.0, 86.8, 72.4, 38.2, 31.9, 31.9, 31.5, 30.1, 29.8, 29.7, 29.6, 29.4, 26.9, 22.7, 14.1, 14.1; MALDI-TOF: calcd for $C_{102}H_{154}N_6O_4$: 1549.188 $[M]^+$, found: 1549.135.

Compound 24

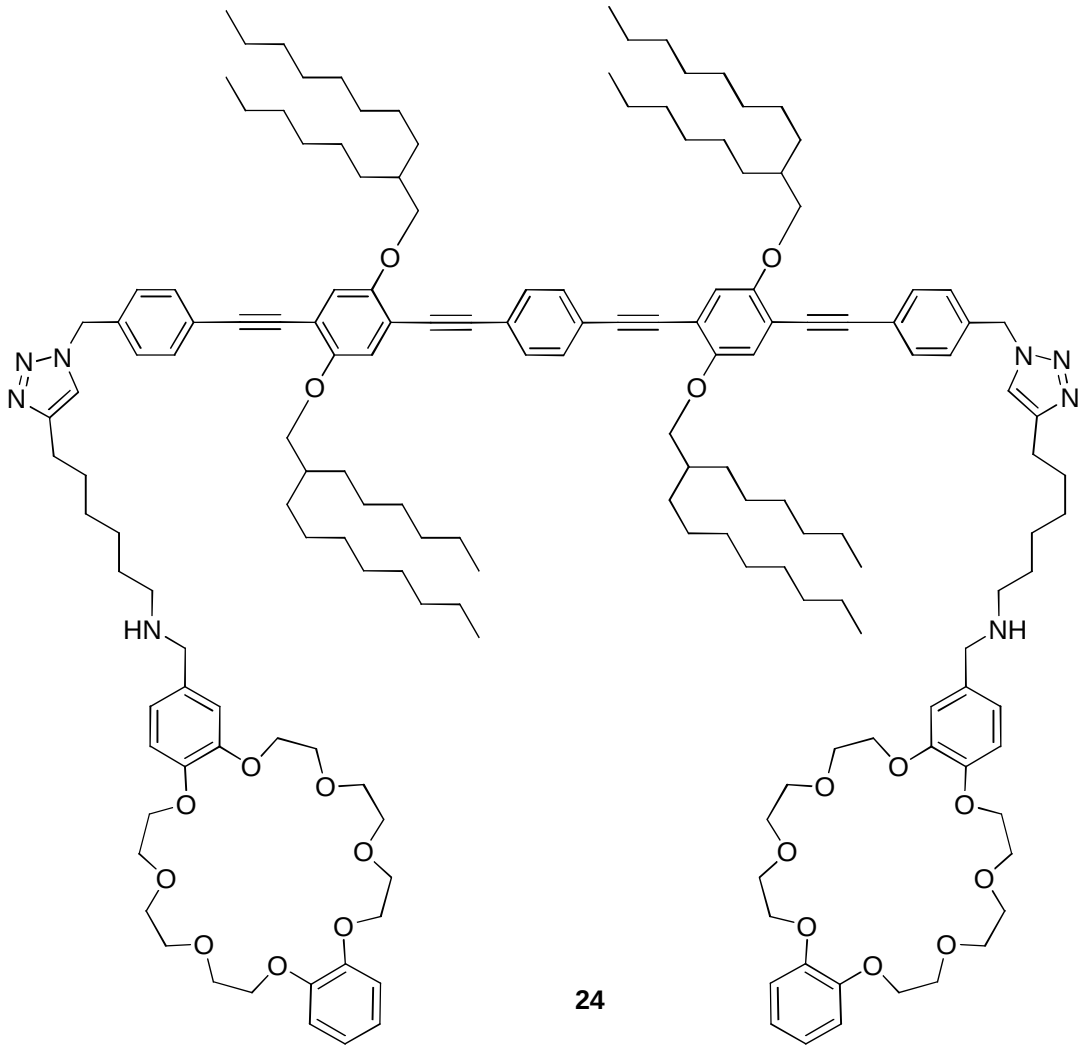

24

Compound **23** (12 mg, 0.0077 mmol) and compound **10** (9.5 mg, 0.0163 mmol) were dissolved in a 1:1 mixture of THF and tetrahydrofuran (600 µL) and then, copper iodide (1.5 mg, 0.0077 mmol) was added and the reaction mixture was stirred overnight at 70°C. After cooling down to room temperature, the solvents were removed, providing compound **24** in a

quantitative manner as a yellow oil. ^{1}H NMR ($CDCl_3$, 400MHz, 25°C): δ = 7.52 (d, *J* = 7.9Hz, 4H), 7.49 (s, 4H), 7.23 (d, *J* = 7.5Hz, 4H), 6.99 (s, 4H), 6.94-6.86 (m, 16H), 5.50 (brs, 4H), 4.23-4.14 (m, 12H), 4.24-3.62 (m, 48H), 2.79-2.60 (m, 4H), 1.89-1.79 (m, 4H), 1.77-1.61(m, 4H), 1.60-1.02 (m, 116H), 0.88-0.81 (m, 24H); ESI-MS: m/z calcd for $C_{170}H_{246}N_8O_{20}$: 1360.93 $[M+2H]^{2+}$, found: 1361.10.

Compound 25

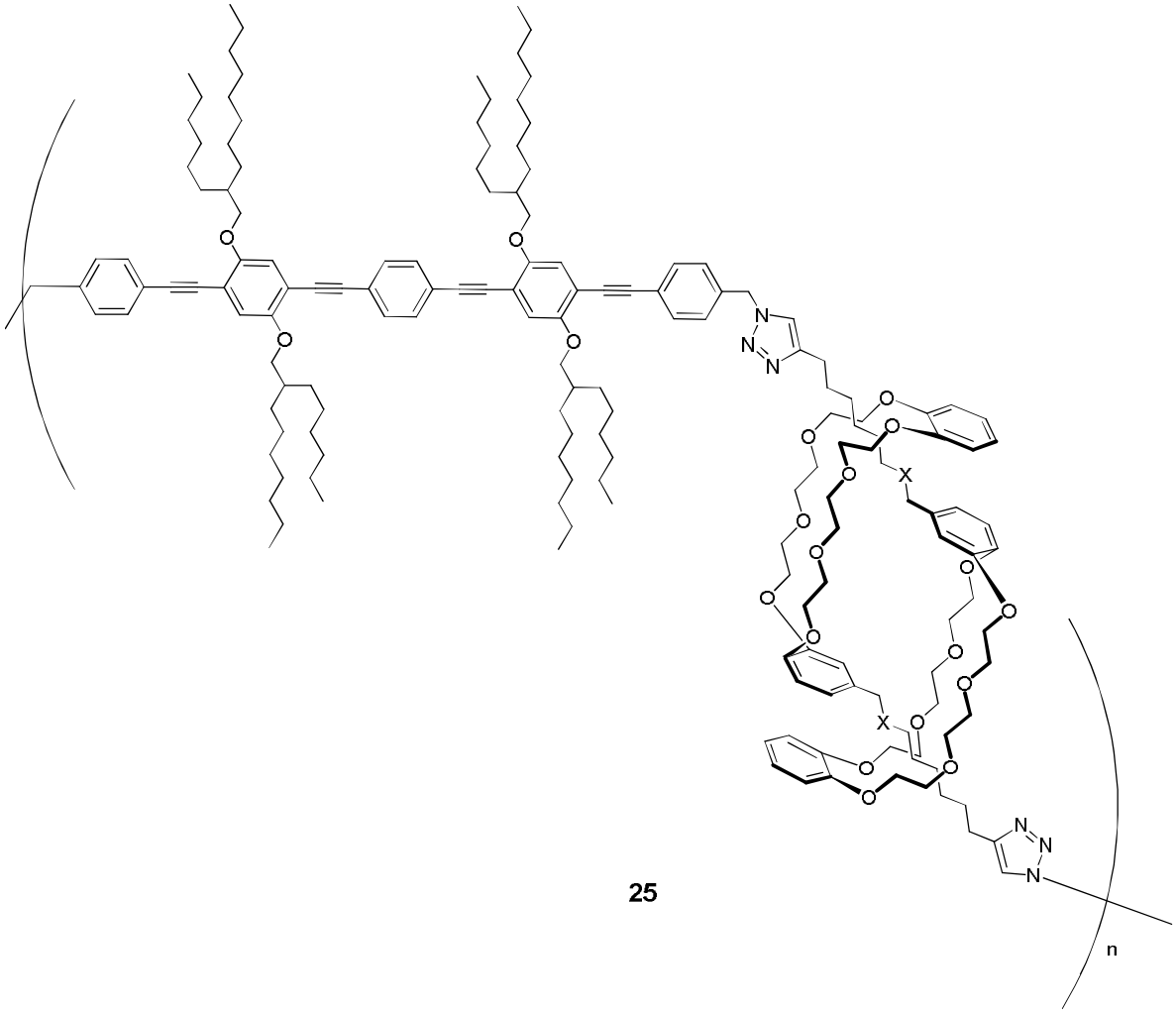

25

To a solution of dumbbell **23** (13.8 mg, 0.009 mmol) and pseudorotaxane **11** (13.0 mg, 0.009 mmol) in dichloromethane (500 µL) was added $Cu(CH_3CN)_4PF_6$ (3.3 mg, 0.009 mmol) and 2,6-lutidine (1.0 µL, 0.009 mmol). The mixture was degassed by using freeze-thaw cycles and stirred at room temperature for almost 5 days. After removal of the solvent, a crude product, soluble only in acetonitrile, was obtained (18 mg, 66%). ^{1}H NMR in CD_3CN displays signals corresponding to a polymer.

Compound 26

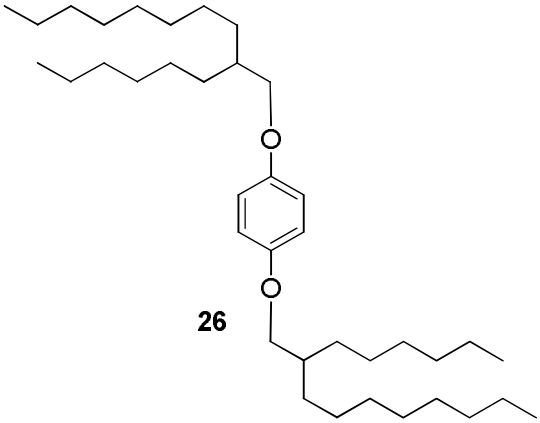

26

Hydroquinone (1.0 g, 9.08 mmol) and triphenylphosphine (5.95g, 22.7 mmol) were dissolved in a 3:1 mixture of CH_2Cl_2 and THF (22 mL). The solution was cooled down to 0 ^oC and DIAD (4.47 mL, 22.7 mmol) was added dropwise over 30 min. 2-hexyldecanol (6.58 mL, 22.7 mmol) was then added over 40 min at 0 ^oC, and the solution was stirred overnight at room temperature. After removal of the solvent, the residue was treated with pentane and filtered to remove undissolved triphenylphosphine oxide. Evaporation of the filtrate followed by purification by column chromatography (SiO_2, pentane → pentane/diethyl ether: 100/1) provided compound **26** (2.8 g, 56%) as a colorless oil. R_f = 0.3 (pentane); ^1H NMR ($CDCl_3$, 400 MHz, 25°C): δ = 6.82 (s, 4H), 3.78 (d, *J* = 5.7Hz, 4H), 1.78-1.69 (m, 2H), 1.50-1.20 (m, 48H), 0.89 (t, *J* = 6.8Hz, 12H); ^{13}C NMR ($CDCl_3$, 100 MHz, 25°C): δ = 153.6, 115.5, 77.2, 71.8, 38.2, 32.1, 32.0, 31.5, 31.5, 30.2, 29.9, 29.8, 29.5, 27.0, 27.0, 22.8, 14.3; Anal. calcd for $C_{38}H_{70}O_2$: C 81.65, H 12.62, O 5.72; found: C 81.99, H 12.98, O 5.59.

Compound 27

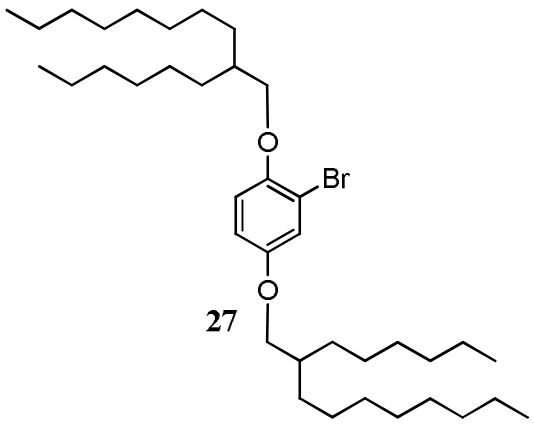

27

Compound **26** (9.78 g, 17.5 mmol) and sodium acetate (1.44 g, 17.5 mmol) were dissolved in acetic acid (85 mL). Bromine (0.896 mL, 17.5 mmol) in acetic acid (20 mL) was then added

very slowly over 8 hours, and the reaction mixture was stirred overnight at room temperature. The mixture was poured into water (300 mL), and extracted with dichloromethane (3 × 300 mL). The combined organic phase was neutralized with $NaHCO_3$ (300 mL), dried over Na_2SO_4. Evaporation of the solvent followed by purification by column chromatography (SiO_2, pentane) afforded compound **27** (9.6 g, 86%) as a colorless oil. R_f = 0.35 (pentane); ^{1}H NMR ($CDCl_3$, 400 MHz, 25°C): δ = 7.11 (d, *J* = 6.7Hz, 1H), 6.80-6.79 (m, 2H), 3.83 (d, *J* = 5.6Hz, 2H), 3.76 (d, *J* = 5.7Hz, 2H), 1.80-1.74 (m, 2H), 1.54-1.20 (m, 48H), 0.89 (m, 12H); ^{13}C NMR ($CDCl_3$, 100 MHz, 25°C): δ = 153.9, 150.1, 119.7, 114.5, 114.4, 112.9, 77.2, 73.0, 71.9, 38.2, 38.1, 32.1, 32.0, 31.5, 30.2, 29.8, 29.7, 29.5, 29.5, 27.0, 27.0, 27.0, 22.8, 14.3; Anal. calcd for $C_{38}H_{69}BrO_2$: C 71.55, H 10.90, O 5.02; found: C 71.63, H 11.19, O 4.99.

Compound 28

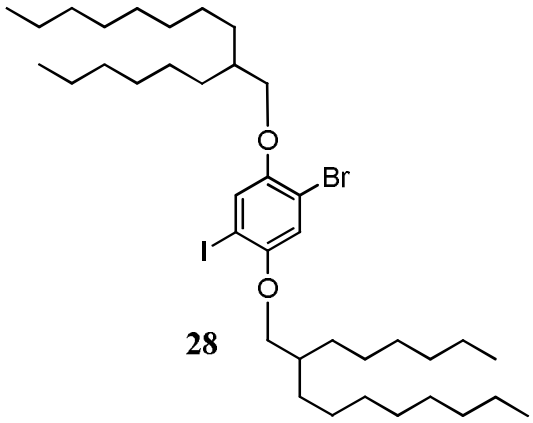

28

Compound **27** (5.0 g, 7.84 mmol), iodine (2.01 g, 7.92 mmol) and potassium iodate (847 mg, 3.96 mmol) were dissolved in acetic acid (19 mL), CCl_4 (1.5 mL), water (0.5 mL) and H_2SO_4 (1 mL). The reaction mixture was stirred overnight at 70 °C, cooled down to room temperature, and a Na_2SO_3 solution (50 mL) was added until the brown color disappeared. The solution poured into water (300 mL) and extracted with dichloromethane (5 × 100 mL). The combined organic phase was neutralized with $NaHCO_3$ solution (100 mL) and dried over Na_2SO_4. Evaporation of the solvent followed by column chromatography (SiO_2, n-hexane) afforded compound **28** (4.87 g, 81%) as a colorless oil. R_f = 0.4 (n-hexane); ^{1}H NMR ($CDCl_3$, 400 MHz, 25°C): δ = 7.26 (s, 1H), 6.97 (s, 1H), 3.81 (d, *J* = 5.6Hz, 2H), 3.80 (d, *J* = 5.4Hz, 2H), 1.83-1.75 (m, 2H), 1.53-1.19 (m, 48H), 0.92-0.85 (m, 12H); ^{13}C NMR ($CDCl_3$, 100 MHz, 25°C): δ = 152.7, 150.6, 124.1, 116.8, 112.6, 84.7, 77.2, 73.1, 72.9, 38.1, 38.1, 32.1, 32.0, 31.5, 31.5, 30.2, 29.8, 29.7, 29.5, 27.0, 22.8, 14.3; Anal. calcd for $C_{38}H_{68}BrIO_2$: C 59.76, H 8.97, O 4.19; found: C 59.97, H 9.21, O 4.58.

Compound 16

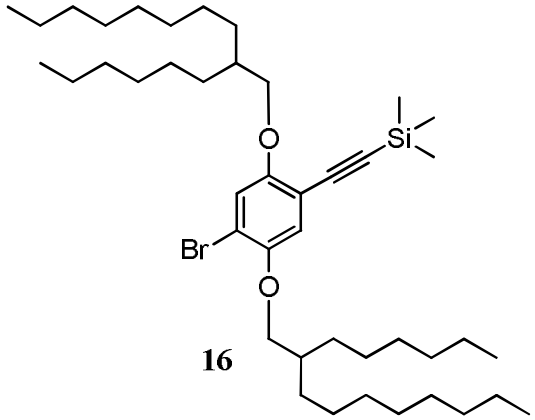

16

Route 2: To an oven dried Schlenk were added compound **28** (4.87 g, 6.38 mmol), trimethylsilylacetylene (1.24 mL, 8.93 mmol), $Pd(PPh_3)_2Cl_2$ (269 mg, 0.38 mmol), copper iodide (243 mg, 1.28 mmol), triphenylphosphine (335 mg, 1.28 mmol) in a 1:1 mixture of triethylamine and THF (34 mL). The solution was degassed using freeze-thaw cycles and the reaction mixture was heated overnight at 30 °C. The reaction was quenched with $NH_4Cl_{sat.}$(20 mL) and extracted with CH_2Cl_2 (30 mL). The organic phase was washed with $NH_4Cl_{sat.}$ (20 mL), water (20 mL) and dried over Na_2SO_4. After removal of the solvent, the product was treated with pentane and filtered. Evaporation of the filtrate followed by purification by column chromatography (SiO_2, pentane/3% CH_2Cl_2) afforded compound **16** (4.1 g, 88%) as a light yellow oil. R_f = 0.3 (pentane); ^{1}H NMR ($CDCl_3$, 400 MHz, 25°C): δ = 7.03 (s, 1H), 6.92 (s, 1H), 3.82 (d, *J* = 5.5Hz, 4H), 1.81-1.74 (m, 2H), 1.54-1.19 (m, 48H), 0.92-0.83 (m, 12H), 0.25 (s, 9H); ^{13}C NMR ($CDCl_3$, 400 MHz, 25°C): δ = 155.0, 149.5, 117.7, 117.5, 113.7, 112.3, 100.8, 99.1, 77.2, 72.9, 72.2, 38.3, 38.1, 32.1, 32.1, 32.0, 32.0, 31.5, 31.4, 31.4, 30.2, 30.2, 29.9, 29.8, 29.8, 29.7, 29.5, 29.5, 27.0, 27.0, 27.0, 26.9, 22.8, 14.3, 0.13; Anal. calcd for $C_{43}H_{77}BrO_2Si$: C 70.36, H 10.57, Si 3.83; found: C 70.58, H 10.9, Si 3.3.

Compound 29

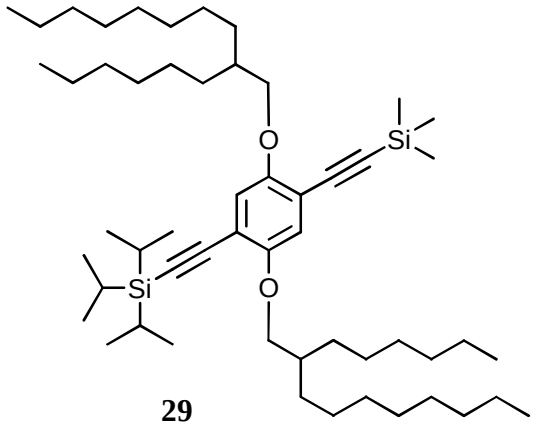

29

To an oven dried Schlenk were added compound **16** (2.0 g, 2.73 mmol), (triisopropylsilyl)acetylene (0.92 mL, 4.09 mmol), $Pd(PPh_3)_2Cl_2$ (115 mg, 0.16 mmol), copper iodide (104 mg, 0.55 mmol), triphenylphosphine (143 mg, 0.55 mmol) in a 1:1 mixture of triethylamine and THF (7 mL). The solution was degassed using freeze-thaw cycles and the reaction mixture was heated overnight at 80 ^oC. The reaction was quenched with $NH_4Cl_{sat.}$(10 mL) and extracted with CH_2Cl_2 (20 mL). The organic phase was washed with $NH_4Cl_{sat.}$ (10 mL), water (10 mL) and dried over Na_2SO_4. After removal of the solvent, the product was treated with n-hexane and filtered. Evaporation of the filtrate followed by purification by column chromatography (SiO_2, n-hexane/4% CH_2Cl_2) afforded compound **29** (2.27 g, 99%) as a light yellow oil. R_f = 0.3 (CH_2Cl_2/ n-hexane: 4/96); ^{1}H NMR ($CDCl_3$, 400 MHz, 25°C): δ = 6.87 (s, 1H), 6.86 (s, 1H), 3.85 (d, *J* = 5.3Hz, 2H), 3.81 (d, *J* = 5.4Hz, 2H), 1.82-1.72 (m, 2H), 1.58-1.21 (m, 48H), 1.15 (s, 21H), 0.89 (t, *J* = 6.7Hz, 12H), 0.26 (s, 9H); ^{13}C NMR($CDCl_3$, 400 MHz, 25°C): δ = 154.3, 154.2, 117.4, 116.4, 114.1, 113.8, 103.2, 101.5, 99.7, 96.3, 77.2, 72.0, 71.8, 38.4, 38.4, 32.1, 32.1, 31.4, 31.3, 30.3, 30.2, 29.9, 29.9, 29.8, 29.8, 29.5, 29.5, 27.1, 27.0, 27.0, 27.0, 22.9, 22.9, 19.0, 14.3, 11.6, 0.17; Anal. calcd for $C_{54}H_{98}O_2Si_2$: C 77.63, H 11.82, Si 6.72; found: C 77.68, H 12.02, Si 6.36.

Compound 30

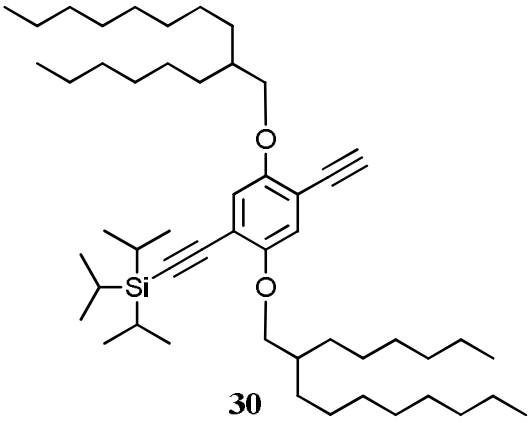

30

To a solution of compound **29** (2.16 g, 2.59 mmol) in a 1:1 mixture of $CHCl_3$ and MeOH (60 mL), K_2CO_3 (1.43 g, 10.34 mmol) was added and the mixture was stirred overnight at room temperature. The reaction mixture was then washed with water (3 × 30 mL) and dried over Na_2SO_4. Further evaporation of the solvent provided compound **30** (1.95 g, 98%) as a light orange colored oil. R_f = 0.35 (CH_2Cl_2/n-hexane: 4/96); ^{1}H NMR ($CDCl_3$, 400 MHz, 25°C): δ = 6.9 (s, 2H), 3.85 (d, *J* = 5.8Hz, 2H), 3.80 (d, *J* = 5.4Hz, 2H), 3.29 (s, 1H), 1.83-1.72 (m, 2H), 1.53-1.20 (m, 48H), 1.14 (s, 21H), 0.88 (t, *J* = 6.8 Hz, 12H); ^{13}C NMR ($CDCl_3$, 100 MHz, 25°C): δ = 154.3, 154.2, 117.9, 116.9, 114.5, 112.8, 103.0, 96.5, 82.1, 80.3, 77.2, 72.7,

71.8, 38.3, 38.1, 32.1, 32.0, 31.5, 31.2, 31.2, 30.2, 30.2, 29.9, 29.9, 29.8, 29.7, 29.5, 29.5, 27.0, 27.0, 22.9, 22.8, 18.9, 14.3, 11.5; Anal. calcd for $C_{51}H_{90}O_2Si$: C 80.24, H 11.88, Si 3.68; found: C 80.38, H 12.07, Si 3.66.

Compound 31

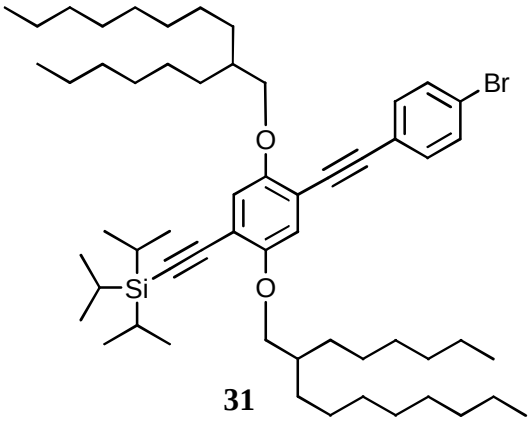

31

To an oven dried Schlenk were added compound **30** (1.81 g, 2.37 mmol), *p*-bromoiodobenzene (1.01 g, 3.56 mmol), $Pd(PPh_3)_2Cl_2$ (100 mg, 0.14 mmol), copper iodide (91 mg, 0.48 mmol), triphenylphosphine (125 mg, 0.48 mmol) in a 1:1 mixture of triethylamine and dry THF (14 mL). The solution was degassed using freeze-thaw cycles and the reaction mixture was heated overnight at 30 °C. The reaction was quenched with $NH_4Cl_{sat.}$(10 mL) and extracted with CH_2Cl_2 (20 mL). The organic phase was washed with $NH_4Cl_{sat.}$ (10 mL), water (10 mL) and dried over Na_2SO_4. After removal of the solvent was removed, the product was treated with pentane and filtered. Evaporation of the filtrate followed by purification by column chromatography (SiO_2, pentane → pentane/ CH_2Cl_2: 1/10) provided compound **31** (1.88 g, 86%) as a light yellow oil. R_f = 0.5 (CH_2Cl_2/pentane: 1/10); ^{1}H NMR ($CDCl_3$, 400 MHz, 25°C): δ = 7.49-7.45 (m, 2H), 7.39-7.36 (m, 2H), 6.93 (s, 1H), 6.92 (s, 1H), 3.88 (d, *J* = 5.6Hz, 2H), 3.84 (d, *J* = 5.4Hz, 2H), 1.85-1.74 (m, 2H), 1.58-1.18 (m, 48H), 1.15 (s, 21H), 0.91-0.83 (m, 12H); ^{13}C NMR ($CDCl_3$, 100 MHz, 25°C): δ = 154.5, 153.7, 133.1, 131.7, 122.7, 122.5, 117.7, 116.0, 114.2, 113.7, 103.1, 96.6, 93.6, 87.5, 77.2, 72.5, 71.8, 38.4, 32.1, 32.1, 32.0, 31.6, 31.3, 31.2, 30.3, 30.2, 29.9, 29.8, 29.8, 29.5, 29.5, 27.1, 27.1, 27.0, 27.0, 22.9, 22.8, 18.9, 14.3, 14.2, 11.6; Anal. calcd for $C_{57}H_{93}BrO_2Si$: C 74.55, H 10.21, Si 3.06; found: C 74.76, H 10.41, Si 3.05.

Compound 33

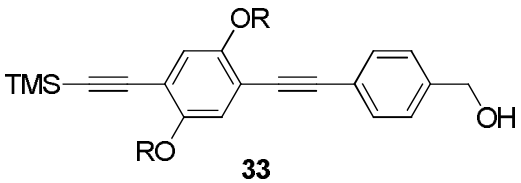

33

To an oven dried Schlenk were added compound **16** (100 mg, 0.14 mmol), 4-ethynylbenzyl alcohol **32** (21.6 mg, 0.16 mmol), $Pd(PPh_3)_2Cl_2$ (10 mg, 0.01 mmol), copper iodide (5.0 mg, 0.02 mmol), triphenylphosphine (4 mg, 0.02 mmol) in a 5:2 mixture of triethylamine and dry THF (7 mL). The solution was degassed using freeze-thaw cycles and the reaction mixture was heated at overnight 80°C. The reaction was quenched with $NH_4Cl_{sat.}$(10 mL) and extracted with CH_2Cl_2 (20 mL). The organic phase was washed with $NH_4Cl_{\ sat.}$ (10 mL), water (10 mL) and dried over Na_2SO_4. After removal of the solvent, the product was treated with n-hexane and filtered. Evaporation of the filtrate followed by purification by column chromatography (SiO_2, n-hexane → EtOAc/n-hexane: 1/2) afforded compound **33** (60 mg, 56%) as a light yellow oil. R_f = 0.5 (EtOAc/n-hexane: 1/4); ^{1}H NMR and ^{13}C NMR data cannot be reported due to a problem faced with the NMR hard drive.

Compound 34

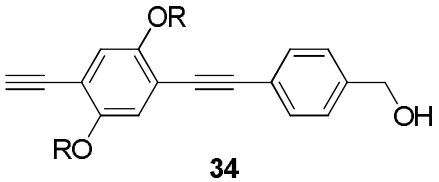

34

To a solution of compound **33** (66 mg, 0.084 mmol) in a 1:1 mixture of CH_2Cl_2 and MeOH (4 mL), K_2CO_3 (137 mg, 1.0 mmol) was added and the mixture was stirred overnight at room temperature. The reaction mixture was then washed with water (3 × 20 mL), dried over Na_2SO_4. Removal of the solvent afford compound **34** (58 mg, 98%) as a red viscous oil. R_f = 0.7 (EtOAc/n-hexane: 1/3); ^{1}H NMR and ^{13}C NMR data cannot be reported due to a problem faced with the NMR hard drive.

Compound 38

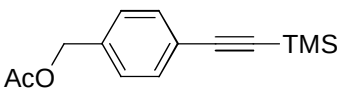

38

4-Trimethylsilylbenzyl acetate. Trimethylsilyl acetylene (3.34 ml, 24 mmol) was added to a solution of copper iodide (767 mg, 4 mmol), $PdCl_2(PPh_3)_2$ (1.41 g, 2 mmol), PPh_3 (1.06 g, 4

mmol) and 4-bromobenzylacetate (4.61 g, 20 mmol) in triethylamine (30 mL). The mixture was degassed by using freeze-thaw cycles and heated up to 70 °C for 36 hours under a nitrogen atmosphere. The resulting dark brown mixture was then filtered and the solvent was removed in vacuo. Further purification by column chromatography (SiO_2, n-hexane/EtOAc: 20/1) provided compound **38** (4.56 g, 89%) as a pale yellow solid. R_f = 0.2 (n-hexane/EtOAc: 20/1); ^{1}H NMR ($CDCl_3$, 400 MHz, 25°C): δ = 7.44 (d, *J* = 8.4Hz, 2H), 7.30 (d, *J* = 8.4Hz, 2H), 5.07 (s, 2H), 2.08 (s, 3H), 0.25 (s, 9H); ^{13}C NMR ($CDCl_3$, 100 MHz, 25°C): δ = 170.9, 136.4, 132.3, 128.0, 123.2, 104.8, 94.8, 65.9, 21.1, 0.1; ESI-MS: calcd. for $C_{14}H_{18}O_2Si$: 247.12 $[M+H]^+$, found: 247.15.

Compound 39

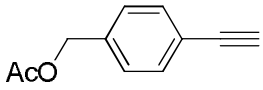

39

4-ethynylbenzyl acetate. A solution of 4-trimethylsilylbenzyl acetate (1.82 g, 8.9 mmol) in THF (10 mL) was treated with TBAF (1M solution in THF, 0.8 mL, 0.8 mmol). The mixture was stirred at room temperature for 30 min and the solvent was removed under reduced pressure. Further purification by column chromatography (SiO_2, n-hexane/EtOAc: 20/1) provided compound **39** (1.10 g, 85%) as a pale yellow solid. R_f = 0.2 (n-hexane/ EtOAc: 20/1); ^{1}H NMR ($CDCl_3$, 400 MHz, 25°C): δ = 7.48 (d, *J* = 8.2Hz, 2H), 7.31 (d, *J* = 8.4Hz, 2H), 5.09 (s, 2H), 3.09 (s, 1H), 2.11 (s, 3H); ^{13}C NMR ($CDCl_3$, 100 MHz, 25°C): δ = 170.9, 136.8, 132.5, 128.2, 122.2, 83.4, 77.7, 65.9, 21.1; Anal. calcd. for $C_{11}H_{10}O_2$: C 75.84, H 5.79; found C 75.17, H 5.86.

Compound 40

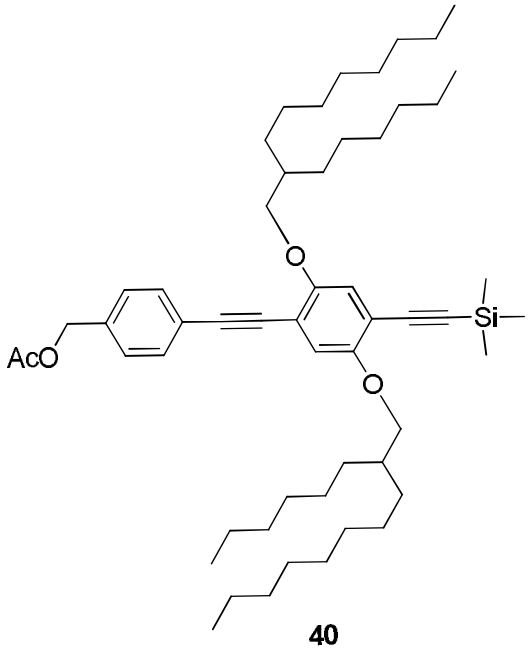

40

To an oven dried Schlenk were added compound **16** (3.2 g, 4.36 mmol), 4-ethynylbenzyl acetate **39** (1.14 g, 6.54 mmol), $Pd(PPh_3)_2Cl_2$ (306 mg, 0.44 mmol), copper iodide (166 mg, 0.87 mmol), triphenylphosphine (229 mg, 0.87 mmol) in a 3:1 mixture of triethylamine and dry THF (20 mL). The solution was degassed using freeze-thaw cycles and the reaction mixture was heated at overnight 80 °C. The reaction was quenched with $NH_4Cl_{sat.}$(10 mL) and extracted with CH_2Cl_2 (20 mL). The organic phase was washed with $NH_4Cl_{sat.}$ (10 mL), water (10 mL) and dried over Na_2SO_4. After removal of the solvent, the product was treated with n-hexane and filtered. Evaporation of the filtrate followed by purification by column chromatography (SiO_2, n-hexane → EtOAc/n-hexane: 1/20) afforded compound **40** (3.14 g, 87%) as a light yellow oil. R_f = 0.3 (EtOAc/n-hexane: 1/20); ^{1}H NMR ($CDCl_3$, 400 MHz, 25°C): δ= 7.52 (d, *J* = 8.0Hz, 2H), 7.33 (d, *J* = 8.7Hz, 2H), 6.96 (s, 1H), 6.95 (s, 1H), 5.11 (s, 2H), 3.88 (d, *J* = 2.3Hz, 2H), 3.87 (d, *J* = 1.8Hz, 2H), 2.11 (s, 3H), 1.87-1.77 (m, 2H), 1.62-1.16 (m, 48H), 0.92-0.83 (m, 12H), 0.28 (s, 9H); ^{13}C NMR ($CDCl_3$, 100 MHz, 25°C): δ = 170.6, 154.4, 153.7, 136.0, 131.7, 128.1, 123.5, 117.0, 116.3, 114.1, 114.0, 101.3, 99.9, 94.3, 86.5, 72.3, 71.9, 65.8, 38.2, 31.9, 31.9, 31.9, 31.5, 31.5, 31.3, 31.3, 30.1, 30.1, 29.8, 29.6, 29.6, 29.4, 29.3, 26.9, 26.9, 26.9, 22.8, 22.8, 20.9, 14.1, 14.1, 0.1; Anal. calcd for $C_{54}H_{86}O_4Si$: C 78.39, H 10.48, Si 3.39; found: C 78.57, H 10.63, Si 3.415.

Compound 41

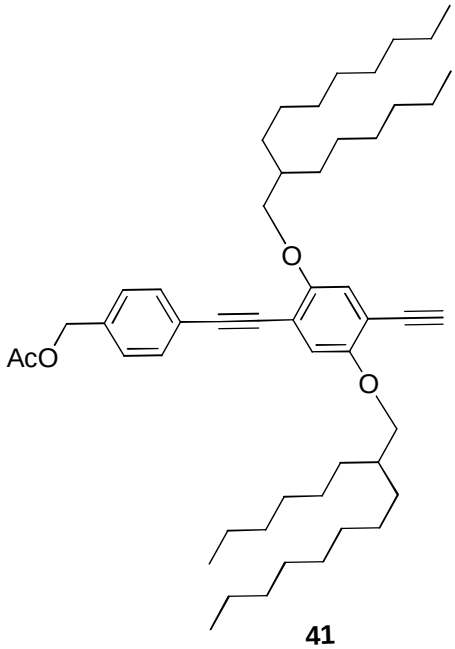

41

To a solution of compound **40** (358 mg, 0.43 mmol) in a 4:1 mixture of THF and water (5 mL), TBAF (0.8 mL, 0.86 mmol) was added. The reaction mixture was then stirred overnight at room temperature, and further diluted with water (10 mL) and extracted with CH_2Cl_2 (3 × 10 mL). Evaporation of the solvent followed by purification by column chromatography (SiO_2, n-hexane → EtOAc/n-hexane: 1/10) provided compound **41** (265 mg, 81%) as a orange colored oil. R_f = 0.55 (EtOAc/n-hexane: 1/10); ^{1}H NMR ($CDCl_3$, 400 MHz, 25°C): δ = 7.52 (d, *J* = 8.1Hz, 2H), 7.33 (d, *J* = 8.1Hz, 2H), 6.99 (s, 1H), 6.97 (s, 1H), 5.12 (s, 2H), 3.88 (d, *J* = 5.6Hz, 4H), 3.31 (s, 1H), 2.12 (s, 3H), 1.87-1.78 (m, 2H), 1.60-1.17 (m, 48H), 0.93-0.81 (m, 12H); ^{13}C NMR ($CDCl_3$, 100 MHz, 25°C): δ = 170.8, 154.6, 153.9, 136.2, 131.8, 128.2, 123.6, 117.5, 116.9, 114.5, 112.9, 94.5, 86.4, 82.3, 80.2, 72.7, 72.5, 66.0, 38.3, 38.1, 32.1, 32.0, 32.0, 31.6, 31.6, 31.5, 30.2, 30.2, 29.9, 29.8, 29.7, 29.5, 29.5, 27.1, 27.0, 27.0, 22.8, 22.8, 21.0, 14.1; Anal. calcd for $C_{51}H_{78}O_4$: C 81.1, H 10.41, found: C 81.31, H 10.57.

Compound 42

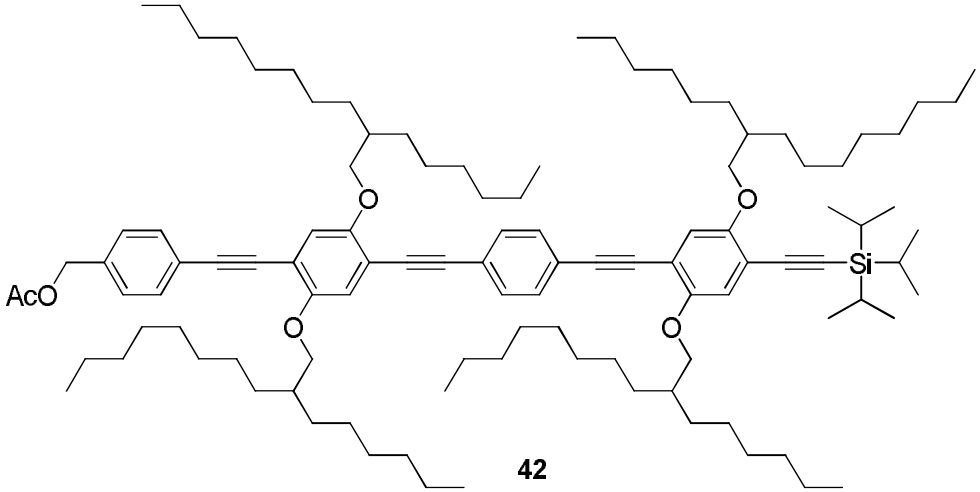

42

Compound **41** (20 mg, 26.5 mmol) was added to a solution of compound **31** (22.2 mg, 26.5 mmol) in a 1:1 mixture of triethylamine and tetrahydrofuran (4 mL). The mixture was degassed by using freeze-thaw cycles and $Pd(PPh_3)_4$ (3 mg, 2.65 mmol) was added. The mixture was degassed once more by using freeze-thaw cycles and then heated up to 70°C overnight. The resulting dark brown mixture was filtered and the solvent was removed in vacuo. Further purification by column chromatography (SiO_2, n-hexane → n-hexane/CH_2Cl_2: 10/1) provide compound **42** (32.9 mg, 78%) as an orange oil. R_f = 0.15 (n-hexane/CH_2Cl_2: 1/20); ^{1}H NMR ($CDCl_3$, 400 MHz, 25°C): δ = 7.53 (d, *J* = 8.0Hz, 2H), 7.49 (s, 4H), 7.33 (d, *J* = 8.0 Hz, 2H), 7.01 (s, 1H), 7.00 (s, 1H), 6.94 (s, 1H), 6.93 (s, 1H), 5.12 (s, 2H), 3.94-3.83 (m, 8H), 2.13 (s, 3H), 1.93-1.73 (m, 4H), 1.63-1.19 (m, 99H), 1.16 (s, 18H), 0.92-0.82 (m, 24H); ^{13}C NMR ($CDCl_3$, 400 MHz, 25°C): δ = 170.9, 154.5, 154.1, 153.8, 136.1, 131.9, 131.6, 128.2, 123.7, 123.6, 123.4, 117.8, 116.8, 116.2, 114.2, 114.1, 114.0, 113.9, 103.2, 96.6, 94.8，94.6, 94.5, 88.3, 88.2, 86.7, 72.6, 72.5, 71.9, 66.0, 38.4, 32.1, 32.0, 31.7, 31.6, 31.3, 30.3, 29.9, 29.8, 29.8, 29.5, 29.5, 27.1, 27.0, 27.0, 22.9, 22.9, 21.1, 18.9, 14.3, 14.3, 11.6; Anal. calcd for $C_{108}H_{170}O_6Si$: C 81.45, H 10.76, Si, 1.76; found: C 81.62, H 11.01, Si 1.743.

Compound 44

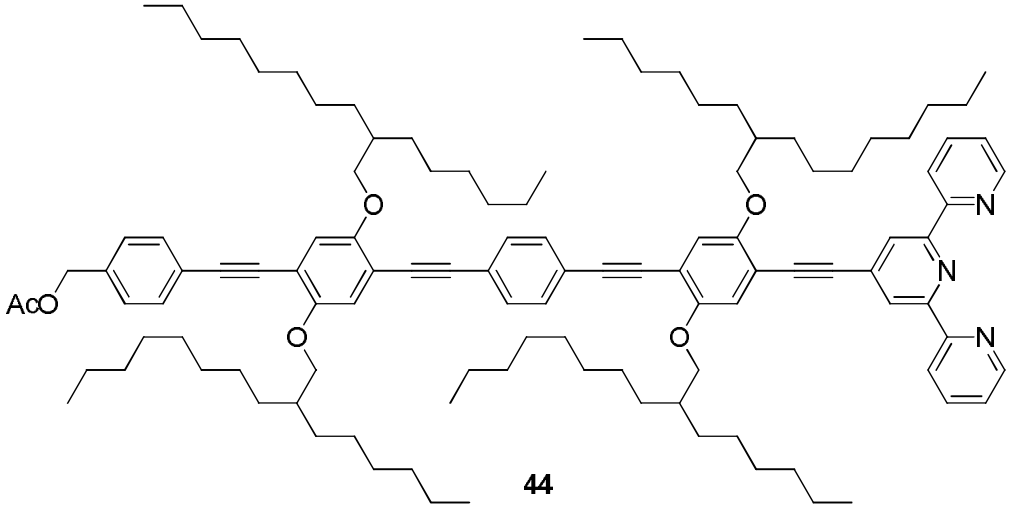

44

To a solution of compound **42** (500 mg, 0.31 mmol) in THF (3 mL), TBAF (0.628 mL, 0.628 mmol) was added and the reaction mixture was stirred overnight at room temperature. The mixture was then diluted with water (10 mL) and extracted with CH_2Cl_2 (3 × 10 mL). Evaporation of the solvent followed by purification by column chromatography (SiO_2, n-hexane → CH_2Cl_2/n-hexane: 1/2) provided the free alkyne intermediate (375 mg, 83%) as a yellow oil, which was used as such in the next step.

2,2′:6,2″-terpyridine triflate (119 mg, 0.31 mmol) was added to a solution of the free alkyne intermediate (375 mg, 0.26 mmol) in a 1:1 mixture of triethylamine and tetrahydrofuran (6 ml). The mixture was degassed by using freeze-thaw cycles and $Pd(Ph_3)_4$ (30 mg, 0.03 mmol) was added. The mixture was degassed once more by using freeze-thaw cycles and then heated up to 60°C overnight. The resulting dark brown mixture was filtered and the solvent was removed in vacuo. Further purification by column chromatography (Al_2O_3, n-hexane → CH_2Cl_2 /n-hexane: 1/2) yielded compound **44** (370 g, 85%) as yellow oil. R_f = 0.6 (CH_2Cl_2 /n-hexane: 1/2); ^{1}H NMR ($CDCl_3$, 400 MHz, 25°C): δ = 8.63 (brs, 2H), 8.54 (brd, *J* = 8.3Hz, 2H), 8.52 (s, 2H), 7.77 (ddd, *J* = 7.5 Hz, 2H), 7.44 (d, *J* = 6.5 Hz, 2H), 7.43 (s, 4H), 7.31-7.22 (m, 4H), 6.99 (s, 1H), 6.95 (s, 1H), 6.93 (s, 2H), 4.50 (s, 2H), 3.90-3.79 (m, 4H), 1.89-1.70 (m, 8H), 1.30-1.10 (m, 4H); 1.09-0.95 (m, 96H), 0.87 (m, 24H); MALDI-TOF: calcd for $C_{114}H_{159}N_3O_6$: 1667.231 $[M-H]^+$, found: 1667.234.

Compound 45

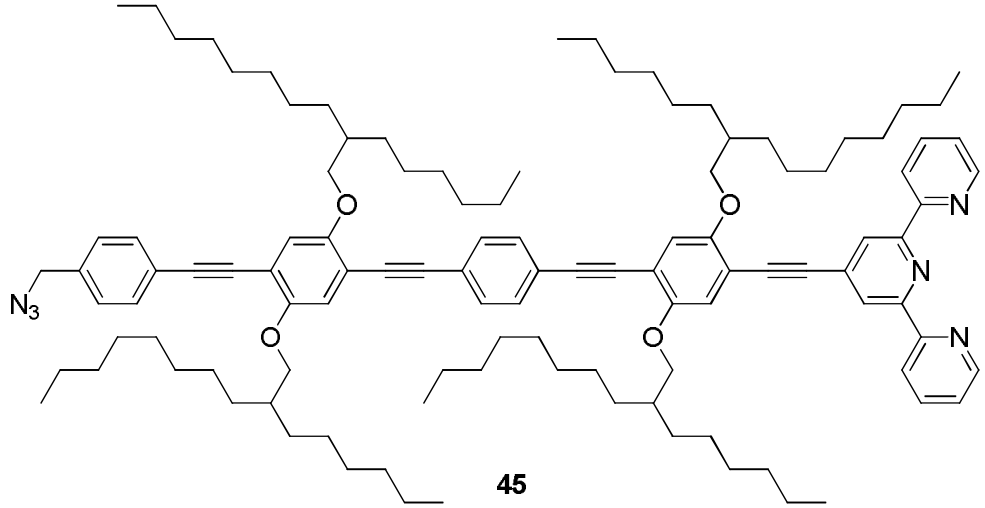

45

A solution of compound **44** (300 mg, 0.18 mmol) in a 9:1 mixture of THF/methanol (10 mL) was treated with K_2CO_3 (249 mg, 1.8 mmol) and the solution was stirred overnight at room temperature. The solvent was then removed in vacuo, and the resulting mixture was dissolved with a mixture of CH_2Cl_2 (10 mL) and water (20 mL), and the aqueous phase was extracted with CH_2Cl_2 (3 × 20 mL). The organic phases were combined, dried over Na_2SO_4, and evaporated in vacuo to give the corresponding-benzyl alcohol, which was pure enough to be used as such in the next step.

A solution of this crude compound in CH_2Cl_2 (10 mL) was cooled down to 0°C and triethylamine (168 µL, 1.17 mmol) and methanesulfonyl chloride (96 µL, 1.17 mmol) were added. The reaction mixture was then stirred overnight at room temperature. The organic phase was then extracted with water (10 mL) and $NH_4Cl_{\text{ sat.}}$ (10 mL), dried over Na_2SO_4 and concentrated in vacuo to provide the mesylated derivative, which was pure enough to be used as such in the next step.

A solution of this mesylate compound in a 1:1 mixture of DMF and THF (5 mL) was treated with sodium azide (152 mg, 2.34 mmol) and heated up overnight at 50°C. After cooling down to room temperature, the reaction mixture was diluted with CH_2Cl_2 (10 mL). The organic phase was then extracted with water (10 mL) and $NH_4Cl_{\text{ sat.}}$ (10 mL), dried over Na_2SO_4 and concentrated in vacuo. Further purification by column chromatography (Al_2O_3, n-hexane → CH_2Cl_2/n-hexane: 1/2) provided compound **45** (297 mg, 60% over 3 steps) as a yellow solid. R_f = 0.45 (CH_2Cl_2/n-hexane: 1/2); ^{1}H NMR ($CDCl_3$, 400 MHz, 25°C): δ = 8.73 (brs, 2H), 8.63 (brd, *J* = 8.3Hz, 2H), 8.61 (s, 2H), 7.86 (ddd, *J* = 7.8Hz, 2H), 7.54 (d, *J* = 5.5Hz, 2H), 7.53 (s, 4H), 7.40-7.32 (m, 4H), 7.08 (s, 1H), 7.05 (s, 1H), 7.02 (s, 2H), 4.60 (s, 2H), 4.00-3.89 (m, 4H), 1.98-1.81 (m, 8H), 1.66-1.53 (m, 4H); 1.52-1.10 (m, 96H), 0.95-0.75 (m, 24H);

^{13}C NMR ($CDCl_3$, 400 MHz, 25°C): δ = 155.8, 155.6, 154.2, 153.9, 153.9, 153.9, 149.2, 137.4, 136.8, 133.6, 131.8, 131.5, 131.4, 128.5, 123.9, 123.8, 123.4，123.3, 122.8, 121.2, 116.9, 116.8, 116.6, 114.6, 113.9, 113.9, 113.4, 94.9, 94.7, 94.4, 92.9, 90.6, 88.1, 88.0, 86.9, 72.8, 72.4, 72.4, 45.9, 38.2, 38.1, 31.9, 31.9, 31.9, 31.5, 30.2, 30.1, 30.1, 29.8, 29.8, 29.8, 29.6, 29.4, 29.4, 29.3, 27.0, 26.9, 22.7, 22.7, 14.1, 14.1, 14.1, 14.1, 14.1, 11.6; MALDI-TOF: calcd for $C_{112}H_{156}N_6O_4$: 1646.21 $[M-N_2+Na]^+$, found: 1646.15.

Compound 48

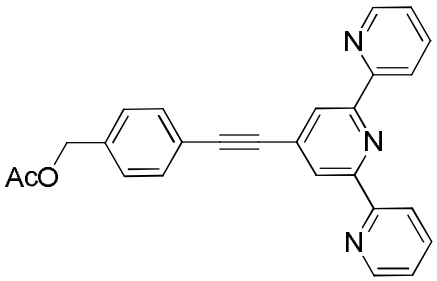

48

2,2′:6′,2″-terpyridine triflate (2.12 g, 5.56 mmol) [115] was added to a solution of compound **39** (1.26 g, 7.23 mmol) in a mixture of triethylamine (40 mL) and tetrahydrofuran (10 mL). The mixture was degassed by using freeze-thaw cycles and $Pd(Ph_3)_4$ (642 mg, 0.56 mmol) was added. The mixture was degassed once more by using freeze-thaw cycles and then heated up to 65°C overnight. The resulting dark brown mixture was filtered and the solvent was removed in vacuo. Further purification by column chromatography (Al_2O_3, n-hexane/CH_2Cl_2: 10/1) yielded compound **48** (1.60 g, 71%) as a white solid. R_f = 0.6 (Al_2O_3, n-hexane/CH_2Cl_2: 10/1); ^{1}H NMR ($CDCl_3$, 400 MHz, 25°C): δ = 8.72 (ddd, *J* = 4.8, 1.7, 0.9Hz, 2H), 8.62 (ddd, *J* = 8.0, 1.0, 1.0Hz, 2H), 8.58 (s, 2H), 7.87 (ddd, *J* = 7.8, 7.7, 1.8Hz, 2H), 7.57 (d, *J* = 8.2Hz, 2H), 7.39-7.34 (m, 4H), 5.13 (s, 2H), 2.13 (s, 3H); ^{13}C NMR ($CDCl_3$, 100 MHz, 25°C): δ = 170.9, 155.8, 155.7, 149.3, 137.1, 137.0, 133.4, 132.3, 128.3, 124.2, 123.0, 122.5, 121.4, 93.4, 88.0, 65.9, 21.1; ESI-MS: calcd for $C_{26}H_{19}N_3O_2$: 406.16 $[M+H]^+$, found: 406.22.

Compound 49

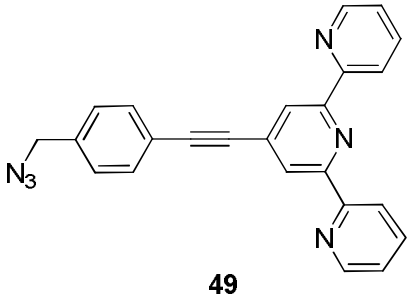

49

[115] Potts, K. T.; Konwar, D. Synthesis of 4'-vinyl-2,2':6',2"-terpyridine. *J. Org. Chem.* **56**, 4815-4816 (1991).

A solution of compound **48** (1.6 g, 3.9 mmol) in a 9:1 mixture of dichloromethane/methanol (60 mL) was treated with sodium hydroxide (320 mg, 12.0 mmol) and the solution was stirred at room temperature for 1 hour. The solvent was then removed in vacuo, and the resulting mixture was dissolved with a mixture of CH_2Cl_2 (50 mL) and water (50 mL). The pH was then ajusted to 5~6 using dilute HCl (2M), and the aqueous phase was extracted with CH_2Cl_2 (50 mL) and EtOAc (3 x 50 mL). The organic phases were combined, dried over Na_2SO_4, and evaporated in vacuo to give 2,2′:6,2″-terpyridineethynylbenzyl alcohol, which was pure enough to be used as such in the next step. ^{1}H NMR ($CDCl_3$, 400 MHz, 25°C): δ = 8.74 (d, *J* = 4.2Hz, 2H), 8.65 (d, *J* = 7.9Hz, 2H), 8.59 (s, 2H), 7.90 (ddd, *J* = 7.8, 7.8, 1.5Hz, 2H), 7.58 (d, *J* = 8.2Hz, 2H), 7.41-7.36 (m, 4H), 4.75 (s, 2H).

A solution of crude 2,2′:6,2″-terpyridineethynylbenzyl alcohol in CH_2Cl_2 (10 mL) was cooled down to 0°C and triethylamine (1.5 mL, 12.9 mmol) and methanesulfonyl chloride (1.0 mL, 12.9 mmol) were added. The reaction mixture was then stirred overnight at room temperature and further dissolved with CH_2Cl_2 (70 mL). The organic phase was then extracted with water (50 mL) and $NH_4Cl_{\,sat.}$ (20 mL), dried over Na_2SO_4 and concentrated in vacuo to provide the mesylated derivative, which was pure enough to be used as such in the next step.

A solution of crude 2,2′:6,2″-terpyridineethynylbenzylmesylate in a 1:1 mixture of DMF and THF (10 mL) was treated with sodium azide (1.5 g, 23.0 mmol) and heated up overnight to 50°C. After cooling down to room temperature, the reaction mixture was diluted with CH_2Cl_2 (70 mL). The organic phase was then extracted with water (50 mL) and $NH_4Cl_{\,sat.}$ (20 mL), dried over Na_2SO_4 and concentrated in vacuo. Further purification by column chromatography (Al_2O_3, n-hexane/CH_2Cl_2: 10/1 →CH_2Cl_2) provided compound **49** (900 mg, 66% over 3 steps) as a white solid. R_f = 0.7 (n-hexane/CH_2Cl_2: 10/1); ^{1}H NMR ($CDCl_3$, 400 MHz, 25°C): δ = 8.71 (d, *J* = 4.7Hz, 2H), 8.60 (d, *J* = 8.0Hz, 2H), 8.57 (s, 2H), 7.85 (ddd, *J* = 7.8, 7.8, 1.8Hz, 2H), 7.58 (d, *J* = 8.2Hz, 2H), 7.35-7.32 (m, 4H), 4.37 (s, 2H); ^{13}C NMR ($CDCl_3$, 100 MHz, 25°C): δ = 155.7, 155.7, 149.3, 137.0, 136.5, 133.3, 132.5, 128.3, 124.1, 122.9, 122.6, 121.3, 93.3, 88.2, 54.4; ESI-MS: calcd for $C_{24}H_{16}N_6$: 389.15 $[M+H]^+$, found: 389.21.

Compound 50

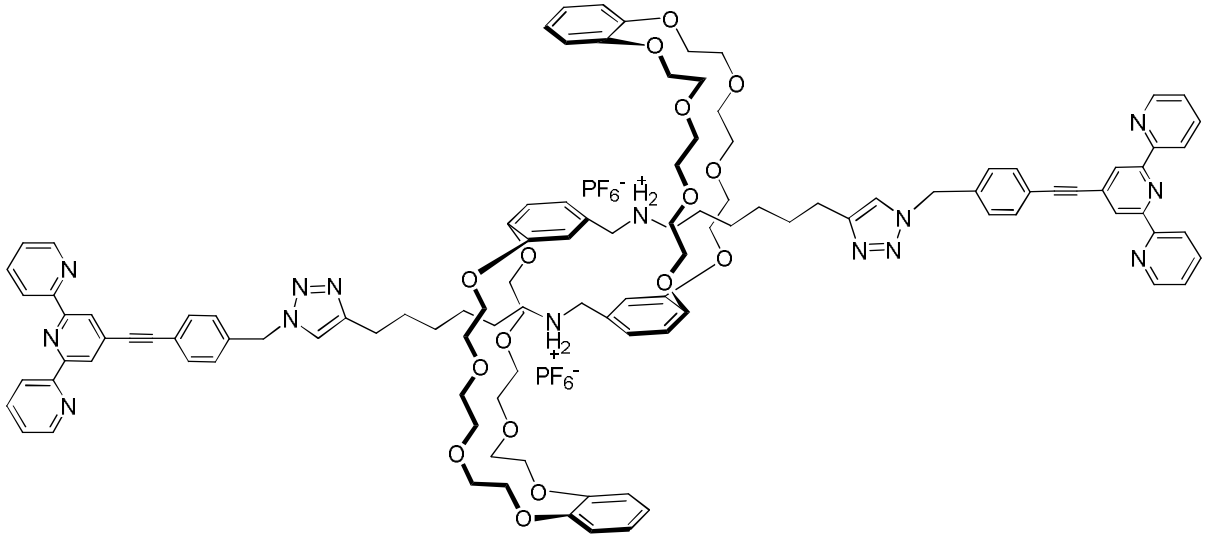

50

To a solution of terpyridine azide **49** (106 mg, 0.27 mmol) and pseudo-rotaxane **11** (200 mg, 0.13 mmol) in a mixture of dry CH_2Cl_2 (10 mL) and dry CH_3CN (4 mL) were added successively $Cu(CH_3CN)_4PF_6$ (408 mg, 1.08 mmol) and 2,6-lutidine (128 µL, 1.08 mmol). The reaction mixture was stirred for 5 min, then heated by microwave irradiation (50 W) for 1hour at 30°C and finally, stirred with an aqueous EDTA-disodium salt solution adjusted to pH ≈ 8-9 (20 mL). The mixture was then extracted with a 3:1 mixture of CH_2Cl_2/ CH_3CN (3 × 20 mL). The organic phases were combined, dried over Na_2SO_4 and finally evaporated in vacuo. Further purification by column chromatography (Al_2O_3, CH_2Cl_2 → CH_2Cl_2/CH_3OH: 100/1) yielded compound **50** (220 mg, 72%) as a yellow solid. ^{1}H NMR ($CDCl_3$, 400 MHz, 25°C): δ = 8.71 (d, *J* = 4.1Hz, 4H), 8.62 (d, *J* = 7.9Hz, 4H), 8.56 (s, 4H), 7.87 (dd, *J* = 7.9, 7.2Hz, 4H), 7.57 (d, *J* = 8.1Hz, 4H), 7.36 (brdd, *J* = 6.1, 5.9 Hz, 4H), 7.29 (d, *J* = 7.8Hz, 4H), 7.23 (s, 2H), 6.94-6.59 (m, 14H), 5.53 (s, 4H), 4.49-4.25 (m, 4H), 4.24-3.62 (m, 48H), 3.54-3.28 (m, 4H), 2.62 (t, *J* = 8.1Hz, 4H), 1.75-1.54 (m, 8H), 1.39-1.27 (m, 8H); ^{13}C NMR ($CDCl_3$, 100 MHz, 25°C): δ = 155.8, 155.7, 149.4, 148.6, 147.8, 147.7, 146.5, 146.2, 137.1, 136.1, 133.2, 132.7, 128.3, 124.8, 124.3, 123.1, 123.0, 122.9, 121.4, 121.3, 121.2, 120.8, 113.2, 112.8, 112.0(x2), 92.9, 88.5, 72.4, 72.0, 71.4, 71.0, 70.9, 70.5, 70.1, 69.6, 67.7, 67.2, 67.1, 66.9, 53.8, 52.3, 48.9, 29.2, 28.7, 26.8, 26.7, 26.6, 25.6; MALDI-TOF: m/z calcd for $C_{114}H_{128}N_{14}O_{16}P_2F_{12}$: 974.48 $[M\text{-}2PF_6]^{2+}$, found: 974.64.

Compound 1^{ext}

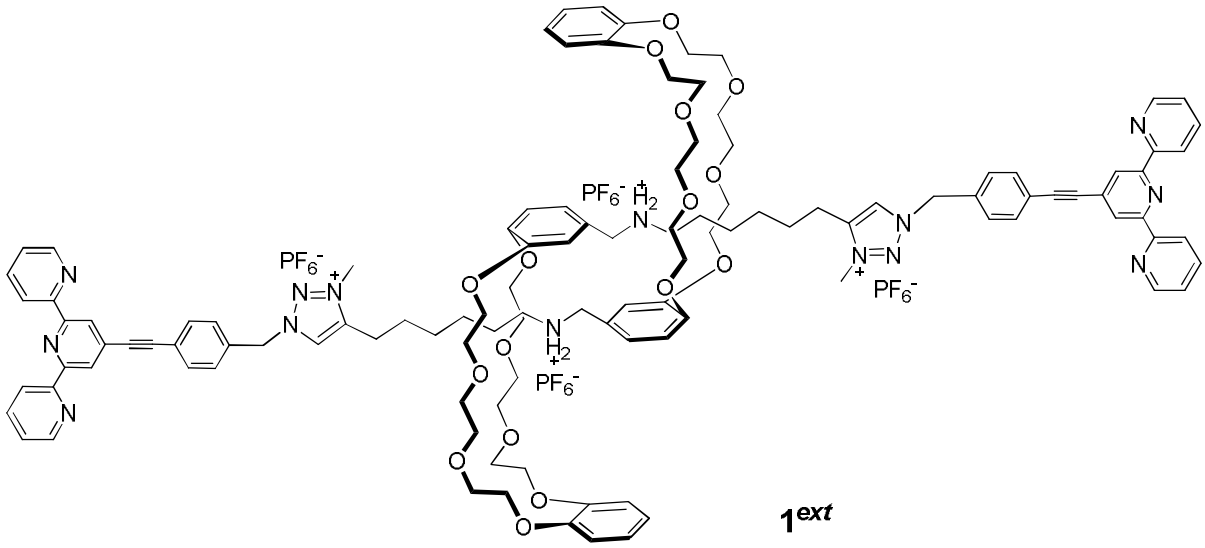

1^{ext}

Rotaxane **15** (45 mg, 0.02 mmol) and $Cu(OTf)_2$ (21.8 mg, 0.06 mmol) were dissolved in a 1:1 mixture of $CHCl_3$ and CH_3CN (6 mL). After stirring for 1 hour at room temperature, the solvents were evaporated in vacuo and a 1:1 mixture of iodomethane and acetonitrile (4 mL) was added. The mixture was stirred for 5 days at room temperature and, then solvents were evaporated in vacuo and the resulting solid was washed with Et_2O (10 mL) to give a brown solid. This crude solid was dissolved in CH_2Cl_2 (20 mL) and the solution was stirred with an aqueous EDTA-disodium salt solution adjusted to pH ≈ 8-9 (20 mL). The mixture was then extracted with a 3:1 mixture of CH_2Cl_2/CH_3CN (3 × 20 mL). The organic phases were combined, dried over Na_2SO_4 and finally evaporated in vacuo. To a solution of this crude residue in water (4 mL) was added NH_4PF_6 (30 mg, 0.18 mmol) and a 3:1 mixture of CH_2Cl_2/CH_3CN (4 mL). The biphasic solution was stirred vigorously for 1 hour. The aqueous layer was extracted with $CHCl_3$ (3 x 20 mL). The organic layers were combined, dried over Na_2SO_4 and concentrated in vacuo to give product **1^{ext}** (51 mg, quantitative) as a brown solid. ^{1}H NMR ($CDCl_3$, 400 MHz, 25°C): δ = 8.69 (brd, *J* = 4.0Hz, 4H), 8.62-8.56 (m, 4H), 8.54-8.48 (m, 4H), 8.30 (s, 1.33H), 8.20 (s, 0.67H), 7.85 (dd, *J* = 7.7, 7.7Hz, 4H), 7.56 (d, *J* = 8.1Hz, 4H), 7.48-7.44 (m, 4H), 7.37-7.32 (m, 4H), 7.05-6.64 (m, 12H), 5.64 and 5.62 (2x s, 4H, isomers), 4.44-4.23 (m, 4H), 4.24-3.51 (m, 48H), 3.49-3.26 (m, 4H), 2.76 (t, *J* = 7.2Hz, 2.67H), 2.65 (t, *J* = 7.0Hz, 1.33H), 1.90-1.66 (m, 8H), 1.49-1.34 (m, 8H); ^{13}C NMR ($CDCl_3$, 125 MHz, 25°C): δ = 155.8, 155.6, 151.0, 149.4, 149.2, 149.0, 147.7, 145.3, 145.0, 137.1, 132.9, 132.3, 129.6, 128.2, 128.0, 126.3, 124.3, 124.1, 122.9, 121.7, 121.4, 118.0, 114.4, 114.3, 92.7, 88.9, 71.4, 71.3, 71.0, 70.8, 70.7, 70.6, 70.0, 69.9, 69.8, 69.6, 69.5, 69.4, 68.2, 65.2, 57.0, 37.6, 27.0, 25.4, 25.0, 23.0, 22.9, 21.5; ESI-MS: m/z calcd for $C_{116}H_{134}N_{14}O_{16}P_4F_{24}$: 1134.469 $[M\text{-}2PF_6]^{2+}$, found: 1134.766.

Compound 1^{cont}

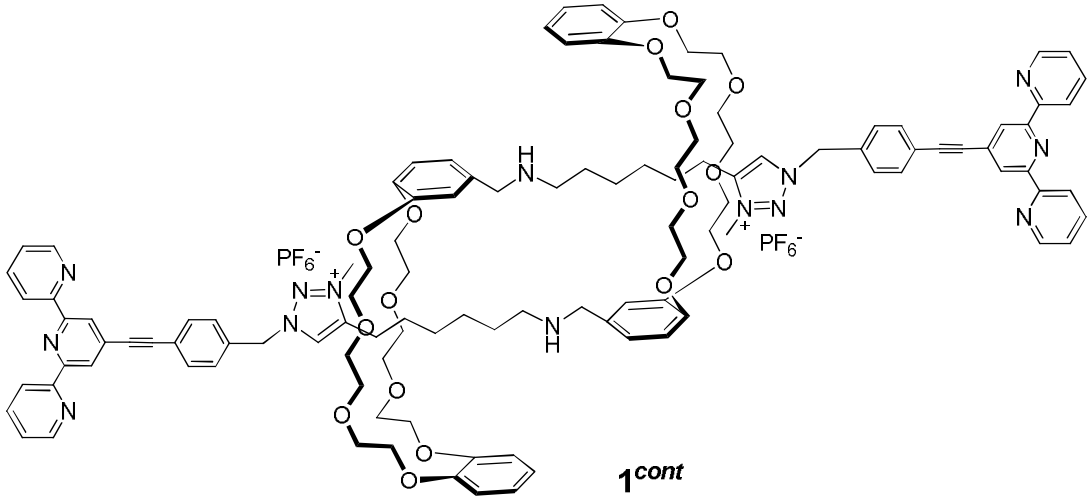

A solution of rotaxane **1**^{ext} (64 mg, 22.8 µmol) in chloroform (10 mL) was washed with an aqueous solution of NaOH 1M (10 mL). The organic phase was dried over Na_2SO_4 and then evaporated in vacuo to provide compound **1**^{cont} (55 mg, quantitative) as a brown solid. As expected, the compound is obtained as a mixture of isomers [64], and only major isomer is described.^{1}H NMR ($CDCl_3$, 500 MHz, 25°C): δ = 8.66 (brd, *J* = 3.6Hz, 4H), 8.56 (brd, *J* = 7.8Hz, 6H), 8.49 (s, 4H), 7.83 (ddd, *J* = 7.7, 7.7, 1.5Hz, 4H), 7.54 (d, *J* = 7.8Hz, 4H), 7.47 (d, *J* = 7.6Hz, 4H), 7.33-7.31 (m, 4H), 7.01-6.62 (m, 14H), 5.67 (s, 4H), 4.40-4.28 (m, 4H), 4.22-3.97 (m, 18H), 3.90-3.52 (m, 30H), 3.47-3.29 (m, 4H), 2.76 (brs, 4H), 1.88-1.55 (m, 8H), 1.50-1.33 (m, 8H); ^{13}C NMR ($CDCl_3$, 125 MHz, 25°C): δ = 155.6, 155.6, 155.4, 150.5, 149.2, 148.9, 148.7, 148.7, 148.5, 144.7, 136.9, 132.7, 132.3, 129.4, 128.4, 124.1, 123.8, 122.7, 121.7, 121.2, 121.2, 178.3, 114.5, 114.4, 111.9, 92.6, 88.7, 72.7, 70.7, 70.6, 70.5, 70.2, 69.6, 69.5, 69.4, 69.3, 69.1, 68.6, 64.8, 56.6, 49.0, 37.5, 27.0, 25.3, 24.9, 22.7, 21.5; MALDI-TOF: calcd for $C_{116}H_{132}N_{14}O_{16}P_2F_{12}$: 988.497 $[M-2PF_6]^{2+}$, found: 988.597.

Procedures for polymerization of terpyridine rotaxanes

Contracted polymers: A solution of $FeCl_2$ (3.2 mg, 25.0 × 10^{-3} mmol, 1.0 equiv.) in CD_3CN (1250 µL) was added rotaxane monomer **1**^{cont} (56.7 mg, 25.0 × 10^{-3} mmol, 1.0 equiv.) in $CDCl_3$ (1250 µL). Immediately the colorless solution turned to purple and the mixture was stirred for 30 min at room temperature prior to further analyzes.

A solution of $Zn(OTf)_2$ (9.1 mg, 25.0 × 10^{-3} mmol, 1.0 equiv.) in CD_3CN (1250 µL) was added rotaxane monomer **1**^{cont} (56.7 mg, 25.0 × 10^{-3} mmol, 1.0 equiv.) in $CDCl_3$ (1250 µL). The colorless solution was stirred for 30 min at room temperature prior to further analyzes.

Extended polymers: A solution of $FeCl_2$ (3.2 mg, 25.0 × 10^{-3} mmol, 1.0 equiv.) in CD_3CN (1250 µL) was added rotaxane monomer **1**^{ext} (64.0 mg, 25.0 × 10^{-3} mmol, 1.0 equiv.) in $CDCl_3$ (1250 µL). Immediately the colorless solution turned to purple and the mixture was stirred for 30 min at room temperature prior to further analyzes.

A solution of $Zn(OTf)_2$ (9.1 mg, 25.0 × 10^{-3} mmol, 1.0 equiv.) in CD_3CN (1250 µL) was added rotaxane monomer **1**^{ext} (64.0 mg, 25.0 × 10^{-3} mmol, 1.0 equiv.) in $CDCl_3$ (1250 µL). The colorless solution was stirred for 30 min at room temperature prior to further analyzes.

Procedures for acidic-basic titrations of monomers 1^{ext} and 1^{cont}

Basic titration: A solution of **1**^{ext} (4 × 10^{-3} mmol) in $CDCl_3$ and a solution of NaOD (0.2 mol/L) in D_2O were prepared separately. 2µL of NaOD solution was added to the 1ext solution for each titration. The complete titration was finished after 22 times (up to 2.2 equiv.).

Acidic titration: A solution of **1**^{cont} (4 × 10^{-3} mmol) in $CDCl_3$ and of *d*-TFA (0.2 mol/L) in $CDCl_3$ were prepared separately. 2µL of *d*-TFA solution was added to the 1cont solution for each titration. The complete titration was finished after 22 times (up to 2.2 equiv.). Finally, the solution was washed with $NaPF_6$ (sat.) aqueous solution to perform a micro-exchange counter ion process.

Compound 51

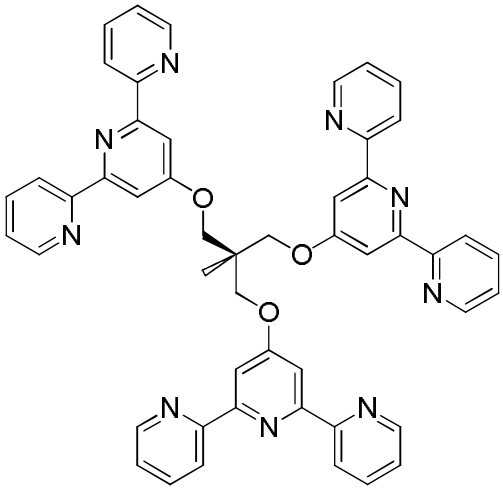

51

1,1,1-Tris(hydroxymethyl)ethane (26.3 mg, 0.22 mmol) was suspended in dry DMSO (8mL) containing powdered potassium hydroxide (184.2 mg, 3.28 mmol). The suspension was stirred for 10 min at room temperature before 4′-chloro-2,2′:6′,2″-terpyridine (234.4 mg, 0.87 mmol) was added, and the mixture was stirred for 72 hours at 70 °C. The color changed from

orange to red-brown. The reaction mixture was stirred for 24 hours more at room temperature, and water (10 mL) was added. The yellow precipitate was filtrated and washed with water (10 mL), methanol (10 mL), and diethyl ether (5 mL), and dried in vacuo to give compound **51** (75 mg, 42%) as a white powder. ^{1}H NMR ($CDCl_3$, 400 MHz, 25°C): δ = 8.66 (d, *J* = 4.8 Hz, 6H), 8.57 (d, *J* = 7.7Hz, 6H), 8.07 (s, 6H), 7.81 (dd, *J* = 7.6, 7.7Hz, 6H), 7.30-7.27 (m, 6H), 4.46 (s, 6H), 1.47 (s, 3H); ^{13}C NMR ($CDCl_3$, 100 MHz, 25°C): δ = 167.1, 157.1, 155.9, 149.0, 137.1, 124.0, 121.6,107.8, 70.0, 40.8,17.5; ESI-MS: calcd. for $C_{50}H_{39}N_9O_3$: 814.33 $[M+H]^+$, found: 814.42.

Compound 58

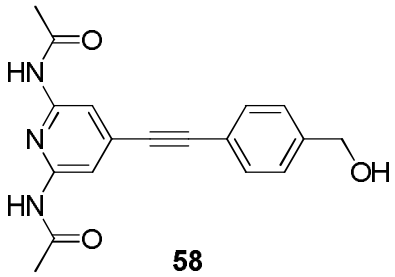

58

4-Bromo-2,6-diacetylaminopyridine (22 mg, 0.08 mmol), 4-ethynylbenzyl acetate **39** (16.9 mg, 0.10 mmol), NEt_3 (2 mL, 14.3 mmol), THF (0.3 mL) and DMF (0.05 mL) were added to a Schlenk tube, and the solution was degassed by using freeze-thaw cycles. $Pd(PPh_3)_4$ (3.7 mg, 0.003 mmol) and CuI (1.3 mg, 0.006 mmol) were then added. The reaction mixture was degassed again and stirred overnight at 85°C. The resulting dark mixture was filtered over Celite and washed with toluene (2 mL), CH_2Cl_2 (4 mL), and MeOH (4 mL). Removal of the solvents under vacuum and purification by column chromatography (SiO_2, n-hexane → n-hexane/EtOAc: 1/1) provide the pyridine-benzyl acetate derivative, which was pure enough to be used as such in the next step as a yellow solid.

A solution of this solid (25 mg, 0.068 mmol) in a 9:1 mixture of dichloromethane/methanol (1 mL) was treated with sodium methoxide (9.2 mg, 0.17 mmol) and the solution was stirred at room temperature for 1 hour. The solvent was then removed in vacuo, and the resulting mixture was dissolved with a mixture of CH_2Cl_2 (5 mL) and water (5 mL). The aqueous phase was extracted with CH_2Cl_2 (5 mL) and EtOAc (3 × 5 mL). The organic phases were combined and dried over Na_2SO_4. Evaporation of the solvent under vacuum and further purification by column chromatography (SiO_2, n-hexane → n-hexane/EtOAc: 1/3) provide compound **58** (16.5 mg, 62%, 2 steps) as a yellow crystalline solid. R_f = 0.1 (n-hexane/EtOAc: 1/3); ^{1}H NMR (MeOD, 400 MHz, 25°C): δ = 7.86 (s, 2H), 7.54 (d, *J* = 8.3Hz, 2H), 7.40 (d, *J* = 7.8Hz, 2H), 4.64 (s, 2H), 2.17 (s, 6H); ^{13}C NMR (MeOD, 100 MHz, 25°C): δ = 171.9, 151.9, 144.5,

136.2, 133.0, 128.0, 122.1, 112.1, 93.9, 87.9, 64.7, 24.1; ESI-MS: calcd for $C_{18}H_{17}N_3O_3$: 324.14, $[M+H]^+$, found 324.05.

Compound 59

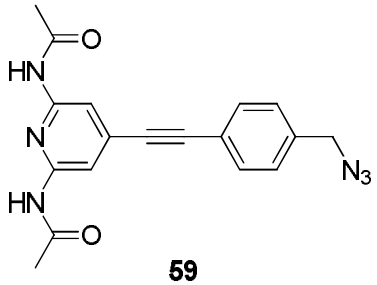

59

A solution of compound **58** (161 mg, 0.50 mmol) in a 4:1 mixture of THF/DMF (10 mL) was cooled down to 0°C and triethylamine (1.5 mL, 0.65 mmol) and methanesulfonyl chloride (50 µL, 0.65 mmol) were added. The reaction mixture was then stirred overnight at room temperature and further dissolved with CH_2Cl_2 (10 mL). The organic phase was then extracted with water (10 mL) and NH_4Cl $_{sat.}$ (10 mL), dried over Na_2SO_4 and concentrated in vacuo to provide the mesylated derivative, which was pure enough to be used as such in the next step.

A solution of the crude mesylated compound in a 1:1 mixture of DMF and THF (4 mL) was treated with sodium azide (380 mg, 5.0 mmol) and heated up overnight to 50°C. After cooling down to room temperature, the reaction mixture was diluted with CH_2Cl_2 (10 mL). The organic phase was then extracted with water (10 mL) and NH_4Cl $_{sat.}$ (10 mL), dried over Na_2SO_4 and concentrated in vacuo. Further purification by column chromatography (SiO_2, n-hexane/EtOAc: 1/4 → EtOAc) provided compound **59** (173 mg, quantitative, over 2 steps) as a brown solid. R_f = 0.2 (SiO_2, n-hexane/AcOEt: 1/4); ^{1}H NMR (MeOD, 400 MHz, 25°C): δ = 7.87 (s, 2H), 7.59 (d, *J* = 8.4Hz, 2H), 7.40 (d, *J* = 7.3 Hz, 2H), 4.42 (s, 2H), 2.17 (s, 6H); ^{13}C NMR (MeOD, 100 MHz, 25°C): δ = 171.9, 151.9, 138.6, 135.9, 133.3, 129.6, 123.2, 112.2, 93.3, 88.6, 55.2, 24.1; ESI-MS: calcd for $C_{18}H_{16}N_6O_2$ 349.14, $[M+H]^+$, found 349.07.

Compound 60

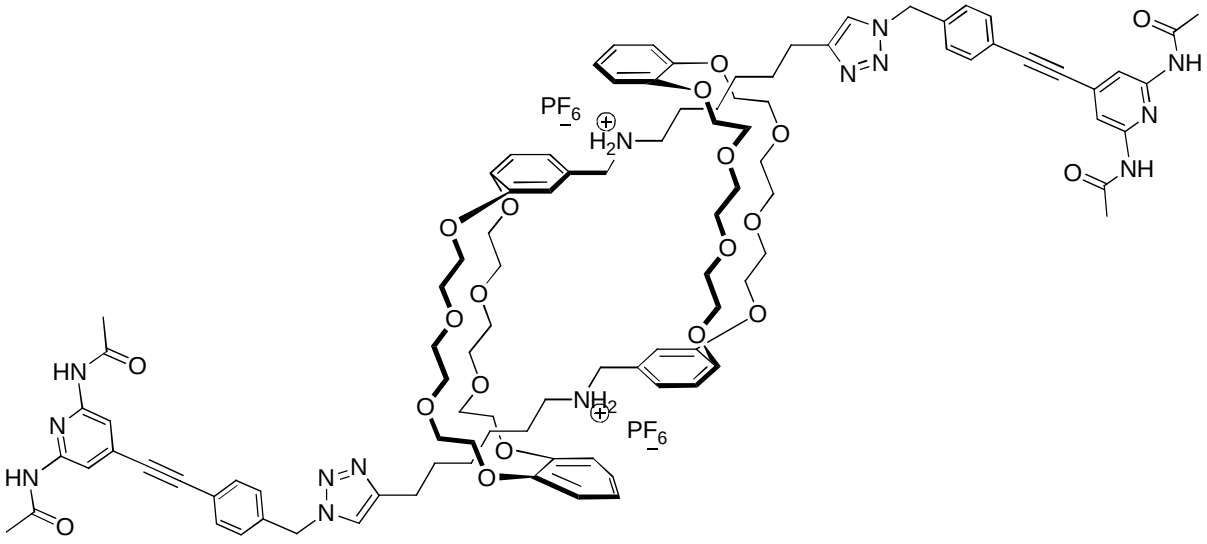

60

To a solution of compound **59** (108 mg, 0.31 mmol) and pseudo-rotaxane **11** (217 mg, 0.15 mmol) in a mixture of dry CH_2Cl_2 (10 mL) and dry CH_3CN (4mL) were added successively $Cu(CH_3CN)_4PF_6$ (231 mg, 0.62 mmol) and 2,6-lutidine (72 µL, 0.62 mmol). The reaction mixture was stirred for 5 min, then heated by microwave irradiation (50 W) for 2 hour at 30°C and finally, stirred with an aqueous EDTA-disodium salt solution adjusted to pH≈ 8-9 (10 mL). The mixture was then extracted with a 3:1 mixture of CH_2Cl_2/CH_3CN (3 × 20 mL). The organic phases were combined, dried over Na_2SO_4 and finally evaporated in vacuo. Further purification by column chromatography (SiO_2, CH_2Cl_2 → $CH_2Cl_2/CH_3OH/Et_3N$: 200/1/1, then $CH_2Cl_2/CH_3OH/ Et_3N$: 200/4/1) yielded compound **60** (220 mg, 75%) as a yellow solid.
ESI-MS: calcd for $C_{102}H_{128}N_{14}O_{20}P_2F_{12}$ 934.60, $[M\text{-}2PF_6]^{2+}$, found: 934.47.

Compound 2ext

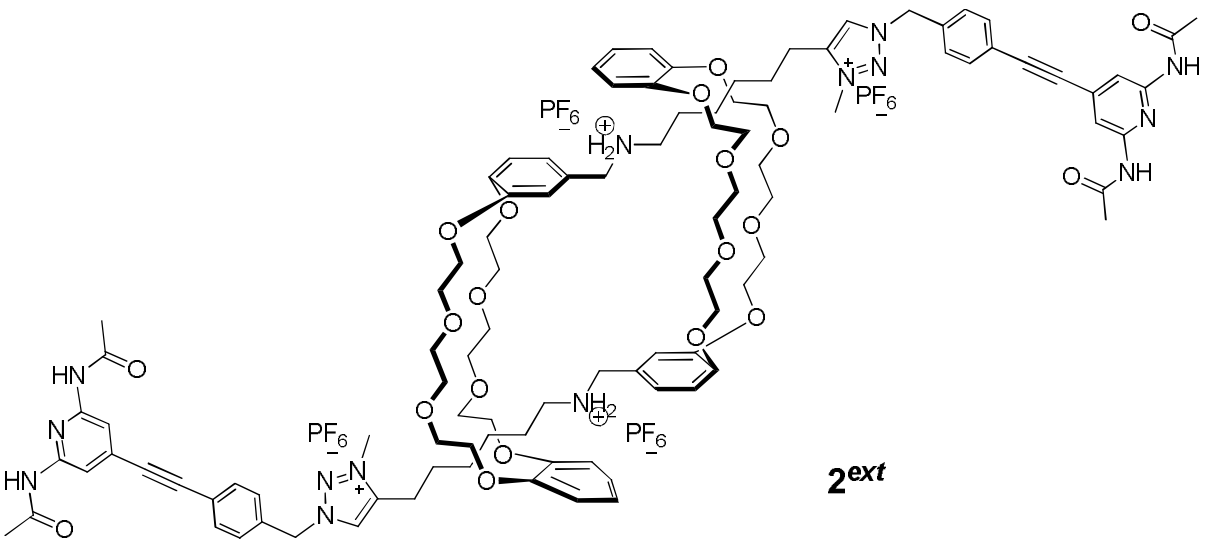

2*ext*

Rotaxane **60** (45 mg, 0.02 mmol) was dissolved in a 4:1:1 mixture of methyl iodide, chloroform and acetonitrile (6 mL). The mixture was stirred for 4 days at room temperature and then, solvents were evaporated in vacuo and the resulting solid was washed with Et_2O (5 mL) to give a brown solid. To a solution of this crude residue in water (4 mL) was added NH_4PF_6 (8.20 mg, 0.05 mmol) and a 3:1 mixture of CH_2Cl_2/CH_3CN (4 mL). The biphasic solution was stirred vigorously for 1 hour. The aqueous layer was extracted with $CHCl_3$ (3 × 5 mL). The organic layers were combined, dried over Na_2SO_4 and concentrated in vacuo to give product $\mathbf{2}^{ext}$ (51 mg, quantitative) as a brown solid. ^{1}H NMR and ^{13}C NMR data cannot be reported due to a problem faced with the NMR hard drive. A ^{1}H NMR spectra is depicted in Annex 3.

Compound 2^{cont}

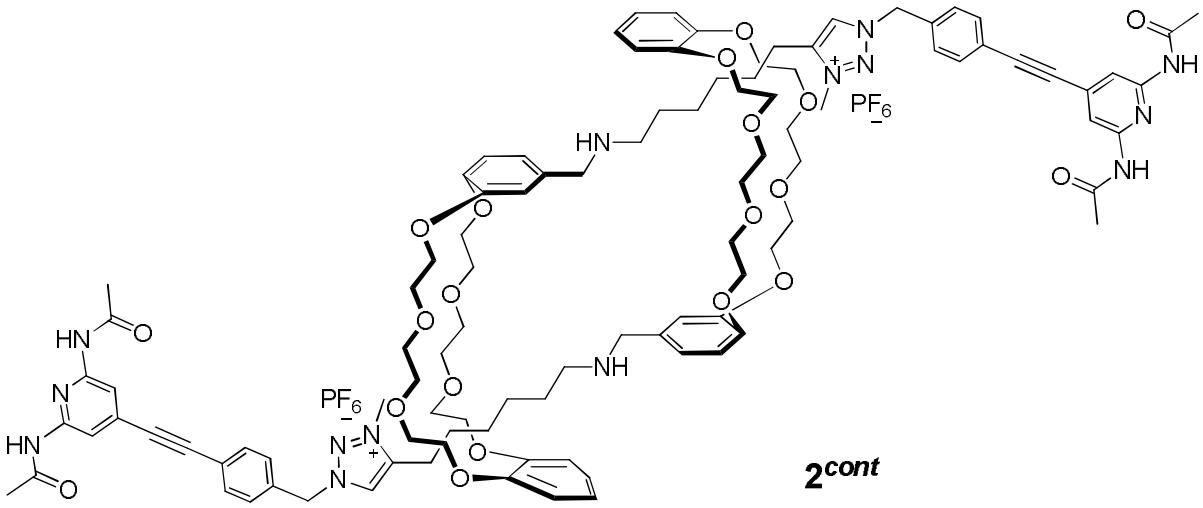

2^{cont}

A solution of the rotaxane $\mathbf{2}^{ext}$ (64 mg, 0.026 mmol) in $CHCl_3$ (6 mL) was washed with an aqueous solution of NaOH 1M (6 mL). The organic phase was dried over Na_2SO_4 and then evaporated in vacuo to provide compound $\mathbf{2}^{cont}$ (60 mg, quantitatively). ^{1}H NMR and ^{13}C NMR data cannot be reported due to a problem faced with the NMR hard drive. A ^{1}H NMR spectra is depicted in Annex 3. ESI-MS: calcd for $C_{104}H_{132}N_{14}O_{20}\ P_2F_{12}$ 948.49, $[M\text{-}2PF_6]^{2+}$, found: 948.30.

Compound 61

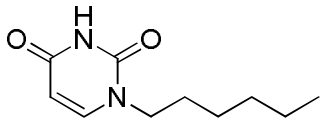

61

1-Hexyluracil. To a suspension of uracil (400 mg, 35.0 mmol) in DMSO (5 mL), dry K_2CO_3 (540 mg, 39.0 mmol) was added, and the suspension was stirred for 15-20 min. 1-

bromohexane (500 µL, 35.0 mmol) was then added and the reaction mixture stirred for 20 hours at 40 °C. The suspension was diluted with $CHCl_3$ (20 mL), washed with 0.1 M HCl solution (2 × 20 mL) and brine (3 × 20 mL), dried over Na_2SO_4, concentrated and poured into cold hexane with vigorous stirring. The resulting precipitate was filtered and washed with cold hexane (20 mL) to afford 1-hexyluracil **61** (490 mg, 71%) as a white solid. ^{1}H NMR ($CDCl_3$, 400 MHz, 25°C): δ = 9.35 (s, 1H), 7.14 (d, *J* = 7.9Hz, 1H), 5.68 (dd, *J* = 7.9, 1.8Hz, 1H), 3.71 (t, *J* = 7.3Hz, 2H), 1.70-1.63 (m, 2H), 1.34-1.26 (m, 6H), 0.88 (t, *J* = 6.8Hz, 3H); ^{13}C NMR ($CDCl_3$, 100 MHz, 25°C): δ = 164.0, 151.0, 144.6, 102.2, 49.1, 31.4, 29.1, 26.2, 22.6, 14.1; ESI-MS: calcd for $C_{10}H_{16}N_2O_2$ $[M+H]^+$ 197.13, found: 197.01.

Compound 62

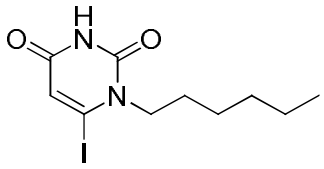

62

1-Hexyl-6-iodouracil. To a THF solution (1.6 mL) of 1-hexyluracil **61** (50 mg, 0.26 mmol), freshly prepared LDA (1.8 M solution in THF, 2.26 mL, 0.56 mmol) was added dropwise, and the resulting solution was stirred at -78 °C for 1.5 hours. Iodine (320 mg, 1.26 mmol) was added and the reaction mixture stirred for 2 hours. The solution was then treated with acetic acid (60 µL) and allowed to warm to room temperature. The organic phase was diluted with $CHCl_3$ (5 mL), washed with saturated aqueous $NaHCO_3$ solution (3 × 20 mL), $Na_2SO_{3\ sat.}$ (3 × 20 mL), and brine (20 mL), and dried over Na_2SO_4. Evaporation of the solvents in vacuo and purification by column chromatography (SiO_2, EtOAc/cyclohexane: 1/1) yielded compound **62** (64 mg, 78%) as a brown solid. R_f = 0.2 (n-hexane/EtOAc: 2/1); ^{1}H NMR (400 MHz, $CDCl_3$): δ = 9.40 (br, 1H), 6.40 (s, 1H), 4.05 (d, *J* = 7.3 Hz, 2H), 1.70-1.65 (m, 2H), 1.35-1.30 (m, 6H), 0.89 (t, *J* = 7.0 Hz, 3H); ^{13}C NMR ($CDCl_3$, 100 MHz, 25°C): δ = 161.0, 148.4, 115.9, 113.9, 53.8, 31.4, 28.8, 26.1, 22.6, 14.1. ESI-MS: calcd for $C_{10}H_{15}IN_2O_2$ $[M+H]^+$ 323.03, found: 323.19.

Compound 64

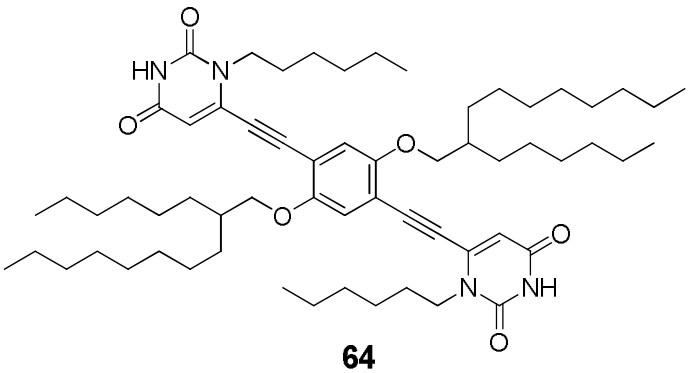

64

1-Hexyl-6-iodouracil (150 mg, 0.47 mmol) was added to a solution of free bis alkyne compound **63** (128 mg, 0.21 mmol) in a 1:1 mixture of Et_3N and THF (6 mL). The mixture was degassed by using freeze-thaw cycles and $Pd(PPh_3)_4$ (20 mg, 0.02 mmol), CuI (6.5 mg, 0.03 mmol) were then added. The mixture was degassed once more by using freeze-thaw cycles and then heated up to 35°C overnight. The resulting dark brown mixture was filtered and the solvent was removed in vacuo. Further purification by column chromatography (SiO_2, n-hexane → n-hexane/EtOAc: 2/1) yielded compound **64** (178 g, 40%) as a yellow solid. R_f = 0.6 (n-hexane/EtOAc: 2/1); ^{1}H NMR ($CDCl_3$, 400 MHz, 25°C): δ = 8.99 (s, 2H), 6.96 (s, 2H), 5.99 (d, *J* = 2.6Hz, 2H), 4.09 (t, *J* = 7.4Hz, 4H), 3.88 (d, *J* = 5.4Hz, 4H), 1.81-1.75 (m, 6H), 1.43-1.25 (m, 60H), 0.90-0.83 (m,12H); ^{13}C NMR ($CDCl_3$, 100 MHz, 25°C): δ = 162.4, 154.5, 150.7, 138.8, 116.4, 113.0, 107.0, 96.8, 86.2, 72.4, 46.8, 38.2, 32.0, 31.9, 31.6, 31.4, 30.2, 29.8, 29.7, 29.50, 29.0, 26.9, 26.5, 22.8, 22.7, 14.2, 14.1; ESI-MS: calcd for $C_{62}H_{98}N_4O_6$ $[M+H]^+$ 995.76, found: 995.99.

Procedures for acidic-basic titrations of monomer 2^{cont}

Acidic titration: A solution of $\mathbf{2}^{cont}$ (4×10^{-3} mmol) in $CDCl_3$ and of *d*-TFA (0.2 mol/L) in $CDCl_3$ were prepared separately. 2μL of *d*-TFA solution was added to the 1cont solution for each titration. The complete titration was finished after 22 times (up to 2.2 equiv.).

Procedures for polymerization of Hydrogen-bonding rotaxanes

Contracted polymers: A solution of compound **64** (24.9 mg, 25.0×10^{-3} mmol, 1.0 equiv.) in $CDCl_3$ (1250 μL) was added rotaxane monomer $\mathbf{2}^{cont}$ (43.8 mg, 25.0×10^{-3} mmol, 1.0 equiv.) in CD_3CN (1250 μL). The mixture was stirred for 30 min at room temperature prior to further analyzes.

Extended polymers: A solution of compound **64** (3.2 mg, 24.9 × 10^{-3} mmol, 1.0 equiv.) in $CDCl_3$ (1250 µL) was added rotaxane monomer $\mathbf{2}^{ext}$ (62.0 mg, 25.0 × 10^{-3} mmol, 1.0 equiv.) in CD_3CN (1250 µL). The mixture was stirred for 30 min at room temperature prior to further analyzes.

Compound 65

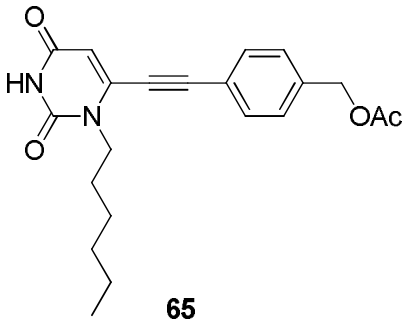

65

4-ethynylbenzyl acetate (91 mg, 0.52 mmol) was added to a solution of compound **62** (140 mg, 0.43 mmol) in a 1:1 mixture of triethylamine and tetrahydrofuran (5.6 mL). The mixture was degassed by using freeze-thaw cycles, then $Pd(PPh_3)_4$ (21 mg, 0.02 mmol) and CuI (6.3 mg, 0.03 mmol) were added. The mixture was degassed once more by using freeze-thaw cycles and then heated up overnight to 45°C. The resulting dark brown mixture was filtered and the solvent was removed in vacuo. Further purification by column chromatography (SiO_2, cyclohexane → cyclohexane/EtOAc: 1/1) yielded compound **65** (137 mg, 86%) as a brown solid. R_f = 0.4 (cyclohexane/EtOAc: 1/1); ^{1}H NMR (400 MHz, $CDCl_3$, 25°C): δ =8.59 (br, 1H), 7.53 (d, *J* = 7.7Hz, 2H), 7.41 (d, *J* = 7.7Hz, 2H), 5.99 (s, 1H), 5.14 (s, 2H), 4.05 (t, *J* = 7.3Hz, 2H), 2.13 (s, 3H), 1.80-1.75 (m, 2H), 1.40-1.30 (m, 6H), 0.87 (t, *J* = 6.8 Hz, 3H); ^{13}C NMR ($CDCl_3$, 100 MHz, 25°C): δ = 170.9, 162.4, 150.8, 138.9, 138.6, 132.4, 128.4, 120.0, 107.0, 100.0, 80.8, 65.6, 46.8, 31.6, 28.9, 26.5, 22.7, 21.0, 14.1; ESI-MS: calcd for $C_{21}H_{24}N_2O_4$ $[M+H]^+$ 369.18, found: 369.15.

Compound 66

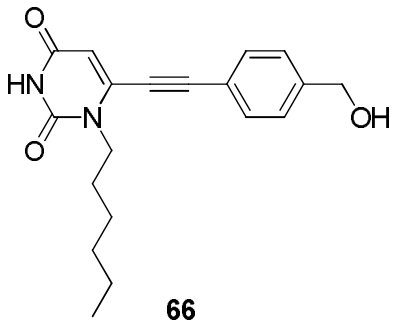

66

A solution of compound **65** (50 mg, 0.14 mmol) in methanol (2 mL) was treated with KOH (1M, 2 Ml, 0.71 mmol) and the solution was stirred at room temperature for 1 hour. The solvent was then removed in vacuo, and the resulting mixture was dissolved with a mixture of CH_2Cl_2 (5 mL) and water (5 mL). The aqueous phase was extracted with CH_2Cl_2 (3*5 mL). The organic phases were combined, dried over Na_2SO_4. Evaporation of the solvent under vacuum and purification by column chromatography (SiO_2, n-hexane/EtOAc: 1/3) provide compound **66** (22 mg, 47%) as a yellow solid. , R_f = 0.1 (n-hexane/EtOAc: 1/3); ^{1}H NMR ($CDCl_3$, 400 MHz, 25°C): δ = 8.34 (s, 2H), 7.53 (d, *J* = 8.3Hz, 2H), 7.43 (d, *J* = 7.8Hz, 2H), 5.98 (s, 1H), 4.77 (s, 2H), 2.17 (s, 6H), 1.80-1.75 (m, 2H), 1.40-1.30 (m, 6H), 0.87 (t, *J* = 6.8 Hz, 3H); ^{13}C NMR ($CDCl_3$, 100 MHz, 25°C): δ = 171.9, 151.9, 144.5, 136.2, 133.0, 128.0, 122.1, 112.1, 93.9, 87.9, 64.7, 24.1; ESI-MS: calcd for $C_{19}H_{22}N_2O_3$: 327.17 $[M+H]^+$, found: 327.34.

Compound 67

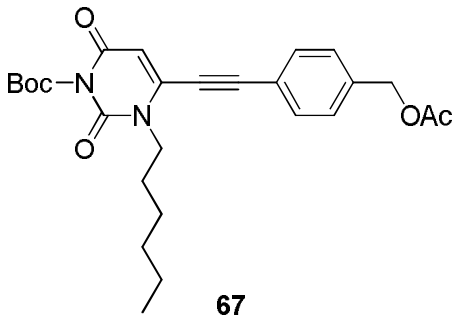

67

Route 1: Compound **65** (150 mg, 0.41 mmol) was dissolved in a mixture of pyridine (110 µL) and dry $CHCl_3$ (850 µL). After stirring the solution for 10 min at room temperature, Boc_2O (266 mg, 1.21 mmol) was added and the whole solution stirred overnight at 40 °C. The reaction mixture was then diluted with $CHCl_3$ (10 mL), and extracted with H_2O (5 mL) and brine (5 mL). The organic phase was dried over Na_2SO_4 and evaporated under reduced pressure to afford brown oil. Further purification by column chromatography (SiO_2, cyclohexane/EtOAc: 5/1) yielded compound **67** (168 mg, 88%) as a brown solid.

Route 2: 4-ethynylbenzyl acetate **39** (158 mg, 0.91 mmol) was added to a solution of compound **68** (320 mg, 0.76 mmol) in a 1:1 mixture of triethylamine and tetrahydrofuran (8 mL). The mixture was degassed by using freeze-thaw cycles, then $Pd(PPh_3)_4$ (35 mg, 0.03 mmol) and CuI (12 mg, 0.06 mmol) were added. The mixture was degassed once more by using freeze-thaw cycles and then heated up overnight to 45°C. The resulting dark brown mixture was filtered and the solvent was removed in vacuo. Further purification by column chromatography (SiO_2, cyclohexane → cyclohexane/EtOAc: 5/1) yielded compound **67** (137 mg, 86%) as a brown solid. R_f = 0.2 (cyclohexane/EtOAc: 5/1); ^{1}H NMR ($CDCl_3$, 400 MHz, 25°C): δ = 7.51 (d, *J* = 8.1Hz, 2H), 7.42 (d, *J* = 8.1Hz, 2H), 6.01 (s, 1H), 5.14 (s, 2H), 4.02 (t, *J* = 7.2Hz, 2H), 2.13 (s, 3H); 1.87-1.73 (m, 2H), 1.41 (s, 9H), 1.39-1.32 (m, 6H), 0.9 (t, *J* = 6.8 Hz, 3H); ^{13}C NMR ($CDCl_3$, 100 MHz, 25°C): δ = 170.8, 151.7, 149.0, 147.9, 139.0, 137.9, 132.4, 128.4, 119.9, 106.6, 100.4, 87.0, 80.6, 65.5, 47.4, 31.6, 28.8, 27.6, 27.0, 26.6, 22.7, 14.1; ESI-MS: calcd for $C_{26}H_{32}N_2O_6$: 429.216 $[M+Na]^+$, found: 492.40.

Compound 68

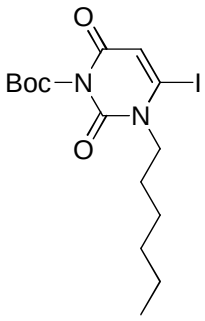

68

Compound **62** (200 mg, 0.62 mmol) was dissolved in a mixture of pyridine (130 µL) and dry $CHCl_3$ (1 mL). After stirring the solution for 10 min at room temperature, Boc_2O (409 mg, 1.86 mmol) was added and the whole solution stirred overnight at 40 °C. The reaction mixture was then diluted with $CHCl_3$ (20 mL), and extracted with H_2O (10 mL) and brine (10 mL). The organic phase was dried over Na_2SO_4 and evaporated under reduced pressure to afford a brown oil. Further purification by column chromatography (SiO_2, cyclohexane/EtOAc: 5/1) yielded compound **68** (233 mg, 89%) as a brown solid. R_f = 0.25 (cyclohexane/EtOAc: 5/1); ^{1}H NMR ($CDCl_3$, 400 MHz, 25°C): δ = 6.43 (s, 1H), 4.04 (t, *J* = 8.0Hz, 2H), 1.74-1.68 (m, 2H); 1.64 (s, 9H), 1.59-1.33 (m, 6H); 0.89 (t, *J* = 6.6 Hz, 3H); ^{13}C NMR ($CDCl_3$, 100 MHz, 25°C): δ = 158.6, 147.4, 146.5, 115.4, 113.1, 87.2, 54.3, 31.4, 28.7, 27.5, 26.1, 22.6, 14.1; ESI-MS: calcd for $C_{15}H_{23}IN_2O_4$: 445.068 $[M+Na]^+$, found: 445.30.

Compound 69

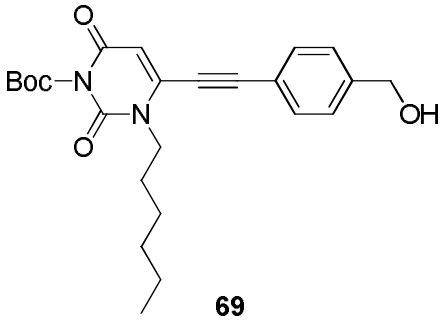

69

A solution of compound **67** (5 mg, 0.012 mmol) in a 2:1:2 mixture of methanol, CH_2Cl_2 and H_2O (2.5 mL) was treated with K_2CO_3 (20 mg, 0.14 mmol) and the solution was stirred at room temperature overnight. The solvent was then removed in vacuo, and the resulting mixture was dissolved with a mixture of CH_2Cl_2 (5 mL) and water (5 mL). The aqueous phase was extracted with CH_2Cl_2 (3 × 5 mL). The organic phases were combined, dried over Na_2SO_4. Evaporation of the solvent under vacuum provide compound **69** (4 mg, 88%) as a yellow solid. ^{1}H NMR ($CDCl_3$, 400 MHz, 25°C): δ = 7.52 (d, *J* = 8.1Hz, 2H), 7.43 (d, *J* = 8.2Hz, 2H), 5.99 (s, 1H), 4.77 (s, 2H), 4.04 (t, *J* = 8.0Hz, 2H), 1.82-1.74 (m, 2H), 1.62 (s, 9H), 1.41-1.31 (m, 6H), 0.87 (t, *J* = 7.0Hz, 3H); ^{13}C NMR ($CDCl_3$, 100 MHz, 25°C): δ = 159.8, 149.1, 147.9, 144.1, 138.1, 132.4, 127.2, 119.3, 106.4, 100.9, 87.0, 80. 3, 64.8, 47.3, 31.6, 28.9, 27.6, 26.6, 22.7, 14.1; ESI-MS: calcd for $C_{24}H_{30}N_2O_5$: 450.213 $[M+Na]^+$, found: 450.34.

Compound 70

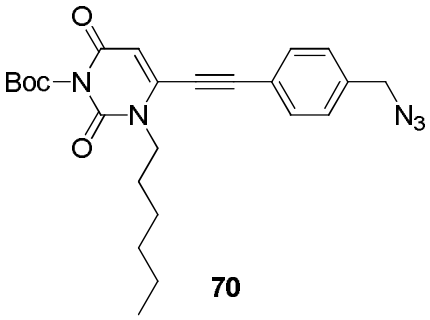

70

A solution of compound **69** (21.8 mg, 0.067 mmol) in a 4:1 mixture of THF/DMF (10 mL) was cooled down to 0°C and triethylamine (200 µL, 0.087 mmol) and methanesulfonyl chloride (7 µL, 0.09 mmol) were added. The reaction mixture was then stirred overnight at room temperature and further dissolved with CH_2Cl_2 (5 mL). The organic phase was then extracted with water (5 mL) and $NH_4Cl_{\text{ sat.}}$ (5 mL), dried over Na_2SO_4 and concentrated in vacuo to provide the mesylated derivative, which was pure enough to be used as such in the next step.

A solution of the crude mesylate derivative in a 1:1 mixture of DMF and THF (1 mL) was

treated with sodium azide (22 mg, 0.335 mmol) and heated up overnight to 50°C. After cooling down to room temperature, the reaction mixture was diluted with CH_2Cl_2 (5 mL). The organic phase was then extracted with water (5 mL) and $NH_4Cl_{sat.}$ (5 mL), dried over Na_2SO_4 and concentrated in vacuo. Further purification by column chromatography (SiO_2, cyclohexane/EtOAc: 1/1) yielded compound **70** (8.7 mg, 37%) as a yellow solid. R_f = 0.4 (cyclohexane/EtOAc: 1/1); ^{1}H NMR ($CDCl_3$, 400 MHz, 25°C): δ = 7.65 (d, *J* = 8.4Hz, 2H), 7.41 (d, *J* = 8.4Hz, 2H), 5.79 (s, 1H), 4.41 (s, 2H), 3.61 (t, *J* = 8.0Hz, 2H), 1.78-1.68 (m, 2H), 1.66 (s, 9H), 1.41 (s, 9H), 1.38-1.26 (m, 6H); 0.9 (t, *J* = 7.0 Hz, 3H); ^{13}C NMR ($CDCl_3$, 100 MHz, 25°C): δ = 159.2, 149.4, 147.7, 145.9, 137.9, 137.5, 129.0, 127.9, 127.6, 105.7, 87.2, 68.0, 54.3, 46.2, 30.9, 28.4, 27.5, 26.0, 22.7, 14.1.

Compound 71

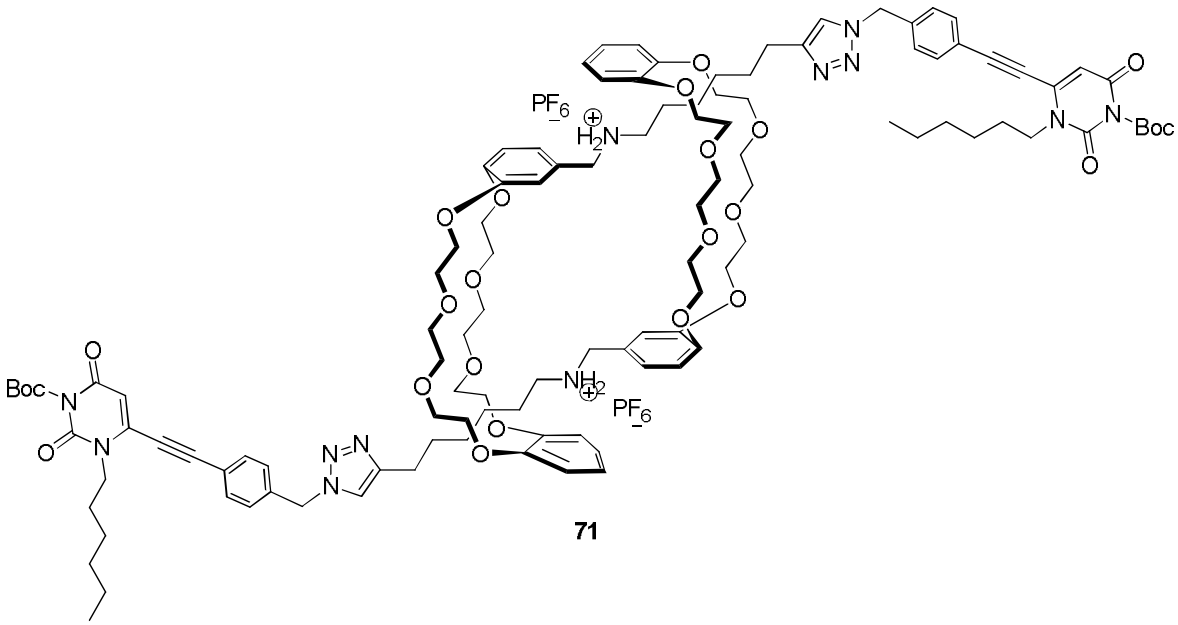

71

To a solution of boc-uracil benzyl azide compound **70** (27 mg, 0.059 mmol) and compound **11** (43.8 mg, 0.029 mmol) in a mixture of dry CH_2Cl_2 (5 mL) and dry CH_3CN (2 mL) were added successively $Cu(CH_3CN)_4PF_6$ (22 mg, 0.059 mmol) and 2,6-lutidine (7 µL, 0.06 mmol). The reaction mixture was stirred for 5 min, then heated by microwave irradiation (50 W) for 2 hours at 30°C and finally, stirred with an aqueous EDTA-disodium salt solution adjusted to pH≈ 8-9 (10 mL). The mixture was then extracted with a 3:1 mixture of CH_2Cl_2/ CH_3CN (3 × 10 mL). The organic phases were combined, dried over Na_2SO_4 and finally evaporated in vacuo. It was not purified further.

Compound 72

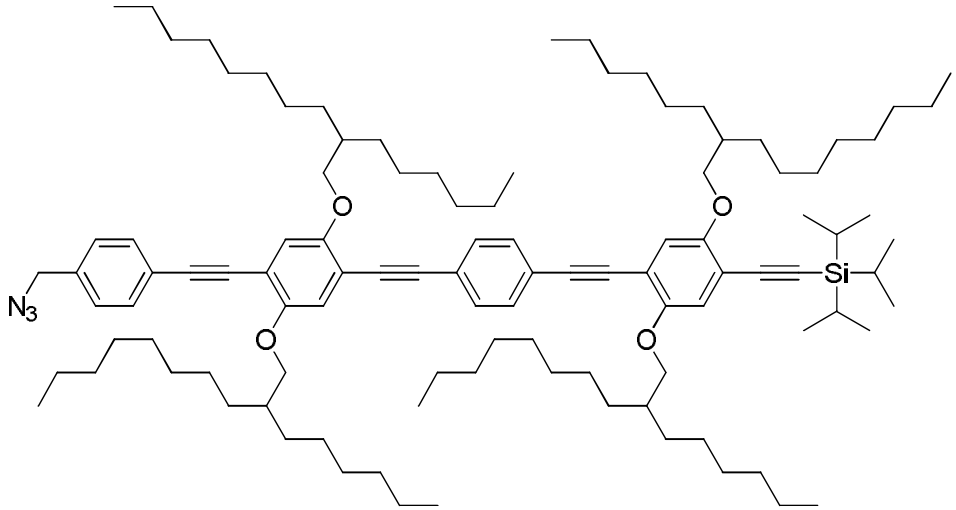

72

A solution of compound **42** (10 mg, 6.28 µmol) in a 1:1 mixture of THF/methanol (300 µL) was treated with K_2CO_3 (3 mg, 9.42 µmol) and the solution was stirred overnight at room temperature. The solvent was then removed in vacuo, and the resulting mixture was dissolved with a mixture of CH_2Cl_2 (5 mL) and water (5 mL), and the aqueous phase was extracted with CH_2Cl_2 (3 × 5 mL). The organic phases were combined, dried over Na_2SO_4, and evaporated in vacuo to give the corresponding alcohol, which was pure enough to be used as such in the next step.

A solution of this crude alcohol (25 mg, 16.7 µmol) in CH_2Cl_2 (520 µL) was cooled down to 0°C and triethylamine (14 µL, 50 µmol) and methanesulfonyl chloride (8 µL, 50 µmol) were added. The reaction mixture was then stirred overnight at room temperature. The organic phase was then extracted with water (5 mL) and $NH_4Cl_{\text{ sat.}}$ (5 mL), dried over Na_2SO_4 and concentrated in vacuo to provide the mesylated derivative, which was pure enough to be used as such in the next step.

A solution of this crude mesylate in a 1:1 mixture of DMF and THF (0.5 mL) was treated with sodium azide (11 mg, 166.6 µmol) and heated up overnight to 50°C. After cooling down to room temperature, the reaction mixture was diluted with CH_2Cl_2 (5 mL). The organic phase was then extracted with water (5 mL) and $NH_4Cl_{\text{ sat.}}$ (5 mL), dried over Na_2SO_4 and concentrated in vacuo. Further purification by column chromatography (SiO_2, n-hexane → n-hexane/EtOAc: 10/1) provided compound **72** (9 mg, 36% over 3 steps) as a yellow oil. R_f = 0.1 (EtOAc/n-hexane: 1/20); ^{1}H NMR ($CDCl_3$, 400 MHz, 25°C): δ = 7.53 (d, *J* = 8.2Hz, 2H), 7.50 (s, 4H), 7.37 (d, *J* = 8.3Hz, 2H), 7.02 (s, 1H), 7.01 (s, 1H), 6.95 (s, 1H), 6.94 (s, 1H), 6.93 (s, 1H), 4.60 (s, 2H), 3.97-3.83 (m, 8H), 1.94-1.73 (m, 4H), 1.63-1.20 (m, 99H), 1.16 (s,

18H), 0.98-0.79 (m, 24H); ^{13}C NMR (100 MHz, $CDCl_3$, 298 K): δ = 154.5, 154.1, 153.7, 137.5, 132.0, 131.6, 128.7, 123.9, 123.5, 123.4, 117.8, 116.7, 116.1，114.2, 114.1, 113.9, 103.2, 96.5, 94.8, 94.5, 94.5, 88.3, 88.1, 87.0, 72.5, 71.9, 45.0, 38.4, 32.1, 32.0, 31.7, 31.6, 31.3, 30.3, 29.9, 29.8, 29.8, 29.5, 27.1, 27.1, 27.0, 27.0, 22.9, 22.8, 18.9, 14.3, 11.6; MALDI-TOF: calcd for $C_{106}H_{167}N_3O_4Si$: 1571.27 $[M-N_2+Na]^+$, found: 1571.22.

Compound 73

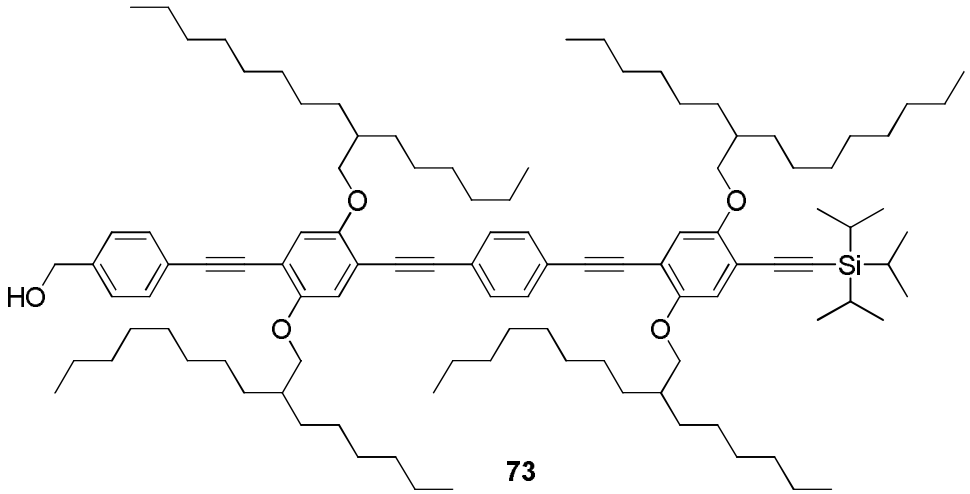

73

To an oven dried Schlenk were added compound **34** (45.6 mg, 0.064 mmol), compound **31** (64.4 mg, 0.077 mmol), $Pd(PPh_3)_2Cl_2$ (6 mg, 0.008 mmol), copper iodide (3 mg, 0.002 mmol), triphenylphosphine (4 mg, 0.002 mmol) in a 1:1 mixture of triethylamine and dry THF (8 mL). The solution was degassed using freeze-thaw cycles and the reaction mixture was heated at overnight 80°C. The reaction was quenched with $NH_4Cl_{sat.}$(10 mL) and extracted with CH_2Cl_2 (20 mL). The organic phase was washed with $NH_4Cl_{sat.}$ (10 mL), water (10 mL) and dried over Na_2SO_4. After removal of the solvent, the product was treated with n-hexane and filtered. Evaporation of the filtrate followed by purification by column chromatography (SiO_2, n-hexane → EtOAc/n-hexane: 1/3) afforded compound **73** (12 mg, 13%) as a light yellow oil. R_f = 0.6 (EtOAc/n-hexane: 1/6); ^{1}H NMR ($CDCl_3$, 400 MHz, 25°C): δ = 7.53 (d, *J* = 8.2Hz, 2H), 7.48 (s, 4H), 7.35 (d, *J* = 8.2Hz, 2H), 7.03 (s, 1H), 7.02 (s, 1H), 6.95 (s, 1H), 6.94 (s, 1H), 4.72 (s, 2H), 3.96-3.83 (m, 8H), 1.89-1.73 (m, 4H), 1.59-1.17 (m, 96H), 1.15 (s, 21H), 0.99-0.79 (m, 24H); ^{13}C NMR ($CDCl_3$, 400 MHz, 25°C): δ = 154.5, 154.1, 154.0, 153.7, 141.1, 131.9, 131.5, 126.9, 123.5, 123.5, 123.0, 117.8, 116.8, 116.2, 114.3, 114.2, 114.0, 113.9, 103.2, 96.5, 95.0, 94.7, 94.5, 88.3, 88.2, 86.3, 77.4, 72.6, 71.9, 65.1, 38.4, 32.1, 32.0, 31.7, 31.3, 30.4, 30.3, 29.9, 29.8, 29.8, 29.5, 27.1, 27.1, 27.0, 27.0, 22.8, 18.9, 14.2, 11.6; ESI-MS: calcd for $C_{108}H_{168}O_5Si$ 1550.27 $[M+H]^+$, found: 1550.85.

Annex 1 –Superimposed ^{1}H NMR Spectra of compounds 10, 23 and 24

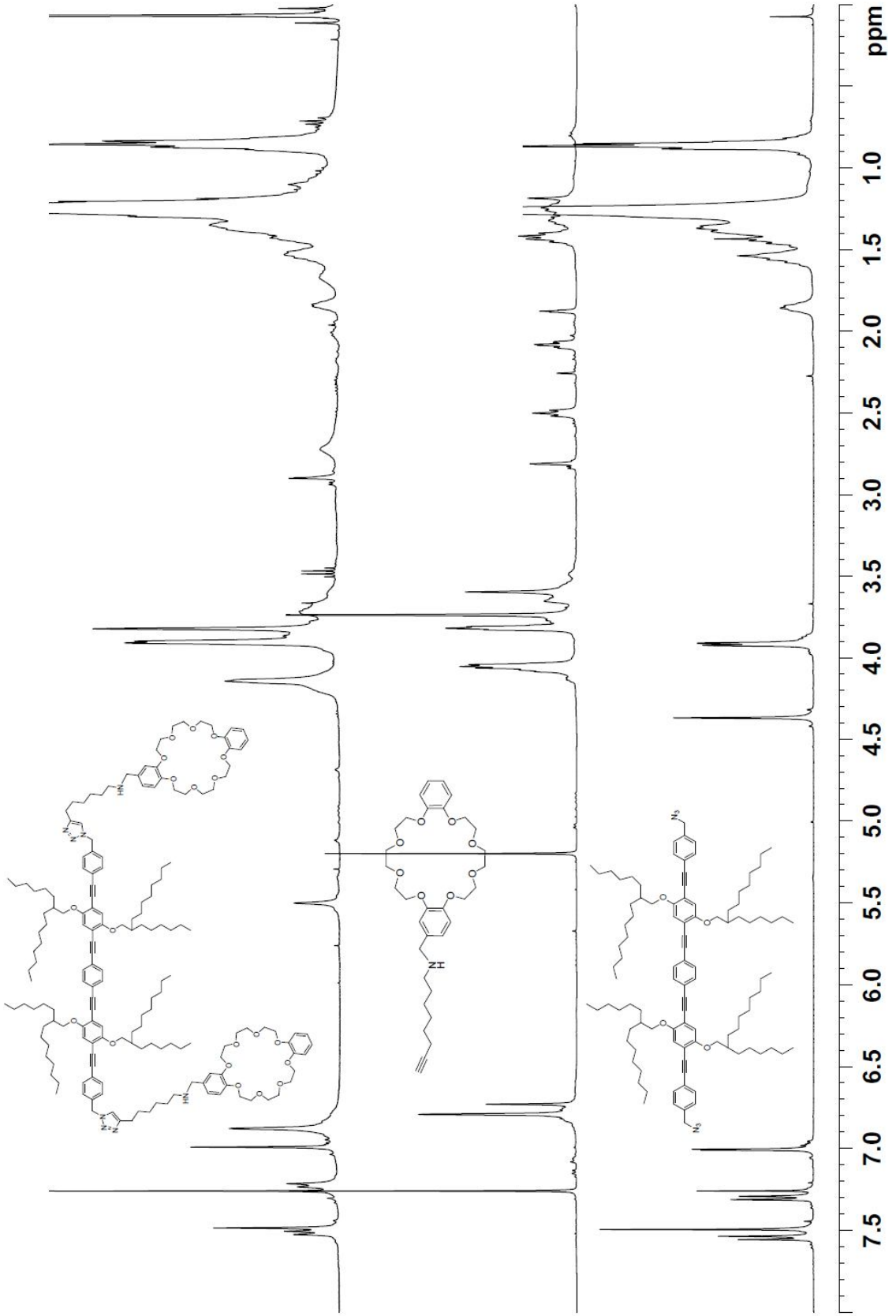

Annex 2 –^{1}H NMR Spectrum of compound 45

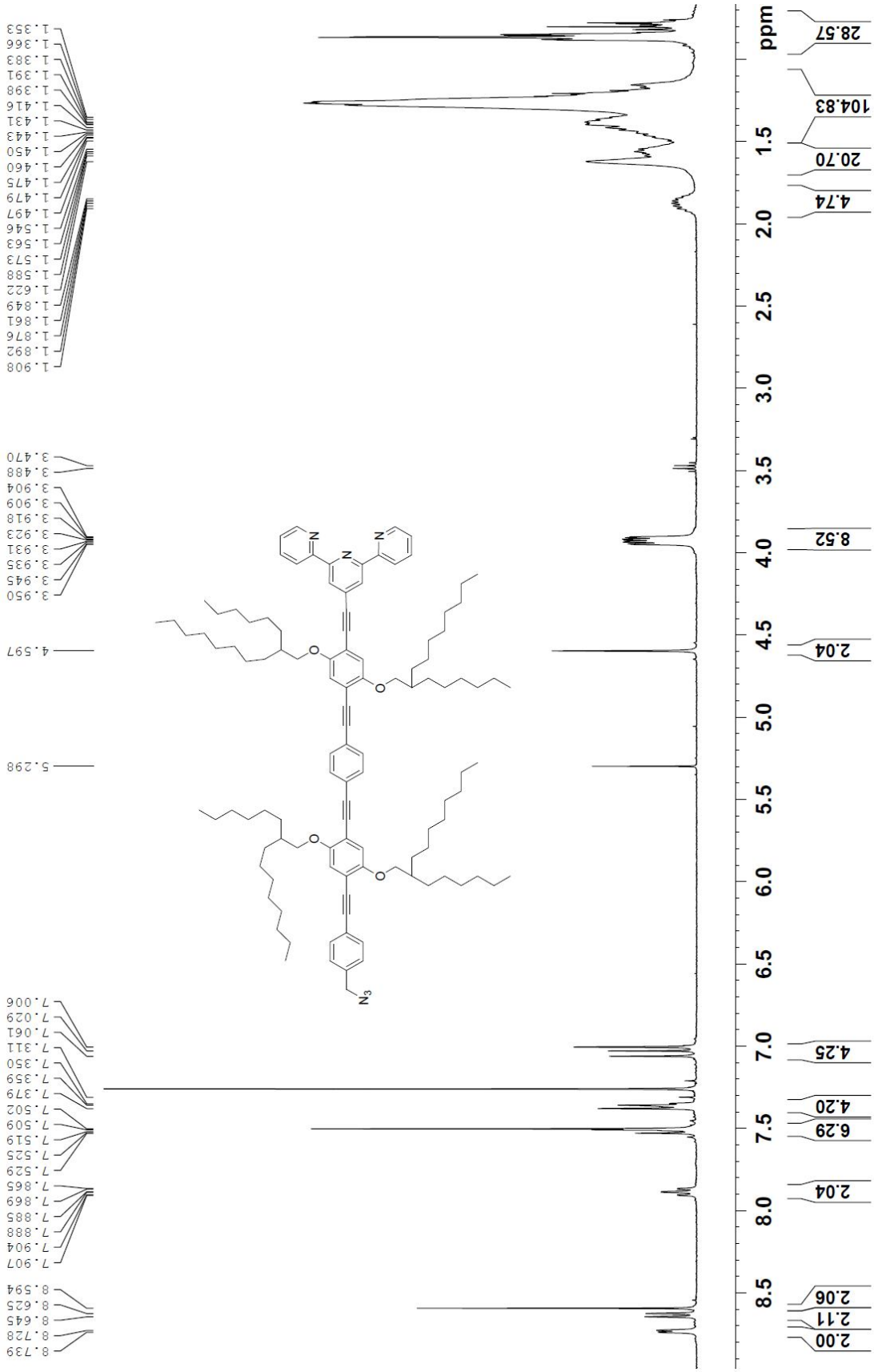

Annex 3 – Superimposed ^{1}H NMR Spectra of compounds 64, 2^{ext}, 2^{cont} and polymers $[64•2]^{cont}$ and $[64•2]^{ext}$